Multi-axial Fatigue Assessment of a Lemniscate Crane

FEA and MBD Analysis

Skirmantas Pargalgauskas

ISBN 2022.MME.8631

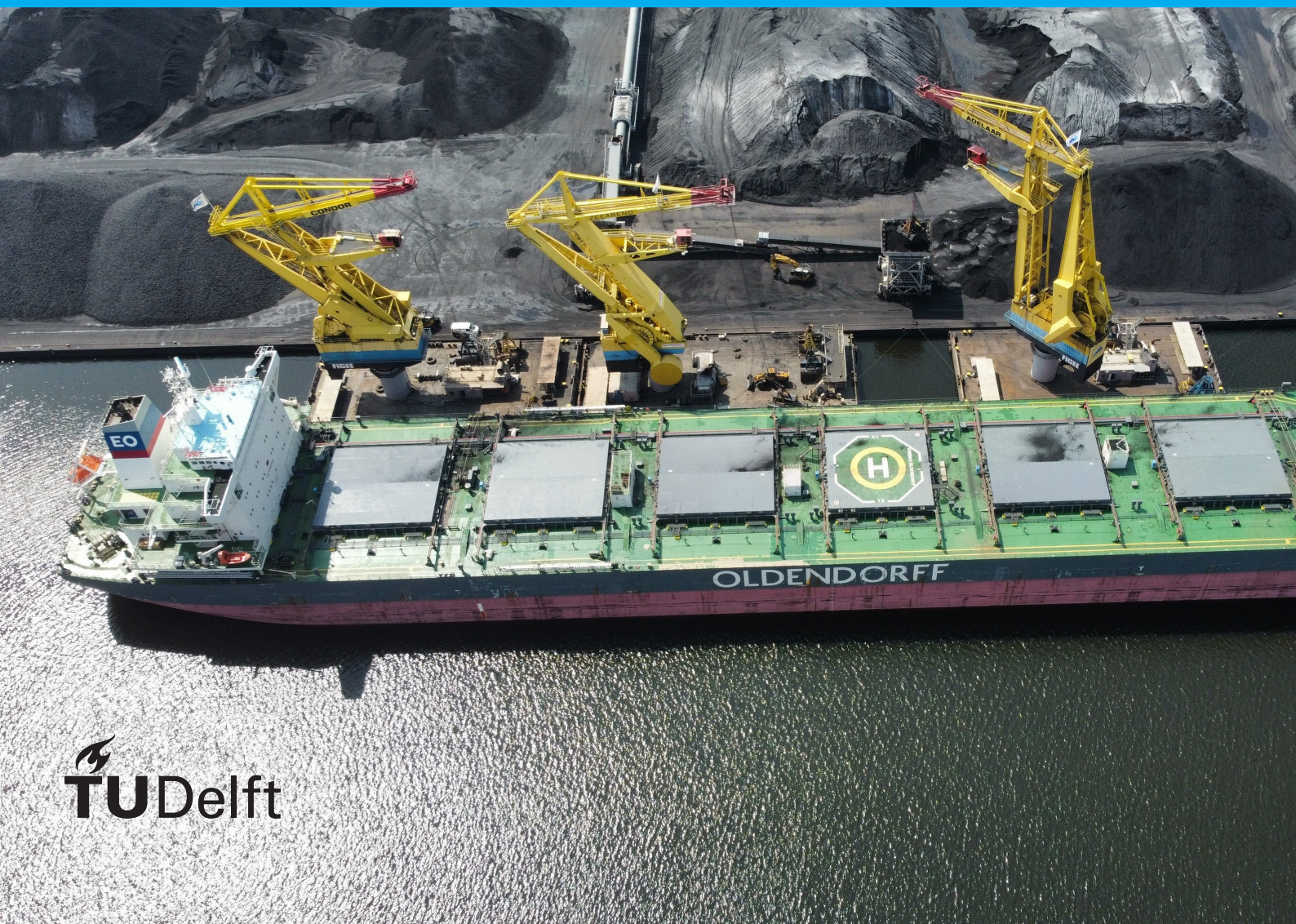

TU Delft

Multi-axial Fatigue Assessment of a Lemniscate Crane

FEA and MBD Analysis

by

Skirmantas Pargalgauskas

to obtain the degree of Master of Science
at the Delft University of Technology,
to be defended publicly on Tuesday May 24, 2022 at 1:00 PM.

Student number:	5122163	
Project duration:	July 15, 2021 – March 30, 2022	
Thesis committee:	Dr. ir. D.L. Schott,	TU Delft, chair
	Dr. ir. X. Jiang,	TU Delft, supervisor
	Dr. ir. J. K. Moore,	TU Delft,
	Mr. M. Edelkamp,	In Summa Innovation B.V.

TU Delft

Preface

Now that I am writing these last paragraphs as the final part of my Master thesis report - it is still hard to believe that the project is finally over. During its process I have accomplished all of my project goals and a little bit extra, yet it still feels like there are more things which I would want to investigate and find answers to. I guess that is the pitfall of all research - it never feels like it is over. Nonetheless, it is time for me to close this particular chapter and open a new one, as life does not stop and I am excited to begin the new things that await me now. This is a document, which in the grand scheme of things will likely not mean as much to me in the future as it does now, however it serves as the final product to commemorate the conclusion of my Master degree studies within Delft University of Technology. Out of this experience I will bring with me not only the acquired knowledge related to my study field, but also good and bad moments encountered during this time, human connections and a matured worldview which hopefully will allow me to see everything in life from an improved standpoint.

Before starting, I did not like the idea of treating this part as a glorified *thank you* message, however now that I am done - I feel that the following people indeed deserve acknowledgement and recognition for being a part of my thesis project or the time I have spent completing my master studies. Firstly, I would like to thank the entire graduation committee, with a special thanks going to my main supervisor, Dr. ir. Xiaoli Jiang, who has provided me with valuable guidance and interesting discussions throughout the duration of the final project. It was a pleasure working with you and I couldn't have asked for a better supervisor. I would also like to extend my thanks to Dr. ir. Dingena Schott for participating as the Chair of this project committee and for being a great stand-out professor within the courses I have taken during my time in TU Delft. Secondly, I would like to show appreciation to my friends: Mr. Gavin Furtado, who from the first days of my time in the Netherlands has become one of my closest friends in the country, even though he still struggles to light a barbecue grill without spilling half a bottle of hand sanitizer on it (I'm just saying - there are better ways to do it); Mr. Sangamesh Balaji for always finding ways to make me laugh at inappropriate moments; Mr. Alexander (Xander) Kragt Mateu, Ms. Nilüfer Özhan and Mr. Bjørn Romijn for not only being great classmates, but also for becoming an amazing group of friends I will continue to cherish; Ms. Esmée Kaman for making all of our study sessions and randomly deep talks an unforgettable part of my time in TU Delft; and Ms. Yiwen Lin for being my go-to person who I can always count on whenever I need support, advice or a little bit of cheering up. Finally I would like to thank my mother who always supports me in my endeavours, for which I will always be grateful.

If you have spent time reading this part - I commend you and I hope that you will have a good time reading the rest of the report as well. So buckle up - quite an extensive read awaits you.

Skirmantas Pargalgauskas
Delft, 2022

Abstract

The main purpose of this report is to investigate flaws within Cornelis Tromp 25T lemniscate crane upper arm joint. This is done in order to figure out why the joint structure is experiencing significant crack propagation and what potentially could have led to a structural joint failure and death of an operator within a crane of the same model.

Assessment is performed by simulating stress distribution within the problematic joint structure and assessing high-cycle fatigue damage accumulation around its welds. Loading conditions affecting crane upper arm are established through multi-body dynamic simulations, which are meant to replicate operation of a lemniscate crane. Multi-body dynamic model is verified for its accuracy using available crane operation measurement data. Loads are acquired within the time domain and include temporal effects of luffing, slewing and hoisting operations as well as pontoon motion.

Fatigue analysis is performed to evaluate damage accumulation within the tubular joint structure of the crane upper arm. A detailed shell finite element model is established to acquire time-dependent stress responses. During stress evaluation stage - a particularly large stress concentration has been observed at the joint brace saddle position. To assess which method best simulate damage accumulation in the joint structure - three specific fatigue assessment approaches are tested: nominal stress approach, hot-spot stress approach and multi-axial fatigue approach. Nominal and hot-spot stress approaches are evaluated and compared to determine how inclusion of stress concentration effects into fatigue assessment influence damage accumulation results. Result comparison has shown a large disparity in results with hot-spot stress approach, indicating that the method capable of determining locations of dangerous stress accumulation, in relation to what has been observed in the real structure.

Evaluation is performed to determine whether multi-axial fatigue assessment is needed to improve calculation results of fatigue damage accumulation. Based on stress direction properties within the analysed structure - most favorable multi-axial fatigue assessment approach (capable of analysing proportional stress responses) is used. Multi-axial fatigue assessment method results are then compared with results of conventional hot-spot stress approach to evaluate the differences in damage accumulation rate. Analysis results have shown that both methods are capable of determining locations of critical points with present disparity within magnitude of damage accumulation. This indicates that hot-spot stress fatigue approach, which uses Von Mises stress, is more conservative out of two methods. Fatigue analysis has also presented that original joint structure is inherently flawed, as its stress concentration locations are not easily accessible without crane disassembly and its structural capacity has been underestimated during design stage.

Finally methods for extending operational life of crane upper arm structure are evaluated. Three methods for reducing stress within the structure are assessed: increase of structural capacity, stress redistribution and load reduction. Increase of structural capacity is performed by adjusting thickness of relevant joint elements, with optimal thickness being established using a sensitivity analysis algorithm, which simultaneously acquires combined thickness setup for multiple joint elements - making the joint capable of surviving predetermined fatigue life. Stress redistribution approach is implemented by producing an alternative upper arm joint design, which could be exchanged with the problematic original joint during crane refurbishment. Load reduction approach is performed to investigate whether it would be possible to increase fatigue life of the original joint structure without affecting work efficiency, by only adjusting crane motion profile within multi-body dynamic simulation environment. All three methods are quantified and compared through fatigue damage factor results acquired using multi-axial fatigue assessment method. Result comparison has shown that joint redesign is the most preferred approach due to its ability to efficiently improve fatigue life of the structure without significant structural weight increase, while exposing any potential points for crack initiation to locations easily accessible for inspection and repair.

Contents

List of Figures

List of Tables

1 Introduction

Fatigue is the most important failure mode to be considered in a mechanical design. According to Gagg and Lewis [29], 60-90 % of the damage on mechanical parts belongs to fatigue damage, while fatigue failure accounts for the majority of mechanical failures worldwide (with the numbers ranging between 50% and 90% between different industry statistics). As fatigue life is difficult to assess experimentally and sources for damage accumulation depend on an extremely large amount of variables - the methodology for fatigue life assessment is based on estimations and generally lack experimental data to provide a unified approach. However, the constantly evolving research and continuously developing tools allows us to move forward and find ways to increase the accuracy of evaluation procedures, implementing less conservative methods than what has been used in the past. This report is meant to analyse the damage accumulation and potentially improve the design of a flawed lemniscate crane boom, with the help of multi-body dynamic simulations for load acquisition and multi-axial fatigue assessment methodology for fatigue assessment. This chapter provides necessary background information on the topic and analysed crane, establishes project goals and lays the foundation on how the rest of the paper is organized.

1.1. Background

The aim of this thesis is to address the issue of premature structural failure due to fatigue damage accumulation within a specific lemniscate crane model used for handling bulk material. This is tackled through determining whether a less conservative fatigue evaluation method could potentially improve assessment procedure of a critical joint structure. The following section is meant to establish background information about the crane subjected for analysis, as well as the specific issue which has lead to the initiation of the objective for this research.

1.1.1. Lemniscate cranes

Lemniscate crane is a variant of a crane, most commonly used in transshipment industry for loading/unloading of various types of bulk material such as grain, coal, iron ore or break bulk like scrap metal. This crane type gets its name from its unique motion and reach profile which allows crane to move the lifted load in a lemniscate pattern due its ability to perform slewing and luffing motions.

1.1.2. Working principle

When it comes to modern lemniscate cranes, most of them consist of similar part setup which defines its working principle. Figure 1.1 provides a visual overview of the main components of the analysed Cornelis Tromp 25T lemniscate crane, with a general naming convention of its parts, which will be used throughout this report.

Lemniscate cranes are generally lifted above ground using a crane foot construction which is meant to increase crane lifting height, as well as free-up space for the crane to spin around its axis (i.e. slew). It includes the spinning joint at the top which drives the slewing motion. This structure is meant to sufficiently support the crane even when it is extended significantly and while carrying maximum allowed load. Machine floor along with the tower structure provides support to the crane arms and upper arm structure.

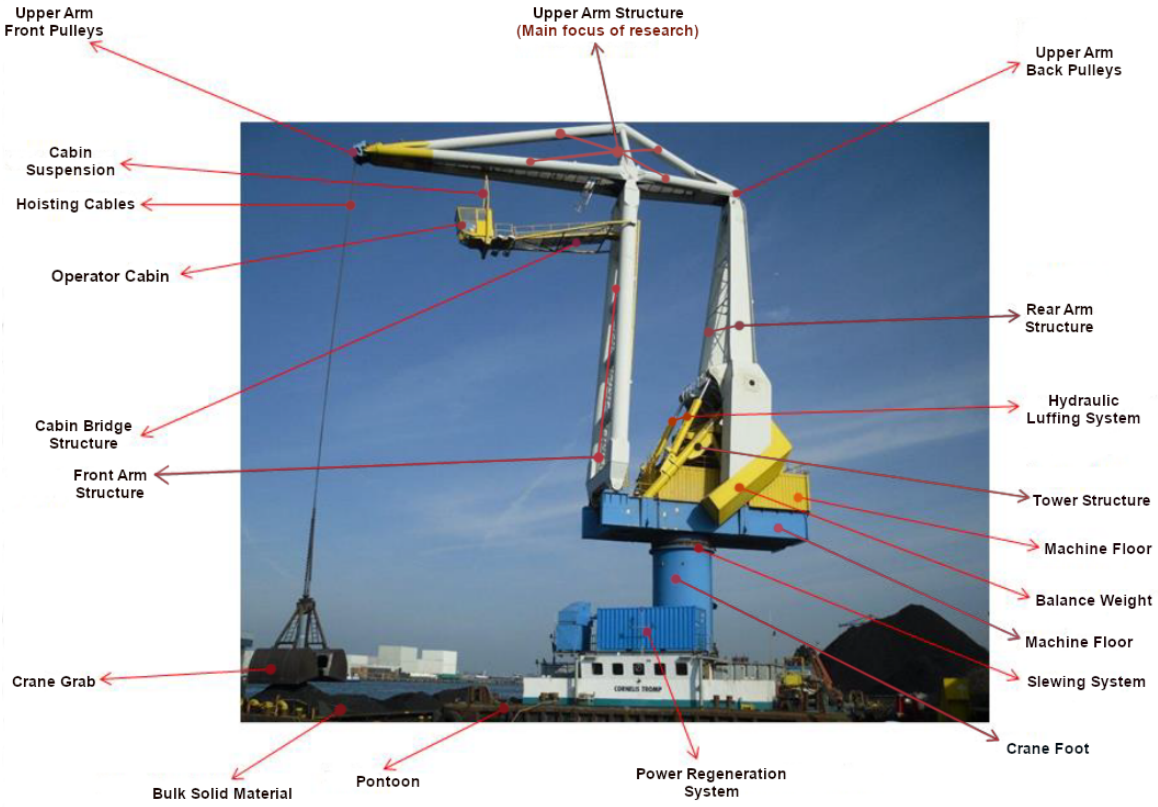

Figure 1.1: Main components of Cornelis Tromp 25T lemniscate crane

When it comes to crane front and rear arms, they both serve as extension and support structures for the upper arm (i.e. boom). Rear arm has two fixed balance weights attached to its lower end sides, which help to balance the center of the mass of the crane when the upper arm is extended. On the other hand, front arm - besides supporting the upper arm structure, also supports the cab bridge which is used for housing the operators cabin. The upper arm plays the part of handling the hoisted load. It is placed at the top of the crane and although it does not experience significant compression, is exposed to most strain, for which it is commonly reinforced.

Operation of this crane is performed manually, with the operator handling crane motions from cabin situated below the crane upper arm structure. This provides significant amount of sight to always have carried load directly in front of the operator. The load of the cabin is generally either supported directly by the boom as in figure 1.1, or by the front and rear arms, depending on model.

1.1.3. Motion profile and applications

Crane motion principles

Lemniscate crane motion and operational principle can be very closely compared to a 3 degree of freedom (DoF) robot manipulator arm. Fixed position lemniscate crane has single a rotation and two translation degrees of freedom available for handling cargo. This involves the following motions:

1. Slewing - Rotational motion around crane foot axis. It allows to change the direction of transshipment operations. This moves all the upper part of the crane above its foot. Motion is driven with electric motor and a planetary gear system located inside the crane foot.

2. Luffing - motion extending and subtracting crane boom position away from its foot. This motion operates on a lever principle, where hydraulic cylinder system assigned to the bottom of the rear arm moves the front arm and the boom of the crane, allowing the operator to reach objects further away from the rotational center.

3. Hoisting - (ideally) motion which changes operational height of the grab and allows the grab to adapt

to differing changes in operational height. Cables travel from the grab throughout the whole length of the upper arm and rear arm and is generally actuated with electric motor system placed in the crane machine floor.

A combination of all three motions allow the lemniscate crane to cover a large area of active operation. Due to this wide operational profile, lemniscate cranes are very handy when material loading and unloading position are not directly in front of each other. Figure 1.2 illustrates motion profile of the crane for combined hoisting and luffing operations.

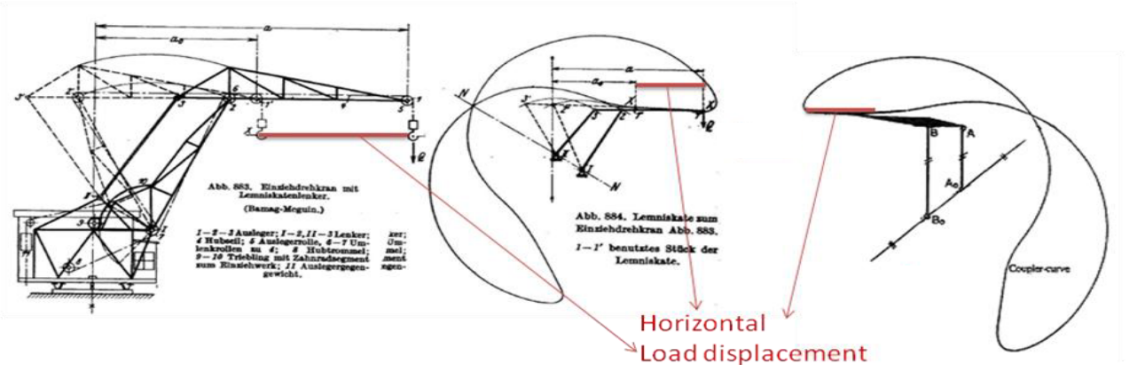

Figure 1.2: Generalised luffing motion profile of a lemniscate crane [86]

Applications
Lemniscate cranes are most commonly used to handle bulk material. Unlike Ship to Shore (STS) cranes, lemniscate cranes provide more versatility due to a different operational profile which allows them to perform loading operations with more freedom of movement. However, this apparent freedom also tends to create more variable swing which has to be controlled by the operator to keep loading direction unchanged. Since these cranes are used for handling bulk material, they tend to be loaded near their maximum loading limit on the majority of work cycles. This is an important distinction, as it means that bulk cranes need to handle heavy cyclic loads throughout their lifetime and require significant reinforcement in their arm structures to contain possible accumulation of fatigue damage. This has consequences towards their size and mass, as well as possible stability.

1.1.4. Research target
The analysed crane is Cronellis Tromp 25T. This is a floating lemniscate crane operated by Maja Stuwadoors Groep B.V. [1] which is mainly stationed to perform bulk handling operations in the Port of Amsterdam. According to Wierenga [90], Cornelis Tromp 25T is mainly used for performing scrap metal loading/unloading operations. However, due to the present availability of different grab types on the floating vessel, it appears that it is also occasionally used for handling granular bulk, such as coal and iron ore. Tawjoeram [86] provides a more extensive overview of the lemniscate crane working principles and main parts of the Cornelis Tromp 25T lemniscate crane.

Figure 1.3 illustrates structural member overview for analysed crane upper arm structure. Upper arm is a construction which in most cases fails first as it is exposed to highest cyclic hoisting loads and is generally prone to more strain imposed onto its structure. Additionally, Cornelis Tromp 25T boom structure is setup in a fairly unique manner, where forestay and backstay beams are load carrying beams responsible for carrying majority of the load. For this purpose, it is estimated to potentially experience highest stress fluctuation at their welded connection, which is worthy of fatigue life estimation.

1.2. Motivation
In the past, flawed design of analyzed lemniscate crane variant has ended in structural failure of the boom and death of the operator. The main reason for crane failure is assumed to be the initiation of crack at the welded connection between forestay and backstay as shown in figure 1.4. An inspection of identical model

[1] https://majastuwadoors.nl/en/

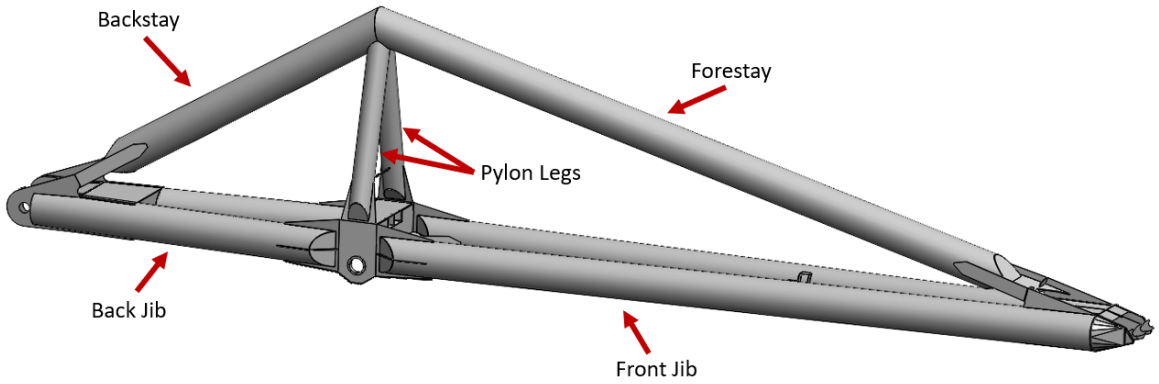

Figure 1.3: Upper arm structural member naming convention overview of Cornelis Tromp 25T crane

variant crane Cornelis Tromp 25T has revealed that it has experienced comparable damage accumulation at the same location, which could lead to structural failure in near future if left unattended. This similarity shows that there is a pattern in cranes of this design and since multiple cranes of this type are still in operation in the Netherlands and around the world - it is worth investigating what is the main contributing factor towards this damage - whether its a specific unattended loading setup, poor design for cyclic loading or something else that is difficult to initially assume.

The current guess is the crack initiation is a result of poor joint design setup, that does not accurately account for directional loading of the lemnicate crane, however that is yet to be proven. It is unclear how fatigue life of analysed lemniscate upper arm structure has been initially evaluated in the design stage, however, the observed magnitude of damage on Cornelis Tromp crane and failure of another crane of the same model clearly indicates that mistakes have been made along the way. Considering the fact that multiple cranes of the same model are currently still in active operation, this possesses a risk of more catastrophic failures occurring in the future.

Figure 1.4: Fatigue crack propagation location on Cornelis Tromp 25T Crane [86]

Additionally cranes which perform rotational motion operations (e.g. slewing motion in lemniscate cranes) are much more prone to continuously changing multi-directional loading than gantry cranes, which move cargo through linear motions. This means that slewing cranes have more complex loading profiles, thus potentially requiring a more intricate approach to assessing fatigue damage. One possible approach to achieve this increase of accuracy is to include the time domain into load , through multi-body dynamic analysis and assess damage using fatigue assessment method which takes into account stress direction - this could provide more insight into how the structure is loaded in real time and how it accumulates fatigue damage.

There has been an attempt made previously by Tawjoeram [86] to validate the crane fatigue damage with a multi-body dynamic model of the Cornelis Tromp 25T lemniscate crane. The author has created a dynamic simulation model and estimated fatigue damage through a Nominal stress method. However the scope of aforementioned MBD model analysis and fatigue assessment methodology did not provide enough confidence within its results. This includes lack of proof for accuracy of MBD model load response, and chosen approach for estimating fatigue damage. Additionally, several questions in the MBD model setup have been

left unanswered, such as which loading conditions tend to be most critical for inducing loads on the crane boom, as well as the determination what effect does part flexibility play in the overall context of load determination. Due to the aforementioned reasons, a conclusion has been made that it is important to determine whether a properly verified multi-body dynamic (MBD) analysis is beneficial for acquiring loads for finite element analysis. Furthermore, as the crane operation is estimated to impose loading and stress in continuously varying directions throughout its operational cycle, thus fatigue evaluation also includes multi-axial fatigue damage estimation and a comparative study with a uni-axial fatigue calculation approach. Finally it is worth investigating how fatigue damage could be reduced within the upper arm, either through changes in joint design or its motion setup adjustments.

1.3. Report goals

The main objective of the research presented in this thesis is to determine why has the crane experienced critical failure and how could that be avoided. This is answered through a following research question:

What is the main reason for fatigue damage accumulation in the upper arm tubular joint and how can structural failure of the crane be counteracted?

The aforementioned main research question is addressed through answering the following research sub-questions in the upcoming chapters:

1. What is the current state of fatigue analysis methodology for structural joints?
2. How can multi-body dynamic simulation approach help with establishing representative loading conditions of a crane work cycle within the time domain?
   (a) Which factors in the MBD crane model setup most significantly affect load responses relevant for acquiring boom stress cycle?
   (b) How to verify that the accuracy of acquired load results is representative of realistic loading conditions?
3. How does incorporation of stress concentrations into fatigue assessment affect resultant fatigue life estimation in relation to nominal stress fatigue analysis?
4. Is incorporation of stress direction into fatigue assessment beneficial for evaluating fatigue damage at the welds of problematic joint? How its results compare to more conventional hot-spot fatigue assessment approach?
5. What is the best potential method to increase fatigue life of crane upper arm?
6. How can problematic joint structure be redesigned to reduce the rate of fatigue damage accumulation?
7. How can fatigue damage of the structure be reduced without changes to crane design? Can this be done without reducing efficiency of crane operation?

These sub-questions are answered first through a literature review of present examples on current state of the art of fatigue analysis methodology for welded structural joints. Second step involves evaluation of multi-body dynamic model of the crane and its accuracy. This is done using statistical screening methodology for assessing critical model parameter impact on the load responses that are relevant for stress accumulation in the tubular joint structure of the crane upper arm. Third step deals with fatigue life assessment of the joint using stress responses acquired from finite element analysis. It evaluates effects of including stress concentration effects into fatigue assessment using a hot-spot stress approach, against the nominal stress fatigue assessment which averages stress result over beam cross-section. Fourth step evaluates how accounting for stress direction affect fatigue assessment results. It compares multi-axial fatigue assessment against previously performed hot-spot fatigue approach results - this determines whether it is beneficial to add multi-axial fatigue assessment methodology for damage estimation of welded joint structures. Final steps deal with determining ways for increasing fatigue life of the crane upper arm. This includes structural design adjustment of the problematic joint, as well as crane motion profile adjustments which would reduce stress accumulation in critical hot spot/-s that are prone to fatigue failure without increasing work cycle time.

Process of how research is performed is summarized in figure 1.5. It presents main steps in the process of acquiring project goals and the bigger picture how each step is linked in the overall structure of the project.

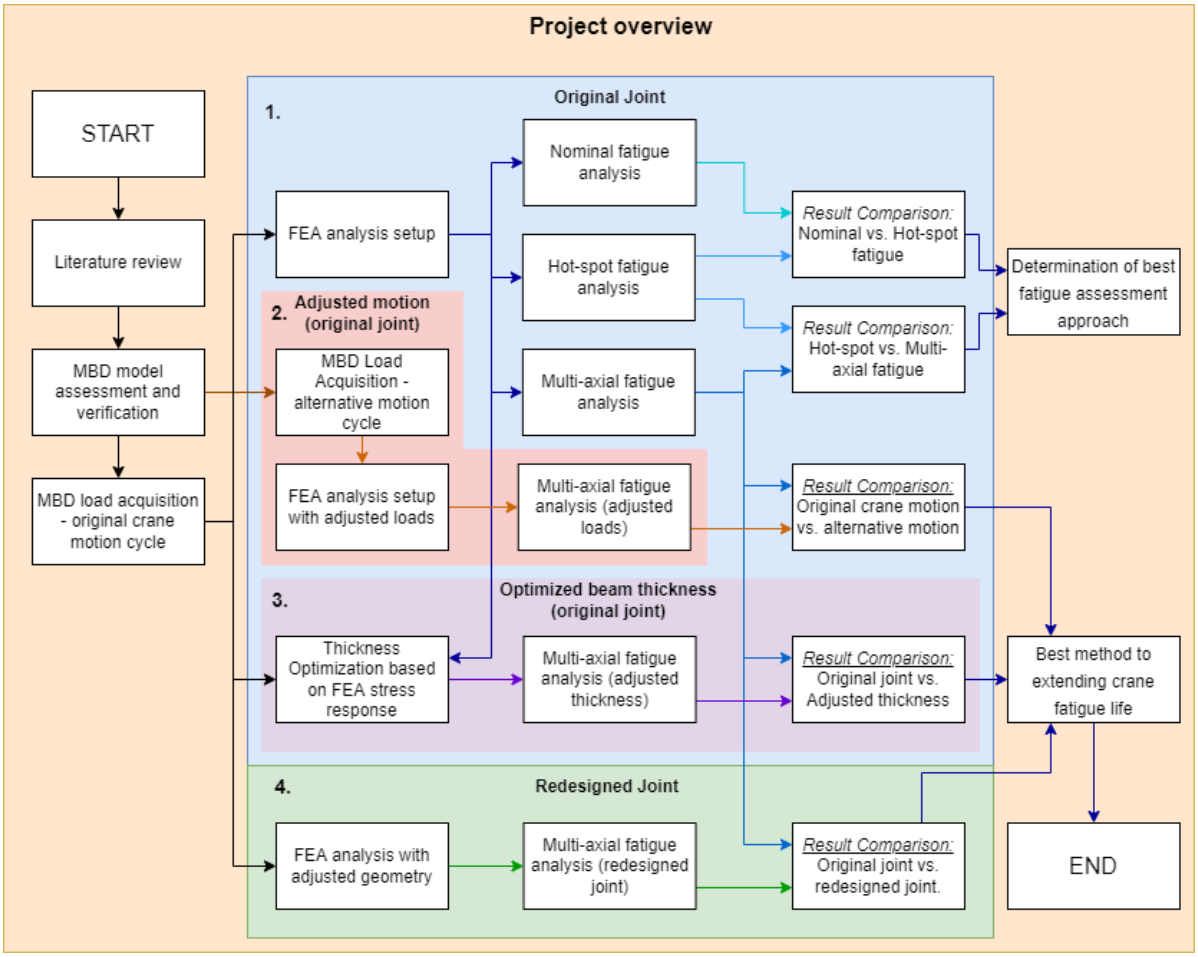

Figure 1.5: Overview of the main research steps towards acquiring project goals.

1.4. Main contributions

Contributions of the research within this paper can be separated into two main groups:

1. Contributions which are applicable to the specific case or analysis performed within this report.
2. Contributions of approaches or results which could be applicable to a general case in broader range of related research.

Separation is meant to provide an idea whether results could be applicable mainly for the specific evaluated structure or can they provide results which could be extended further to other applications and different analysis cases.

1.4.1. Contributions towards specific analysis

Multi-body dynamic model of the crane initially created as described in Tawjoeram [86] is evaluated and adjusted in a manner which is meant to improve the accuracy of acquired loads relevant for fatigue analysis of upper arm. This is done by:

1. Fixing errors in the MBD model setup through quantification of parameters important for load establishment to determine the magnitude of their significance towards relevant load responses.
2. Testing incorporation of flexibility into rigid components.
3. Adjusting and verifying significant parameter values to improve result accuracy.

Strategies are proposed to potentially prolong fatigue life of the crane upper arm. This task is approached from two different points of view:

1. Design adjustments to upper arm joint structure - where design changes and/or reinforcements are made to the current model of the upper arm. These changes are meant to increase the structural capacity of the joint or redistribute stress thus increasing its fatigue life;

2. Adjustment of analysed motion profile - which assesses whether its possible to reduce loads imposed on the crane through change in crane motion without increasing work cycle time of crane operation;

1.4.2. General contributions

1. Approach for acquiring time-dependent loads, using multi-body dynamic simulations can be used for a large array of different mechanisms which experience a certain type of displacement during their operation. If there is a sufficient amount of data for model verification, this can be a method for potentially acquiring accurate load responses, which could be used for stress and/or fatigue analysis, or for the purpose of evaluating various motion setups of the mechanism.

2. Comparison of fatigue assessment methodologies between nominal stress and hot-spot stress approaches present how inclusion of stress concentration effects affect fatigue assessment results for complex welded joint structures.

3. This report includes an assessment on how incorporation of stress direction within fatigue analysis affect fatigue life results for welded joint connections. Comparison of multi-axial fatigue assessment method of DNVGL-RP-C203 [20] and conventional hot-spot stress fatigue assessment (which uses Von Mises stress) is used to indicate the difference in results.

4. Thickness optimization approach for reducing rate of fatigue damage accumulation using Design of experiments Screening analysis approach can be potentially applied to any joint structure modelled in finite element analysis environment using shell elements. This method is however best applicable using methods which are not sensitive to stress direction (e.g. using conventional hot-spot stress rather than multi-axial fatigue assessment methods).

1.5. Assumptions and research scope limitations

Due to the lack of data or for the sake of limiting analysis complexity to a manageable degree - some research scope limitations are present. Because any presence of assumptions can affect the accuracy of results, they have to be understood and clearly defined. Main assumptions and scope limits within the research presented in this report can be summarized as follows:

1. Multi-body dynamic model used for load establishment considers only a single work cycle, which is meant to represent a general main loading case of the crane. Occasional loads appearing from construction, assembly, transportation, passive wave and wind loads are not considered.

2. Multi-body dynamic model pontoon setup has not been reevaluated in terms of its optimal or fully accurate setup, but rather has been calibrated to match real motion of a specific work cycle. Further work is needed for the pontoon to accurately define its displacement during crane operation.

3. It is assumed that unaccounted motion of the crane in surge, sway and yaw directions do not contribute significantly to overall loads experienced within the crane structure. This is due to the fact that there is a very limited presence of motion in these particular directions. They are not modelled within multi-body dynamic simulation environment.

4. Since crane is sometimes used to handle scrap metal, there is a potential for metal parts during hoisting to bind and lock-up, which could require additional force to release them from the pile. This could potentially increase experienced loads and stress magnitude during initial load pull. This however is not explicitly modelled due to lack of data on particular load magnitude increase and frequency of occurrence.

5. Hot-spot stress fatigue assessment has been performed using Von Mises stress. Although there are conflicting statements in the literature about the proper stress type for calculating hot-spot stress - additional stress variants have not been investigated but are expected to have a significant effect of hot-spot stress fatigue results.

6. Verification of Multi-body dynamic simulation model is limited by available data to only evaluating pontoon roll and pitch motions.

7. Validation to assess the most suitable fatigue assessment approach is not performed due to lack of empirical data.

8. Performed assessment on how inclusion of stress direction affect fatigue damage accumulation rate is limited to proportional stress response. It is possible that presence of non-proportional stress within joint weld stress response could affect accuracy of provided conclusions.

9. Performed multi-axial fatigue analysis is meant for evaluating fatigue damage within welded joint structures. For different type of geometry, it is possible that performed method might not be applicable.

10. Joint redesign which is meant to increase fatigue life of the upper arm structure is limited to providing a reasonable improvement over the original joint structure mainly in terms of fatigue damage reduction, rather than finding the most optimal structural design.

11. Motion profile adjustment which is meant to increase fatigue life is limited to evaluating the feasibility of the approach. An implementation of a more advanced approach to acquire best possible motion setup (either through optimisation or controller implementation) is left for future research.

1.6. Organization

The rest of the thesis is formulated in a following manner: Chapter 2 discusses the present literature on fatigue assessment for structural joints and incorporation of MBD analysis for load acquisition. Chapter 3 deals with the process of evaluation for the state of the MBD model created by Tawjoeram [86], effects acquired from incorporating flexibility into specific model parts, quantification of most critical parameters of the MBD model for result accuracy and result evaluation. Chapter 4 deals with setting up finite element analysis for stress acquisition and investigates how incorporation of stress concentrations into fatigue assessment influences fatigue damage accumulation results - this is done through a comparative study of nominal and hot-spot stress fatigue assessment results. In chapter 5 multi-axial fatigue assessment is performed to analyse how accounting for stress direction influences fatigue damage in comparison to a conventional hot-spot stress fatigue assessment. Chapter 6 discusses possible ways to increase fatigue life of the analysed lemniscate crane, which could be achieved by changing design of crane upper arm joint. Additionally it evaluates whether the magnitude of fatigue damage accumulation could be potentially reduced without design changes. Chapter 7 provides concluding remarks and summarizes the main findings in the report and provides recommendations for future research.

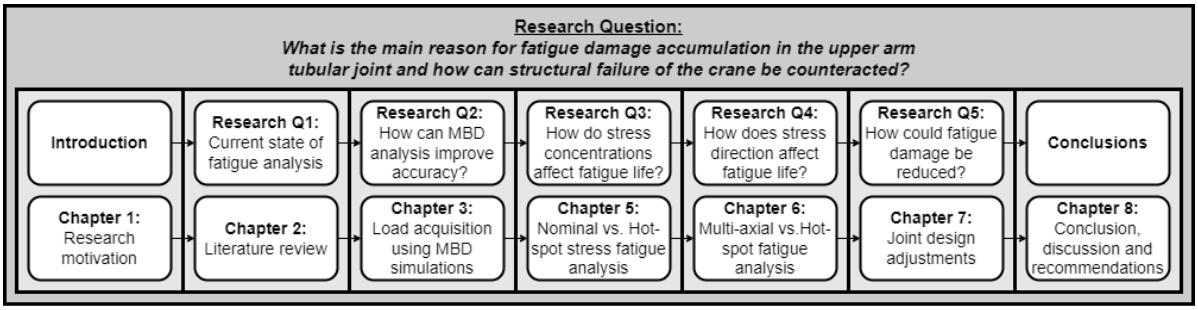

Figure 1.6: Thesis structure overview

2

Structural joint fatigue assessment methods

The initial step of establishing and performing fatigue analysis in a manner which is applicable for joint structures and which provides sufficient amount of accuracy - first requires understanding of principles on how it is done in the scientific literature. There are multiple aspects of fatigue relevant to the topic of this report, such as the possible approaches for assessing fatigue, the principle of choosing right methodology, as well as ways for improving the accuracy of the final result. This chapter is meant to discuss the state of the art of fatigue assessment for joint structures that can be found in scientific literature. The main goal of this chapter is to answer the research question:

What is the current state of the art of fatigue analysis methodology for structural joints?

The answer is found through a review on conventional and more complex fatigue assessment methods found in the literature. It discusses methods how fatigue life of a structure is commonly estimated for structural joints, provides an overview the main standards used and what are the ways to improve result accuracy of fatigue assessment - specifically through incorporation of various multi-axial fatigue approaches.

2.1. Background on fatigue analysis in welded structures

This section provides some background for fatigue analysis, that is important for analysing welded structural joints.

There are many aspects which have to be taken into account when performing fatigue analysis. When it comes to structural joints, it is important to understand how such aspects as geometry, material, weld quality and loading setup affect fatigue life. Because each combination of these factors is unique - this shows that the concept of fatigue analysis is based on damage estimation rather than its precise definition. Here the main aspects which influence fatigue assessment are briefly introduced.

2.1.1. Geometry

Fatigue resistance is highly dependent on the geometry of the part that is being loaded. Since structural beams come in various shapes, setups and thickness, they have different applications relating to different loading types and support directions. In a similar fashion, strengths and weaknesses can be distinguished within different joint sections. As the subject of this report concerns fatigue assessment of crane upper arm structure which is constructed out of welded beams, the focus of literature study mainly concerns fatigue assessment of structural joints.

By definition - structural joint is a connection between two or more beams of identical or differing cross-section profiles [76]. These types of joints are widely applied in the design of mechanical structures which experience heavy loads such as high rise buildings, offshore installations and crane structures. As the setup of analysed crane is created mainly out of beam of tubular cross-sections, it is worth to understand their specific benefits. The popularity of their application comes from inherent properties of tubular joints to posses high torsional rigidity as well as higher strength to weight ratio compared to the conventional steel sections [76]. Figure 2.1 illustrates most commonly used connection variants of uni-planar tubular joint setups.

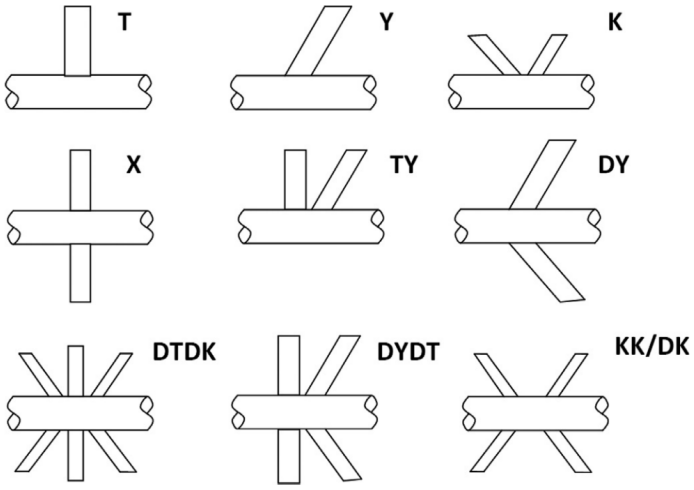

Figure 2.1: Tubular joint types with their nomenclature [76]

However these are not all potential combinations of structural joints - depending on application type, some joints can be setup in a 3-dimensional plane, creating multi-planar joint setups. These include KK, TT XX joint variants, among others. The specific analysed lemniscate crane boom joint, which has been observed as being prone to failure - is a multi-planar joint. It connects forestay and backstay beams of the crane upper arm with the pylon legs. All aforementioned parts are constructed with circular hollow section (CHS) steel tubes that do not conform to any of the popular tubular joint connection setups described here or visualised in figure 2.1. Throughout its lifetime, crane boom experiences the cycling weight load effects appearing from transportation of bulk material, as well as the reactionary inertial loads appearing due to crane operation and pontoon motions. All of these loads impose a certain amount of stress which affects the crane boom structure. Each stress cycle contributes towards the accumulation of fatigue damage which limits operational lifetime of the structure. In a general case if the timeline and scope of analysis allows - to ensure that the structure will fulfil its intended function, a fatigue assessment (supported where appropriate by a detailed fatigue analysis) should be carried out for each individual member, which is subjected to fatigue loading [6]. Thus in order to properly assess fatigue damage it is critical to understand the setup of analysed structural joint as it establishes measurement positions and loading conditions at each measurement point.

2.1.2. Material

Material is an important factor when it comes to fatigue evaluation. Material properties define its mechanical characteristics and determine how structure performs under loading conditions, including cyclic loads. Brittle and ductile materials fail differently, with different stress components having unequal contributions towards failure. Shear stress or strain usually initiates cracks in ductile behaving materials, where tensile stress or strain typically causes crack initiation for brittle behaving materials [79] and this have to be taken into account when evaluating fatigue.

Additionally, understanding when material experiences plastic deformation is an important aspect of fatigue assessment as it helps estimating damage magnitude that is defined for a specific experienced stress range and what kind of fatigue assessment should be performed. In a general case, fatigue analysis is performed when material is within the elastic deformation region over its loading cycle, without acquiring enough stress to impose plastic deformation on a macro level. This means that materials used are commonly capable of experiencing wide stress ranges and allow for prediction of fatigue damage based on present experimental data.

For industrial applications, steel is the most common material type used for manufacturing structural joints. Other common materials such as cast iron can also be used in some cases, however due to poor roughness qualities and potential internal flaws within its structure which could create stress concentrations and cracking under cyclic loads - is rarely used. This report mainly deals with fatigue analysis of structural steel, which is in principle a ductile material commonly used within welded structural components.

2.1.3. Loading conditions

For fatigue assessment - establishing accurate stress response is critical for ensuring accuracy of the analysis. This cannot be achieved without precise definition of loading conditions, which include acquisition of the magnitude, direction and frequency of the cyclic loads acting on analysed geometry. When stress acquisition is performed with the help of Finite element analysis, loading conditions have to be acquired and applied manually to properly represent their setup on a real body. For fatigue assessment, loads are generally not large enough to fail a structure within several loading cycles and generally deals with stress ranges that inflict damage over a large time period. This mainly includes cyclic operational loads (e.g. hoisting load acting on a crane structure when cargo is being loaded/unloaded), but can also include occasional loads which occur due to such factors as installation and transportation of the equipment, as well as potential overload which can occur unexpectedly and inflict significant amount of damage. However, in a general case, operational loads accumulate the largest amount of fatigue damage to the structure [57]. Normally there are two types of ways to model loads:

1. Static loading setup - where it is assumed that all loading can be formulated using a single time step of load increase and decrease. This is a method which makes loading setup very simple to establish, however in general it excludes effects of additional residual load fluctuation effects which can occur in a real scenario. Due to its simplicity - this is the most common way to establish loads acting on analysed structures then finite element analysis is used for fatigue damage estimation.

2. Dynamic loading setup - loads established with multiple time steps, which can potentially include residual loading fluctuations and provide a more accurate definition of a real setup. They are measured over time and in each overal loading cycle they can contain multiple smaller loading effects which vary over the cycle duration. It is a method which is more computationally intensive and more difficult to verify, but in turn presents more realistic loading cases, specific to evaluated operation of analysed structure.

Along with their parametric differences, each of these methods require a different way to create its setup. Static load establishment procedure for structures such as cranes can be defined with the help of specific standards such as [66] and [67], which provide steps and formulas needed to acquire values of important loads through hand calculations, as well as safety factors which are meant to account for residual load effects that are not present in the static load setup. When it comes to dynamic loads, the most reliable way to model them is through physical measurements. This can include various parameters, from measurements of body as well as inertia loads. Multiple sources in the literature base their loading conditions on some variant of measurements taken from analysed structures [83, 86, 90]. Under a reliable load acquisition technique which uses accurate sensor measurements, this method tends to provide more reliable loading data than simulations. However this is a very time and effort consuming task which requires direct access to an active structure for measurement acquisition.

In cases when dynamic load data cannot be directly acquired, Multi-body dynamic (MBD) simulations can prove as a feasible alternative for both aforementioned methods. MBD analysis allows users to acquire forces acting on a dynamically loaded body through a process of simulation procedure. Its setup generally relies on the same measurements used for standard-based calculation methods. However unlike conventional load acquisition approaches which operate in the frequency domain, MBD analysis operates in time domain. It simulates dynamic behaviour and loading conditions of a real system while taking into account load magnitude and direction at pre-specified time steps, thus acquiring a much more realistic loading profile. This is especially convenient when assessing load changes which are assumed to significally affect the body and have a tendency to fluctuate throughout each loading cycle (generally from dynamic motion effects) [47, 50, 51].

Multi-body dynamics and fatigue

Traditional finite element (FE) methods used to analyze structure dynamics are linear and operate in the frequency domain. They can address only one type of loading problem at a time and cannot account for coupled motions or non-periodic responses [24]. This is a simplification of most loading conditions affecting specific body, yet it tends to be sufficient in most cases. However there is a possibility to increase the accuracy of evaluation by assessing loads with the inclusion of time domain in the analysis.

When it comes to incorporation of multi-body dynamic analysis for fatigue damage and life estimations - impact or rolling contact fatigue (RCF) and rotary systems tend to be the most common application for the aforementioned approach. RCF analysis is a popular application for acquiring loads using MBD simulations

[22, 23, 42, 47, 50]. In the case of rolling contact, analyses of train axle fatigue, which are exposed to cyclic loading through wheel rotation are widely discussed. Karttunen et al. [42] investigates dynamic impact loads appearing from uneven wear of train axles. Modaresahmadi et al. [63] involves a co-simulation of MBD and FE analyses to estimate fatigue life of magnetic gearbox components. Other variants of contact fatigue are also investigated, especially in the area of aforementioned rotary systems. Bilodeau et al. [14] employs use of MBD to analyse relationship between contact fatigue damage appearing on surfaces and stiffness of car suspensions moving over the surface. Alemayehu and Ekwaro-Osire [4] moves fatigue analysis away from contact location and uses MBD software Adams to determine contact loads affecting a gear coupling teeth, which are used to acquire fatigue life of the gears when crack initiates at the root of gear teeth. Kuka et al. [47] expands the scope away from RCF and studies fatigue damage on the train rail axle-box links that are a loaded indirectly through part interaction. When it comes to fatigue damage in joint connections, it generally accumulates not through direct contact at the fracture position/-s. In these situations, stress concentrations appear due to bending, torsion or extension/compression loading. As it has been observed, although present to a limited degree [86, 90], there are not many cases in the literature which employ use of multi-body dynamics for establishing crane loads or loads affecting structural joints. This is due to the fact that in most applications structural joints are not loaded dynamically in a complex loading setup, unless it involves wave motions, which can be more efficiently modelled using such approaches as spectral analysis. However it is possible to do so and in some can prove beneficial, as in the case of mechanisms and constructions which experience acceleration and large motion effects, such as lemniscate cranes.

Multi-body dynamic simulation software
There is a number of possible software and simulation algorithm choices available which are able to perform multi-body dynamic simulations. In the past, this has mainly included locally-produced algorithms, such as *DIFF3D* [22], however, in the past 2 decades, commercial software has become the dominant option for MBD applications. Nowadays there are a large number of algorithms and software available, which can be chosen based on the analysis requirements. Modaresahmadi et al. [63] uses *JMAG* software to acquire loads for magnetic components in a gearbox system. Karttunen et al. [42] uses *GENSYS* for gear contact load estimation on flexible bodies. Bilodeau et al. [14] estimates loads of a moving truck suspension system due to uneven roads using *MBDyn*. *SIMPACK* appears to be a popular choice of MBD software used by researchers in contact load acquisition [47, 91]. However, by far it seems that *Adams* multi body dynamic software is most commonly used in the reviewed research literature [4, 36, 86, 90]. The popularity of this software package is assumed to be a result of its versatility and feature setup, as it includes dynamic simulations for not only load acquisition but also for acquiring stress and strain data, fatigue life estimation, selective parameter optimization, motion control implementation, among other uses. Lu [58] provides a comprehensive overview of multi-body dynamic simulation software packages, along with the algorithms on which their operation is based. This provides significant amount of options for choosing optimal MBD software for specific required application.

2.1.4. Uncertainty of weld fatigue assessment

Since structural joints are commonly constructed through welding operations, it is important to understand what kind of role welds play within fatigue life. It has been known that in the case of welded structural joints, fatigue damage accumulation is largest at the connection points, specifically at the weld toe [20]. Figure 2.2 illustrates the position of the weld toe within a fillet weld cross-section. Most structural joint fatigue assessments focus on analysing fatigue damage specifically at these positions, making them critically important.

However, accurately predicting fatigue crack initiation in welded structures is a difficult task without real world data. This is due to the fact that there is a large number of factors which can reduce potential fatigue resistance of a welded structure. According to Lotsberg [57], this can include:

1. Planar defects
    (a) Lack of penetration in a weld - where weld does not reach the full thickness of welded component connection (both for single-sided or double-sided welds), leading to stress concentration at the weld root.
    (b) Lack of fusion - this can include the lack of fusion between weld and material, in the area of weld root, or between weld beads themselves. This is generally a result of poor choice of weld procedure or too little heat input.
2. Three dimensional defects

(a) Weld undercut - when weld does not fill entire weld sink, leading to stress concentration present near the weld toe.

(b) Wormhole - large cylindrical cavity on the inside of the weld.

(c) Inclusions - such as irregular or clustered slag that could weaken a specific position of the weld.

All of these factors can cause internal stresses within the weld and can become a cause for premature crack initiation. The appearance of internal stress is often due to high difference in temperature along the thickness of welded beams. Thermal cracks are formed when the surface material is welded, which imposes restrained thermal expansion during heating. Subsequent cooling will then induce tensile residual stresses that may promote crack propagation under a certain amount of strain imposed through external loading [23]. Additionally, lack of smoothness on the weld surface can also be a probable cause for crack initiation - sharp edges and holes tend to concentrate stress when structure is deformed, leading to a much lower yield limit. The quality of a weld determines its resistance to cyclic loading and determines its class [2]. However, this also means that there are ways to reduce residual stress in the weld, post-processing techniques such as post weld treatment or polishing, which relieve weld stress and improve its class for analysis - thus reducing fatigue damage accumulation.

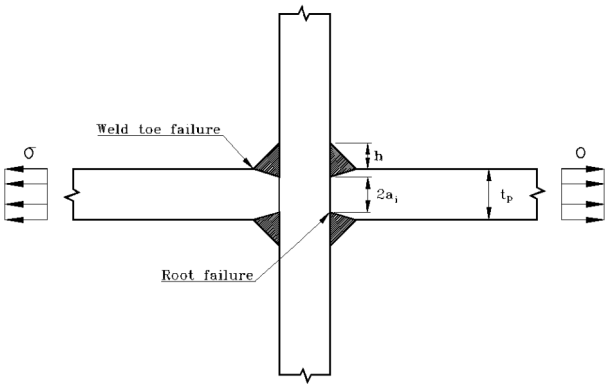

Figure 2.2: Cross-section of a structural joint welded using partial penetration welds, indicating locations of weld root and toe [20].

Additional defects that are applicable for both planar and three-dimensional cases include small effective throat thickness or cracking appearing during weld solidification as a result of large residual stresses. Possibility of all these factors to affect analysed structure leads to a large amount of uncertainty present in the analysis. However since the principle of fatigue assessment is based on damage approximation, it has to be taken into account that it cannot account for all uncertainties with high precision, thus in the actual formulation of analysis tools (e.g. within definitions of stress-life curves) a certain safety factor is commonly added upon acquired experimental results to reduce uncertainty effects.

2.1.5. Low vs. high cycle fatigue

From the standpoint of expected number of stress cycles that the structure is meant to survive, a distinction has to be made between two types of fatigue assessment - it can be separated into low cycle fatigue and high cycle fatigue:

1. Low cycle fatigue - which deals with structural loading that induces stress surpassing material yield limit. Presence of plastic deformation each cycle affects the rate of fatigue failure and limits the maximum amount of operational cycles to a lower value. Although it is debated between different literature sources, the general transition between low and high cycle fatigue lies at the range between 10^4 and 10^5 operational cycles [57].

2. High cycle fatigue - which deals with mainly elastic deformation induced on cyclically loaded structures. The lack of plastic deformation within high cycle fatigue calculations means that it generally deals with a significantly larger number of cycles than high cycle fatigue. This is where most offshore and crane structural evaluations are focused.

Fatigue cracks under low cycle fatigue usually nucleate from localized notch regions [56], while in the case of high cycle fatigue it generally appears at the weld toe locations. Deformation within the material elastic region is the main focus of this report, thus further assessment of potential fatigue analysis approaches for tubular joints and problematic lemniscate crane is focused on high cycle fatigue and mainly focus on the fatigue damage at the weld toe locations.

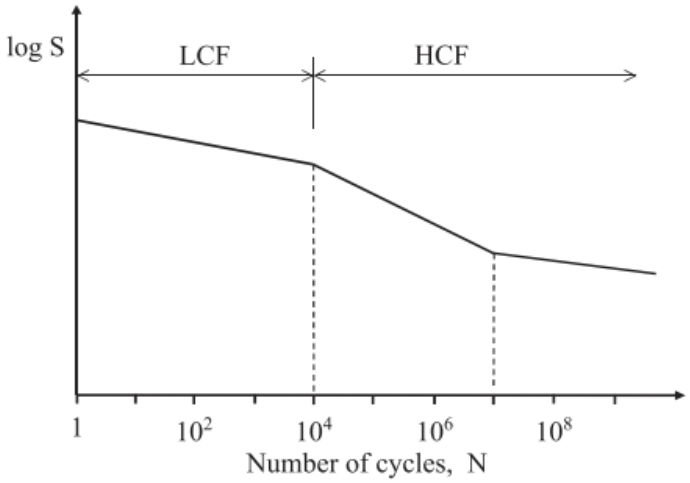

Figure 2.3: S-N diagram indicating low cycle fatigue (LCF) and high cycle fatigue (HCF) regions [57].

Figure 2.3 illustrates the rate of failure in relation to stress induced within the limits of low and high cycle fatigue. As it is seen from the figure, stress within the limits of LCF is higher and generally contains a certain presence of plastic deformation in each cycle, which factors into the rate of failure for the structure. When LCF limit is reached, it is commonly agreed that the relation between rate of fatigue failure and stress range changes, thus requiring a separation between two types of fatigue. In general, for this purpose the types of fatigue assessment approaches also differ depending whether the structure is dealing with predominantly plastic or elastic deformation.

2.1.6. Analysis domains

Values for evaluating fatigue damage accumulation can be done either within static or time domains:

1. Static domain - presents a fatigue assessment variant where stress/strain responses needed for performing fatigue analysis are limited to a single loading step, indicating presence of one loading cycle per operation. These methods have a benefit of simplicity and often rely on addition of coefficients to account for smaller effects which could be dependent on the specific application case.

2. Time domain - approach which includes stress/strain response that is sampled at a certain rate to define its time history. These methods provide the benefit of accuracy as they can include effects of not only the most damaging stress/strain cycle, but also effects of smaller cycle ranges within the time history. Time history is commonly acquired either through direct measurements or by incorporating advanced modelling approaches into load acquisition such as inclusion of power spectral density functions into spectral analysis of wave motion [88] or by simulating operation of the analysed equipment (e.g. crane) using such tools as multi-body dynamic simulations [51].

Both methods are used in fatigue assessment, with only static method having limitations towards application for some fatigue assessment approaches, such as multi-axial fatigue. Time-domain approach however is applicable with all general fatigue assessment approaches, but such fatigue assessments often lack data which is required for evaluating stress/strain time histories and require application of cycle counting approaches which can make the fatigue assessment significantly more complex. Additional information on cycle counting approaches can be found in section 2.3.2.

2.2. Fatigue assessment methodology

This section introduces most common fatigue assessment methods and standards used for analysing operational life of cyclically loaded structural joints

Due to lack empirical data to establish clear relations between various parameters of the structure and its operational life - fatigue analysis is a science field which is heavily based on principles of estimation. There is not a single assessment approach which is capable of ensuring accuracy of results applicable for all structural joints. Depending on such factors as application background and needed accuracy or speed of analysis - different fatigue approaches can be taken. Here the most common fatigue assessment approaches and standards for estimating life of structural joints are presented.

2.2.1. Conventional fatigue assessment

Within the principles of fatigue damage evaluation, most commonly used approaches can be summarised into 4 main variants - Nominal stress, Hot-spot stress, Notch stress and Fracture mechanics. Stress approaches are meant to calculate damage accumulation of an intact structure, before any crack initiation takes place. Each stress variant acquires stress values differently and due to expected different values of stress which account for the same amount of fatigue damage - they also use different S-N curves. Here the aforementioned most commonly used conventional approaches are introduced. On the other hand fracture mechanics method has a distinction from the group as it is mostly meant to assess structural fatigue life when crack initiation has already began and the crack definition is included in the analysis model. Additionally its application principles are different from the aforementioned stress models. Each approach is illustrated in figure 2.4 and briefly introduced within this section.

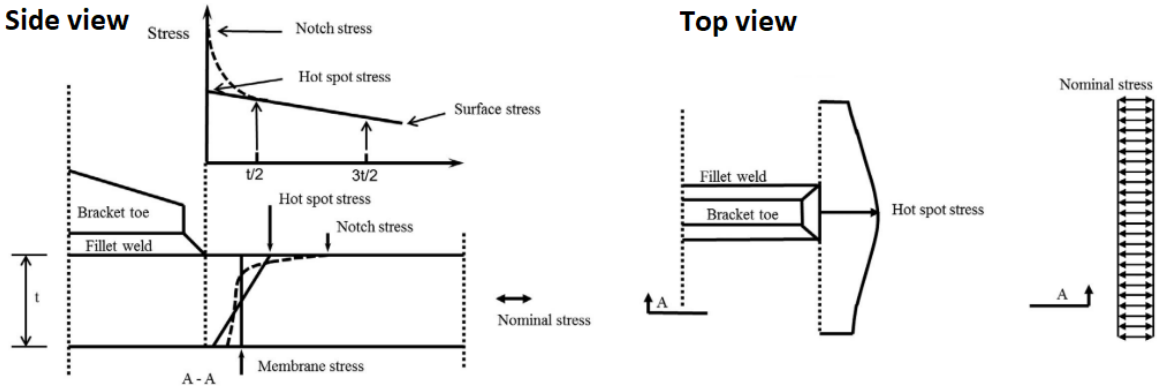

Figure 2.4: Comparison of stress definition between nominal, hot-spot and notch stress at fillet weld toe location [57].

Nominal stress

Nominal stress is the most basic method for evaluating fatigue as it includes the largest amount of estimation within its stress definition. In principle, for its application on welded joint structures - nominal stress is the average stress in the weld throat or in the plate at the weld toe [2]. This method establishes stress values using beam theory based on linear elastic behaviour, by evaluating the properties of analysed beam cross-section. To determine nominal stress values at specific points of the beam, this method averages out the stress in relation to distance between measured point location and center of mass of measured cross section - and this is also represented within the definition of specific S-N curves used for nominal stress fatigue life assessment. Figure 2.4 presents how nominal stress is averaged over entire cross-section in comparison to real stress distribution. Stress averaging part however is also the largest weakness of the approach, as averaged stress does not account for effects of stress concentrations which could be present within the model and which could significantly hasten fatigue failure.

Nominal stress is used in fatigue analysis when quick fatigue life calculations are needed or when analysed geometry is modeled within finite element analysis using simple beam elements, but it can also be used with shell or solid element models and does not require heavy mesh refinement to be performed. It is commonly applied to simple components for which properties such as cross-sectional moment of inertia can be easily derived based on beam thickness and shape. This method becomes more complex when it is applied

on complex geometry, such as overlapping joints. A nominal stress application case which uses detailed assessment presented and explained in further detail in section 4.3, while more theory on the methodology of nominal stress approach can be found in A.F. [2].

Hot-spot stress
In order to include stress concentration effects which are not present within the response of nominal stress - a hot-spot stress can be used. This is the most commonly used stress variant in general fatigue assessment that is performed with finite element analysis. Hot-spot stress includes the effects of stress concentrations in its formulation, without modelling the actual welding profile within the assessed geometry. Measurements for this method are not taken directly but are rather extrapolated to weld toe with multiple points for each measurement as shown in figure 2.4 to acquire stress values used for establishing stress ranges and evaluating fatigue damage.

Structural hot spot stress approach is typically used where there is no clearly defined nominal stress due to complex geometric effects, or where the structural discontinuity is not comparable to a classified structural detail [2]. It is capable for evaluating more complex stress properties of multi-axial stress, which could prove to contain multiple relevant stress components and/or non-proportional stress effects within the measurement location - this is not possible to measure using nominal stress. Additionally, if detailed geometry is being analysed for its ability to handle fatigue damage (e.g. through a finite element analysis established using shell or solid elements and representing detailed structure geometry) it is generally advised to use hot-spot stress fatigue analysis instead of performing nominal stress fatigue assessment [20]. A hot-spot stress application case with additional detail is presented in section 4.4 with a more in-depth explanation of hot-spot stress acquisition methodology found in Lotsberg [57] and A.F. [2].

Notch stress
Notch stress approach is the most detailed variant of conventional stress approaches for fatigue analysis. For this method, the geometry of the weld is included within finite element analysis and the effective notch stress is measured directly from the weld. According to Lotsberg [57], under right conditions of model definition, this is the most accurate fatigue assessment approach for estimating damage within structural joint connections. It however requires establishment of weld material properties and its detailed geometry at measurement locations. In addition to that, this method requires heavy computation resources as accurate notch stress response generally needs a very detailed 3-dimensional stress component definition. Weld size and any discontinuities should be also included into the model as they affect accuracy of assessment results.

As a comparative simplification of detailed notch stress fatigue analysis - is the effective notch stress, which replaces the actual weld contour with its effective counterpart. It uses notch radius which is standardised to a common value and proves as a relatively accurate approximation of the actual notch stress, being capable of accounting for both the variation of the weld shape and potential non-linear material behaviour. One large benefit of notch stress fatigue assessment is within its accuracy and that it uses only a single S-N curve for all weld measurements, regardless of joint setup, which is dependant only on the qualities of weld material A.F. [2]. It also allows measurements to be taken directly from the position of the points where fatigue is to be assessed (which is not possible with either nominal or hot-spot stress approaches) and can be treated as real stress at measurement position, having generally the highest stress value out of three methods as illustrated in figure 2.4. Just as the hot-spot stress - notch stress is also applicable for assessment of fatigue when there is multi-directionality present within the stress response. A more in depth explanation of a notch stress fatigue analysis is presented in van Lieshout [88] and Lotsberg [57].

Fracture mechanics
When fatigue life is being assessed for a structure which has already developed cracks - fracture mechanics approach is commonly applied. This is a fatigue assessment approach focused on understanding when a present crack within the geometry becomes critical by changing the structural integrity of the analysed construction from a stable to an unstable state. It uses the principles of stress intensity factor (SIF), which relates the stress and crack length parameters through application of a geometric factor, which is a function of size of the crack and which is specific for each analysed case. Properties of stress intensity factor for this fatigue assessment method is dependent on the type of loading and is generally more complex to determine for non-proportional loading cases. With this method, crack geometry is modelled in the simulated environment and requires present detailed definition of the crack that is present within the structure in order to analyse its qualities. A more in depth explanation and additional information on the principles and application of fracture mechanics-based fatigue assessment can be found in Freundenthal [28].

2.2.2. S-N curves

The large majority of fatigue assessment approaches within high cycle fatigue region rely on the use of Stress or strain life (S-N) curves to evaluate fatigue life of analysed constructions. In principle, S-N curves establish a relation between magnitude of fluctuation range for stress or strain and the number of loading cycles the construction is expected to survive before structural failure.

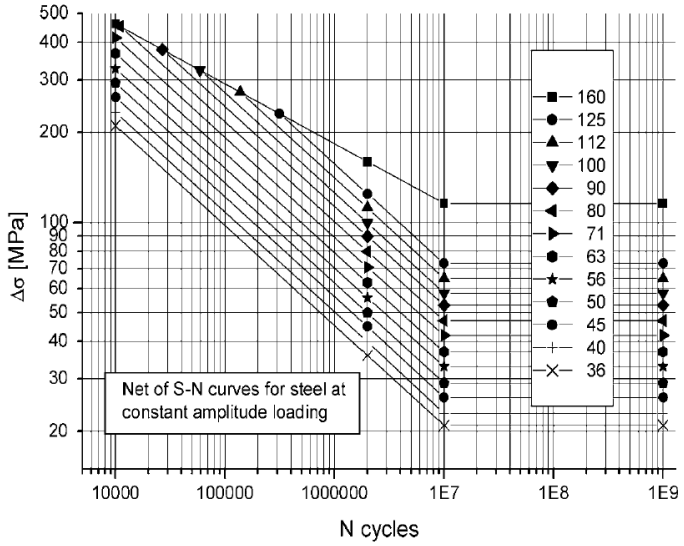

Figure 2.5: Example illustration of nominal stress S-N curves used for different class welded connections [2].

S-N curves are however not universal and they are generally established based on the type of material, stress type used for evaluation (nominal, hot-spot, notch) as well as the type of geometry/weld type that is being evaluated. According to these factors they are also separated into weld classes. Figure 2.5 illustrates a number of different class high cycle fatigue S-N curves used for evaluating welded steel structures using nominal stress response. It shows a stress-life relation for range between 10^4 and 10^9 cycles.

As seen in figure 2.5, after a certain number of cycles, the slope of damage accumulation changes - within shown nominal stress S-N curves this happens at 10^7 cycles and the slope becomes constant for all values above this limit. This shows a value of infinite life below specific stress limit. However this is not a quality of all S-N curves and some variants tend to introduce multiple changing slopes even for cycles above 10^7. In order to acquire value of stress ranges - stress-time histories have to be evaluated with the help of cycle counting algorithms. Figure 2.6 illustrates a common time history which includes multiple stress cycles which have to be extracted and counted. From this point forward - fatigue damage is calculated using S-N curve and a damage equation specific to fatigue assessment method for each cycle, and then summed up to determine the amount of damage which is accumulated over the length of time history [57]. This value is then multiplied by desired fatigue life for which damage accumulation is to be evaluated.

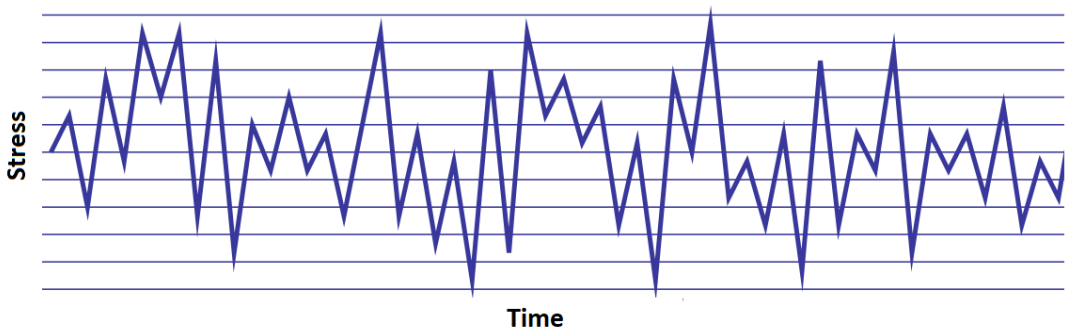

Figure 2.6: Example illustration of stress history used for counting cycles and extracting stress ranges for fatigue assessment using S-N curves [2].

It is worth noting that fatigue analysis in principle is a science based on estimations, thus established S-N curves also serve as only approximation of actual damage, which could differ in a realistic scenario due to a wide array of external influences. However it is the most popular approach to estimate fatigue damage, due to its simplicity and straightforward process of fatigue life assessment within high-cycle fatigue range, where performing experiments is difficult within reasonable time duration limit.

2.2.3. Fatigue assessment standards

It is worth noting that for structural joint fatigue, the assessment methodology is commonly standardised. It is generally established based on joint or its detail geometry, type of connecting welds, application and loading specifics. Here the most commonly used standards for fatigue assessment applicability on structural welded joints are introduced:

1. *EN 1993-1-9:2005, Design of steel structures – Part 1-9: Fatigue* [19] - also known as *Eurocode 3*, this is a fatigue assessment standard that is focused on the performance of nominal stress fatigue analysis on most common welded structural components. It uses distinctive 3-level S-N curves which are separated into shear and normal stress assessments. It separates fatigue assessment approaches into damage tolerant and safe-life methods. Although not the focus of the standard, it also present the principle of performing hot-spot fatigue analysis.

2. *DNVGL-RP-C203 (2020), Fatigue design of offshore steel structures* [20] - this a European maritime standard used for fatigue life design and evaluation of offshore steel structures. It can effectively be applied to all loaded welded structural joints due to mutual structural, geometric and loading setup. Fatigue assessment methods described in this standard present extensive hot-spot and notch fatigue assessment approaches along with S-N curves and formulations of stress concentration factors for differently loaded conventional joint setups. Additionally it includes more advanced assessment approaches such as a hot-spot multi-axial fatigue evaluation method.

3. *ANSI/AISC 360-16, Specification for Structural Steel Buildings* [3] - This is an American national standard used within United States, focusing on steel building constructions and is based on AISI certification procedures. Its intention is to provide design criteria for routine use to provide specific criteria for infrequently encountered problems, which occur in the large part within welded structural joint constructions. Along with design principles it defines fatigue assessment procedure using nominal stress approach.

4. *ISO 19902:2020, Petroleum and natural gas industries — Fixed steel offshore structures* [34] - This is an European standard for structural design and inspection of offshore steel constructions. The document contains requirements for planning and engineering of the design, fabrication, transportation and installation of new structures, as well as (if relevant) their future removal. Most importantly it provides extensive procedure for fatigue assessment using not only S-N curve-based approaches (i.e. nominal, hot-spot, notch stress), but also with fracture mechanics method.

5. *IIW Recommendations for fatigue design of welded joints and components* [2] - this is an international standard which is specifically focused on fatigue assessment of welded joint structures. These recommendations are aimed to provide a basis for the design and analysis of welded components loaded by fluctuating forces, to avoid failure by fatigue. It provides recommendations of fatigue assessment for both steel and aluminum structures and includes substantial detail on performing assessment nominal, hot-spot, notch stresses as well as with fracture mechanics approach.

6. *API-2A-WSD, API Recommended Practice 2A-WSD* API [9] - This is a standard focused on planning designing and constructing fixed offshore platforms. For structural joint applications it provides procedure for fatigue assessment of welded joint structures using hot-spot stress and fracture mechanics methods.

Each standard has its own specific application and although some assessment methodology regional differences are present - generally all aforementioned standards can be applied for analysing fatigue of structural joints. In principle, performing fatigue assessment based on the methodologies provided within aforementioned standards is an efficient way to ensure correct process of fatigue analysis which provides ways to verify that the method is applied correctly.

2.3. Multi-axial fatigue

This section introduces the principles and methodologies for evaluating fatigue damage using various multi-axial fatigue assessment methods.

An important aspect which conventional fatigue assessment methods do not account for is effects of stress direction towards accumulation of fatigue damage. When it comes to welded steel structures - stress rarely develops in a uniform direction, thus creating potential presence of multi-axial stress. Tubular beams are particularly prone to develop complex stress distribution around its welded connections, which should be accounted for if accuracy of fatigue assessment is of high importance. Uni-axial stress approaches described in section 2.2.1 can be applied to these situations as well with limited accuracy, however multi-axial fatigue assessment methods are generally meant to increase the precision of the analysis. For this purpose, it is worth to investigate methods of fatigue life estimation which analyse life of structural joints from the standpoint of multi-axial fatigue.

It is important to note that multi-axial stress properties are not uniform and can encompass different aspects. This can be distinguished in two main factors:

1. Presence of multiple stress components acting on the same position - when construction is loaded with multi-directional loads or contains complex geometry, it is possible to induce complex stress response within the structure which has more than one significant stress component (e.g. comparable tension and bending stress, bending along with torsional and plane shear stress, etc.) From the standpoint of principal stress - this could be understood as presence of two or even three principal stress components of comparable magnitude at a single measurement point. This comes in contrast with uni-axial stress where only a single significant stress component is present (e.g. presence of axial tensile stress in a beam under pure tension).

2. Non-proportionality of stress response - this links to the presence of phase shift within stress measurements where effects on multiple loads acting out of phase can induce stress fluctuations which create variation within magnitude of different stress components. From the standpoint of principal stresses, this can be envisioned as a continuous varied change in direction of principal stress. When magnitude of variation within stress direction is large - its effects have to be accounted with application of specific multi-axial fatigue approach.

Both aforementioned factors indicate presence of multi-directional stress and potential need for fatigue damage estimation using multi-axial fatigue assessment methods. Additionally there are other factors which influence fatigue damage from the standpoint of stress direction, such as material, loading frequency, presence of residual stress and geometry effects [88]. In general, a good multi-axial fatigue model should be physically-based, sensitive to material deformation behavior, robust, and applicable to variable amplitude loading [79]. However, no single multi-axial fatigue method has been found to this date which is capable of addressing all aforementioned factor combinations to provide uniformly correct results in all multi-directional stress cases - there are a number of different methods which are best suited for a specific application and in order to understand which multi-axial fatigue assessment approach is best suited for the specific application, it is worth investigating their differences and where each method is best implemented.

Each multi-axial fatigue assessment method includes four main parts within its formulation - a constitutive model, cycle counting method, damage model and cumulative damage rule. Upcoming sections are meant to introduce the main multi-axial fatigue and cycle counting methods which can be potentially applied on structural joints.

2.3.1. Multi-axial fatigue assessment models

There are several ways to classify multi-axial fatigue assessment methods. Shamsaei [79] classifies them into two main categories: classical and critical plane approaches. However, there are additional approach groups present which are defined based on their methodology, in particular - integral and invariant models [88]. Each class can be briefly described as follows:

1. Classical approaches - such as Gough [70] or Sines [59] models use distortion energy criterion variants (e.g. Von Mises) and have been commonly used in the past. However they generally do not reflect damage mechanism affecting analysed geometry and do not correlate well with fatigue data when loaded with multiple load components out of phase (i.e. non-proportional loading and stress) Shamsaei [79].

2. Critical plane approaches - these approaches rely on the fact that fatigue cracks in most cases initiate on the planes of maximum stress or strain. They evaluate stress/strain within most damage-inducing planes at a specific moment in time and are able to counteract the aforementioned weaknesses of classical models, such as inability to address presence of non-proportional stress. They commonly consider either maximum principal or shear plane as focus point of fatigue assessment. There is a very large number of critical plane approaches, such as Structural Stress Critical Plane, Stress-strain-based, Brown-Miller, Modified Wohler curve, among others.

3. Integral approaches - when critical based methods cannot properly account to specific requirements of analysed case (such as the reduction of fatigue lifetime of ductile materials) - integral methods can be used. These methods, in order to account for non-proportionality of stress response, integrate fatigue parameters over the volume of material. They are however more computationally intensive than other multi-axial fatigue assessment methods as there is not a simple way how the application procedure of this methodology could be streamlined. Some examples of integral approaches include Energy and Effective Equivalent Stress methods.

4. Invariant approaches - when there is a need to reduce complexity of fatigue assessment method, invariant approaches can be effectively used. These approaches estimate fatigue damage using a term which, unlike other methods, generally account for change in volume (using hydrostatic stress to represent it) and material yield (through use of deviatoric stress), while incorporating the use of stress invariant properties (i.e. where definition of a stress matrix includes terms that are not affected by transformation). This leads to a relatively simple definition of fatigue criteria, allowing for reduction of computational complexity. The most common invariant approach is Projection-by-Projection method.

In addition to this, fatigue assessment methods are commonly separated into stress-based and strain-based models depending on which response is used to evaluate fatigue damage. Some multi-axial fatigue models use both stress and strain. Some examples of stress-strain models include Smith-Watson-Topper (SWT), Fatemi-Socie (FS), Glinka approaches.

Following subsections are meant to introduce some of the multi-axial fatigue assessment approaches which can be potentially considered for application of analysing directional fatigue damage within welded structural components (such as the problematic upper arm joint of Cornelis Tromp 25T lemniscate crane upper arm joint). Table 2.1 provides an overview and references to all presented multi-axial fatigue assessment methods and indicates their class, whether it is a stress or strain based method, type of components used, whether approach is applicable for evaluating non-proportional multi-axial stress/strain response and indicates its relevant reference.

Findley [93]
This is one of the most fundamental critical stress plane approach for evaluating multi-axial fatigue, which considers the influence of normal stress on a critical shear stress plane. As it can be understood - this method derives orientation of the critical plane based on a Findley damage parameter through the amplitude of shear stress on the plane and the maximum value of normal stress. It uses the principal concept of Sines fatigue assessment and assumes that fatigue damage is in principle dominated by shear stress, which is also used to define orientation of the critical plane. This criterion is effective for a proportional combination of tension and torsion loading configurations, thus making it difficult to apply for non-proportional multi-axial stress response. Xu and Yuan [93] contains more information on the theory and applicability principles of this fatigue assessment method.

Modified Wöhler Curve (MWC) [10]
This is a stress-based critical plane approach which uses multi-axial shear response to define a modified variant of a Wöhler Curve, through which fatigue lifetime is estimated. It calculates fatigue damage by quantifying shear and normal stress values into stress amplitude ratio acting within the critical plane. Such method has the benefit in terms of its low computational complexity because its critical plane is defined in advance, thus leading to it being independent from further specifics of stress time history. The orientation of critical plane is determined using a Maximum variance method [85] which assumes that fatigue damage is proportional to the variance of the stress signal. This although also means that the method is not applicable for evaluating complex out-of-phase loading setups, thus keeping it for use only with proportional loading. According to this approach, crack initiation is assumed to form in the direction where shear stress range has the highest

magnitude. For more information on the methodology of Modified Wöhler Curve method, refer to Araujo et al. [10].

Multi-axial Hot-spot [20]
This is a multi-axial fatigue assessment method defined in DNVGL-RP-C203 [20] is relatively similar to a conventional hot-spot stress approach described in section 2.2.1. It uses principal hot-spot stress to establish critical planes for each measurement location, where two main principal stress components are separated into parallel and perpendicular stress. There damage is estimated using two specific hot-spot stress S-N curves with an identical damage criterion as is used for conventional hot-spot stress fatigue assessment method. The choice of which S-N curve is used is dependent on angle of each stress component. As the cycle counting for this approach is performed using a conventional Rainflow cycle counting algorithm - this method is best suited for evaluating mainly proportional multi-axial fatigue. Application for non-proportional stress is possible, but it is quite limited and is not expected to provide high accuracy results when there is a large phase shift within different components of stress response. Additionally, this method is specifically focused on evaluating multi-axial fatigue within structural welds, making it potentially applicable for the purposes of this research. DNVGL-RP-C203 [20] provides a step-by-step application guide for this fatigue assessment approach, where more information can be found.

Structural Stress Critical Plane (SSC) [37]
This is a multi-axial critical plane approach used for evaluating both proportional and non-proportional stress, through response of normal and shear stress acting locally at the measurement location. Stress planes are established based on Euler angles of evaluated stress component directions (with a fatigue life formulation using 45 degree angle for ductile materials, and a 0 degree value for brittle counterparts). Fatigue life is calculated with the help of Modified Wöhler Curves described in Araujo et al. [10]. The benefit of this approach for assessing structural joints is that it has been created specifically to assess multi-axial fatigue damage for welded structures [88], meaning it is expected that the method is applicable for evaluation of analysed lemniscate crane joint. More information on the Structural Stress Critical Plane approach can be obtained in Jiang et al. [37].

Brown and Miller (BM) [16]
Relatively similar to previously described Findley method, this strain-based critical plane approach, uses both normal and shear strain to evaluate fatigue damage. According to this method, cyclic shear strain is responsible for crack initiation, while presence of normal strain result in further crack propagation. Here the critical stress plane is acquired in the orientation setup which includes highest combined normal and shear strain response. It is a method which damage parameter formulation depends on the type of multi-axial loading, thus making it relatively difficult to apply for complex stress time histories, even though it is meant to handle non-proportional stress responses. Brown and Miller [16] provides the original formulation of of the Brown-Miller multi-axial fatigue assessment method with additional information on its formulation.

Smith-Watson-Topper (SWT) [55]
Stress-strain-based critical plane approach which has been originally derived as a method for evaluating fatigue damage of structures failing due to mode I loading (which loads the crack propagation zone by cyclically opening the crack). It is formulated in terms of directions of maximum strain and maximum normal stress components, although shear mode is still considered in its damage parameter formulation. This method allows one to account for effects of mean stress in multi-axial problems, while also incorporating effects of potential non-proportional cyclic strain hardening. Refer to Lopez-Crespo et al. [55] for formulation and additional explanation of aforementioned Smith-Watson-Topper damage model. It is applicable for non-proportional multi-axial fatigue approaches, however as it has been observed by Wu et al. [92], it appears to provide relatively non-conservative results.

Fatemi-Socie (FS) [41]
Stress-strain-based approach which uses shear strain and normal stress components to establish its critical plane by finding the plane with maximum magnitude of its fatigue parameter. It uses a scalar quantity, named as damage parameter based on the maximum shear strain amplitude influenced by the maximum normal stress on the maximum shear strain amplitude plane. It additionally takes into account the effects of cyclic hardening into its formulation, by addressing potential changes of material response throughout application of the structure within its lifetime in the boundaries of high-cycle fatigue. According to Reis et al. [73], it

provides solid results when multi-axial fatigue response is out-of-phase, although it does use a relatively simple Rainflow cycle counting method, which is difficult to apply for non-proportional stress responses due to continuously changing orientation of critical plane. However, as later found in Jiang et al. [38], Fatemi–Socie criterion is not practically influenced by the definition of the critical plane. Refer to Karolczuk et al. [41] for a more detailed explanation of this multi-axial fatigue assessment approach.

Liu Virtual Strain Energy (VSE) [73]
This is a stress-strain based critical plane model for calculating multi-axial fatigue, which separates strain criteria into failure modes - for tensile and shear failure. For this method critical planes are acquired separately for each mode, by finding a plane with largest quantity of virtual strain energy, to which the value of tensile or shear work is added (depending on evaluated failure mode). According to Reis et al. [73], virtual strain method is applicable for non-proportional loading but based on experimental comparison, shear based methods such as Findley, Wang-Brown and Fatemi-Socie tend to provide results which are more in-unison with experimental data, making virtual strain energy approach more reliable for evaluating proportional multi-axial fatigue.

Modified Carpinteri Spagnoli (MCS) [74]
This is the final critical plane approach presented in this section. It is a method which combines the effects and relation between principal stress and fracture plane on which crack initiation is expected. Here critical plane is established through observing the direction of principal stress components to the fracture plane. Angular change and determination of critical plane orientation is defined through Euler angles, and the location setup of fracture plane is defined either being at 0 degrees or 45 degrees (depending if material is brittle or ductile). It is a method which is applicable for evaluating both proportional and non-proportional stress response, with only difference between two stress variants is the choice of cycle counting algorithm. However according to van Lieshout [88], this approach has been validated only for planar structures, raising questions on its applicability for structural joints due to their diverse geometric combinations and properties. Ronchei et al. [74] provides a more extensive introduction to this approach, however it does lack validation data to confirm its good applicability for evaluating fatigue damage in structural joints.

Effective Equivalent Stress Hypothesis (EESH) [84]
As indicated in the name, this is an integral class, stress-based approach which uses local result of Von Mises stress response. However instead of using direct equivalent stress, this method uses a corrected value that is supplemented with equivalent shear stress. The value of equivalent shear stress is acquired by integrating shear stresses acting on multiple planes within material thickness - making use of evaluating interaction between slip bands. In principle it serves as an extension of critical plane approaches incapable of properly evaluating fatigue damage when stress at the measurement location is out of phase and exposed to variable amplitude loading. However this is a method that is mainly applicable with notch stress, making its application limited for non-detailed weld geometries. Sonsino [84] explains the formulation and application case of this method.

Energy Method (EM) [15]
It is an integral class approach which uses fatigue parameter that is based on energy theory. To establish its evaluation response, this approach can be defined as a stress-strain-based method using both stress and strain component responses converted into energy density. Elastic strain energy is used as its damage parameter for evaluating fatigue, under the assumption that in high-cycle fatigue loading the structure behaves elastically. One aspect of this approach is that it does not involve the step of cycle counting due to its specifics of establishing response used for fatigue damage evaluation. Instead damage is evaluated through mathematical transformation of the response using auto and cross-power spectra functions. This method does lack validation data for weld damage evaluation when they are exposed to complex loading combinations. More information on the methodology can be found in Braccesi et al. [15]

Projection-by-Projection (PbP) [13]
This is an invariant approach which is based on the assumption that fatigue damage can be correctly established when summing up resulting fatigue damage of all individual stress components. Normal and shear stress are evaluated within five dimensional Euclidian space to define signals which are not mutually correlated though are acting within a mutual reference frame. It uses multi-axial cycle counting approach to

establish stress cycles and ranges, which are then evaluated in terms of fatigue damage accumulation using S-N curve in combination with Modified Wöhler Curve approach for multi-axial fatigue assessment. Benasciutti et al. [13] contains an extensive overview of this fatigue assessment method.

Table 2.1: Summary of multi-axial fatigue assessment methods which could be applied for fatigue assessment of structural joints and their main properties.

Approach	Method class	Response applicability	Response components	Applicable for non-proport. response?	Ref.
Structural Stress Critical Plane	Critical Plane	Stress	Normal and Shear	Yes	[37]
Findley	Critical Plane	Stress	Normal and Shear	No	[93]
Multi-axial hot-spot	Critical Plane	Stress	Principal	No	[20]
Brown-Miller	Critical Plane	Strain	Normal and Shear	Yes	[16]
Smith-Watson-Topper	Critical Plane	Stress-Strain	Normal	Yes	[55]
Fatemi-Socie	Critical Plane	Strain	Shear	Yes	[41]
Liu Virtual Strain	Critical Plane	Stress-Strain	Normal and Shear	No	[73]
Modified Wöhler Curve	Critical Plane	Stress	Shear	No	[10]
Modified Carpinteri-Spagnoli	Critical Plane	Stress	Principal	Yes	[74]
Effective Equivalent Stress	Integral	Stress	Von Mises	Yes	[84]
Energy Method	Integral	Stress-Strain	Energy density	Yes	[15]
Projection-by-Projection	Invariant	Stress	Normal and Shear	Yes	[13]

2.3.2. Cycle counting models

Due to the time-dependent quality of multi-axial fatigue assessment - each approach that is based on use of S-N curves requires a method to evaluate fatigue damage using stress cycles and ranges acquired from the entire loading history. This is done using cycle counting models. However not every cycle counting model is applicable to all multi-axial fatigue assessment approaches. Depending on the method and multi-axial properties of stress/strain measurements, a cycle counting approach has to be chosen. This section provides an overview of cycle counting models which can be used for deriving stress/strain cycles for multi-axial fatigue applications.

Rainflow counting [5]

Being the most common method for counting cycles in uni-axial fatigue - Rainflow cycle counting approach in some cases can also be used for multi-axial fatigue applications. This model for calculating stress ranges and cycle number is based on rain falling down on a roof represented by the history of valleys and peaks. The main principle of it is based on formulating hysteresis loops where for each closed hysteresis loop one cycle is counted, and for an open hysteresis loop, half a cycle is taken into account.

It is only applied when evaluating multi-axial fatigue where stress/strain response is proportional (i.e. does not heavily change stress direction during operation). In such method multi-axial stress or strain is converted into equivalent separate stress or strain responses for each evaluated component and fatigue damage is then calculated in terms of particular relevant fatigue damage model specific to multi-axial fatigue assessment method. When it comes to non-proportional stress, the assessment procedure becomes computationally complex due to the need to reevaluate critical stress planes at each time step, which is counteracted by other methods explained in this chapter. A more detailed explanation of Rainflow cycle counting is presented in section 4.3.4 and can be found in Amzallag and Gerey [5].

Virtual counting [7]

When non-proportional loading cases are of interest, alternative methods of cycle counting should be used. One of the method examples, capable of evaluating out-of-phase stress response for fatigue damage evaluation is Virtual cycle counting approach. This method, unlike conventional cycle counting approaches (such as the aforementioned Rainflow counting), does not consider cycle counting from the standpoint of establishing hysteresis loops. This method separates stress components within critical stress plane into axial and shear components. It uses equivalent shear stress response to find zero up-crossing points and to define load blocks of the loading history. The load block in principle is is a time interval including a certain amount of virtual load cycles which are counted. From here, the largest stress range is chosen to calculate resulting fatigue

damage, with the process repeated for entire time history. This method however has a limited applicability potential, as it can only be used with Stress Scale Factor multi-axial fatigue assessment approach. More information about the applicability of the approach can be found in Anes et al. [7].

Wang-Brown counting [89]
Wang-Brown cycle counting approach is a strain-based method fitted for establishing multi-axial fatigue approach strain cycles when non-proportionality is present within the stress/strain response. It uses equivalent Von Mises strain and is best suited for mainly counting strain cycles using critical plane approaches. The basic principle of application performed with the help of equivalent strain method, using Von Mises strain as its response. Strain reversals are then defined from the zero to the maximum value using the chosen strain response to establish the cycle for fatigue assessment. From this point forward, the counted reversal is removed from the time history and in the case that there are any reversals left - the method of application is repeated until the entire time history is covered.

This method is applicable for non-proportional strain planes due to its quality which requires reestablishment of data after each reversal, if there is presence of phase shift within maximum strain plane. Wang and Brown [89] and Meggiolaro and Castro [60] provides a more in-depth look at the methodology and applications of Wang-Brown cycle counting method.

Modified Wang-Brown counting [60]
This method is created to fix the weakness of original Wang-Brown cycle counting approach by including the sign convention into Von Mises strain formulation. It improves over the original approach to more directly apply for multi-axial fatigue cycle counting, because here it reduces computational complexity of the assessment due to the way it establishes measurements within the deviatoric Euclidian space and does not require to calculate intersecting stress components at each time step [60]. It however requires introduction of additional assessment steps that are not present in the Wang-Brown approach. Unlike the original, this method can also be applied for both strain and stress responses as the cycle counting procedure can be converted to suit this method as well. Refer to Meggiolaro and Castro [60] for a more extensive explanation and full extended step overview of this cycle counting method.

Bannantine-Socie counting [82]
This is another cycle counting approach fitted for calculating multi-axial fatigue with critical plane approaches that use strain as response for damage evaluation. It separates fatigue failure into tensile and shear strain components and calculates them separately using Rainflow cycle counting algorithm. Magnitude and shape of each strain plane, as well as other components needed for different fatigue assessment approaches (e.g. maximum normal stress needed for Smith-Watson-Topper parameter) are all calculated separately for each reversal. This method is well suited for cycle counting when there isn't a single constant critical plane present - specifically when non-proportional stress/strain response is observed within results. It however requires evaluating all potential failure planes. Socie and Bannantine [82] and Shamsaei [79] explain the Bannantine-Socie method in further detail and present an application case for this cycle counting approach.

Multi-axial Rainflow counting [48]
In contrast to conventional Rainflow cycle counting that is efficiently applied mostly for cases which experience proportional multi-axial stress response - the Multi-axial Rainflow method expands the original approach to improve the procedure of evaluating non-proportional stress responses. This is done in principle by separating stress and strain responses by their loading modes and then determining the critical stress plane by evaluating damage of all components. However, unlike some other cycle counting models, such as Wang-Brown or Bannantine-Socie, this approach does not fully discount non-critical plane effects, but rather define them as auxillary channels for which stress/strain reversals are also counted. It has been determined by Langlais [48] that methods which do not include effects of auxillary channels can potentially under predict the effects of evaluated stress and strain components, which is counteracted by multi-axial Rainflow counting approach. More information on this method can be fount in Langlais [48] and van Lieshout [88].

Path-dependent counting [21]
One particular cycle counting method which takes into account loading path effects when evaluating multi-axial stress responses. The general procedure of this approach is based on finding the largest range or distance between two points in stress space over a given time history [21]. The overall length path is calculated by

following a monotonic increase in distance and adding length points throughout the entire time history. This method uses Von Mises stress criterion for evaluation and is capable of accounting for potential complex non-proportionality within multi-axial stress response.

One weakness of this approach is high computational complexity when multiple complex loading modes are acting on the structure. Additionally this cycle counting method requires a specific S-N curve for estimating fatigue damage, known as Master S-N curve [88]. The benefit of this approach for application on structural joints lies in the fact that this method for cycle counting has been successfully applied and validated for evaluating fatigue damage in welded structural joints by Dong et al. [21]. Refer to Dong et al. [21] and its subsequent research for more information on the algorithm and application cases of this approach.

2.3.3. Choosing the right method

Additionally it should be noted that multi-axial fatigue assessment might not always be necessary and conventional fatigue analysis methods might be sufficient. For this purpose before choosing the right method it is advised to evaluate whether there is presence of multi-axial stress within the measurement locations. When deciding on whether to perform a uni-axial or multi-axial fatigue assessment, it is also important to take note that stress magnitude and angle definition is also dependent on whether the crack has already initiated or the stage of its propagation - each potentially affecting fatigue results, especially when fatigue assessment takes into account stress direction - which can potentially lead to reduced result accuracy.

If multi-axial fatigue assessment is needed, it is worth evaluating assessment methods based on both what kind of multi-axial fatigue it is (whether it is proportional or non-proportional) and application case of fatigue analysis. Some methods are best suited for specific applications, geometry as well as loading setup and stress response, thus a single method does not necessarily have sufficient experimental data in the literature to be applicable for required case. For this purpose method is best chosen on information provided in this chapter as well as selection criteria which is described in more detail in section 5.1.

2.4. Conclusion

This section concludes results and observations made and provides answers to research question indicated at the beginning of this chapter.

Survey of fatigue assessment methods and load acquisition approaches have been performed in this chapter. Observations made during literature survey help answering the first research question:

What is the current state of fatigue analysis methodology for structural joints?

Fatigue damage accumulation is heavily dependent on experimental data and on a large number of factors which are difficult to quantify. Because it is hard to account for all factors and situations based on performed fatigue experiments, the entire science of fatigue assessment relies on principle of estimation. Conventional methods, such as nominal, hot-spot and notch stress approaches are commonly applied in the literature and the industry to evaluate fatigue life of designed structures, however each method has their own benefits and weaknesses. Since stress direction can play a large role towards fatigue damage accumulation for different materials - a large amount of multi-axial fatigue assessment methods which could be applicable for fatigue damage estimation in welded structural joints have been surveyed. Methods of multi-axial fatigue assessment are different both in terms of their application (whether they are capable of measuring proportional or non-proportional stress response), as well as in terms of their proposed application. Although there are many approaches present in the literature, a large number of them still lack validation data to ensure their applicability towards estimating fatigue damage accumulation within welded structural joints. It is critical to choose a method which is applicable for specific analysis both in terms of stress response and evaluated geometry.

3

Load acquisition

When fatigue analysis is performed using stress responses acquired with the help of finite element analysis - it is important to establish representative loading conditions acting on a analysed body. Correct loading results is a precondition to acquire accurate stress response both in terms of its distribution and magnitude. Since precision of fatigue analysis is heavily dependent on accuracy of stress response, loading setup establishment is a critical step leading to a successful fatigue damage assessment.

As it has been determined from literature review in chapter 2, load and stress response can be established either using a static approach or within a time domain with the use of such methods as multi-body dynamic (MBD) simulations. Because MBD analysis is used to acquire loads for the purpose of this fatigue assessment, it is important not only to define crane operation model and its parameters, but also ensuring the best possible accuracy of dynamic model loads. If the model is properly defined - it can potentially have solid benefits over more commonly used static load approach. This defines an important research question which has to be answered in order to assess fatigue damage of the crane upper arm in a manner which ensures the validity of final results. In this chapter, following questions will be answered:

1. How can multi-body dynamic simulation approach help with establishing representative loading conditions of a crane work cycle within the time domain?
   (a) Which factors in the MBD crane model setup most significantly affect load responses relevant for acquiring boom stress cycle?
   (b) How to verify that the accuracy of acquired load results is representative of realistic loading conditions?

These questions are closely linked and thus will be answered simultaneously in order to move forward into stress acquisition and fatigue damage assessment stage. For this purpose, the focus of this chapter is to answer the aforementioned questions in a systematic manner through the following actions:

1. Definition of a multi-body dynamic simulation model of the analysed crane.
2. Establishment of multi-body dynamic load setup acting on the upper arm structure that is relevant for implementing loading conditions in a finite element analysis environment.
3. Definition and performance of screening experiments used for quantifying statistical significance of applied loads towards imposing stress and determination of factors, relevant towards changing the value of applied dominant load/-s in the MBD model.
4. Adjusted load calibration and verification of results.

3.1. Multi-body dynamic model setup

This section attempts to establish a feasible and accurate multi-body dynamic model for acquiring accurate loads affecting upper arm structure of the crane. This is done through reassessment and adjustment of the existing multi-body dynamic model of Cornellis Tromp 25T lemniscate crane.

A critical part of fatigue assessment of a structure is the establishment of its representative stress cycle. As stress in the analysed structure is dependant on loading conditions which affect the model - the accuracy of stress cycle is directly related to the accuracy of applied loads. Multi-body simulation is an approach which allows users to acquire loading profiles in the time domain for dynamically loaded structures, which in turn can provide more accuracy to the procedure of fatigue life damage assessment. However, in order for acquired loading results to be reliable, the specific MBD model has to be sufficiently accurate in representing real system. This accuracy cannot be ensured without factual assessment of model parameters and its working principle.

3.1.1. Choice of software

As stated by Kuka et al. [47], in order to reach the goal of studying realistically the dynamic behaviour of a complex system using multi-body dynamic simulations, two main conditions are required:

1. The modelling capabilities of the multi-body dynamics tool should allow the reproduction of the dynamic characteristics of each single component that influences the dynamic performance of the focus point of analysis.

2. The simulation tool should be able to perform in acceptable/reasonable time a large number of parametric calculations.

These points provide a solid reference point for choosing a right methodology and software for running multi-body dynamic simulations and thus acquiring accurate loads affecting the boom structure of analysed lemniscate crane. For the purpose of this thesis, it is also critical that the software would also be able to:

1. incorporate non-rigid parts for assessing the effects of flexibility on the loading results.

2. Include capabilities to incorporate an optimization algorithm and/or controller for motion adjustment for optimizing motion profile.

As discussed in section 2.1.3 of chapter 2, there is a relatively wide array of possible choices for MBD analysis software, but each one has its own specific strengths, weaknesses and use cases. For the purposes of this thesis, *Adams View* software is used. This is a MBD analysis software developed by *MSC Software*, which is user-friendly and has a wide array of features available. It does not only have the basic requirements for acquiring dynamic loading conditions, but also fulfills the additional requirements specific for this research as it allows incorporation of flexibility into modelled parts and provide interface for both optimization and controller implementation, which makes it a great choice for acquiring and analysing dynamic loads acting on the lemniscate crane.

The multi-body dynamic simulation model of Cornellis Tromp 25T lemniscate crane has been created prior to the beginning of this research as described in Tawjoeram [86]. However, in order to acquire loading results affecting upper arm structure that are representative of real-world loading conditions - it is important to evaluate the current state and improve accuracy of the model.

3.1.2. Model setup

The multi-body dynamic model of the crane is created out of 19 body elements (including ground elements) which all consist from variable number of rigid parts. Most parts of the crane originate as imported 3-dimensional models of key components of a floating crane (e.g. crane foot, rear arm, upper arm, etc.) as illustrated in figure 1.1. Based on the principle of multi-body dynamic systems, each body element has limited degrees of freedom, which are defined through joint connections with other body elements. This is meant to allow according slewing and luffing motions of the crane.

Figure 3.1 illustrates the crane model established within multi-body dynamic simulation environment and marks its main components. In this model hoisting motion is simulated through a system of 4 cables (2 for opening the grab, 2 for hoisting). Cable system is implemented in a manner which includes 4 sets of 4 pulleys (16 in total) which are positioned on the upper arm (1x4), rear arm (1x4) and the tower structure of the crane (2x4). As Cornellis Tromp 25T is a floating crane which is operated on a floating platform, the MBD model includes these motions by fixing the crane on a simulated pontoon that has 3 degrees of freedom (for roll, pitch and heave motions). Each degree allows motion in a particular direction but the magnitude of displacement is limited through respective rotational or linear springs. Movement limitation through introduced springs also means that the platform is able to experience fluctuation that is generally comparable to

motions imposed on floating objects. Comparably, luffing motion is supposedly limited by a a pair of linear compression springs which are connected between rear arm and tower structure of the cranes. This additional spring system is meant to imitate the effects of hydraulic cylinders which support the arm during its motion or static position as well as to damp braking effects.

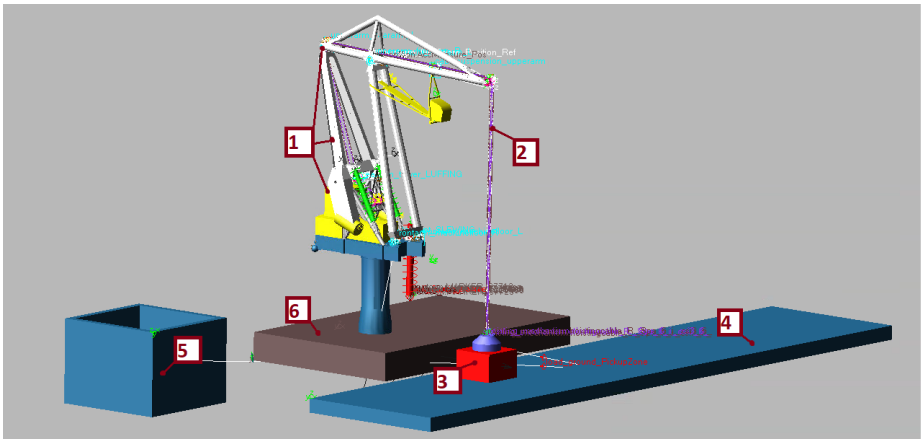

Figure 3.1: Overview of the main components establishing a setup of multi-body dynamics model of Cornelis Tromp 25T lemniscate crane.

Finally load is simulated as a separate non-descript object with a pre-assigned mass that interacts with the ground and grab based on body-to-body contact model. Grab is able to simulate effects of grabing the loads and its pull through contact body attraction force which is switched ON/OFF when necessary throughout the process of crane work cycle. Definition of the model which was created by Tawjoeram [86], allows to approximate operation of the actual crane. This however still leaves unanswered questions towards the accuracy of resulting model, which is addressed in the upcoming section.

3.1.3. Ensuring model accuracy

Due to the large scope of the work required to create a realistic operational representation of the crane and the lack of real life measurement data, a significant amount of parameters have not been fully verified in Tawjoeram [86]. Due to these reason this model has been initially deemed to be a promising tool yet simultaneously insufficient for research cases when high accuracy of dynamic operation assessment is required. A review of Tawjoeram [86] work, although extensive, indirectly presents following flaws visible in the published work:

1. Lack of reasoning or explanation on how forces affecting the crane are defined
2. Working cycle of the crane has been defined based on a combination of assumptions and talks with the company operating the crane. This data according to Tawjoeram [86] is difficult to verify in terms of its accuracy.
3. Flawed design of pontoon motion system.
4. Measurements taken for fatigue analysis do not represent loads exerted on the structure. Hoisting loads are not modelled at their application positions, rather reaction forces in joints are used, which is a misinterpretation of model loading. Additionally load appearing due to the mass of operator cabin is missing.

When analysing the actual MBD model of the crane created by Tawjoeram [86], additional flaws in the model has been observed by Wierenga [90]. This included:

1. movement definition though displacement rather than velocity, which leads to non-realistic velocity profiles of slewing, luffing and hoisting operations.
2. Incorrect definitions for center of mass
3. Wind load setup that does not provide realistic loads

In order to improve the accuracy of the dynamic model Wierenga [90] has reevaluated and adjusted multiple parameters of the crane:

1. Center of Mass positions for crane parts,
2. Motion profile has been linked to velocity rather than displacement
3. Slight changes to operational profile
4. Removal of wind loads from the model due to their irregular behaviour that was deemed not to coincide with real effects.

Along with the aforementioned changes, the main focus in Wierenga [90] has been on the rework of ship motions. As the analysed Cornellis Tromp 25T crane operates as a floating crane on a ship platform, it experiences floating dynamic effects that are commonly linked to ship and pontoon operations. As actual work by the crane is done when the ship is stationary, the ship platform has been modelled as a pontoon. To model the motions of the pontoon to match real working conditions Wierenga [90] has performed measurements for roll, pitch and heave motions as illustrated in figure 3.2. Using gathered data the initial pontoon working principle in the simulation environment has shown to be significantly inaccurate and has been reworked and validated in accordance to gathered data. The work of Wierenga [90] has significantly improved the accuracy of the model, but is not perfect due to assumed inaccuracy for assigned damping coefficient values and the fact that pontoon model still relies on static center of mass during operation, when in reality, during crane slewing, luffing operations and changing mass from lifted material hoisting procedures, the center of mass is prone to continuously change. However, it is not fully clear how much additional improvements would increase the accuracy of the model.

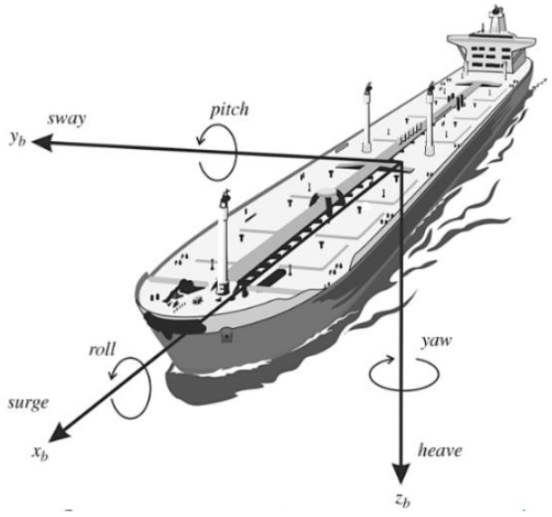

Figure 3.2: Degree of freedom classification for ships and floating structures [71]

To further reevaluate the accuracy of a model - Exterkate et al. [25] has taken on the task to quantify most important factors of crane dynamic model accuracy and to acquire additional measurements from the crane. The work has resulted in evaluation procedure for most critical factors for improvement, that was based on reviewing work of Wierenga [90] and Tawjoeram [86], definition of gaps in previous research and their evaluation on a scale of importance based on subjective criteria and information found in the literature. As the approach was not based on concrete data or a particular methodology, the evaluation has not yielded significant conclusions which parts of the model should be adjusted, and which parameters still require quantification. However the performed measurements and captured video data in this work can be beneficial in defining a significantly more accurate operational profile of a crane work cycle than what has been seen in work of Tawjoeram [86], Wierenga [90].

Overall, aforementioned previous work on developing crane MBD model had provided some important improvements either to the model itself or through acquisition of measurement data which can be used to develop a more accurate representation for lemniscate crane operation. The rest of this chapter is meant to

acquire a more realistic and accurate representation of the crane loads which are important for establishing a representative stress within crane upper arm structure.

3.2. Model setup adjustments

This section deals with performing parameter adjustments in the model, which due to their nature, can be verified through available data.

With additional data acquired by Exterkate et al. [25], it is possible to improve the multi-body dynamic model by adjusting its general simulation and body parameters. These changes are meant to establish a general setup of a crane operation which can then be further improved by evaluating load effects in the later sections of this chapter.

3.2.1. Simulation setup

An important parameter which requires adjustments from the original MBD model is the choice of dynamic integrator, which defines how MBD model calculates body dynamics. Choosing an improper integrator or the wrong integration setting setup can lead to divergence of solution, computational instability or erroneous results [44]. Based on descriptive dynamic formulations and recommendations of Kertész and Palčak [44], a WSTIFF (Wielenga stiff) integrator with a Stabilized index 2 (SI2) formulation has been chosen for running MBD simulations of lemniscate crane. This is a stiffly stable integrator which is capable of solving stiff differential equations, with a index formulation which prioritizes accuracy over efficiency. Chosen dynamic integrator setup assembles mathematical equations using the following formulation [44]:

$$\begin{aligned} &M\dot{\bar{q}} - A^T \bar{F}_A(\bar{q}, \dot{\bar{q}}) + \Phi_{\bar{q}}^T \bar{\lambda} = 0 \\ &\bar{u} - \dot{\bar{q}} + \Phi_{\bar{q}}^T \bar{\mu} = \bar{0} \\ &\bar{\Phi}(\bar{q}, t) = \bar{0} \\ &\dot{\bar{\Phi}}(\bar{q}, \bar{u}, t) = \bar{0} \end{aligned} \tag{3.1}$$

where M is the system mass matrix; $\bar{q}$ is generalized coordinate vector; A^T is the transformation matrix projecting forces into coordinates of q_j; F_A is the vector of action forces and inertial forces; $\bar{\Phi}$ is the vector of constraint equations; and $\bar{\lambda}$ is vector of Lagrangian multipliers.

WSTIFF is a robust, multi-step implicit integrator which uses backward differentiation formula (BDF) as a corrector and Newton's divided differences as its predictor. Such setup has the additional benefit of computational stability in simulations which include flexible bodies, as it does not lead motion speed and erroneous load and acceleration spikes (artifacts) that are present in non-stiff integrator load responses (e.g. Newmark formulation). This is an important aspect as part flexibility is to be incorporated into a specific crane MBD model, with the goal to determine their effect on load response. The main drawback of using WSTIFF integrator with SI2 formulation is its computational complexity as it does compute significantly slower than comparable integrator models.

3.2.2. Motion modelling principle

In addition to integration parameters, it is worth evaluating how acceleration change is modelled within MBD environment. An acceleration vector profile establishment in Adams is calculated based on the formulation of the second form of Lagrange equation [90]:

$$F_j = \frac{d}{dt}\frac{\partial L}{\partial \dot{q}_j} - \frac{\partial L}{\partial q_j} + \sum_{i=1}^{m} \frac{\partial \phi_q^T}{\partial q_j}\lambda_i - Q_j = 0 \tag{3.2}$$

where F_j is the equilibrium equation of generalized coordinate q_j; $\dot{q}_j$ represent second order derivative of generalized coordinate for establishing smooth change of motion profile; L is the Lagrangian; m is unconstrained degrees of freedom in the model; ϕ_q algebraic constraint equation for the generalized coordinate; T is kinetic energy in the model; λ_i is the lagrangian multiplier; and Q_j is the generalized force applied to the model. This formulation covers the principle of how acceleration changes are smoothed out over time, in order not to create acceleration instantly as can be observed in figure A.9. This setup leads to non-instant jerk reaction for all body motions, which is estimated to realistically imitate gradual acceleration/braking that is imposed by electric motor-gearbox combination used for moving crane joints. Additionally, this setup allows

motion implementation in MBD environment through displacement, velocity or acceleration, rather than direct imposition of rotational force.

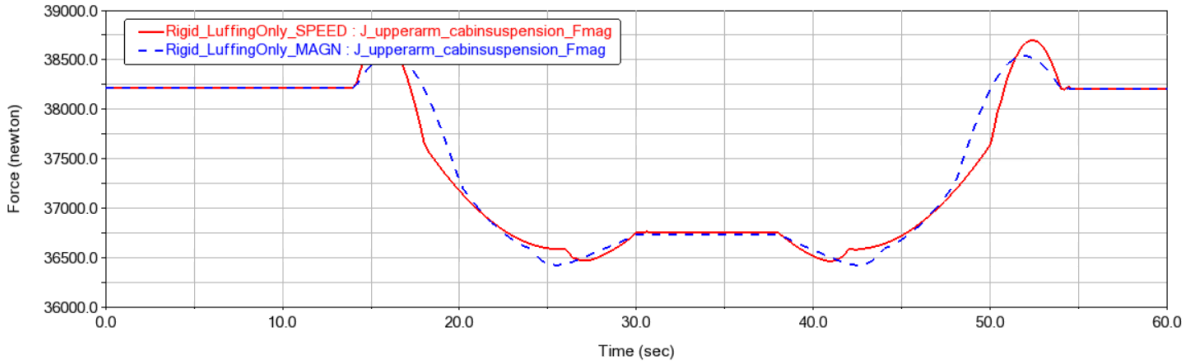

Figure 3.3: Comparison of loading profiles appearing from changed luffing velocity approaches - with increased jerk (red) and increased acceleration magnitude (blue)

3.2.3. Part mass

Although body motions of the crane are established not through forces but rather using velocity - majority of crane part mass does not have a particularly large importance towards derived results. However, since the crane is positioned on a floating platform through incorporation of springs - body load and its distribution can significantly affect how springs deform. For this purpose, crane body part mass has been adjusted using measurements which were acquired during Cornellis Tromp 25T crane disassembly which has been performed in 2020 by crane operator Maja Stuwadoors B.V.[1]. Current mass setup established in Tawjoeram [86] has been compared with measurement results and adjusted accordingly to fit real world values. Table 3.1 summarizes part mass setup based on aforementioned part weight measurements. Concerning the changes to mass, the only two measurements do not have measurement data present to prove their mass value: 1. Crane house; and 2. Hydroset. Mass setup of these parts are kept as per recommendations set in Tawjoeram [86].

Table 3.1: Overview of adjusted component mass setup of crane parts in MBD simulation

Part	Adjusted Mass, kg	Part	Adjusted Mass, kg
Load	16000	Machine_Floor	81000
Cabin_w_Bridge	3500	Pedestal	3000
Cabin_Suspension	500	Foot	20000
Counterweight	42000	Pontoon	980000
Rear_Arm	48000	Grab	9000
Tower	32000	Hydroset	2000
Crane_House	8000	Ballance_Weight	47500
Front_Arm	35000		

3.2.4. Part inertia

Correct setup of diagonal terms for body moment of inertia is a critical part of multi-body dynamic modelling. When it comes to moment of inertia itself, its values are to be directly linked to geometry and mass values of specific parts. However, evaluation of moment of inertia values defined in the original model has shown that for most parts, they are linked to geometry, but not to the part mass. As values of diagonal inertia moment terms scale directly with the change of mass, analysis of material properties for the part computer aided design (CAD) models the link is not present - for example, for the front arm, setup of Tawjoeram [86] uses 20% higher values on all terms than expected. This obervation presents an obvious mistake in simulation setup, which has to be fixed in order to acquire sufficiently accurate simulation results.

The principle of establishing part inertia setups is completed in the following manner:

[1] Maja Stuwadoors B.V. URL: https://majastuwadoors.nl/en/

1. Geometry of each model part is extracted as a parasolid and imported into computer aided design (CAD) software.

2. Each part is assigned an arbitrary material and using geometry measurement tools, part inertia setup is acquired based on the arbitrary material setup.

3. Based on required part mass and its present difference in its value, a coefficient is calculated which is meant to determine how inertia setups acquired in the cad model have to be scaled up or down.

4. Part inertia setups are scaled accordingly and applied to the MBD model setup to represent real dynamics of the crane, which inertia is linked to modelled part geometry and part mass.

Linking part inertia terms to their defined mass has lead to significant change in comparison to the original setup - with components having a difference of magnitude change between 0.7 and 280 times, depending on a particular part. Based on adjusted result setup, it appears that inertia model adjustments have a significant effect on how pontoon reacts to motion and load effects. Figure 3.4 illustrates how results of hoisting load have reduced of the current setup by adjusting the inertia model present in the analysis. The change has led to a 30% average decrease of crane load present at joint location between upper arm and rear arm of the crane, as it has been seen in the original crane MBD model.

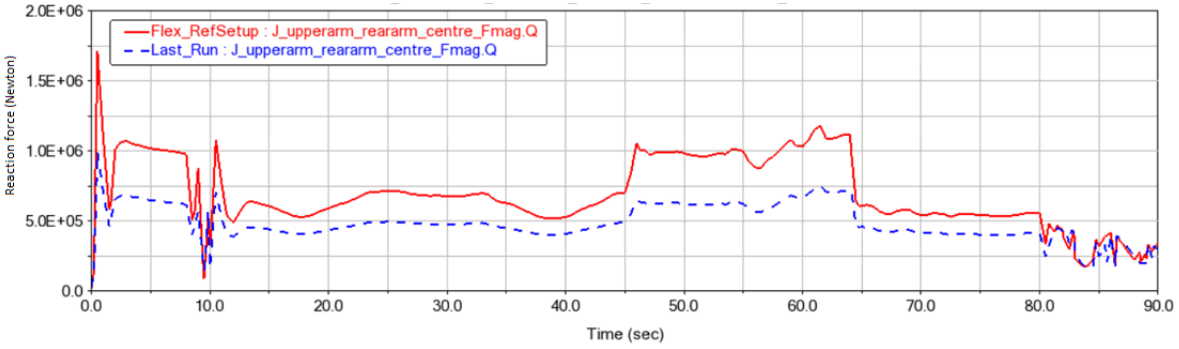

Figure 3.4: Reduction of load exerted on the back joint of the crane with an adjusted component inertia setup in MBD model (red line being original response and blue line adjusted response)

3.2.5. Surface-to-surface contact

When it comes to surface-to-surface contact modelling - it concerns the setup for simulating body responses when two disconnected parts come into contact while at least one of them is in motion. The main issue of this original setup is that Load-Ground impact does not provide realistic behaviour as it includes a non-stiff contact which is at the same time poorly damped, leading to direct impact imposing fluctuating motion (bodies begin to rotate in sway and roll directions) which can be considered as unwanted behaviour as it doesn't represent real contact. This is generally a byproduct of too low stiffness and damping coefficient that is assigned to the contact of aforementioned interacting geometries. The accuracy of this behaviour is most critical when crane grab impacts the ground, as the present motion creates fluctuating pulling motion on the hoisting system, thus imposing additional cyclic loads onto the analysed crane structure. According to the current setup, the preset stiffness-damping ratio for geometry interaction is equal to 1. According to Giesbers [30], the maximum damping coefficient should not be higher than 0.01 of the stiffness value. This statement is supported by the default contact stiffness-damping ratio that is set for Adams impact force setup which is equal to 1+E-4. For this purpose, load-ground impact is worthy of investigation.

When it comes to specific values of damping and stiffness coefficients for ground to body impact, the best way to make adjustments and find optimal value is to adjust results through multiple simulations until the output sufficiently resembles real life contact behaviour [30]. However, a much more simple method for sufficiently accurate behaviour is approaching contact setup from the standpoint of Coefficient of Restitution (CoR). This is a ratio of initial and final velocity between collided objects [1]. CoR values are standardized for commonly interacting materials and are readily available online. For the purpose of modelling load-ground interactions - since the model assumes that the handled material is scrap metal - the value of restitution coefficient has been chosen for to be 0.8 in accordance to dry steel-steel interaction as found in Giesbers

[30]. This change of contact setup based on material coefficient of restitution has lead to slight reduction in grab to lifted mass impact response which in turn has reduced amplitude of roll and swing motions by 30% - leading to more realistic behaviour. This does increase the load impact response between the grab and lifted mass, which slightly increases loads experienced by the boom at the moment of contact, but that is a result of realistic grab to load impact.

3.2.6. Part flexibility

As the purpose of this research also deals with determining the effects of part flexibility present in the crane model, three specific parts are converted from rigid to flexible as shown in figure 3.5:

1. Upper Arm - the main part of analysis, carrying most of the hoisting load and experiencing largest inertial loads (picture A in figure 3.5).
2. Front Arm - part connecting upper arm to the machine floor (picture B in figure 3.5).
3. Rear Arm - part exerting luffing motion on the upper arm and connecting upper arm to the tower structure (picture C in figure 3.5).

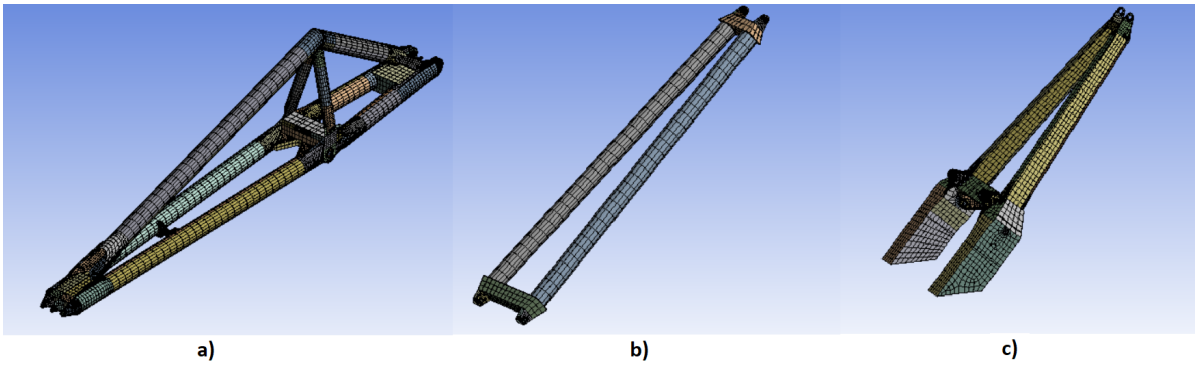

Figure 3.5: Slender crane components, made flexible for incorporation in MBD simulations: a) upper arm; b) front arm; and c) rear arm

The principle of how each part is made flexible in the MBD model is as follows:

1. Part geometry is extracted as a CAD model, assigned material parameters and connected in FEA environment.
2. Each part is assigned a coordinate system representing MBD model origin, remote points, which are at the locations of representative marker locations as it is modelled in MBD rigid components. These remote markers use stiff beam connections to connect floating point to a mesh and is a reference point for positioning meshed geometry model when importing in MBD environment.
3. Within finite element analysis environment the part is meshed with a uniform rough hexagonal mesh (as part deformation is not sensitive to mesh size [57]). No loads or constraints are assigned to the part.
4. A modal analysis is run for the part to determine bodies natural frequency response and critical frequencies for imposing vibration in the geometry (first 20 modes are extracted).
5. Using a custom script, part model is exported in a .mnf file format, which contains mesh geometry, part remote points and natural frequency setup.
6. Part file is imported into the MBD environment where it replaces its rigid counterpart using remote points which have to match locations of specific manually assigned markers.

This is a time-intensive operation, but it provides a component in the model which can potentially acquire more accurate load setup that includes dynamic inertia setup, predefined mass, flexibility effects and (if needed) stress and strain responses. Preparation for further screening analysis and reasoning why these specific parts are made flexible will be discussed in more detail in section A.0.3.

Computational complexity

Under ideal conditions, all parts could be made flexible to incorporate non-rigid inertia setup into the MBD model, however this methodology has its own drawbacks. The main drawback of incorporating flexibility into crane MBD models is linked to reduced computational efficiency as incorporating flexible parts significantly increases simulation time. All simulations in this report are run in CPU mode on a computing node of four Intel(R) Core(TM) i5-6500 CPU @ 3.20GHz CPU cores, 8 GB of RAM, Win10 x64, while utilizing its full computing power. Figure 3.6 presents how computation time of performed MBD simulations vary based on the number of flexible parts introduced to the model. Although the setup of this simulation is relatively complex with several moving and interacting parts - rigid body simulations compute quickly (<5 mins). This fact also takes into account that a working cycle of the crane requires a significant amount of time steps (700 in particular for a 70 second simulation) for simulating and gathering data to acquire accurate representation of crane work cycle motion, which leads to a large amount of data saved. However this factor has small effect on the total computational time. Some factors, such as the choice of dynamic integrator (which is used for establishing the methodology for formulating body dynamics in MBD environment) does influence the simulation efficiency, yet it is apparent that inclusion of flexibility tends to affect simulation with the largest significance. Tested setup for rigid vs. flexible upper arm structure simulations has shown a clear difference in computation time: 4 mins per simulation for rigid variant with almost a linear relative increase in simulation time of extra 20 minutes per each additional flexible part as presented in figure 3.6.

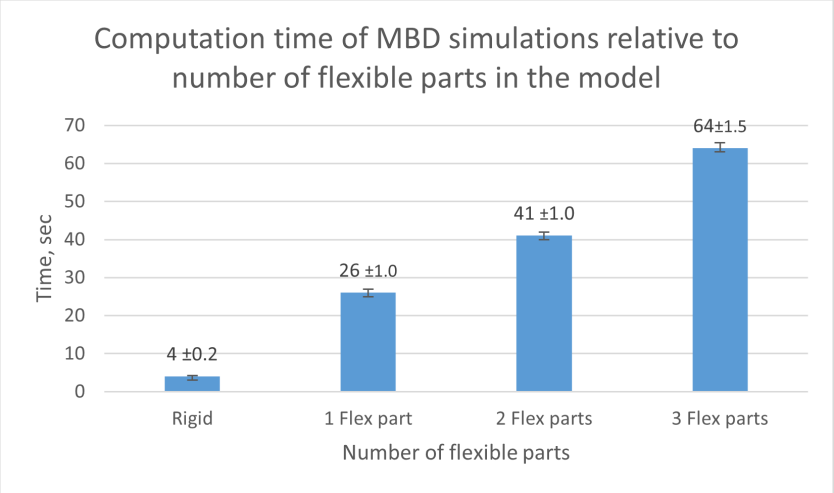

Figure 3.6: Comparison of computation times for multi-body dynamic simulation of lemniscate crane work cycle, dependent on the amount of flexible parts in the model

Finally it is worth taking into account that the current principle of correctly incorporating flexible parts into the MBD simulations is a time consuming process, which requires accurate meshing and eigenmode acquisition of a modelled part, as well as includes a mandatory process of applying rigid links between markers and the flexible parts in order to correctly translate relevant loads to specific measurement markers.

3.2.7. Work cycle setup

This part deals with defining motion profile of analysed crane motion model. Generally for fatigue analysis it is common to assess the main operational cyclic loads acting on the body through its normal operation, as well as occasional and exceptional loads (e.g. wind and strom loads and any associated wave motion, installation and transportation loads, as well as critical hoisting overload, etc.) which happen less frequently. However, in most cases due to the fact that normal operation contains by far the largest amount of significant stress cycles - it tends to accumulate the largest amount of fatigue damage [68]. Combining this fact with the lack of validation data for additional situations as well as complexity of performing time-dependent fatigue assessment with several methods and multiple time steps for stress acquisition - additional loading will not be included and only the regular crane work operation will be modelled and evaluated during fatigue assessment.

When it comes to normal crane operation, a standard working cycle of a lemniscate crane consists of several standard motion operations which are used to transport material between loading-unloading zones.

These operations can can be summarized as follows:

- *Slewing* - rotational motion imposed between the machine floor and the foot of the crane which changes direction to which crane faces. It is modelled as rotational motion to rotate around center axis of crane foot.
- *Luffing* - tilting motion imposed on the front and back legs of the lemniscate crane. It moves crane boom front and back in a linear motion and in turn changes reach of the crane. Luffing is modelled as rotational motion around the lower rear arm joint of the crane foot.
- *Hoisting* - lifting and lowering motion of the crane grab using a cable system, which allows to change the height at which handled material is loaded and unloaded. It is modelled as rotational motion transmitted throughout the entirety of pulley-cable system.
- *Grabbing* - this operation is meant to grab or release material after it is transported with the aforementioned motions. In MBD environment it is modelled as a contact force that attracts grab and the grab body surface and which can be turned on and off when needed.

These operations create the entirety of lemniscate crane motion cycle. Although operation overlaps are expected, regular work cycle is performed as shown if figure 3.7, in the following sequence:

1. Work begins when grab is ready to initiate grabbing of the load. Once the load is secured in the grab, the load is lifted upwards through hoisting.
2. Crane begins to slew from loading zone to unloading zone in a rotational motion around its axis of rotation.
3. Crane is luffing backwards (or forwards depending on the difference of required reach between laoding and unloading position). This moves the center of mass of the crane inwards towards its centre, reducing experienced torque on the slewing mechanism as well as experienced loads on the boom.
4. Handled material is lowered down through downward hoisting operation for release.
5. Grab opens to release the load.
6. Empty grab is lifted up through a hoisting operation
7. Crane slews to the opposite direction than previously in order to reach loading position.
8. Crane luffs to the opposite direction than previously in order to reach required loading position.
9. Grab is hoisted down to prepare for load pickup.

As additional data on crane motions which has been gathered in Exterkate et al. [25] has become available, it is possible to establish how an actual crane operation is performed. Video footage taken from the operator cabin of 57 consecutive work cycles performed with the Cornellis Tromp 25T crane is used, and it allows data extraction for the length of each work cycle, hoisting, luffing, slewing and and grab opening operation times, as well as their duration. This footage also provides sensor data showing travel distance and the mass of lifted material to be acquired and allows reevaluation of crane work cycle with a large level of accuracy.

The process of establishing data-based work cycle and operation duration times is performed in the following manner:

1. Review of video data is performed. This includes calculation of times for each cumulative operational work cycle, as well as determination which cycles are non-feasible for evaluation. The non-feasibility is determined through inclusion of stops in the operations due to unexpected reasons, such as operator breaks, failure to pickup material or halts in operations for adjusting unloaded piles of material. The findings show that out of 57 recorded cycles, 29 cycles have been determined as representative variants, which were performed without unexpected stops, delays or failure to pickup.
2. From resulting 29 cycles, sample population is defined and each cycle is then assigned a number. Using a random number generation algorithm 5 cycles were chosen from the population, for which detail operation times were calculated. Results are used to statistically determine average operation lengths under a normal distribution with a 95% confidence interval.

3. Due to the requirement of extracting sensor data for cycle recreation, a cycle has been chosen from the sampled variant which resembles statistical average values of each operation duration the closest. This cycle is used as representative setup for established new work cycle that will be used to acquire loads for fatigue analysis.

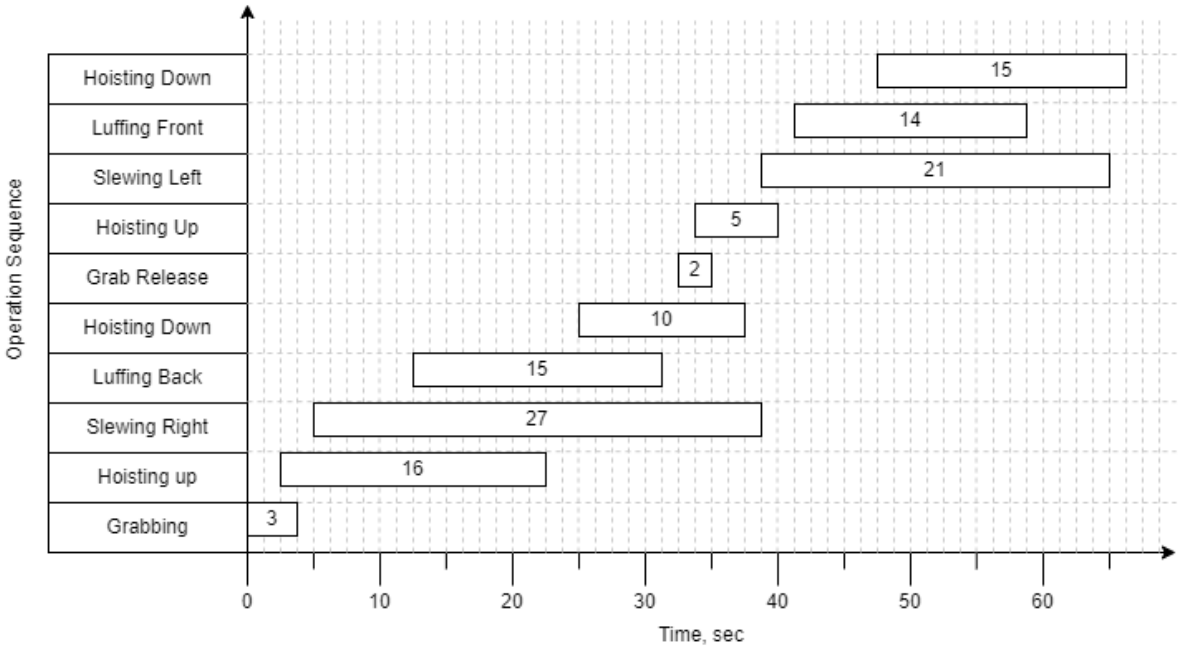

Figure 3.7: Analysed lemniscate crane motion operation temporal setup.

Figure 3.7 presents time bounds on how each crane motion operation is defined based on observing real operation of the crane. The total operation time is equal to 66 seconds during which crane completes loading/unloading operations and gets back to its original pick-up position. What the adjusted crane work cycle achieves is a definition of a realistic work cycle that is based on measurement data and visual evaluation. Although a single work case is not a perfect example for all loading cases, this provides an accurate view towards how the crane is operated in reality, and this information provides at least reasonable basis for evaluating realistic loading conditions experienced by the crane.

3.3. Load factor screening

This section describes the principle of recognising and establishing the most influential loads affecting the upper arm of the crane, while at the same time defining which aspects in the crane loading setup can be considered as not particularly significant to be worth of a detailed establishment in terms of load accuracy.

Establishing loading conditions on the structure for fatigue analysis with the help of multi-body dynamic analysis serves a purpose of potentially increasing the accuracy of the final result. Inclusion of time domain allows acquisition of changing loading response over time, which in turn allows to define stress cycle in FEA environment in relation to time. As result accuracy is important part of performed fatigue assessment, establishing a representative loading setup becomes a critical aspect of MBD model definition. However, as the present crane MBD model itself is complex and involves an abundance of loads and other model parameters which could be adjusted to create a continuously more accurate representation of the real crane operation - it is worth recognising that different factors affect the operational precision of the crane in varying levels - thus limiting the focus to most influential factors is often seen as a reasonable approach. Additionally, since the focus of this research lies mainly in the fatigue assessment of the crane upper upper arm, scope limitations for model improvement also stays on the parameters which influence only loading conditions of the upper arm.

3.3.1. Relevant load overview

The main motivation for establishing a multi-body dynamic model of the crane is to simulate relevant, time-dependent load profiles that affect the FEA model of the analysed crane upper arm structure. During its operation lifetime, the upper arm structure is affected by loads linked not only to body loads such as the weight of handled material and its grab, but also directional inertial loads appearing due to body motion. Figure 3.8 illustrates all relevant loads that potentially affect structure of the upper arm.

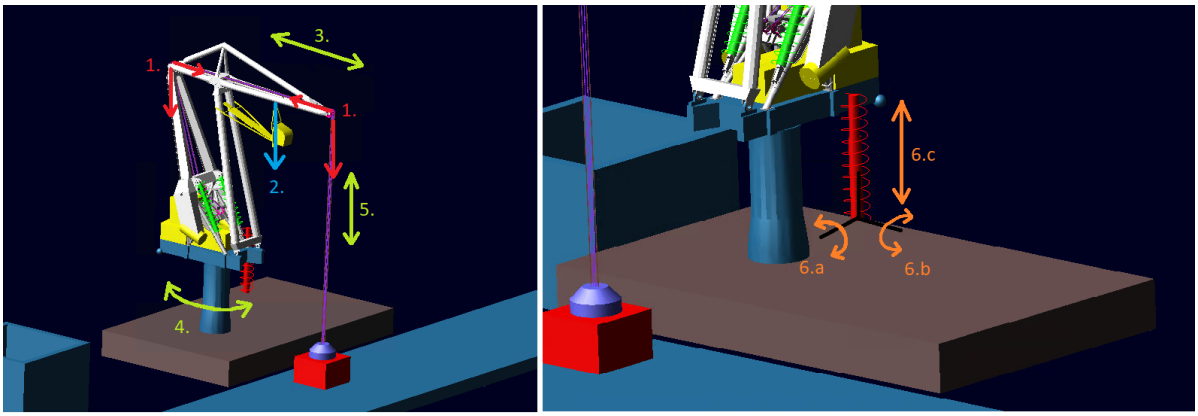

Figure 3.8: Overview of the loads imposed on the crane model: 1. Hoisting load (coloured in red); 2. Operator cabin structure weight (blue); 3. Luffing direction (green); 4. Slewing direction (green); 5. Hoisting direction (green); 6.a Heave direction (orange); 6.b Roll direction (orange); 6.c Pitch direction (orange);

Descriptions of each relevant load for the crane upper arm structure can be summarized up as follows:

1. *Hoisting load* – this is a body load that is a combined result of grab weight and specific load lifted by the crane to perform loading/unloading operations. It includes mass of the lifted material and grab, relevant weight of the cable system. As this load is present when crane is both static state and when it is in motion - the magnitude and direction of the load also is affected by acceleration due to hoisting luffing, slewing operations as well as pontoon motion. Hoisting load is exerted at both front and back of the upper arm, at locations where cable pulleys are positioned. This approach of load application is based on the operational principle of crane cable system: as the drive system of hoisting mechanism for this lemniscate crane is located inside the machine house which stays below the rear arm – cables which support the weight of the grab and lifted material run through the entirety of the rear and upper arm length. This leads to cable tension that inflicts hoisting load on both front and back pulleys installed on the upper arm.

2. *Operator cabin structure weight* – as operator cabin is suspended between upper front arms, it also imposes a load on the upper arm at its suspension point. This load includes the weight of the operator cabin, cabin suspension connected to the boom and cabin bridge that is connected to front arm.

3. *Luffing acceleration*– this is acceleration which imposes crane motion in the forward/backward direction (along its length). It is a motion that is used for extending the reach of the crane.

4. *Slewing Acceleration* - this is a radial acceleration of the crane which rotates around an upward facing axis of motion. This motion allows the crane to significantly increase its reach in multiple directions.

5. *Pontoon motion* - as the analysed crane is installed on a floating pontoon, this motion is meant to simulate crane loads that are imposed by pontoon displacement during crane operation. Out of possible six degrees of freedom illustrated in figure 3.2, pontoon motion in the analysed model allows only three relevant motions that are present in the simulation setup:

   (a) Pitch - rotational acceleration around the side-to-side axis of the pontoon/ship, taken at the center of mass position.

   (b) Roll - rotational acceleration around the front-to-back axis of the pontoon/ship, taken at the center of mass position.

(c) Heave - translation acceleration in the upwards direction of the pontoon.

The decision to limit pontoon motions to only three directions is based on observations made in Wierenga [90], which state that during crane operation of floating lemniscate crane pontoon does not experience translation motion on XY plane (in surge and sway directions) and neither is affected by significant rotational motion along the upward (Z) axis (Yaw). This limits pontoon to a single translation direction (Heave) and two directions for rotation (Pitch and Roll).

3.3.2. Screening goal

The main purpose of performing screening experiments which are described in this section is to determine which factors are most significant towards influencing the imposed stress in the finite element model of the crane upper arm. Under static conditions (when analysed structure experiences only small displacements and slowly changing loading profile) this is a straightforward task which would involve a single screening experiment for which all data could be gathered in FEA environment - as all loads acting on a static structure are predictable based on the principle of load application and can be computed within a single time step. Because the subject of analysis (i.e. upper arm structure of a lemniscate crane) experiences dynamic loading in the form of multi-directional inertial loads which change their magnitude and direction at a relatively rapid pace throughout each loading cycle - establishing accurate loads with a single step is more difficult. For this purpose, a multi-body analysis is used to include time domain in the procedure of load acquisition, which captures loads at multiple time steps over its operation duration. Additionally, it is estimated that effects of inertial loads have an influence on the stress response not only directly (through imposing stress on the body weight of the structure), but also indirectly (by affecting loading profile of other applied loads - e.g. directional load fluctuations appearing from the mass of the grab and hoisted material), however the significance of each inertial load effect is still unknown and thus has to be investigated. Finally as Tawjoeram [86] has speculated - presence of flexibility in the setup of MBD components of analysed lemniscate crane could potentially lead to more accurate results of applied loads - this is a setup aspect worth of further investigation and can be performed with screening experiments. For the aforementioned purposes, screening of indirect inertial load effects and effect of structural flexibility within MBD model will be made in apparent order after first screening experiment, which checks load factor effects on the stress response.

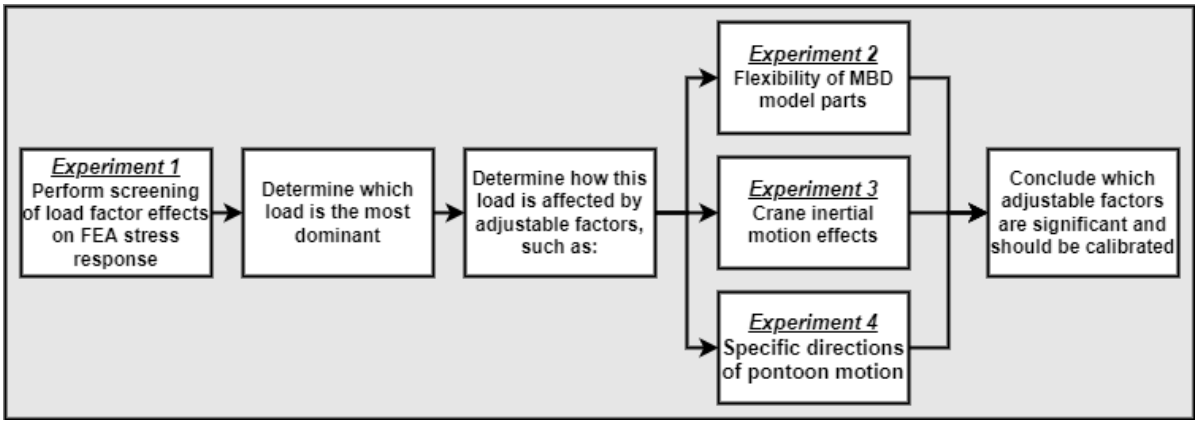

Figure 3.9: Relation and workflow of performed screening experiments.

Figure 3.9 illustrates the relation and workflow principle and relation of performed screening experiments. In total, screening setup performed for assessing significance of loads acting on the crane are separated into four separate experiments:

1. *Experiment 1*: Screening for effects of all loads applied to the finite element model of the crane upper arm towards influencing stress response present in the crane upper arm structure.
2. *Experiment 2*: Screening for effects of flexibility incorporation into the crane MBD model and its influence on the dominant load which imposes most stress in the structure (i.e. specific load determined in experiment 1).
3. *Experiment 3*: Screening for effects of inertia loads on the response of dominant load, which imposes most stress in the structure (i.e. specific load determined in experiment 1)

4. *Experiment 4*: Screening for effects of specific directional pontoon motion influence on response of the dominant load, which imposes most stress within the structure (i.e. specific load determined in experiment 1)

All experiments are linked together in terms of their purpose to acquire accurate load response for fatigue analysis. Experiment 1 establishes significant load factors and the dominant load which imposes most stress in the finite element model. Additional screening experiments are then performed to determine how different factors affect response of the dominant load, as it is defined in figure 3.9. Each experiment, its setup and results are described in extensive detail in appendix A.

3.3.3. Conclusion of Screening Experiments

With the help of Design of Experiments Screening approach, dominant factors relating to stress and load responses has been found. The main takeaways of the screening can be summarized as follows:

1. The most significant load affecting the average and maximum stress response of a detailed finite element model of the crane upper arm belongs to the hoisting load, with operator cabin structure weight being second by a fairly large margin. Presence of other (inertial) loads do provide statistically significant effect towards resultant stress response, but in comparison to the effect of hoisting load, their effect is relatively low. *This concludes that establishing good hoisting load accuracy is most critical towards acquiring accurate stress conditions of the upper arm structure.* In order to achieve accurate response, it is important to establish which factors affect the response of dominant (hoisting) load. That is done with the three additional screening experiments.

2. Flexibility of slender crane components (upper arm, front arm and rear arm structures) do not have any significant effect on resultant hoisting load response. This means that for the purpose of acquiring accurate loads affecting upper arm of the crane, there is no actual need to include flexibility in the MBD model, and for further analysis the whole crane structure will be kept as rigid.

3. Although inertial loads do not impose significant stress in the upper arm, it does however have an effect on the dominant hoisting load. Luffing acceleration being relevant for changing total hoisting force and std. dev. values; slewing acceleration being significant only when combined with luffing acceleration, as a second order effect; while hoisting acceleration affecting mainly the load variation (std. dev.). *Hoisting and Luffing acceleration profile should be adjusted as closely as possible to acquire realistic loading results. When it comes to slewing acceleration, very large accuracy is not critical for final result accuracy - fitting an accurate displacement profile in a predefined time window is sufficient.*

4. Pontoon extension length is a parameter which has a significant effect on hoisting load response when crane is affected by various inertial loads. It has to be defined with largest possible accuracy for acquisition of reliable results.

5. Pontoon motion has strong effects on the resultant dominant hoisting load in terms of its total, maximum values as well as its variation over time. *It is important to establish correct roll and pitch acceleration motions which match real world pontoon operation*, while heave motion effects are mostly negligible.

3.4. Model verification

This section is meant to establish representative values of significant loads affecting crane upper arm and provide verifiable proof that values can be considered as correctly defined.

The most reliable method for verifying the model is to perform a separate experiment and compare the accuracy of acquired data between simulation and separate experiment. This is a common practice for verifying all kinds of simulation models in multiple areas of research [83] and is not limited to only MBD analysis. When direct data is not available, there are other ways which can substitute real data, although to a lower level of confidence. As the data for verifying accuracy of analysed crane MBD model is limited to only pontoon displacement, the rest of acquired data is based on findings in the literature.

Based on screening analysis results, it is clear that there are five main factors which require calibration and verification:

1. Hoisting load in terms of its magnitude and effects relating from other loads affecting its response.
2. Operator cabin structure load which contains constant weight but experience some variation due to dynamic motion of the crane.
3. Crane motion and acceleration profile linked to luffing acceleration and extension length setup.
4. Hoisting acceleration setup defining how quickly transported material is lifted up or down during operation.
5. Pontoon roll and pitch setup which experience motion when crane is luffing forward or grabs/releases material.

Each of these factors are important for acquiring accurate loading conditions of the evaluated structure and can be calibrated and verified in the following manner:

1. Hoisting load - calibrated with the adjustments to maximum rated load by the crane, adjustments to motion profile and pontoon motion calibration. Hoisting load magnitude can be verified through hand calculations of hoisting load as defined in NEN2018 [66] crane standard.
2. Operator cabin structure load - acquired based on measurements taken during crane disassembly (4000 kg) - accurate value is known and possible to confirm based of static measurements of cabin weight.
3. Crane motion and acceleration profile - defined through available video footage of crane in operation, which also contains analog measurements for establishing motion in terms of both length of operation and displacement of luffing, slewing and hoisting.
4. Pontoon roll and pitch setup - calibrated based on acquired sensor measurement results, using inertial loads which were defined as sensitive towards imposing motion on the crane. Possible to verify with independent work cycles that are available in the measurements.

3.4.1. Body loads

Body loads refer to relevant non-inertia-based loads affecting the structure of the upper arm, specifically hoisting load and operator cabin structure load. Their accuracy can be determined in a similar fashion by comparing loads when they are not affected by dynamic motion in the simulation and when using hand calculations.

Hoisting load

For hoisting load, in the simulation environment when crane does only a single motion - grabbing and hoisting up the load - it experiences force magnitude equal to 3.07E+05 Newton. This value can be compared using hand calculations based on NEN2018 standard for *Crane loads and load combinations*, which provides a way to establish a general load case based on crane parameters, with a load factor value. The hoisting load under acceleration is calculated using:

$$F_h = m_h * g * \phi_h \tag{3.3}$$

where F_h is the hoisting force; m_h is the hoisted mass (grab mass + material mass); g is the gravitational acceleration constant; and ϕ_h is the hoisting coefficient value.

Hoisting coefficient for specific crane motion is defined through tables illustrated in figure 3.10 where first hoisting class is defined based on the stiffness of the cable and smoothness of acceleration. For analysed crane, it is done using a relatively slack cable setup with potentially uneven hoisting acceleration present in the model - this establishes hoisting class A. As hoisting class A coefficient χ is equal to 0.3 - meaning that under common crane hoisting acceleration of 2 m/s, hoisting coefficient value is equal to 1.3 (as seen in the picture B of figure 3.10). Based on this estimation, value of the hoisting force F_h is equal to:

$$F_h = m_h * g * \phi_h = 25000 * 9.81 * 1.3 = 3.19E+05\ N \tag{3.4}$$

When comparing both values it is clear that the error of 3.7% between values is heavily comparable and it can be assumed that simulation results present calculated values with reliable precision.

character of the crane system incl. hoisting cable [1]	Course of the accelerations during the hoisting movement [2]		
	even	uneven	very uneven (bumpy)
relatively slack	a	a	b
normal	a	b	b
relatively stiff	b	b	c

a)

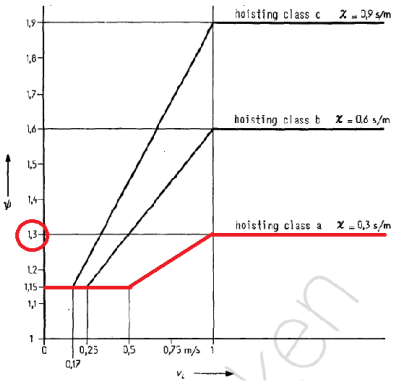

b)

Figure 3.10: Value setup for acquiring hoisting coefficient value, with A showing chosen hoisting class and B showing hoisting coefficient value based on acceleration speed [66].

Operator cabin structure load

When it comes to operator cabin load - its result can be confirmed using a simple static weight calculation:

$$W_{cs} = m_{cs} * g = 4000 * 9.81 = 3.92E+04\ N \tag{3.5}$$

where W_{cs} is the static weight force; m_{cs} is the total measured mass of the operator cabin structure; and g is the gravitational acceleration constant. Comparison with results acquired in MBD analysis when crane is static show that result of cabin suspension load setup is comparable, having the magnitude value equal to *3.89E+05 N*, presenting an error of 0.8%, which is acceptable and shows that simulation results are reliable.

3.4.2. Operational inertia loads

This section concerns setting up hoisting and luffing acceleration profile, as well as extension position of the crane. As this data is not directly available from standards or taken digital measurements, verification of these factors is assessed by observing video data of crane operation taken from inside of the operator cabin which contains analog measurement setup for all relevant crane displacements. Under closer inspection of this video footage it is visible when crane starts hoisting and luffing as well as how operator uses his controls.

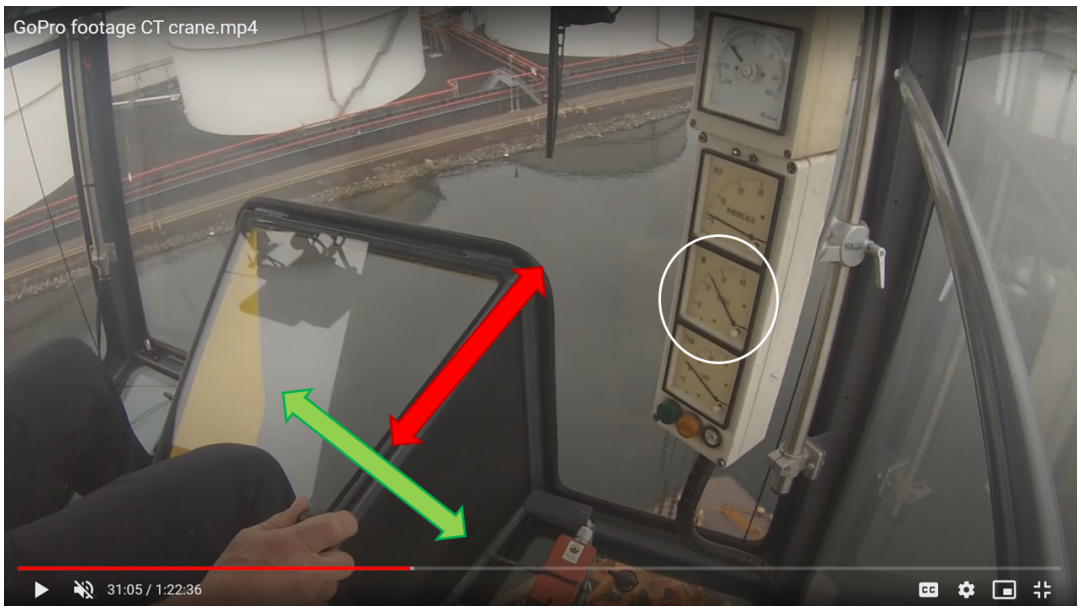

Figure 3.11: Operator control principle of hoisting (red), luffing (green) and luffing extension position (white)

.

As illustrated in figure 3.11, the operator initiates hoisting acceleration/braking by pulling the handle in forward/backward directions (red arrow) while luffing is initiated through pulling the handle left or right (green arrow). This, along with the analog measurement of luffing extension length provides enough information to how much distance has been travelled and when acceleration/braking is initiated for each motion. By calculating travelled distance and lifted height based on previous measurements discussed in chapter 3 - acceleration speeds of each operation has been established: maximum hosting acceleration being equal to $0.8 m/s^2$ and luffing acceleration equal to $0.6 m/s^2$. These values are then adjusted in acceleration setup of MBD model. Along with defined luffing extension positions based on the analog measurement results at specific moments in time - verification the accuracy for the operational inertia loads can be considered as successful.

Pontoon motion effects

This verification step deals with calibrating and verifying the motion of pontoon. As pontoon motion can impose acceleration effects relevant to crane hoisting load response, it is important to define accurate values of both pitch and roll, so their displacement would match real pontoon displacements. As the video footage of crane operator motion (which has been described in last subsection) is accompanied by digital measurements of pitch and roll displacements - it is possible to have very accurate data for evaluating how these motion measurements differ in the simulation model and real life when identical motion profile is established in both situations.

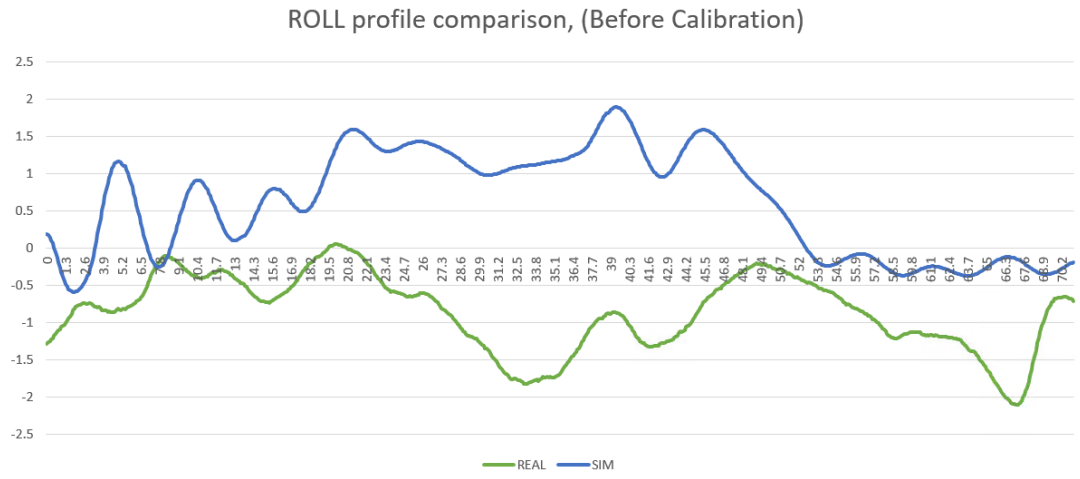

Figure 3.12: Comparison of roll profile between measured (green) and not calibrated simulation values (blue).

Figure 3.12 illustrates a comparison between resultant pontoon roll displacement in the model and when it is taken from the sensor measurement. It is clear that the error in the standard model is very significant and crane pontoon parameters need to be calibrated accordingly. Similar observation could be made from observing pitch displacement result comparison. This simulation setup experiences displacements of higher total magnitude and appears to experience high fluctuation, giving the impression that spring setup for pitch and roll implementation in MBD environment is modelled incorrectly. Additional differences between crane motion visible in the model are result of slight misalignment of other motion effects present in the model, such as luffing and slewing times and accelerations.

The calibration procedure for this motion has been completed using *Design Evaluation Tool* of Adams MBD software, with which it is able to optimize the specified factor variables until a more optimal measured response is reached. The process of optimization is meant to even out the magnitude and damping values of pitch and roll displacement through an introduction of error measurement, which calculates average difference of two displacement measurements (real and simulation). Measurement data is imported into Adams and used as a constant reference point for run simulations. Factors present for adjustment are pitch and roll spring parameters: damping coefficient, stiffness coefficient and spring preload. Simulations for pitch and roll has been run separately and each simulation has a set maximum iteration number set to 50 runs.

Optimization algorithm has been run several times as through initial runs as it has been observed that displacement is also sensitive to crane motion setup. This meant that first slight adjustments to crane motion profile had to be made, otherwise the optimized error was too large and inconsistent for evaluation through

optimization algorithm as load peak values did not properly match in specific time moments. This shows that load peak values have to be first adjusted to match between simulation and real measurements and only then reliable results can be acquired.

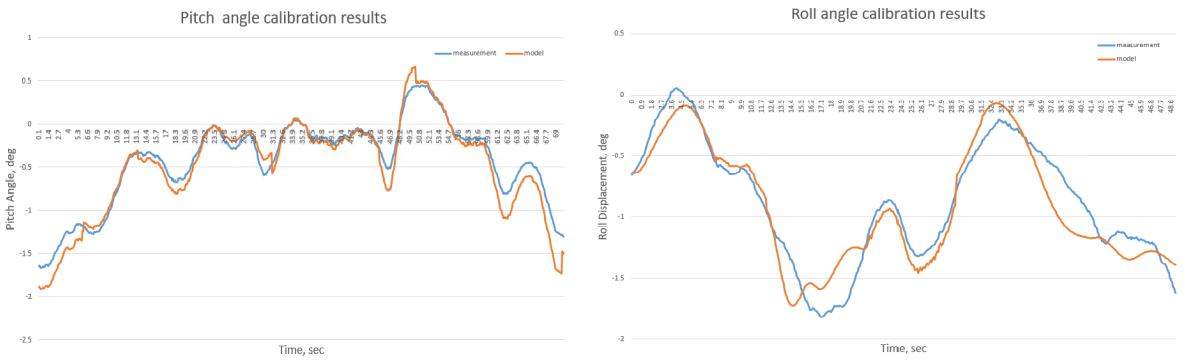

Figure 3.13: Comparison of pitch and roll profiles after calibration, in relation to motion measurements.

Figure 3.13 presents the profile of pitch and roll angular displacements after completing calibration on used crane operational profile. Each optimization run completed the full amount of 50 simulation runs in order to find most optimal result value. Error between operational runs has been reduced to a mean value of 8% and which is a result that ensures consistency in crane and pontoon motion. It is possible that increasing allowable simulation run limit might allow to increase accuracy, however the current error margin is already low and thus calibration result can be considered as satisfactory for the purposes of this research. Optimization experiment setup overview is presented in table 3.2.

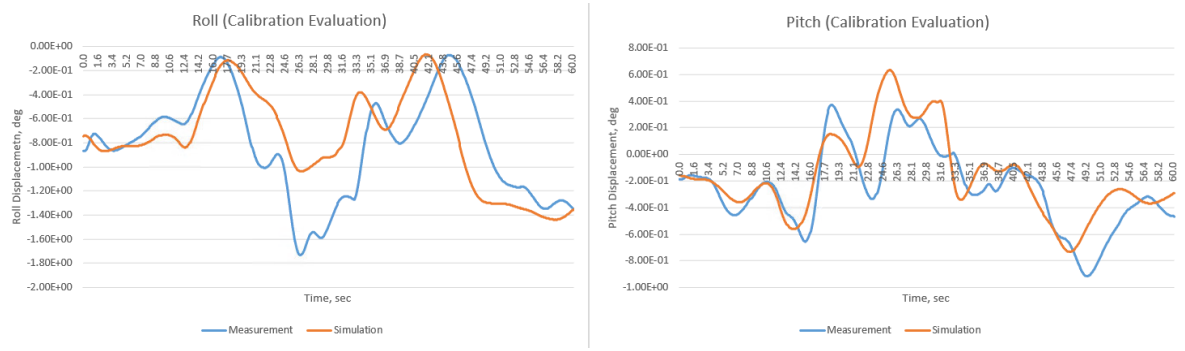

Figure 3.14: Comparison of pitch and roll profiles of an independent run, meant to check the validity of calibration.

However, since this is a specific case for which experiment has been calibrated, it is worth investigating how calibration profile fares against an independent operational profile, as illustrated in figure 3.14. Results show that an independent motion profile still maintains relatively reasonable accuracy to the crane motion model, however the error between measurement and simulation results have increased to 34% for roll simulations and 16% for pitch motion. This result shows that it is almost impossible to fully calibrate pontoon motion to minimize run error to zero, however the resultant independent model is still representative of pontoon motion and can be considered as verified. Additionally, it is assumed that adjusting crane motion profile of an independent run to more realistically fit acceleration profile of real motion, the error could be further reduced as not the entirety of present error is assumed to be result of spring component calibration. Heave stiffness and damping coefficient calculations are based on hand calculation principles described in Wierenga [90]. Due to the lack of measurements and low statistical significance of the measurement, it has been validated by its maximum amplitude of displacement staying under 0.45 meters (actual value being 0.29 m), as it has been defined as a max heave displacement limit for container vessels by Smitz [45].

Table 3.2: Overview of optimization experiment setup for pitch and roll spring parameter adjustments meant to reduce average error between simulation and measurement results.

Experiment 1 (Pitch)		**Experiment 2 (Roll)**	
Goal:	Minimize average error between real measurement and simulation	Goal:	Minimize average error between real measurement and simulation
Optimized variables	1. Spring Preload 2. Spring Damping Coefficient 3. Spring Stiffness Coefficient	Optimized variables	1. Spring Preload 2. Spring Damping Coefficient 3. Spring Stiffness Coefficient
Max number of iterations	50	Max number of iterations	50
Result	6% error	Result	8% error

3.5. Result overview

In this section, final loading results are summarized which will be used for applying body and inertial loads into the finite element analysis of the upper arm.

When it comes to the final outcome of load quantification procedure, final results have been gathered to represent load setup which will be used for establishing stress states in the FEA model and for performing fatigue assessment in the upcoming steps. Responses have been acquired from the Adams Post-processor which show the time history of hosting load, operator cabin structure load as well as experienced accelerations by the upper arm at its center of mass. Results are gathered with a time step of 0.1 seconds for a total duration of 70 seconds - equaling to a overall setup of 700 steps. Results are illustrated and summarized in this section.

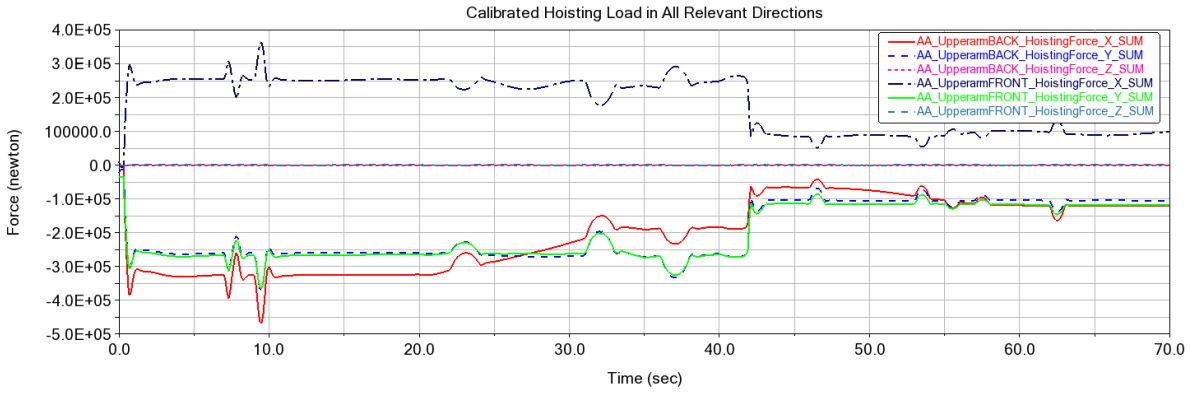

Figure 3.15: Results of calibrated hoisting load for front and back setup of the upper arm structure, separated into cartesian X Y Z directions

Figure 3.15 illustrates cumulative calibrated hoisting load setup for both front and back positions of the upper arm. Results show that overall front and back of the crane being loaded to a relatively similar degree, only the X direction (along the length of the upper arm) being linked to the luffing angle of the crane - experiencing higher force when crane is retracted, and undergoing a reduction in force during forward extension.

3.16 shows how temporal profile of operator cabin load changes over time. As it can be seen from the results, cabin load experiences load spiked present due to dynamic motion that is exerted on the crane. It appears that presence of this motion is beneficial for cabin load as crane motion reduces load response in this direction, which would otherwise stay constant. However fluctuating response does lead to loading cycles, which effects will be quantified in upcoming chapter.

Finally, figure 3.15 illustrates how crane is accelerated in different directions during its normal operation. Judging from the results it is clear that acceleration in X direction (along the length of the crane structure) appears to be largest in magnitude throughout almost entire time history of crane motion. These are results of cumulative motion of the crane including luffing, slewing, pitch, roll and heave acceleration effects. Acceleration spikes are experienced by the crane when specific motions are initiated as well a large spike during load release is also present. All these load responses can be exported in text format and imported as load histories in ANSYS to continue towards fatigue assessment, which will be discussed in upcoming chapter.

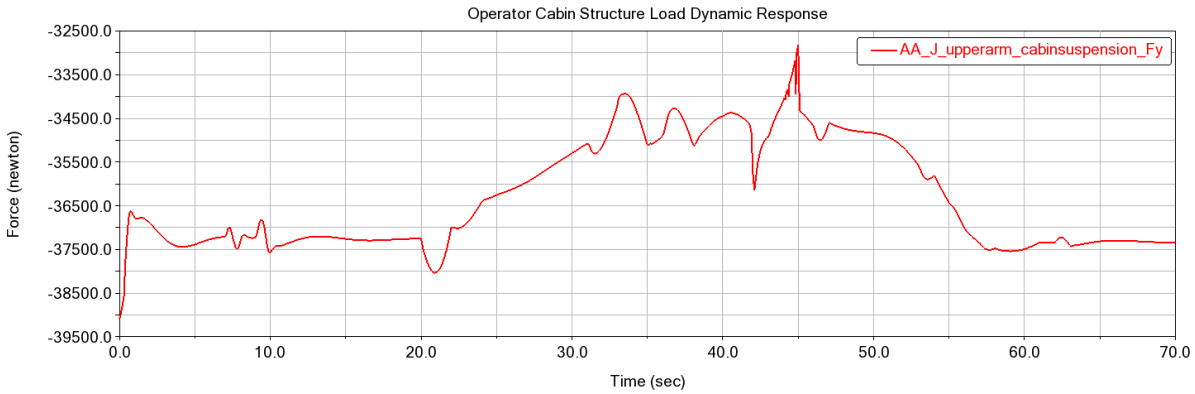

Figure 3.16: Results of calibrated cabin load in the dominant Y direction

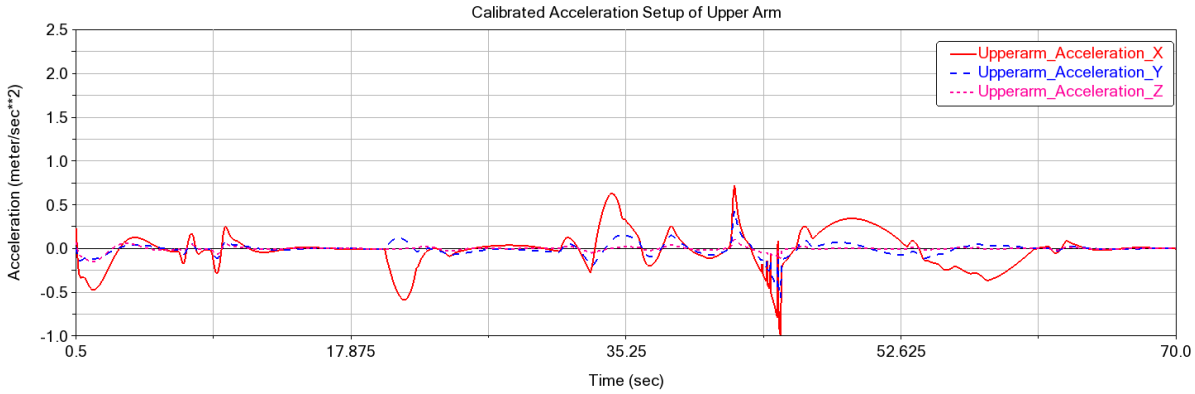

Figure 3.17: Results of calibrated acceleration setup experienced by the crane upper arm structure under regular work cycle conditions.

3.6. Conclusion

This section concludes results and observations made and provides answers to research questions indicated at the beginning of this chapter

In this chapter, a temporal stress response has been established using multi-body dynamic simulations of analysed crane operation. Crane model setup, which was initially established in Tawjoeram [86] has been evaluated in terms of its accuracy through available data of part mass and inertia setup, body contact formulation and introduced flexibility to slender parts such as crane upper arm, front arm and rear arm. A motion profile has been established using available video footage of crane operation in a manner to fit a common working cycle, representative of real motion in terms of time of each action (grabbing, luffing, slewing, hoisting), as well as resulting magnitude of displacement. Using the aforementioned model, relevant body and inertia loads have been evaluated using a design of experiments screening technique to assess how they impact stress accumulation within the upper arm structure, which loads are most statistically significant and which aspects affect their responses the most. Using the aforementioned steps, answers to the following sub-questions have been found:

Which factors in the MBD crane model setup most significantly affect load responses relevant for acquiring boom stress cycle?

1. Hoisting load is objectively the most dominant load factor for affecting magnitude of stress response in the crane upper arm - in order to accurately simulate FEA stress response it is critical to acquire accurate hoisting load response with MBD simulations.

2. As hosting load response is heavily influenced by dynamic effects (specifically luffing and hoisting acceleration, pitch and roll motion) that create swinging motion and impose fluctuation in force on hoisting load response - these inertial loads had to be established with accuracy in mind. Additional load factors, such as slewing acceleration and heave motion do not have a large effect on hoisting load,

meaning their establishment can be sufficient based on general predefined setup without need for particular verification.

3. It has been observed that including flexibility effects into crane upper arm, front arm and rear arm does not particularly effect relevant load responses. Combined with the fact that inclusion of flexibility significantly increase computational complexity of multi-body dynamic simulations - it is clear that flexible components are not needed to acquire accurate loads for finite element analysis.

How to verify that the accuracy of acquired load results is representative of realistic loading conditions?
Establishment of statistically significant factors determined through screening analysis can be verified to match real world results through either available measurement values (as for pontoon roll and pitch motion and luffing and hoisting speeds), or calculations based on relevant standards (as was done for hoisting and cabin suspension load setups). Working with a limited amount of empirical data acquired from the actual crane does limit the scope of model validation, however most important loads were setup in a manner which matches present measurements of pontoon motion and video footage of crane displacement and load data acquired during real crane operation. This provides a solid basis to conclude that load adjustment has been completed successfully and it can be used for application within finite element analysis.

With the answers to these sub-questions it is now possible to answer the research question:
How can multi-body dynamic simulation approach help with establishing representative loading conditions of a crane work cycle within the time domain?
Multi-body dynamic simulation of crane motion allows to establish load setups experienced by the crane within the time domain - meaning that loads acquired using this method include data of any potential load fluctuation and acceleration effects at multiple time steps, which are not present when establishing loads using static loading approach (which uses one time step for each load). MBD approach is less conservative when compared to static method as static method uses safety factors to account for any potential dynamic load effects, while multi-body dynamic simulations capture all load responses in real time making it potentially more accurate. Finally, the addition of time domain within load acquisition allows to evaluate stress response within time domain as well, which is important if multi-axial fatigue analysis is to be performed. Measuring how stress angle changes over time of crane operation can present whether there is a significant presence of non-proportionality within stress response, which influences both the choice of multi-axial fatigue assessment approach as well as potentially having effect on the magnitude of fatigue damage accumulation. These aspects will be evaluated in upcoming chapters.

4

Fatigue assessment

This chapter deals with establishing and performing fatigue assessment meant to evaluate potential fatigue damage accumulation in the main joint of analysed crane upper arm and to assess why joint appears to be prone to crack propagation. Fatigue assessment is performed using two approaches - based on nominal stress and hot-spot stress methods. Results are compared to evaluate their accuracy in accordance to their strengths and weaknesses as well as to crack propagation locations in the real joint structure.

Here the following research questions will be answered:

1. *How does incorporation of stress concentrations into fatigue assessment affect resultant fatigue life estimation in relation to nominal stress fatigue analysis?*

2. *What is the main reason of joint failure for the analyzed lemniscate crane?*

4.1. Background

This section provides an introduction into the chapter and briefly explains why and how fatigue assessment is performed

The key goal of research described in this report is to evaluate fatigue damage accumulation in the problematic joint that is located at the crane upper arm. This is the location of aggressive crack propagation which has been observed within the Cornelis Tromp 25T and the point of previous structural failure for a crane of identical design. As fatigue damage is most commonly evaluated using nominal stress approach, which is popular for its simplicity - results presented in this chapter are meant to assess whether it is possible to observe potential fatigue failure in the crane using nominal stress approach. Additionally, because nominal stress has a weakness of not including effects of stress concentrations - an additional fatigue assessment approach that is based on hot-spot stress is performed to observe difference in estimated fatigue damage. Results of both approaches are compared to assess whether for analysed tubular joint structure it is preferable to include effects of stress concentrations into its problem formulation.

For welded tubular joint structures fatigue damage tends to accumulate around weld toe. According to Kawahara and Iwasaki [43], cracks often initiate as multiple surface cracks at the toe of weld reinforcement of the chord-brace interface for circular beams. Over time under cyclic loading, crack growth extends in two directions: growing around the circumference of the beam and increasing in crack depth. Because stress in welded structures is a critical factor for estimation of fatigue life for welded structures, it is critical to assess the fatigue damage accumulation at the welds of problematic upper arm joint.

Fatigue life is commonly established though experimental tests which assess different geometries, materials, loading conditions and environmental conditions. However as high cycle fatigue testing is a very time-intensive process - the amount of tests is always going to be limited. Additionally there is a very large variety of factors which can influence fatigue life. This includes:

1. Material qualities

2. Geometry setup and surface quality

3. Environmental effects such as temperature changes, wind and wave load effects, exposure to corrosive chemicals.

4. Loading conditions, both cyclic and exceptional loads.

5. Weld quality and any impurities/defects, etc.

Combinations of all these factors continuously increase the amount of tests that have to be performed for accurate fatigue life data. This limitation concerning the lack of experimental data poses a need to rely on estimations and calculated assumptions when assessing fatigue life of a structure. Most common cyclic damage estimations rely on simplification strategies, such as:

1. implementing static loads with use of safety factors which help to approximate dynamic load effects

2. Using simplified beam elements in FEA environment to model analysed structures.

3. Performing fatigue assessment using nominal stress approach.

These strategies allow to perform fatigue damage evaluation in a streamlined fashion, thus saving time and resources required to assess integrity of the structure. However, since these strategies heavily rely on simplifications, it is possible that they might be unable to account for all important factors which lead to failure of a particular structure. As it has been seen within the analysed lemniscate crane variant - cracks tend to propagate at the same locations in the upper arm joint. It is assumed that reliance of estimations during structural assessment of the design has missed some flaws in design or load definitions which tend to accumulate fatigue damage over the lifetime of the crane.

Fatigue analysis methods presented in this report all consider a detailed geometric model of the crane with applied loads that are linked to time history of crane working load cycle. Within this chapter these parameters are assessed with two different fatigue damage estimation approaches - specifically nominal fatigue and hot-spot fatigue described in sections 4.3 and 4.4 respectively.

4.2. Finite element model

This section discusses the principle and process of establishing a reliable finite element model that could be used to assess stress states and fatigue life of analysed crane upper arm structure. It describes main steps and tasks performed to acquire a representative model capable of completing its defined task of representing real-world setup of the crane.

In order to evaluate fatigue damage, finite element analysis is used to acquire relevant response values. To ensure result accuracy - the FEA model has to be setup to characterise real-life crane structure as representatively as potentially possible, while reducing computational time and taking into account the requirements of performed fatigue analyses. This section is meant to explain definition of finite element analysis setup that is used for assessing crane stress and fatigue damage.

4.2.1. Scope of model setup

First step in establishing a FEA model is defining simulation scope. This concerns establishing the extent of geometry that should be modelled for acquiring stress results. Oftentimes it is not beneficial to include the entirety of evaluated structure into fatigue analysis if only localised results are relevant. This means that if a specific model can be realistically defined with a partial structure setup - it can significantly simplify both simulation establishment process and its computational complexity. For this purpose, it important to determine how much of the crane has to be included in finite element simulation to accurately estimate stress responses appearing in the problematic upper arm joint.

As the subject of analysis is localized to the joint, located within crane upper arm structure - modelling an entire crane might not be the most efficient approach. On the other hand - limiting FEA model scope to only the main joint provides issues with potential setup of boundary conditions that tend to affect simulation results. A sufficiently limited analysis scope has to be determined based on the specifics of analysed problem.

Whether it is beneficial to model full crane for FEA analysis highly depends on specific crane type. During loading/unloading procedures ship-to-shore (STS) and other types of gantry cranes contain only a limited amount of moving parts (e.g. trolley and grab) which are generally not modelled in an FEA environment. However portal cranes which move cargo by performing luffing and slewing motions include a large amount

of moving parts - crane legs continuously change position creating a large number of setups that should be assessed for realistic results as illustrated in figure 4.1, making modelling of a full crane much more complex - this is the case for analysed lemniscate crane as well.

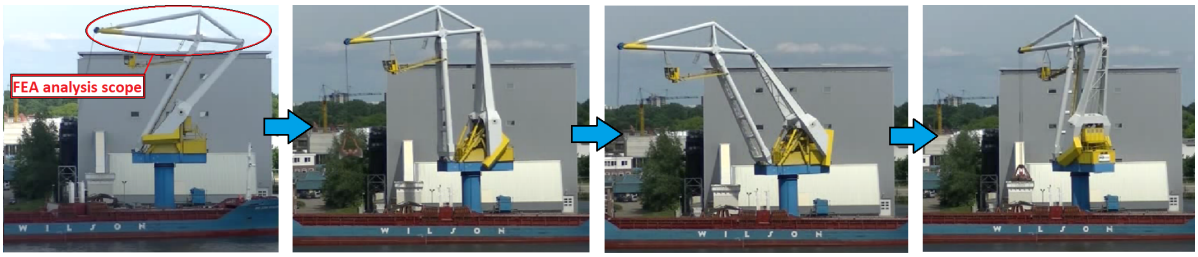

Figure 4.1: Crane position overview of Cornelis Tromp 25T lemniscate crane during its work cycle. Finite element analysis model scope is highlighted in red.

Nevertheless there are examples in the literature which show that modelling a full crane for fatigue assessment is a feasible approach. Both simplified [52, 86, 94] or fully detailed [77] models of analysed cranes can be applied, depending on the analysis scope and requirements. Modelling of the full crane is beneficial when finite element analysis of crane structure deals with the entirety of the structure as in Li et al. [52], Samchuk and Bos [77], Tawjoeram [86]. However this approach has multiple drawbacks that limit the scope of analysis, potentially affecting accuracy of results or requiring a significant amount of work and computational resources to setup and perform FEA simulations. Drawbacks of modelling entire lemniscate crane structure include:

1. Requirement to create multiple sets of crane model at different extension positions (when crane is contracted and extended at different levels). This is a time and effort-intensive process which is not able to capture all possible load situations - potentially missing the critical load setup.

2. Setup requires a large amount of modelling work that relies on the accuracy of the whole crane model setup (errors in modelling of one part might lead to errors in the rest of the model).

3. A large number of mesh elements and nodes is needed - this can significantly increase computational complexity.

4. This approach does not allow importing of loading results gathered through multi-body dynamic analysis for luffing cranes, as loads experienced by the structure are time-dependent and directly linked to current crane extension position at each moment in time.

Due to the aforementioned weaknesses of modelling a full crane setup - a different approach to FEA modelling will be taken - localization of simulation scope has to be performed. The prime focus of this research concerns the analysis of fatigue damage in the joint of the upper arm structure which connects forestay, backstay and pylon legs. As limiting FEA model to only the main joint geometry can be compared to model setup of conventional tubular joints - this has potential benefit of modelling simplicity. On the other hand this approach also possesses weaknesses of tubular joint setup - specifically difficulty to realistically constrain the model while applying realistic loads affecting the structure. This issue is commonly solved by extending the length of joint beams which is not possible for the purpose of crane joint analysis as it would provide unrealistic results. For this purpose the scope of finite element analysis is set at an intermediate point - specifically limited to modelling mainly the structure of the upper arm, highlighted in red in figure 4.1. With this approach, crane upper arm is separated at all joint positions from the rest of the crane (disconnected from crane front and rear arms, as well as operator cabin structure), leaving only the main upper triangle present in the FEA model. This allows to avoid issues of modelling a full crane while at the same time providing ability to accurately define loads and boundary conditions, which affect the upper arm joint in a manner that wouldn't be possible if only the joint itself was to be modelled. Finally this method of modelling mainly the upper arm allows to streamline load import procedure from MBD to FEA environment and apply them at representative locations of their effects, without sacrificing application accuracy.

4.2.2. Geometry definition

Finite element model is established using a detailed computer aided design (CAD) model of crane upper arm structure, acquired as a parasolid from representatives of Maja Stuwadoors B.V[1], which operate Cornelis Tromp 25T crane in the port of Amsterdam (The Netherlands). This upper arm geometry is illustrated in figure 4.2. This is a fully detailed production variant of Cornelis Tromp 25T crane upper arm and the model serves as a realistic representation of crane geometry. Using a detailed geometry setup allows to model and evaluate stress concentration effects which potentially contribute towards fatigue damage accumulation.

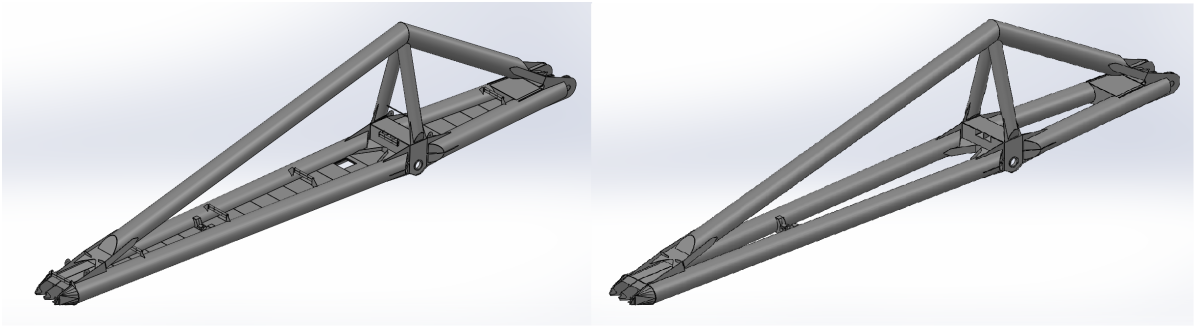

Figure 4.2: Result of CAD model simplification for crane upper arm. Here a) original model of the structure; and b) simplified model used for FEA analysis;

To simplify analysis FEA setup - CAD model of the upper arm is simplified as shown if figure 4.2. This simplification is performed by removing difficult-to-mesh parts that objectively do not add any particular benefit towards changing stress results for the analysed joint structure. In summary, following main changes have been made between original and adjusted crane models:

1. small, low-weight parts have been removed - this includes cable rollers, bearings, bearing covers, sheet metal plates used mainly for walking access, and connection points for components not present in the model;

2. Fastener holes used mainly for assembly purposes have been filled up to create uniform components, meant for optimal mesh creation;

Aforementioned changes allow to create a more streamlined process of meshing the structure and reduce number of mesh nodes without affecting simulation results. Adjusted model is the final part of geometry setup that is used in FEA environment for acquiring stress responses needed for fatigue assessment.

For the purpose of FEA analysis *ANSYS Workbench* software is used. This is a streamlined simulation environment which is able to combine multiple tools for a versatile simulation procedure. A static structural analysis is used for creating FEA model of the upper arm with established detailed crane geometry imported as a parasolid.

4.2.3. Material properties

Material assigned to the entirety of the crane model is S235 structural steel. It is a low carbon manganese steel that is very well suited for welding. It is ductile material, commonly used in the industry for manufacturing structural components, such as crane structures. This is the steel from which actual crane structure is made, which should provide a good representation of the actual crane in simulation environment. Main material properties are summarized in table 4.1.

Table 4.1: Material property overview for S235 structural steel used in upper arm construction.

Material Grade	Standard	Density, kg/m-3	Youngs Modulus, Pa	Poissons Ratio	Yield Strength, Pa	Ultimate Strength, Pa
Steel S235	EN 10025-2: 2004	7850	2.50E+11	0.3	2.50E+09	4.60E+08

[1] https://majastuwadoors.nl/en/

Because the purpose of finite element analysis is to evaluate fatigue damage in the problematic joint - a linear material is used. This is based on the principles of high-cycle fatigue damage evaluation which deals with continuous cyclic loading over an extended period of time. This means that the analysed structure is not expected not to experience plastic deformation on a macro scale. In the FEA simulations it is assumed that structure remains in elastic region, thus measured stress is not capped to material yielding limit and the FEA model results do not take into account potential stress redistribution in the case that the structure experiences stress above its yielding point.

4.2.4. Boundary conditions

The key in successful boundary setup is defining constraints and loads in a manner which most accurately mimic real setup of analysed structure. As finite element analysis scope is limited to modelling crane upper arm structure, this allows representative definition of model boundaries. This section explains the setup for FEA boundary conditions which are used to acquire stress setup that is capable of representing stress distribution in the real upper arm joint.

Constraint setup

Establishing representative constraints is an important aspect of finite element analysis, because the way how structure is constrained can significantly affect resultant stress response. A model that is over-constrained can locally limit deflection around constraint locations, while an under-constrained model can impose unrealistic deflections in directions which should not experience deformation. Both aforementioned approaches result to an unrealistic stress distribution within the analysed structure.

Approach for defining realistic constraint setup for crane upper arm is based on the principle of emulating real crane setup. As modelled upper arm is connected to the front and rear arms at two main locations with rotary bearings (in the middle and back of the upper arm respectively as shown in figure 4.3). Based on this setup constraints are applied accordingly.

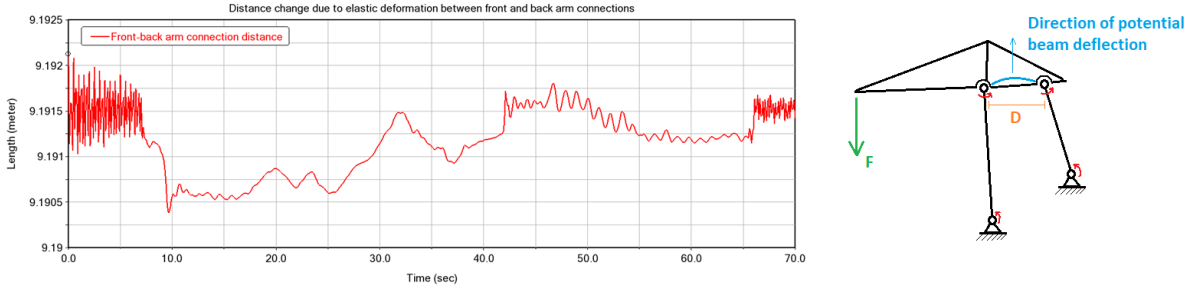

Figure 4.3: Results of distance change between upper arm connection joints during crane operation cycle.

Secondly, there is a possibility that an additional translational degree of freedom might have to be released. This assumption is based on the hypothesis that deformation of the upper arm during hoisting operation might allow retraction of the distance between upper arm connection points of the front and rear arms (as connecting beams are flexible and tend to bend during hoisting operation). To determine whether this change in distance is significant enough for inclusion of additional degree of freedom in direction along the length of upper arm - a flexible multi-body dynamic model of the crane has been used to measure distance between both upper arm connections during crane operation. Graph illustrated in figure 4.3 presents the measurement results, which show a maximum distance change ΔD between both connections is equal to $1.6E-3$ m, which accounts for a 0.018% change in total distance between connections - concluding that distance change is insignificant to require an inclusion of additional degree of freedom.

Based on aforementioned assessment - for a static structural analysis of the crane, which will be used for assessing crane fatigue life, structure is constrained only with rotational joints (each providing 1 rotational degree of freedom) as shown in figure 4.4.

It can be concluded that constraints should be applied at two positions:

1. Rotational joint on two circular faces in the middle of the upper arm, where it is connected to crane front arm.

2. Rotational joint placed on four circular surface faces at the back of the upper arm, where it is connected to crane rear arm.

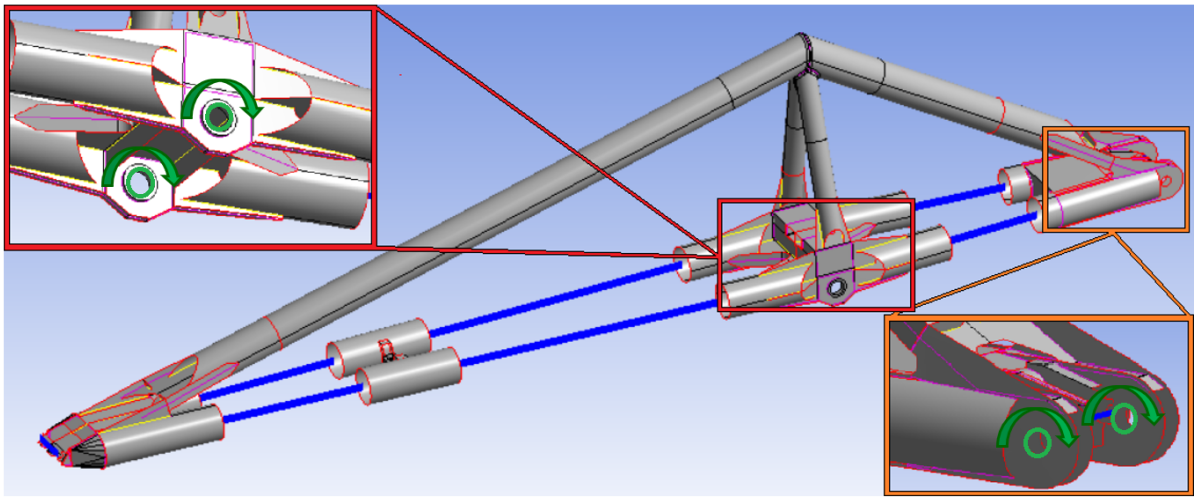

Figure 4.4: Constraint positions as well as directions of free motion for each constraint (green).

Both constraints are meant to imitate operation of a rotary ball bearings which allow a single rotational degree of freedom per connection. This fully constrains the structure while allowing flexible displacement of the joint around the joints. Final constraint setup is illustrated in figure 4.4 which indicates positions and surfaces where constraints are applied (with specific surfaces coloured in green) as well as direction of their allowed motion (marked with green directional arrows). Setup of this constraint structure is meant to simulate the connection of upper arm to the front and read arms using representative joint setup as it is present in the real crane structure.

Load setup

Load setup defines external effects which affect analysed structure and are modelled in FEA environment in the form of forces, moments and accelerations. Loads affecting the crane upper arm structure are marked in figure 4.5 and can be summarized as follows:

1. Earth gravity - it exerts constant inertial load towards the ground direction (from top to bottom of the crane) (marked A in figure 4.5).

2. Body acceleration - it encompasses all inertial loads related to crane motion and subsequent upper arm displacement (luffing, slewing operations, as well as pontoon pitch roll and heave motion) in the form of body acceleration at a specific moment in time. This acceleration is positioned at the center of mass for the upper arm structure at the same location it has been measured at within MBD environment (marked B in figure 4.5).

3. Hoisting load - it simulates weight imposed on the upper arm structure when it is hoisting and transporting cargo. Load is modelled through cable tension as it affect crane structure at the positions where cable pulleys are connected at the front and back ends of the boom. It is thus separated into two load entities - one at the front boom and one at the back of the upper arm. (C and D in figure 4.5).

4. Operator cabin structure load, which models cabin weight exerted on the upper arm structure and provides downward pull in the middle part of the upper arm front jibs (located at position E in figure 4.5).

An important part of performed fatigue assessment is inclusion of time domain into the stress input. As analysed lemniscate crane upper arm structure experiences significant motion during its operation - all aforementioned loads affecting modelled upper arm structure have been modelled in time steps, with a time-domain included in the setup. Temporal loads were acquired using multi-body dynamic simulations as described in chapter 3. These loads, sampled at 0.2 seconds are imported into FEA environment as inputs of cartesian X Y Z components, and then modelled into a continuous loading cycle in a time step format (330 steps in total) lasting a total duration of 66 seconds. Temporal hoisting load applied to the front pulley location is illustrated in figure 4.6.

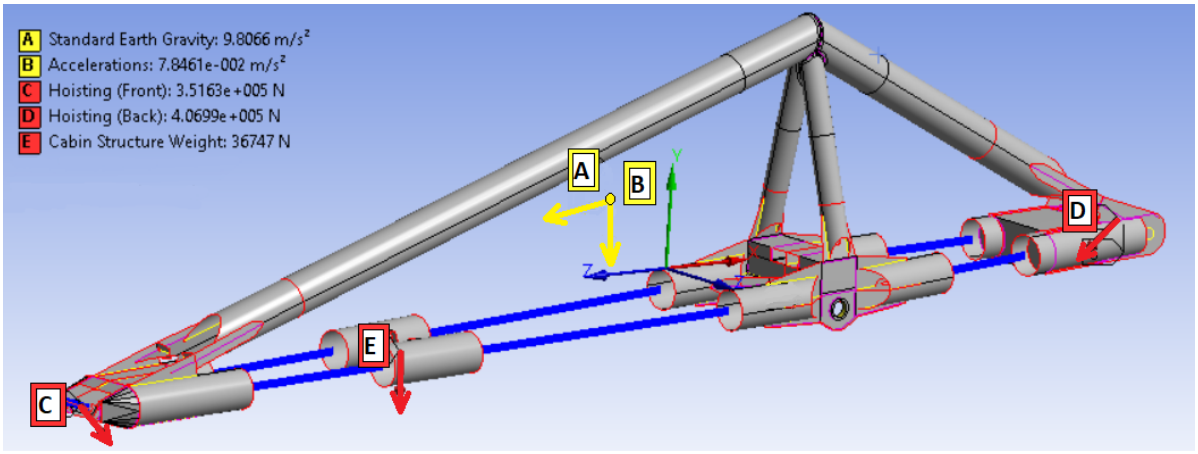

Figure 4.5: Position of inertial (yellow) and body (red) loads affecting crane upper arm structure

Limitations within load establishment

It is worth noting that loads have been acquired using simulations rather than measurements. These simulations have been verified in chapter 3, but their validation has been limited to pontoon motions, due to lack of empirical data. More importantly, the load setup applied to the upper arm structure is established for a single loading setup case. Although it is set up in a manner which presents a representative general operational case that has been modelled in accordance to real operation of the crane, it has to be acknowledged that each operational cycle has some variation present which cannot be fully represented with a single loading/unloading operation cycle. These limitations have to be taken into consideration when evaluating accuracy of implemented load establishment.

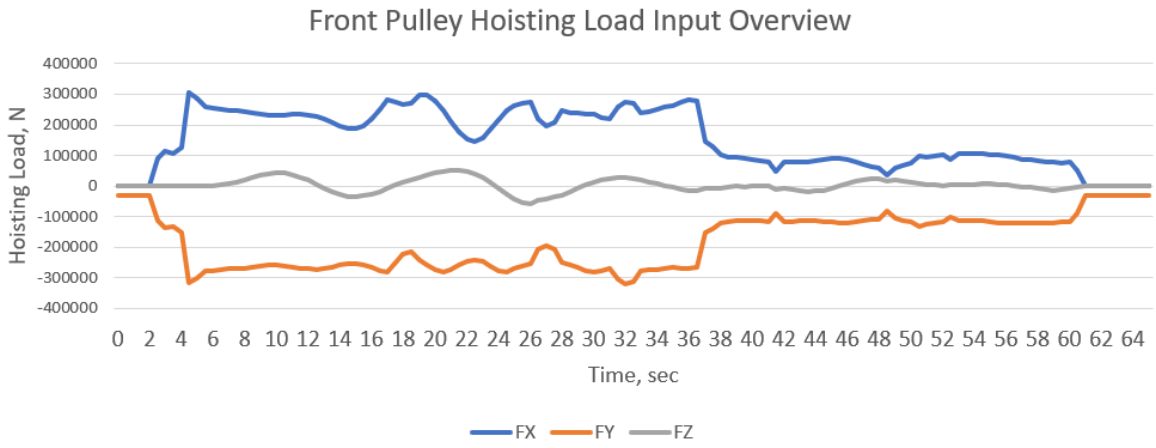

Figure 4.6: X Y Z components of hoisting load input applied to front pulley location of the upper arm

4.2.5. Mesh setup

A critical aspect of FEA analysis is a definition of model mesh. Mesh quality, type and size significantly affects result accuracy and computational complexity of the model, thus requiring establishment of FEA analysis that provides sufficiently accurate results, while limiting simulation run-time to a sufficiently reasonable duration. For this to be possible, several important factors have to be accounted for. Establishment of mesh setup which fulfills the defined requirements is explained in this section.

Element type

For thin walled components such as hollow beams and plates, it is often possible to assume that the FEA setup can be modelled using surface shell elements. Such setup is applicable in cases where plane stress conditions can be fulfilled, which state that the overall majority of the stress experienced by the structure acts

in a 2D plane. For circular structural components, such as those used in tubular beams and thin plates (which compile the majority of analysed crane upper arm structure), there is an existing contribution of stress along both the length (axial stress) and around circumference of the beam (hoop stress) establishing presence of planar stress. However, when it comes to radial stress (through the thickness of the beam), its component is not expected to be significant. This makes modelling crane upper arm using shell elements a good option. As the purpose of performed research is to assess fatigue damage in the crane joint - it is worth to additionally note that 3D stress states are hardly ever relevant for fatigue, cracks always start at a free surface. Even with sub-surface initiation it can be argued that the stress state is 2-dimensional, cracks start at inclusions or voids [32].

Based on the aforementioned statements and observations, the structure of the main joint and the majority of the upper arm mesh is established using 2D shell elements. This simplifies computation and setup complexity of the model from a 3-dimensional to a 2-dimensional problem. It uses bending and axial forces at the shell position to calculate stress at extended extreme fibers of the element, however it has been established that using shell elements to model thin components, such as tubular beams is a practice that is both accurate and computationally efficient [57]. The reason for this being that thin plates and thin beam elements contain comparably small and non-complex values of stress in its thickness direction, thus not sufficiently contributing to overall stress magnitude. Normal and shear stresses at the surfaces are always equal to zero and in cases of thin structures, it can often be assumed that stress variation throughout its thickness cannot be very large, and likely close to zero - thus fulfilling plane stress condition. Additionally, since a comparable accuracy can be acquired with both solid and shell elements, definition of model mesh using shell elements has a benefit of containing less mesh nodes - reducing computational complexity and streamlining process of establishment of high quality mesh. Finally, since notch stress of fracture mechanics fatigue assessments (which requires detailed weld modelling with solid mesh elements) is not a part of research scope for this report - a shell model provides a sufficiently enough accuracy to reach project goals. Fatigue assessment that is performed using a hot-spot stress approach can successfully use shell elements as per recommendations of DNVGL-RP-C203 [20].

To further reduce the amount of calculation nodes, front and back boom beams are partially remodelled with beam elements as shown in figure 4.7. This is done by modelling intermediate connecting tubular beam parts in-between local detailed joint connections with simple 1-dimensional beam elements. 1-dimensional components are connected to 2-dimensional shell elements of detailed geometry through rigid spider mesh connections which connect an ending vertices of a beam element to to adjacent shell geometry edge nodes. Rigid connection is used for modelling spider mesh which implies that the tubular member form is stiff, and does not transfer cross-sectional deformation from one side to the other. Stress response assessment at the analysed joint structure welds has been performed to determine if exchanging these particular shell components with beam elements will affect stress results. Assessment has shown that there is 0% change in stress responses present in the main joint structure, meaning that simplification can be efficiently implemented in FEA analysis without affecting relevant results. This lack of response can be explained by Saint Venants principle [62], which states that stress redistribution in an elastic body affects stress results only locally, and has a negligible effect sufficient distance away from the actual connection. This however has concluded that the same exchange of forestay and backstay beams with beam elements is not a feasible approach as these beams are too close to the analysed joint geometry and it affects stress responses at locations relevant to fatigue assessment. Thus the rest of geometry is kept in the form of shell elements.

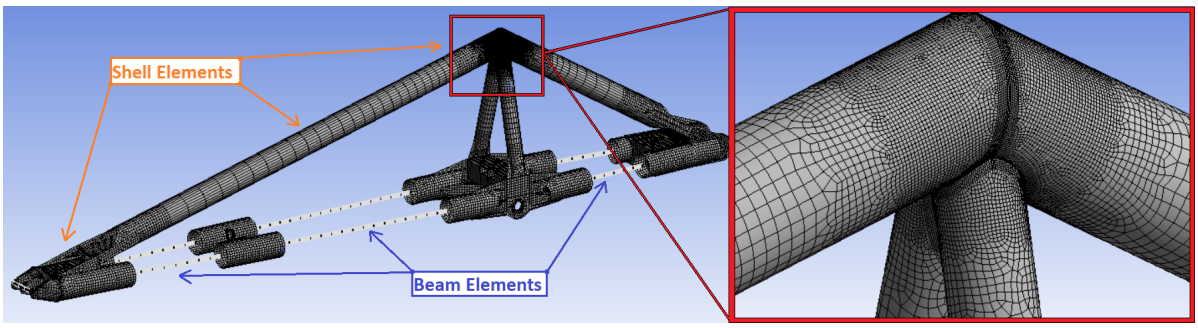

Figure 4.7: Mesh setup for simulated model of crane upper arm

When it comes to element order - the entire FEA model uses quadratic elements to establish mesh. This

means that crane upper arm structure is created out of SHELL281 and BEAM189 elements which consist of 8 and 3 nodes respectively. Figure 4.8 illustrates the nodal setup for both mesh elements. The main purpose of using quadratic elements in the crane upper arm model can be summarised as follows:

1. to avoid stiff deformations in complex geometry that is present in the model;
2. to allow performance of stress extrapolation needed for hot-spot fatigue analysis which uses stress responses of element mid-side nodes;
3. to avoid creating a multi-faceted model that can create inaccurate axial stress and spurious circumferential bending moments.

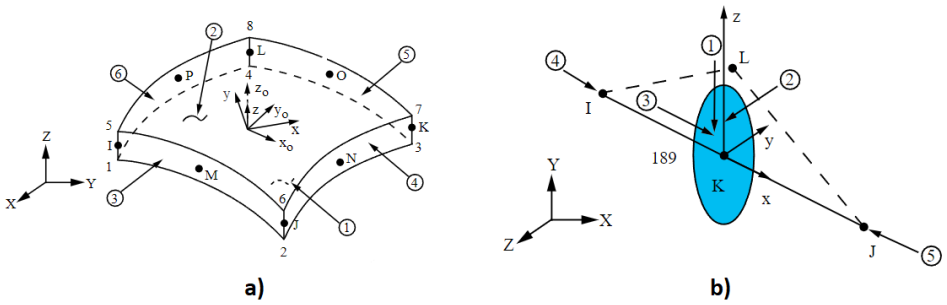

Figure 4.8: Mesh elements used for establishing finite element model a) SHELL281 b) BEAM189.

Additionally, use of quadratic elements in many cases supports quadratic variation of displacement and provides more accurate stress results than linear elements, with fewer number of elements and total degrees of freedom [8]. As stress result accuracy is critical to the precision of fatigue analysis - this concludes that establishing mesh elements in the aforementioned manner allows to acquire stress responses that are of sufficient quality for fatigue assessment within tubular joint welds.

Mesh pattern

Element shape and pattern is an important factor of finite element analysis that affects result accuracy. As element deformation is modelled using quadrilateral elements and transferred through connecting nodes, it is important that both the shape and element node distribution around important measurement locations is kept uniform. To achieve this for the problematic tubular joint - a specific meshing approach has been used based on methodology described in Caoa et al. [18], where meshing done on a plane is then adapted to the shape of the beam as presented in figure 4.9. The principle is based on mesh transformation from a circle to a profile that is adjusted with the angle at which pylon leg beams connect with the forestay/backstay beams. This methodology is applied to all weld lines for beam connections of the analysed tubular joint. It allows maintaining mesh uniformity around the welded connections where stress is to be evaluated for fatigue assessment.

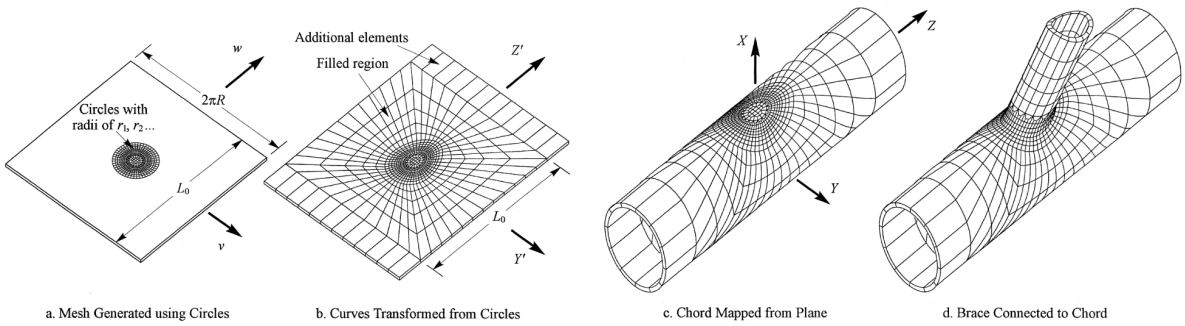

Figure 4.9: Principle steps of procedure applied for meshing tubular joint [18]

Figure 4.10 illustrates the defined mesh pattern for the analysed problematic joint chord (forestay and backstay beams). The end result establishes a uniform mesh pattern around complex beam connections

while maintaining mesh node connections between each body component in the joint and the entire crane upper arm setup.

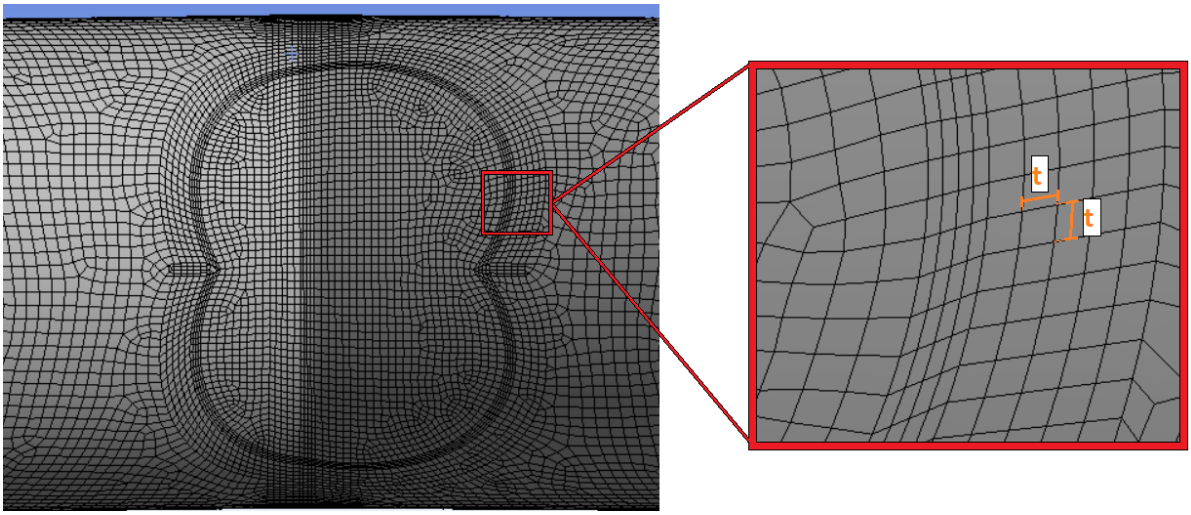

Figure 4.10: Mesh pattern setup and size definitions for the analysed upper arm joint (with t indicating thickness of the structural member)

Element size

Mesh element size has a large influence on the measured stress response. As quality of fatigue analysis is very sensitive to accuracy of stress results, it is critical to establish mesh of size which is capable to acquiring realistic stress that is experienced by the analysed structure at relevant measurement points. As a rule - smaller sized elements lead to closer distribution of mesh nodes, thus providing higher accuracy of nodal and element stress. However, the number of nodes in the model also negatively influences computational complexity, which means that mesh element size has to be established in a manner which provides accurate results while efficiently using computation resources.

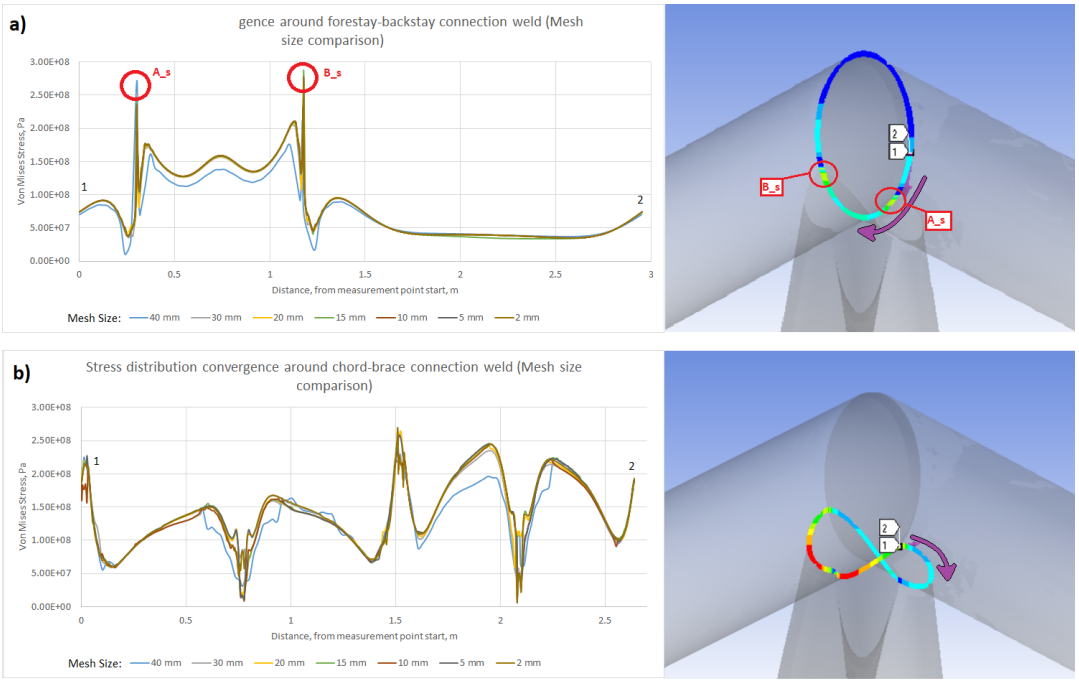

Figure 4.11: Mesh convergence comparison of different mesh sizes around a) forestay-backstay and b) chord-brace connection welds.

For the entirety of the crane structure, the default mesh size is set is 0.1 m, with significant mesh refinement setup for analysed joint as presented in figure 4.7. To ensure that stress result accuracy is sufficient - mesh convergence tests are performed around the problematic joint weld lines for the analysed joint structure. This test is a critical part of FEA setup as it verifies that stress response acquired from the analysis contains values that are approximated to a sufficiently accurate degree. The limit at which accuracy can be considered sufficient is determined when reduction of mesh size no longer affects stress response.

For the purpose of evaluating convergence of entire weld line - convergence test has been performed by measuring stress around two circumference welds - around forestay-backstay chord weld and around the chord-brace weld which connects pylon legs to the chord as illustrated in figure 4.11. This allows to simultaneously measure a large number of stress responses in terms of their convergence and streamlines the process.

Results show that the optimal mesh size around the majority of the weld lines converges best at 10 mm. Thus the acquired mesh size at the weld toe is set to be equal to 10 x 10 mm as indicated in figure 4.10. This is a value that is consistent with mesh size requirements of DNVGL-RP-C203 [20], which suggest using eight node shell element mesh of sizes between t x t and 2t x 2t for hot-spot stress fatigue analysis. Here t refers to beam thickness on which mesh size is being setup. For this specific structure - recommendation of mesh size around welds is bound to fall into a region between 9.5 mm and 19 mm, which the chosen defined setup of 10 mm is well positioned.

It is important to note that convergence test results also highlight several points around the weld which do not appear to converge - it is specifically apparent from graph A in figure 4.11 where highlighted stress spikes A_s and B_s indicate a presence of stress singularity, as stress values at these positions are not capable of converging. This stress point will be analysed further in section 4.2.7.

In the final mesh setup - entire FEA model consists of 54500 elements and 151500 nodes. Analysed joint contains approximately 1/3 of the entire node and element count this model (with 19600 elements and 58500 nodes). This concludes mesh setup of the crane upper arm model and it is meant to provide results of sufficient accuracy required for performing fatigue assessment with several methods, which will be discussed in upcoming sections. Mesh setup overview can be found in table 4.2.

Table 4.2: Overview of main parameters for mesh and boundary condition setup

Mesh Properties		
	Full Model	**Main Joint**
Element type	Mixed	Shell
Element class	SHELL281	SHELL281
	BEAM189	
MAX mesh edge size	500 mm	100 mm
MIN mesh edge size	100 mm	10 mm
Element type	Quadrilateral-dominant	
Element order	quadratic	
Number of elements	54500	19600
Number of nodes	151500	58500

Constraints		
Connection	Front Arm	Rear Arm
Degrees of Freedom	1	1
DoF type	Rotation X	Rotation X

Applied loads		
	Type	**Condition**
Hoisting (Front)	Force, N	Variable
Hoisting (Back)	Force, N	Variable
Cabin Suspension	Force, N	Variable
Gravity	Inertia, m/s^2	Static
Acceleration	Inertia, m/s^2	Variable

4.2.6. Static vs. dynamic analysis

As fatigue assessment is performed using loads defined within a time domain, it is worth determining whether a static or dynamic finite element analysis should be performed. As per recommendations of ANSYS [8], if load excitation frequency is higher than 1/3 of the lowest structure natural frequency - a dynamic analysis provides more accurate results.

Modal analysis has been performed with the defined crane upper arm FEA setup to acquire natural frequency responses for the assessed structure. Table 4.3 provides value overview for the first six natural frequency of the upper arm. Results of the lowest natural frequency (equaling to 3.37 Hz) is within the limits of static FEA assessment approach (which experiences highest load excitation of 0.8 Hz). Based on this observation a static analysis contains enough accuracy and will be used for acquiring stress in all upcoming FEA simulations. When it comes to deformation setup - because structure does not appear to experience large deformations (which are common for cables, membranes and spinning structures) - stress results are acquired with large deflection effects turned off.

Table 4.3: Overview of first six natural frequencies for the upper arm structure, with defined constraint setup.

Mode	1	2	3	4	5	6
Frequency, Hz	3.37	5.62	10.70	11.46	13.83	15.23

Dynamic analysis frequency limit, Hz	>1.12
Highest excitation frequency	0.8
Recommended analysis type	Static

4.2.7. Evaluating presence of stress concentration

Accuracy of fatigue analysis is heavily dependent on the accuracy of peak stress calculations. This indicates that establishment of accurate peak stress values at measurement locations is critical for precision of fatigue assessment results. Since stress values used in fatigue assessment in this research are acquired with the help of finite element analysis - it is worth determining if acquired results are representative and realistic stress response in the structure.

Ductile materials (such as structural steel used in the crane upper arm) tend to experience plastic deformation before undergoing a fracture. As a rule of general high-cycle fatigue assessment - structures should be designed in a way where they stay within the elastic limit and do not yield [31]. When a measurement shows localised stress higher than or close to material yield limit - this is an indication that a potential dangerous stress concentration is present in the structure.

In the analysed FEA model it appears that a critical measurement location in the problematic joint (specifically at the saddle location for both braces, indicated in figure 4.12) is experiencing large stress during load hoisting operation (stress reaching values close to material yield limit of 250 MPa), which is potentially a result of a stress concentration and could be a reason of crack initiation and propagation in the real crane.

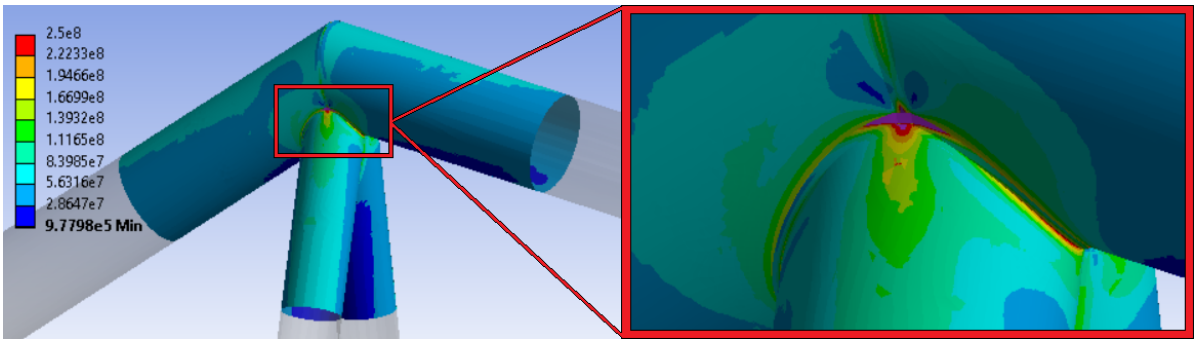

Figure 4.12: Stress response distribution in the upper arm joint surface, concentrating at the chord-brace connection saddle during load hoisting (stress capped at material yield limit of 250MPa).

However the location of stress concentration also casts some uncertainty within the observation - specifically linked to the fact that it is located at a point which in FEA analysis can be prone to formation of a *stress singularity*. As it has been observed by a mesh convergence test (which results have been presented in section 4.2.5) - stress value at this specific location does not appear to converge with additional mesh refinement (highlighted in figure 4.11). This is a common property for showing that a stress singularity might be present in the model, which adds an error factor into stress measurement results at this specific location.

Because observation of damage in the real crane present a crack propagation at this specific location (i.e. brace saddle) - it is an important measurement point for fatigue assessment, which requires additional attention to determine whether stress response is dominated by a stress concentration of presence of stress singularity.

Stress concentration vs. stress singularity

To better understand how both stress responses compare - it is worth taking a look into their similarities and differences.

A stress concentration is a natural stress distribution which indicates that stress appears to concentrate at a specific location with a magnitude that is higher than its surrounding area. Stress concentrations are a

common occurrence in real structures which have to be taken into account when checking structural stability and fatigue life of analysed geometry.

On the other hand - a stress singularity is an artificial stress concentration in a finite element model where stress value is unbounded [8] (continuously increasing measured stress response with reduction of mesh element size). This is a potential consequence of such finite element analysis setup principles as:

1. Point load being applied to a single mesh node as a force or moment.

2. An isolated constraint point where resulting reaction force behaves like a point load.

3. A sharp re-entrant corner, with zero fillet radius.

Singularities are commonly expected in a FEA analysis and do not create an issue if the location of a stress singularity is far away from a measurement locations. However when they are located close to locations where stress has to be measured as in the case of stress at joint brace saddle - it is important to either remove the stress singularity or determine how to avoid its effects in measured stress results.

Stress concentrations and stress singularities in principle are not exclusive - often when a stress singularity is present it also indicates a presence of a stress concentration in the local region. Only the opposite is not always the case as formation of stress singularities can often be avoided.

To verify whether there is a singularity present in the model - a localized mesh convergence test has been performed at the localized node, which location is illustrated in figure 4.13. Test results have shown that indeed a stress singularity is present - as stress values at saddle brace connection to the chord do not converge to a specific value and continue to grow. This is a consequence of using shell elements to model the crane joint, as it contains sharp re-entrant corners between chord and brace element connection.

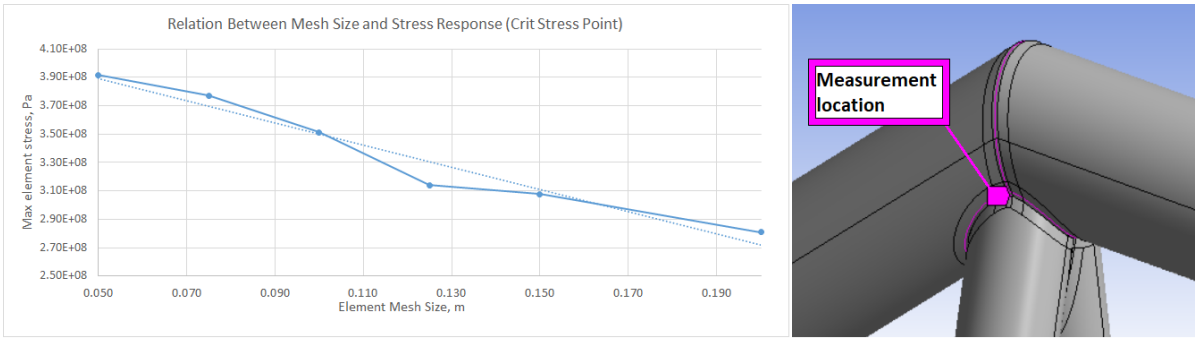

Figure 4.13: Localised mesh convergence test measured at brace saddle, indicating presence of stress singularity.

This conclusion however does also require assessment whether area away from the singularity node is a result of stress concentration or is mainly a residual stress effect appearing from aforementioned stress singularity. This will be assessed next.

Dealing with stress singularities

Depending on analysed model setup, there are methods to avoid stress singularities in a way that they do not affect required measurement results or potentially remove the singularity altogether. Commonly stress singularities appearing from sharp re-entrant corners can be dealt with by following approaches:

1. Modelling re-entrant corners with fillets. This is the most common practice for removing singularities as it allows stress to distribute realistically over the fillet area in a way which shape function modelling stress response in finite element analysis are able to handle. This is however not always possible to do, as in the case of analysed tubular joint.

2. For ductile materials, a stress singularity can potentially be solved by implementing a non-linear (e.g elasto plastic) material setup in the FEA analysis. This would allow geometry to locally yield and redistribute stress over the model in a manner which would approximate towards more reasonable simulation results once stress singularity point experiences local yielding.

3. When possible, a common practice is to completely ignore presence of stress singularities. This assumption is based on the St. Venant's principle, which states: if the forces acting upon a body are restricted to several small parts of the surface, each included in a sphere of radius, then the strains and stresses produced in the interior of the body at a finite distance from all those parts are smaller in the order of magnitude when the forces for each single part are in equilibrium than when they are not [62]. In layman's terms, applied for finite element analysis - it translates to the fact that even when a stress singularity is present a particular distance away from the singularity point, the results of stress and strain will remain correct. This means that stress singularities generally do not lead to incorrect simulation results in other locations of the model, both in terms of stress and deformation. If it is possible to measure stress away from the singularity point - singularity effects can be discounted from adding error to measurement results.

Because assessed model is composed out of shell elements - completely removing stress singularity through addition of fillets is not a feasible approach. As an alternative, to minimize singularity effects appearing from a sharp re-entrant corner - joint has been remodelled with inclusion of welds. Figure 4.14 illustrates comparison between original and adjusted joint models. The presence of sharp corners have been reduced. However as results show - the presence of overall stress distribution and overall magnitude in the region around brace saddle has not changed. As indicated in results with adjusted joint models - stress tends to propagate too far to indicate sole effect of stress singularity. This specifies that outside the main singularity nodes which connect brace to the chord - the rest of the elements experience effects of a present stress concentration.

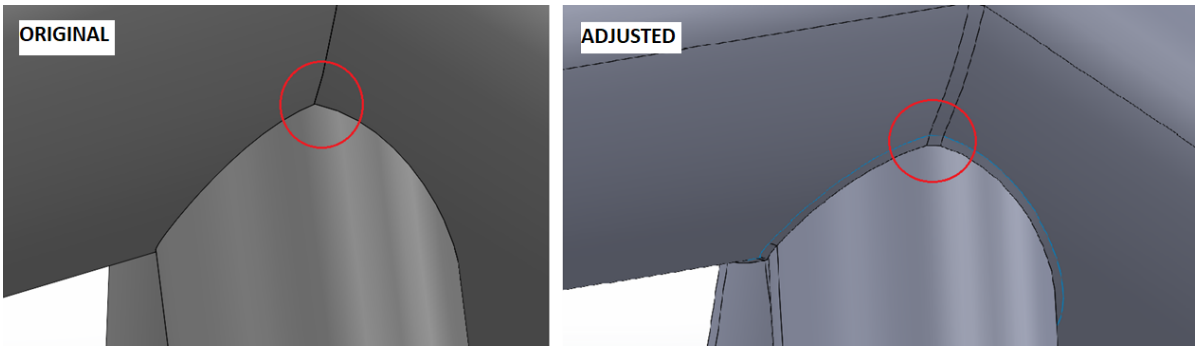

Figure 4.14: Comparison of analysed upper arm joint geometry between original setup and model with included weld geometry.

Mesh convergence tests have shown that approximately at the distance of 6 mm away from the singularity node - stress appears to converge. This observation is important for measuring hot-spot stress in the upcoming chapters because it highlights that although it is not possible to completely remove a stress concentration around the welds of analysed model - it is however possible to avoid its effects by measuring stress away from the weld and then extrapolating its value to approximate actual stress at the weld toe.

Conclusion

An important observation is visualized in figure 4.15, which shows how stress distribution at brace saddle compares with crack propagation locations in real cranes of the same model as Cornelis Tromp 25T lemniscate crane. It appears that the analysed measurement point which indicates presence of stress singularity is also the location where cracks tend to propagate (and potentially initiate) in the real crane. This observation combined with the fact that stress does not reduce after weld lines have been introduced into the joint, concludes that outside the first node - the rest of stress response is a result of stress concentration, rather than a singularity. This is an important conclusion because it already shows a presence of dangerous stress response at the saddle of the joint brace connection, with stress values nearing material yield limit.

It is worth noting that although the presence of stress singularity cannot be completely removed from this critical point - it is not expected to affect fatigue assessment results. This is due to the methodology of how stress is measured for each assessment approach - specifically because nominal stress fatigue analysis uses force and moment reaction values instead of nodal stress (which are not sensitive to mesh size), and because hot-spot fatigue analysis extrapolates stress away from the singularity point to avoid its potential effects. These methods will be discussed in more detail further in sections 4.3 and 4.4, which discuss performance of aforementioned fatigue analyses.

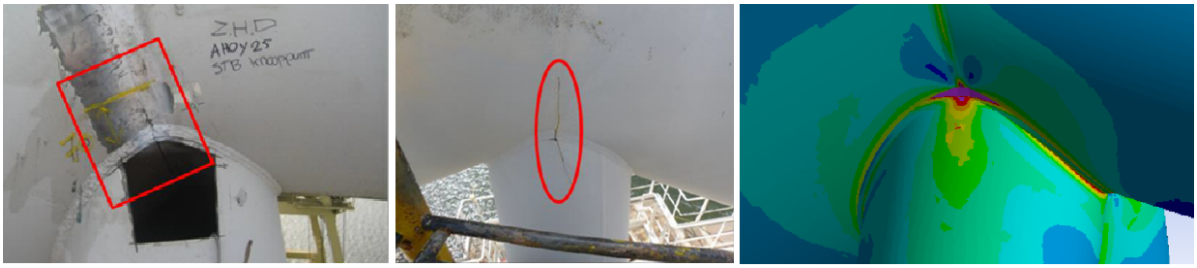

Figure 4.15: Crack propagation location comparison in a) Cornelis Tromp 25T crane b) crane of the same model and c) stress distribution in developed FEA model

4.3. Nominal stress fatigue assessment

This section presents setup procedure and results of fatigue assessment which uses nominal stress approach. Additionally it includes description of measurement point setup for the problematic tubular joint as well as presents definition of operational life and stress cycle counting approach that will be used for all upcoming fatigue assessments.

The key of performed research is to assess whether crane upper arm structure joint is problematic in terms of its accumulated fatigue damage. With a representative FEA model established (as defined in section 4.2) - it is now possible to perform fatigue analyses and assess resultant damage accumulation. As the first step - fatigue damage is evaluated using nominal stress fatigue assessment approach which does not localize stress concentration effects to their specific location. Its results are used as a base point of comparison for further fatigue assessment that includes effects of stress concentrations, which will be described in section 4.4.

4.3.1. Fatigue assessment methodology

In this report nominal fatigue assessment is performed using a detailed finite element model which consists out of 2-dimensional shell mesh elements with a load setup that is established within a time domain. This approach for nominal stress fatigue assessment is not the standard in the industry, as it is more complex in its setup and thus requires a specific methodology to be performed. Figure 4.16 summarizes the procedure of how nominal stress fatigue assessment is performed when FEA model is established with a non-beam element model and included temporal loads.

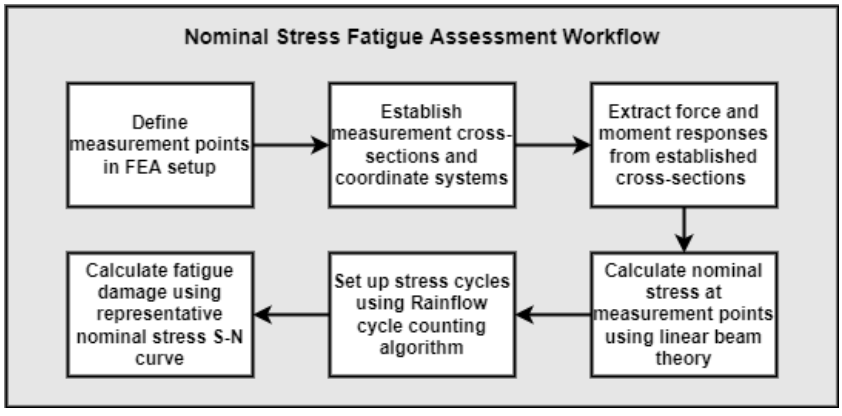

Figure 4.16: Workflow overview for nominal stress fatigue assessment

The main steps for performing fatigue assessment can be described with the following main steps:

1. Measurement point locations are chosen for assessing fatigue. These positions are constant for all fatigue assessment methods of problematic tubular joint welds, including for nominal stress, hot-spot stress and multi-axial stress assessment methods.

2. Cross-sectional surface areas are defined for measurement purposes. These surfaces are located slightly away from the weld around the weld lines of assessed joint geometry as illustrated in figure 4.18. Coordinate systems are setup for each surface to align measurement directions in relation to the beam length direction.

3. Force and moment reactions are extracted from previously defined cross-sectional measurement surfaces within FEA environment. Values are of each cross section are summed up into a single force and moment value respectively for further calculations.

4. Using force and moment reaction values and based on the specifics of cross-section area, shape inertia and measurement position value - nominal stress values are calculated for all measurement points based on the principles of linear beam theory equations.

5. Using Rainflow counting algorithm, stress cycles are defined in terms of their amount and range magnitude. Stress ranges are then combined with representative S-N curves and a particular cumulative damage rule to calculate fatigue damage accumulation.

These main steps of aforementioned fatigue assessment procedure are detailed further in following subsections.

4.3.2. Measurement location setup

Fatigue assessment is performed to measure fatigue damage at the weld toes of problematic joint. To limit the scope of performed fatigue assessment - measurements are taken at a limited number of points around the circumference of the welds present in the tubular joint. As per recommendations of DNVGL-RP-C203 [20] and as illustrated in figure 4.17, measurement points are setup in 8 locations per circular connections (related to forestay-backstay weld), with same point distribution principle defined for chord-brace connection. Due to the fact that pylon legs overlap - this limits method applicability to 12 points for two leg beams (points P1-P12 and C1-C12) and extends measurement setup to additional 3 points defined for the weld connecting overlapping pylon leg beams (points P13-P15). In total 43 measurements positions are defined to assess fatigue damage in the problematic tubular joint, which will be discussed in upcoming sections.

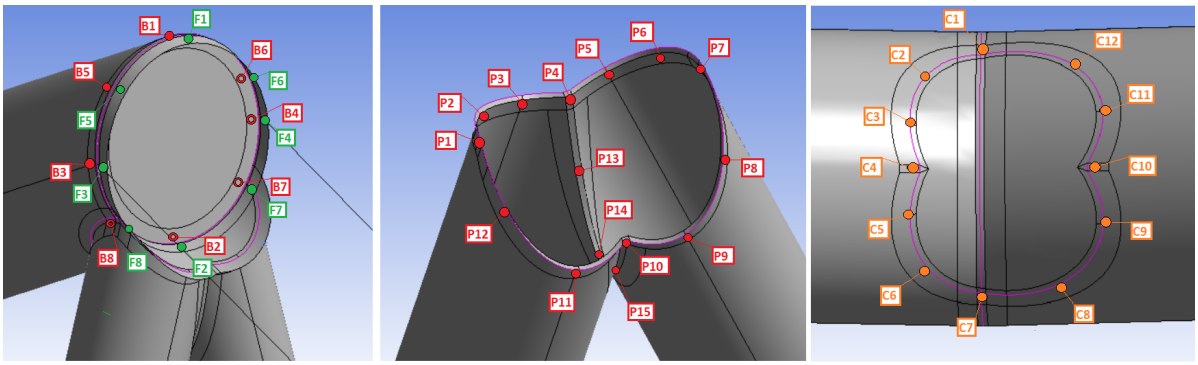

Figure 4.17: Fatigue damage measurement location setup for crane upper arm joint

4.3.3. Stress acquisition

As nominal stress by definition does not include stress concentration effects into its formulation - acquiring nominal stress values directly from FEA model established with detailed geometry is not a feasible approach. Direct acquisition of stress values for nominal stress fatigue assessment is possible only for FEA models which are defined using 1-dimensional beam elements. Since analysed structure of crane upper arm joint is modelled using detailed 2-dimensional shell elements - stress has to be calculated using measurements of force and moment reactions, acquired in FEA environment close distance away from analysed welds.

Figure 4.18 illustrates how cross-sectional surfaces are setup for acquiring force and moment reaction values, which are then used to calculate nominal stress using beam theory equations. Surface shown in picture A defines how points located on the forestay and backstay connection are measured; Pictures B and E measures points around the brace, while pictures C and D define principle for measuring reactions appearing on

the chord side. According to measurement point location - distances are defined for each point away from the center of cross-sectional surface so nominal stress values can then be acquired.

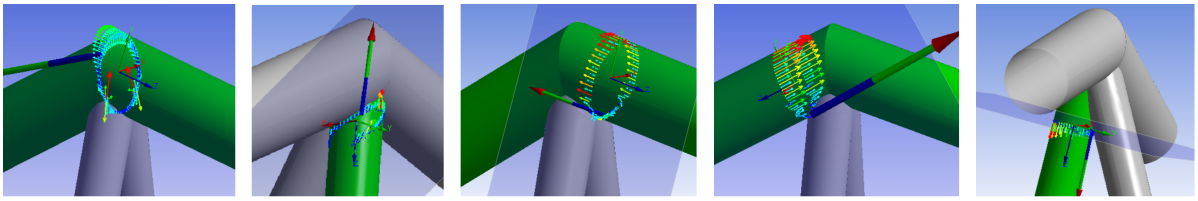

Figure 4.18: Force and moment cross-section reaction measurement setup for evaluating nominal stress fatigue of problematic upper arm joint

Because reaction measurements are taken from the entire cross-section and then summed up - it is not possible to directly acquire stress values at specific measurement points on the beam surface. Instead, all stress measurements are averaged out and depend on the distance from the center of specific measured cross-sectional area. Stress at all measurement points relevant for fatigue assessment (illustrated in figure 4.17) are defined through aforementioned cross-section surfaces using this approach.

As stated by Kam and Dover [40], there are three major stress axes important for nominal fatigue loading in tubular joints - namely axial loading, in plane bending (IPB) and out of plane bending (OPB). Because nominal stress fatigue analysis assumes that normal stress components are dominant for fatigue damage accumulation - only normal stress components are used. Normal stress σ_i of point i at time step t for fatigue assessment are thus calculated based on the formula presented in Lee and Ball [49]:

$$\sigma_i = \frac{F_z}{A} - \frac{M_x y_i}{I_x} + \frac{M_y x_i}{I_y} \tag{4.1}$$

where F_z is force reaction in tension direction; A is cross-sectional area of measured cut; M_x and M_y is out-of-plane and in-plane bending moment reactions; y_i and x_i are planar distance values from center of cross-section to location of measurement point in X and Y directions; I_x and I_y being values of cross-sectional area moment of inertia in X and Y directions, established based on the shape of evaluated beam cross section. For tubular joints, $I_x = I_y$ and is calculated using the following formula:

$$I = \frac{\pi(D^4 - d^4)}{64} \tag{4.2}$$

where D is the outer diameter of the tubular beam; and d is the inner diameter of the tubular beam. This allows to acquire nominal stress values at each time step, which are then compiled into stress time histories for all measurement points.

4.3.4. Cycle counting

Once nominal stress values are acquired for time steps containing entire operation duration - stress cycles are distinguished from the loading cycle using a conventional *Rainflow counting algorithm*. This algorithm is used for simplifying temporal stress spectrum into countable stress variation cycles, which can then be used for fatigue damage assessment. Counting procedure is performed with the following steps:

1. Time history of a complex stress setup is reduced to a simplified temporal set of stress peaks and valleys.
2. Based on the principle of natural phenomenon of rainflow - each tensile peak is defined as a flow source which allows establishing stress lines following the time history.
3. Number of half-cycles are then counted based on the criteria on whether flow line reaches time history, merges with a flow that started at an earlier tensile peak, or flows when an opposite tensile peak has greater or equal magnitude.
4. Step 3 is repeated for all stress peaks and valleys in stress time history.
5. Stress range is then established by comparing minimum and maximum stress values for each half-cycle.

6. Identical half-cycles are summed to acquire a number of stress cycles, which can then be used for fatigue damage evaluation.

Based on the aforementioned approach temporal stress ranges and cycles are evaluated for all measurement points. The same methodology for establishing stress ranges is used for calculating hot-spot and multiaxial fatigue approaches as well, which will be discussed further in the report.

Cycle calculations are performed with a Rainflow counting algorithm established in *SFAT*[2] software. The accuracy of used script has been verified by performing hand calculations for nominal stress cycle, which has provided comparable stress cycle results with an error margin between two calculation variants containing only ±2% of the total stress value. Figure 4.19 illustrates the principle of manually performing stress cycle counting through flow line establishment, as it has been calculated for point C6 (please refer to figure 4.17). This provides an overview of how rainflow cycles are set up for establishing stress ranges.

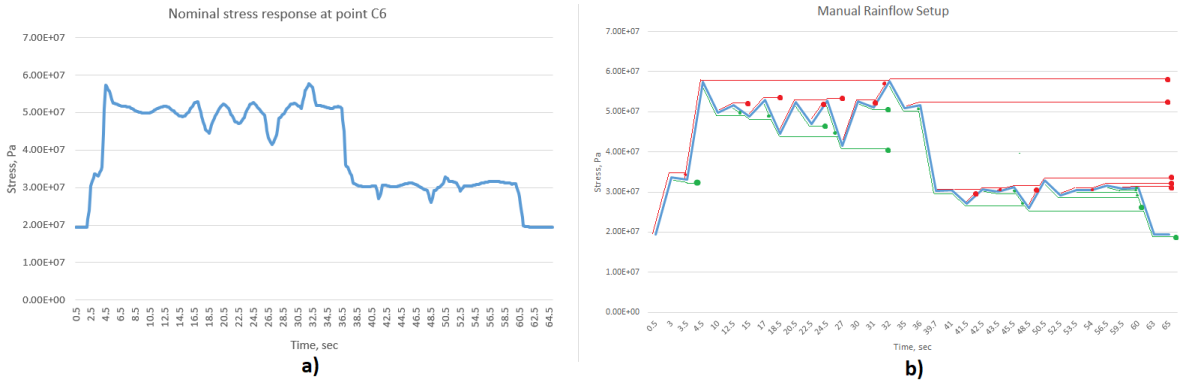

Figure 4.19: Stress response comparison between a) calculated nominal stress and b) simplified Rainflow cycle counting peak-valley setup of the same cycle.

Aforementioned approach is performed for time histories of stress at all measurement points, which then are compared to empirical stress life data established in the format of S-N curves.

4.3.5. Operational life definition

Operational life of all performed fatigue assessments within this report is evaluated for a timeline of 23 years. This value is defined to represent life of Cornelis Tromp 25T lemniscate crane before it has been temporarily taken out of operation due to observed crack at the main joint of the upper arm in year 2020.

In order to accurately represent this measurement in a number of operational cycles - the following approach has been performed:

1. It is known that the crane has been in operation between 1997 and 2020 concluding a damage accumulation lifetime of 23 years.

2. Based on transshipment data acquired from crane operator *Maja Stuwadoors B.V.* - between the years 2006 and 2018 crane has transshipped 16.1 million metric tons of cargo (approximately 1.34 tons per year).

3. Basing transshipment on the crane capacity (rated at 25 tons with included variation of 20-25 tons in realistic operation) - crane is performing between 53.6 to 67 thousand operational cycles per year.

4. Throughout crane exploitation period between 1997 and 2020 this sums up to a total number of cycles in the range between 1.23 - 1.54 million operational cycles.

In order to average out the number of cycles to a reasonable limit - final number of operational cycles in fatigue life estimations have been defined as 1.31 million. This value takes into account that the crane experiences cargo loads which do vary in their tonnage and thus keeping total number of assessed operations within defined cycle range. This value of 1.31 million cycles will also be used in other fatigue analyses along with nominal stress fatigue assessment discussed in this section.

[2] `https://fatigue-life.com/sfat/`

4.3.6. S-N curve

As indicated in section 4.3.4 - fatigue assessment determines the type of Stress-life (S-N) curves which can be considered for damage estimation. For the purpose of nominal stress fatigue assessment - nominal stress S-N curves are used and are chosen based on recommendations of A.F. [2]. These S-N curves are specifically meant to be used for evaluating fatigue damage using a nominal stress approach and are not applicable for other types of fatigue assessment (e.g. with hot-spot or notch stress).

Chosen S-N curves for calculation of normal components of nominal stress is of class 56 and 71:

1. Class 56 S-N curve is used for defining fatigue damage for measurement points around the weld connecting forestay beam to backstay beam (specifically for points F1-F8 and B1-B8). It is treated according to weld classification provided in Barsoum [11] as a weld circular hollow section reinforced with an intermediate plate, with potential failure spanning from weld toe. Comparison of failure for weld toe is consistent with upcoming analysis for hot-spot stress, which specifically focus on measuring fatigue accumulation at the weld toe.

2. Class 71 S-N curve is used for all welds within chord-brace connection - joining pylon legs to the forestay-backstay beams. It is treated in accordance to weld classification of Barsoum [11] as a weld for connecting tubular hollow section to another hollow section, with section width < 100 mm. It accurately defines specific joint setup, both in terms of sections used, as well as their connection principle.

Specified S-N curves are illustrated in figure 4.20 and are used for assessing nominal fatigue damage at all relevant measurement locations.

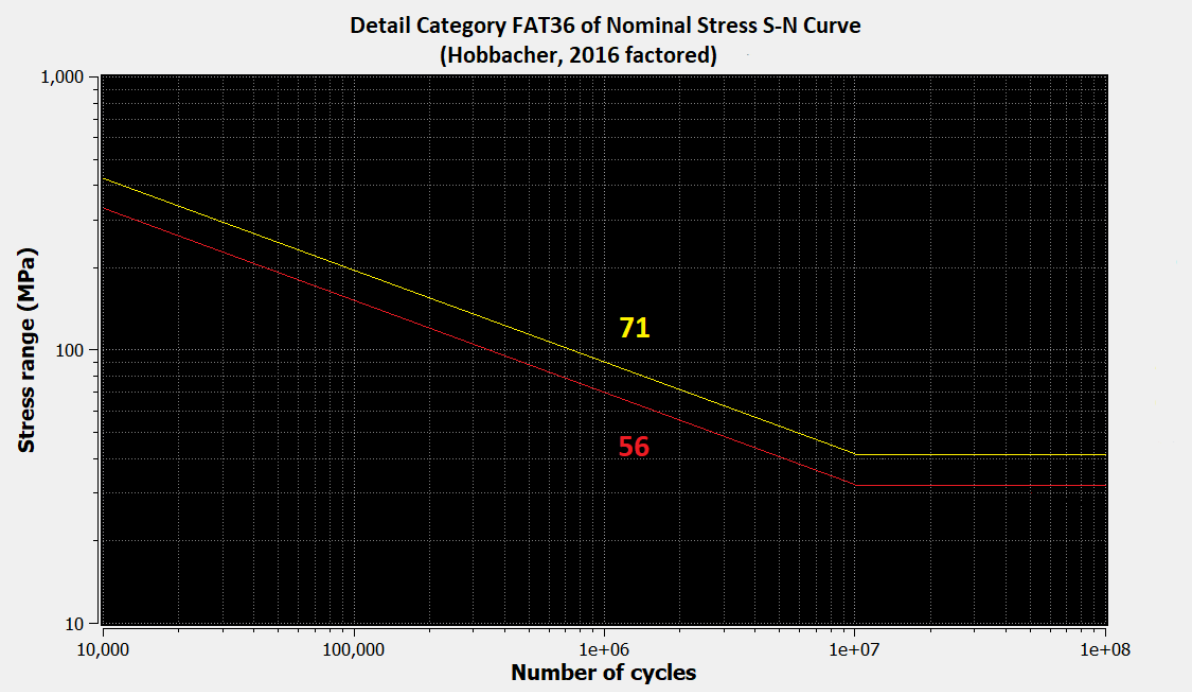

Figure 4.20: Nominal stress S-N curves used for evaluation of upper arm joint fatigue damage

As it can be observed in the representative S-N curves - for nominal stress fatigue assessment a detailed fatigue analysis can be omitted if the largest local stress range for actual detail is less than the fatigue limit at 10^7 cycles DNVGL-RP-C203 [20]. This indicates that measurement point theoretically has infinite fatigue life as stress cycle is too low to impose enough damage to initiate a crack over operational lifetime of the structure. This is the estimation within used S-N curves, which is taken into account for performed fatigue assessment. For very high cycle fatigue applications (with expected life above 1E+7 cycles) slope of m=5 is introduced, but this is not expected fatigue life region in assessed structure, for which S-N curve high cycle fatigue setup illustrated in figure 4.20 is sufficient.

4.3.7. Fatigue damage estimation

Nominal stress fatigue damage factor D_i values for specific stress cycle of measurement point i is calculated based using following cumulative damage formula, which is derived from a combination of Haibach equation and Palmgren-Miner rule [86]:

$$D_i = \sum (\frac{\Delta\sigma_{range}}{\Delta\sigma_{FAT}})^3 \frac{Cn}{N} \tag{4.3}$$

where $\Delta\sigma_{range}$ is stress range measured for evaluated stress cycle; $\Delta\sigma_{FAT}$ is fatigue life at 2 million cycles specific for applied S-N curve (equal to $5.6E+7$ and $7.1E+7$ for chosen class 56 and 71 S-N curves respectively); C is the number of identical stress cycles within stress time history; n is the evaluated fatigue life of the structure (1.31 million cycles); and N being the reference cycle limit for fatigue life S-N curves (2 million cycle).

Because each operational cycle of the crane structure includes a number of stress cycles of varying magnitude - it has to be taken into account that not only the largest stress cycle accumulates fatigue damage at the measurement point. According to Ekberg et al. [23], The total fatigue damage D then needs to be evaluated from a fatigue damage accumulation rule, by summing up damage of all subsequent stress cycles D_i to acquire final damage factor value:

$$D = \sum_{i=1}^{k} D_i \tag{4.4}$$

where (theoretically) $D = 1$ corresponds to fatigue failure. This final value is then considered as fatigue damage factor which serves as a result for evaluating whether measurement points and thus entire structure is capable of surviving defined fatigue life. If there are points which fatigue damage factor value is above 1 - it indicates that there is potential for fatigue failure at specific location. Acquired values of damage ratio also serve as quantifiable results for comparing differences between fatigue assessment methods and structure designs, which will all be discussed in upcoming chapters.

4.3.8. Results

Performing fatigue assessment of problematic upper arm joint structure based on the aforementioned methodology - fatigue damage factor results have been acquired as summarized in table 4.4. This table presents damage factor results for all measurement points with color indicating severity of each value.

Table 4.4: Accumulated fatigue damage factor D_{i_N} around the welds of analysed lemniscate crane upper arm structure, acquired using nominal stress fatigue assessment method (for 23 years of operation).

Brace	**Point**	**P1**	**P2**	**P3**	**P4**	**P5**	**P6**	**P7**	**P8**
	D_{i_N}	0.376	0.302	0.037	0.099	0.046	0.374	0.661	0.381
	Point	**P9**	**P10.2**	**P11**	**P12**	**P13**	**P14**	**P15**	
	D_{i_N}	0.082	0.026	0.070	0.005	0.009	0.233	0.005	
Chord	**Point**	**C1**	**C2**	**C3**	**C4**	**C5**	**C6**	**C7**	**C8**
	D_{i_N}	0.018	0.055	0.070	0.072	0.079	0.068	0.024	0.080
	Point	**C9**	**C10**	**C11**	**C12**				
	D_{i_N}	0.100	0.104	0.111	0.095				
Forestay	**Point**	**F1**	**F2**	**F3**	**F4**	**F5**	**F6**	**F7**	**F8**
	D_{i_N}	0.037	0.064	0.058	0.070	0.040	0.054	0.076	0.058
Backstay	**Point**	**B1**	**B2**	**B3**	**B4**	**B5**	**B6**	**B7**	**B8**
	D_{i_N}	0.042	0.061	0.072	0.059	0.059	0.043	0.056	0.074

Results show that when assessing fatigue damage using a nominal stress approach - structure can be considered as safe to operate at the life limit of 23 years (1.31 million cycles). No point passes the critical limit value of $D = 1$, with only point P7 (highlighted in figure 4.21) indicating highest damage output ($D = 0.661$) and being the only point surpassing damage threshold of 0.5. Results indicate that the point which accumulates most damage correlates well with real life position where cracks appear to propagate in Cornelis Tromp upper arm structure.

On the other hand there is appearance of relatively high damage accumulation (in comparison to the rest of the model) at positions P6 P8 and P14. This result poses some questions about result accuracy as it is spec-

ulated that this increase in damage accumulation at aforementioned points could be a residual effect from averaging out force and moment reactions over measured cross-sectional area. As in the case of pylon legs, the cut cross section is an ellipse - points P7 along with points P6, P8 and P14 are furthest away from measurement centre, which leads to approximation of higher stress value and thus can explain the fatigue damage magnitude in the setup. Whether this is a realistic damage accumulation representation in the structure, it will be evaluated further into analysis when nominal stress fatigue assessment results will be compared with results of fatigue assessment method which is capable of localising stress concentration effects.

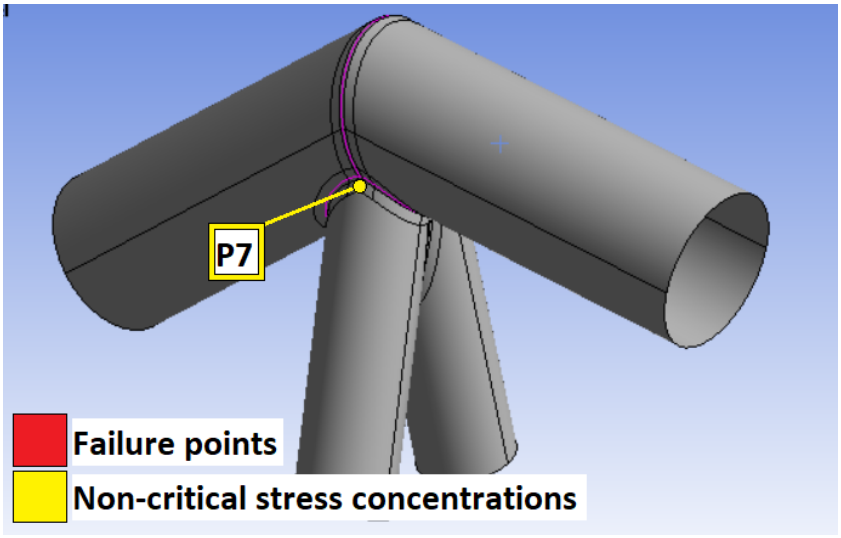

Figure 4.21: Locations of failure points (D > 1) and non-critical stress concentrations (0.5 > D > 1) as measured using nominal stress fatigue assessment approach (marked in red and yellow respectively).

Additionally it is worth noting that even though there are present questions about the accuracy of nominal stress fatigue assessment results - one important factor which determines fatigue damage definition for each measurement point is directly linked to how measurement cross-sections (figure 4.18) are defined. As the cross section plane placement position and angle in a 3D space is not always straightforwards for complex geometry - resulting plane placement can be somewhat prone to subjective judgement of engineer performing measurement plane setup. This can lead to variation of results and can potentially miss force and moment reaction effects acting in the location of a stress concentration, leading to reduced stress response and reduced fatigue damage measurement. Secondly, because stress calculations are performed by averaging out acquired force and moment reaction response in the assessment - this means that any captured reaction effects indicating a presence of stress concentration are distributed over entire area of measured cross-section, leading to results showing inconsistent fatigue damage response that redistributes to more measurement locations on the same plane. This factor of averaging out reaction effects over a subjectively defined cross-section area in complex geometry can lead to lack of consistency in measured fatigue damage. When evaluating fatigue assessment results which were acquired using a nominal stress - this potential effect should be taken into consideration.

4.4. Hot-spot stress fatigue assessment

This section presents procedure of fatigue assessment which includes effects of stress concentrations (using hot-spot stress approach). Section details the steps of performing hot-spot stress fatigue analysis using finite element model approach, provides verification of stress acquisition method by assessing fatigue damage using stress concentration factor calculations and presents results of fatigue assessment.

As it had been established in section 4.3 the main weakness of a nominal stress approach for fatigue assessment is that it does not include stress concentration effects in its formulation. Depending on geometry and loading conditions, stress concentrations commonly are a source and location of crack initiation which can potentially lead to accumulation of fatigue damage and eventual failure of the structure. As it has been observed in section 4.2.7 - the analysed crane upper arm tubular joint contains at least one serious stress concentration at the brace saddle location, where the initial crack propagation has been observed in the

analysed crane. As nominal stress fatigue assessment did not predict structural failure - it appears it is not able to properly account for fatigue damage accumulation in the joint. This is a serious point of interest for assessment of fatigue damage, meaning that including effects of stress concentrations into fatigue analysis is pivotal for understanding why this crane joint structure is prone to failure.

In order to understand how stress concentrations affect accumulation fatigue damage for the specific analysed tubular joint - an additional fatigue assessment is performed. This section describes the assessment process and result evaluation of fatigue damage using a conventional hot-spot stress approach. It is meant to use more representative stress results in fatigue assessment, in relation to nominal stress fatigue assessment which is used for result comparison purposes in section 4.5.

4.4.1. Fatigue assessment methodology

It is possible to acquire stress values in a manner which include stress concentrations using two methods - specifically hot-spot stress and notch stress approaches. A detailed notch stress approach allows to acquire realistic stress response by directly measuring stress in the weld. It however requires definitions of realistic weld geometry and material properties. On the other hand, a hot-spot stress approach provides a simplified approach which does not require incorporation of detailed weld geometry but still allows to analyse fatigue damage while taking stress concentration effects into consideration. Because detailed weld geometry and properties are not available for the analysed joint structure - the welds which a been modelled are only approximations of actual welding profile, without consideration of detailed weld composition. This is a sufficient amount of detail for nominal and hot-spot stress fatigue assessment, but it is not sufficient for evaluating fatigue using notch stress approach. For this purpose - fatigue analysis which includes stress concentration effects is performed using a hot-spot stress methodology

Hot-spot stress (also known as structural stress) describes the stress raising effect caused by the global geometric discontinuity of the welded joints, without considering the local notch geometries of the welds [27]. Unlike nominal stress fatigue assessment - hot-spot stress approach uses stress values acquired from a detailed finite element analysis model. For this purpose the process of hot-spot stress fatigue assessment is performed in a different manner than nominal stress. Overview of adjusted fatigue damage evaluation approach is illustrated in figure 4.22.

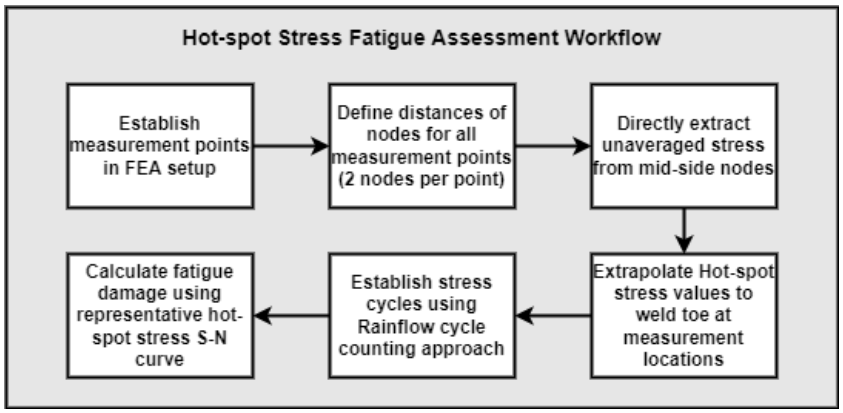

Figure 4.22: Workflow overview for hot-spot stress fatigue assessment

The principle of performing hot-spot stress fatigue assessment can be summarized in following steps:

1. Measurement points are defined for assessment at the same locations as it has been established using nominal stress approach. This allows to directly compare accumulated fatigue damage between both approaches.

2. For each measurement point - two mesh element mid-side nodes are assigned for stress acquisition. Locations and distance away from measurement point for each node are defined based on the qualities of beam size and thickness on which measurement point is located.

3. Based on stress values for each of two nodes (per measurement point) stress is extrapolated to location of weld toe. This serves as the value for hot-spot stress at measurement location.

4. Stress cycle ranges and quantity is calculated using conventional rainflow cycle algorithm.
5. Fatigue damage is evaluated for defined operational life of structure using hot-spot S-N curves, which are chosen depending on weld and joint setup specifics for each analysed measurement point.

Main aspects of aforementioned steps are explained in further detail in the upcoming sub-sections.

4.4.2. Stress acquisition

Stress responses for hot-spot stress fatigue assessment are acquired directly from finite element analysis. This means that it also incorporates stress concentration effects into its formulation. This is the main difference between hot-spot and nominal stress fatigue assessments.

Stress extrapolation

Because a shell element model does not allow measuring stress at actual location of weld toe (due to presence of stress singularities at modelled sharp re-entrant corners and lack of detailed definition of weld geometric and material properties), any stress acquired would not be a realistic representation of a real stress in the structure. For this purpose stress for hot-spot fatigue assessment approach has to be acquired through a stress extrapolation technique. The general procedure for acquiring hot-spot stress response using the method defined in DNVGL-RP-C203 [20] is performed as follows:

1. A detailed geometry finite element model is established with representative geometry and boundary conditions.
2. Detailed uniform mesh of size *between t x t and 2t x 2t* is created using quadratic mesh elements. Here t is refers to the wall thickness of specific meshed beam member.
3. Stress measurements are taken a predefined distance away from the hot-spot location, at two mid-side nodes as shown in figure 4.23.
4. Stress responses are acquired and based on their stress magnitude value specific distance away from the weld - stress is linearly extrapolated to weld toe location to acquire value which can be considered as hot-spot stress;

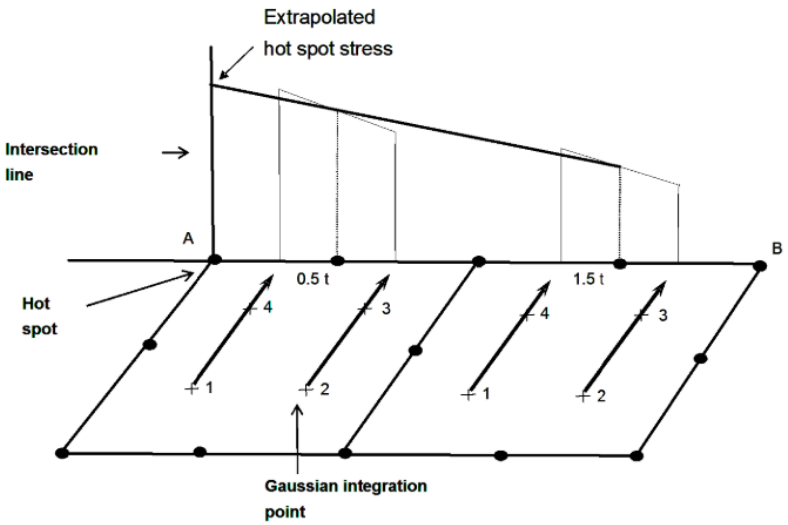

Figure 4.23: Principle of linear stress extrapolation using mesh element mid-side nodes [20]

Because finite element analysis setup described in section 4.2 was established considering requirements for hot-spot fatigue assessment - no additional changes to the simulation setup has to be made, either in terms of its geometry, boundary conditions or mesh setup - simulation model remains identical as used for nominal stress fatigue assessment.

Stress node locations (a and b) where stress is directly measured in a finite element analysis model for further stress extrapolation are calculated based on two criteria defined in DNVGL-RP-C203 [20]:

1. Where assessed measurement point is positioned - different equations are defined depending whether measurement point is on the chord or brace side, as well as depending on whether is can be considered as crown or saddle position.

2. Geometric properties of assessed beam member - this specifically concerns beam radius and thickness on which measurement point is positioned.

Picture A of figure 4.24 illustrates point setup acquisition principle. Locations for points a and b can be acquired based on representative formulas which are chosen depending on point position. For extrapolation of stress along the brace surface normal to the weld toe:

$$a = 0.2\sqrt{rt} \tag{4.5}$$

$$b = 0.65\sqrt{rt} \tag{4.6}$$

For extrapolation of stress along the chord surface normal to the weld toe at the crown position:

$$a = 0.2\sqrt{rt} \tag{4.7}$$

$$b = 0.4\sqrt[4]{rtRT} \tag{4.8}$$

For extrapolation of stress along the chord surface normal to the weld toe at the saddle position:

$$a = 0.2\sqrt{rt} \tag{4.9}$$

$$b = \frac{\pi R}{36} \tag{4.10}$$

Here r and R are radius of brace and chord beams, while t and T are beam thickness values for brace and chord respectively. Based on calculated distance positions - points a and b are averaged out to closest mesh mid-side nodes to acquire stress measurement locations.

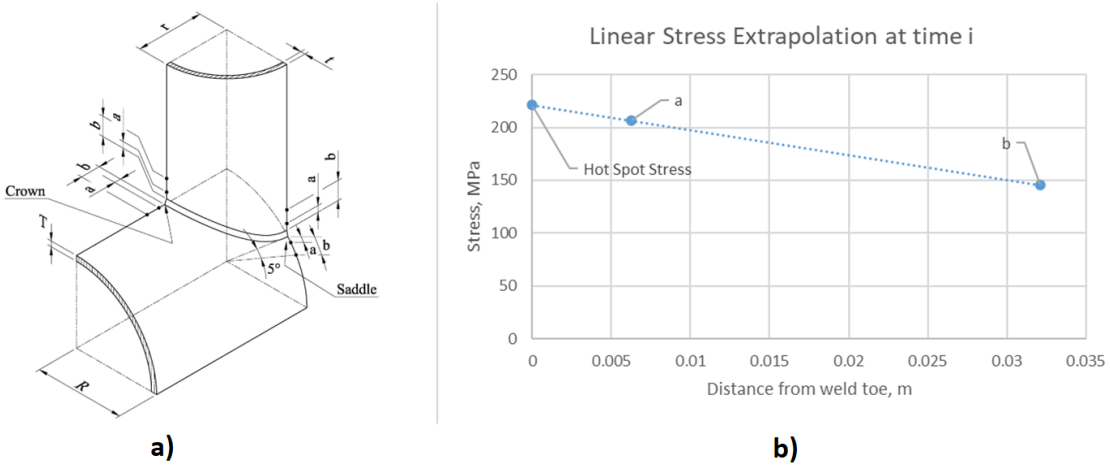

Figure 4.24: a) Node setup used for stress measurements [20] and b) single time-step linear extrapolation result for acquisition of hot-spot stress at measurement point P7.

Once point a and b nodes are defined, hot-spot stress values are acquired using a linear extrapolation technique defined in Lotsberg [57]. As it has been observed by a comparative study of Liu et al. [54] - linear extrapolation technique yields sufficient stress results which are very comparable to quadratic extrapolation method. Thus using linear extrapolation approach is preferred due to methods simplicity in comparison to the quadratic counterpart. Acquired stress value is treated as hot-spot stress value that can be used for fatigue assessment purposes.

Stress type

Regarding location of stress measurement acquisition - hot-spot stress approach specifically measures fatigue at the weld toe of joint beam outer surface [57]. This leads to a conclusion that fatigue assessment will use stress values acquired on the outer surface of shell elements. This does have an impact on FEA analysis stress results as values for top, bottom and middle stress values differ significantly, with outer surface stress generally containing highest stress values.

When evaluating fatigue damage using a hot-spot stress approach - there is a possibility to choose specific stress type. Choosing a particular stress variant for fatigue assessment can have significant consequences to acquired stress response. To determine which stress variant should be used for hot-spot stress fatigue assessment, it is worth investigating general qualities of most commonly used stress types. Use of maximum principal stress is recommended by DNVGL-RP-C203 [20]. However this could potentially lead to relatively non-conservative results, as two additional principal stress components are not considered. This choice is based on the fact that fatigue damage is expected to propagate perpendicular to the largest principal stress range, therefore this stress range determines the fatigue behaviour. However such approach discounts potential effects of stress acting in second and third principal directions as it considers fatigue effects of stress that acts in only single direction and does not account for possibility of non-uniform stress direction between multiple hot-spot locations. Liu et al. [54] uses transverse stress that is perpendicular to the crack direction as it reasons it as being the main stress which governs crack propagation.

It is worth taking into account standard approach used for stress estimations based on region: common practice fatigue assessment of ductile materials in European Standards, Von Mises stress is the main variant used. Von Mises stress includes all stress components into stress formulation, which tend to have highest stress magnitude out of all aforementioned stress variants. Tensile stress in the direction normal to the cracking plane opens the crack and reduces crack closure, resulting in decreased fatigue life, while a compressive normal stress has the opposite effect [26]. This means that evaluating fatigue with Von mises stress that considers compressive stress values in its overall magnitude indicate potential overvaluation of actual fatigue damage and there have been cases reported in the literature where a significant overestimation of fatigue lifetime was observed under combined fatigue response of bending and torsion [88]. On the other hand - when compressive stress is a result of bending - it creates tension on the other side of the surface. As fatigue is assessed only on the outer surface - using Von Mises stress could allow estimations to account for potential fatigue damage appearing on the inner surface of the weld. This indicates that compressive stress can play a part if fatigue damage accumulation and potentially should be accounted for when assessing fatigue damage in joint welds, especially for geometry which is prone to induce complex stress responses - such as tubular beam sections as used in problematic joint.

Overall this stipulates that there is not a unified agreement in the literature on which stress variant should be used for hot-spot stress analysis. Thus in order to consider potential effects of all stress components acting at a measurement point location - Von Mises stress will be used as stress response for hot-spot fatigue assessment performed to estimate fatigue damage in crane upper arm joint. All stress inputs into fatigue analysis will be acquired using this specific type of stress, with considerations about its conservative nature taken into account when comparing results.

4.4.3. Evaluation of method applicability

In principle, hot-spot stress can be evaluated with two main approaches:

1. Using extrapolated nodal stress responses of a detailed shell or solid joint finite element model, as performed for the analysed crane upper arm joint.

2. Calculating nominal stress at hot-spot locations and multiplying its values with stress concentration factors (SCF) ,that are specific for joint setup, loading type and hot-spot location.

In order to ensure that the approach for acquiring hot-spot stress using extrapolated stress values obtained directly from finite element analysis is correctly performed - FEA setup for hot-spot stress acquisition should be verified using a *Stress concentration factor* approach.

Stress concentration factor is a stress multiplier for specific geometry and loading type, which combined with nominal stress value allows to directly convert nominal stress results into hot-spot stress. This allows to simplify the process of stress acquisition and allow to account for stress concentration effects when only nominal stress results are available. Additionally it is a good verification tool which helps assessing whether

hot-spot stress acquisition setup is performed correctly if hot-spot stress is being acquired directly from FEA analysis.

When analysing conventional joints, which are loaded with static non-complex loads - this verification is performed using model setup of the joint that is being analysed. However this is not possible for verifying results of analysed joint because of the following reasons:

1. Due to unique geometry setup of analysed joint (i.e. chord is comprised out of two beams positioned at an angle with a stiffener plate, brace beams overlapping in an unconventional manner, etc.). Such setup has not been investigated in scientific literature, thus it does not have specific stress concentration factor values defined.

2. SCF factor values of similar tubular joints cannot be used because joint is defined in a non-conventional manner and does not compare well with commonly studies joints which have their SCF values established in the literature.

3. Because SCF value is dependent on loading type and direction - it is not well applicable to assess complex loading setups which are present in the analysed crane upper arm joint.

4. SCF factor values are generally established only for joint setups where only joint brace beams are loaded, while in analysed case both chord and brace beams result in loading during crane operation.

Because of the aforementioned points - methodology of defining FEA model setup for stress acquisition is verified using a separate analysis of hot-spot stress of a uni-planar K-joint (figure B.1). For comparability purposes K-joint FEA simulation setup is established based on the same principles as for crane upper arm structure, which can provide proof that analysis is performed correctly.

Verification process is performed in the following manner:

1. Finite element analysis is established for a uni-planar K-joint, based on the same principles as it has been done for analysed structure of the crane upper arm (described in section 4.2)

2. Hot-Spot stress of a well-studied uni-planar K-Joint loaded in different directions is calculated through several static simulations, using approach that uses nominal stress multiplied by SCF values found in the literature.

3. Hot-Spot stress is calculated using stress extrapolation technique of FEA analysis stress results, which are then divided by nominal stress to acquire representative stress concentration factor values.

4. Stress concentration factor values are then compared between two aforementioned approaches to check whether the results approximately correspond to each other.

If stress concentration factor values are comparable - it means that the approach for setting up finite element analysis for acquisition of nominal and hot-spot stress is defined correctly and stress results can be trusted.

Model establishment

The principle setup for establishing joint model and its stress concentration factor values is based on procedure defined in DNVGL-RP-C203 [20]. Table 4.5 summarizes parameter setup of analysed K joint with positions of specific parameters illustrated in figure B.1. Used parameter values are setup in a way to represent analysed crane upper arm joint by using same values of chord-brace diameters and thicknesses. Both chord and braces and sufficiently extended to minimize effects of constraints.

Table 4.5: Evaluated K-Joint parameter value overview.

K-Joint Parameter							
d =	0.559	m	t =	0.0095	m	C =	0.7
D =	0.914	m	T =	0.0127	m	C_1 =	0.4
L =	15	m	g =	0.12345	m	C_2 =	0.35
θ_1 =	45	deg	θ_2 =	45	deg	C_3 =	0.14

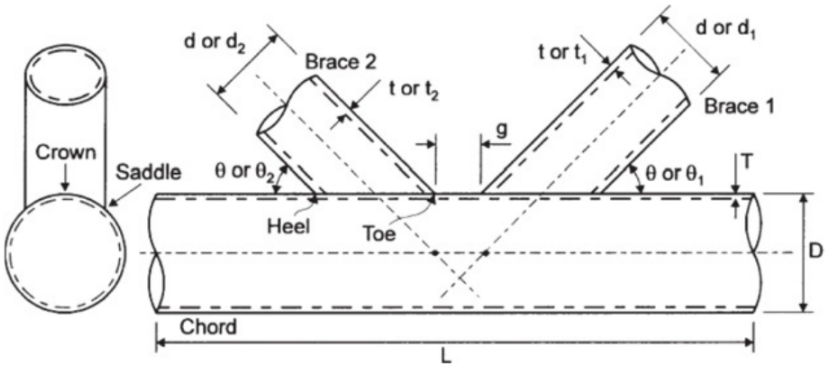

Figure 4.25: Setup parameters of K-Joint used for FEA analysis method verification [17].

Mesh setup is defined based on the principles of in section 4.2, with sizing adapted in a manner which provides significant mesh refinement around chord-brace welds that keeps element edge with the same length as beam thickness.

To establish boundary conditions - fixed joints are used as constraints for fixing the joint (0 degrees of freedom). These constraints are located on two endings of chord beam. This sufficiently constrains the structure which, combined with the long beam extensions for chord and brace beams, do not affect stress distribution locally around joint chord-brace welds. Stress measurements are taken around left brace weld at 8 locations as illustrated in figure 4.26. With four points located on the brace (B1-B4) and four points on the chord (C1-C4). Positions of points 1-2 for both chord and brace are defined for measuring stress at crowns positions and points 3-4 measure stress at saddle positions.

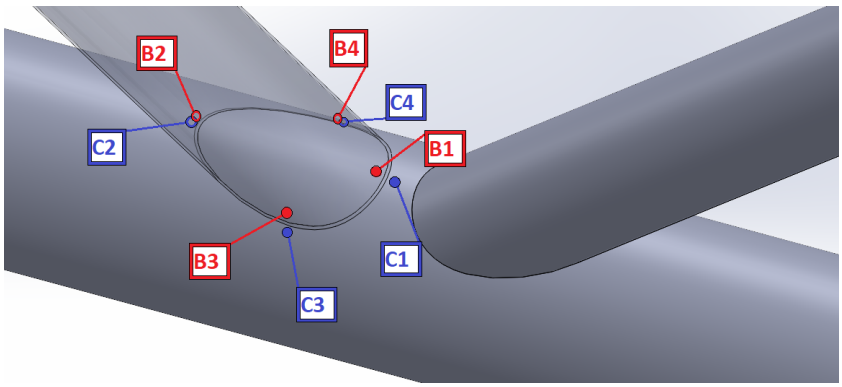

Figure 4.26: Measurement points used for methodology verification.

As stress concentration factors are dependent on loading type and direction - six loading cases are evaluated. Each loading case measures stress concentration factors for different points by using different loading direction as well combinations of whether one or two brace beams are being loaded. Assessed loading setups are illustrated in figure 4.27 and can be summarized as follows:

1. Balanced axial load - applied loads affecting both braces in their length axis direction, with one brace load applied inwards, while the other is applied outwards. SCF is measured for the outwards loaded brace with SCF values acquired for all measurement points (B1-B4 and C1-C4).

2. Unbalanced in-plane bending - bending loads applied on both brace beams in joint definition plane. Bending direction for both braces is applied counter-clockwise, with SCF values acquired only for chord and brace crown points (B1-B2 and C1-C2).

3. Unbalanced out-of-plane bending - bending loads applied on both brace beams in a plane that is perpendicular to joint definition plane. Bending is applied counter-clockwise for both braces, with SCF values acquired only for chord and brace saddle points (B3-B4 and C3-C4).

4. Axial load on one brace only - load is applied along brace axis in an outwards direction to a single brace only. SCF is measured for the loaded brace with SCF values acquired for all measurement points (B1-B4 and C1-C4).

5. In-plane bending on one brace only - load is applied to a single brace in joint definition plane. Bending direction to the brace is applied counter-clockwise, with SCF values measured on the loaded brace, acquired only for chord and brace crown points (B1-B2 and C1-C2).

6. Out-of-plane bending on one brace only - load is applied to a single brace in plane that is perpendicular to joint definition plane. Bending is applied to the brace counter-clockwise, with SCF values measured on the loaded brace, acquired only for chord and brace saddle points (B3-B4 and C3-C4).

Static, single step load setups are established without including time domain into simulations and not combining aforementioned loading setups. This is required to properly establish nominal and hot-spot stress values which are representative of stress concentration values defined in DNVGL-RP-C203 [20].

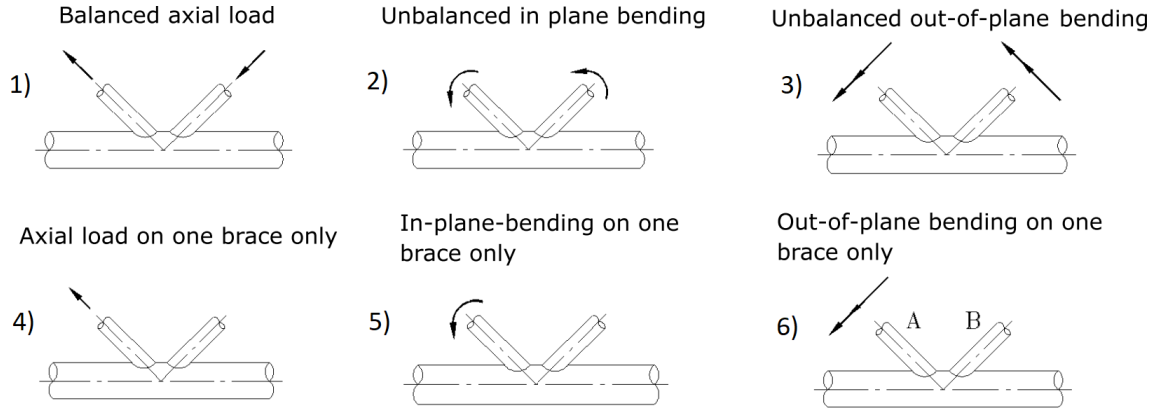

Figure 4.27: Analysed load setups of K-Joint [20].

Because nominal stress consists mainly of normal stress components (sum of axial tension/compression and two bending stresses) compared stress result that is acquired for hot-spot stress comparison also uses normal stress as its response. This allows for direct comparison to assess how stress concentration factors correlate between two calculation methods.

Result acquisition and comparison

Nominal stress values were calculated using the methodology for nominal stress acquisition principles defined in 4.3, where force and moment reaction values are used for manual stress calculations, based on linear beam theory. Manual calculations of stress concentration factors have been acquired using equations of DNVGL-RP-C203 [20], with all used equations summarized in appendix B. Hot-spot stress acquisition for the same measurement points is performed using linear stress extrapolation technique explained in section 4.4.2. These values are then divided by corresponding nominal stress result to acquire FEA stress concentration factors. These SCF values are then compared to their counterparts which were calculated using equations of DNVGL-RP-C203 [20]. Result overview for stress concentration factors acquired from DNVGL-RP-C203 [20] standard methodology (DNV) and finite element analysis (FEA) is summarized in table 4.6. Coloured value indicate which SCF value is higher for each measurement point depending on the method used.

Results show that majority of stress concentration factor value comparisons (29 out of 32 measurement pairs) provide analogous results with larger value (highlighted in blue) being 1.03-1.52 times larger than its lower counterpart. This comparison can be considered as corresponding well between two stress concentration factor establishment methods. Only a small margin of points (specifically SCF measurements for point B2) provide relatively poor comparison between results (leading to >2 times larger value is acquired when performing SCF value assessment using manual calculations based on recommendations of DNVGL-RP-C203 [20]). This is estimated to be a result of using identical stress concentration factor value in DNVGL-RP-C203 [20] calculations for both crown positions, when K-joint brace is defined at an angle and thus is expected to experience stress of higher variation between both crown points.

Table 4.6: Stress concentration factor result comparison for uni-planar K-joint crown and saddle points, between SCF values defined in DNVGL-RP-C203 [20] and acquired though FEA analysis.

	Balanced axial load		Unbalanced in-plane bending		Unbalanced out-of-plane bending		One Brace: axial load		One Brace: in-plane bending		One Brace: out-of-plane bending	
SCF	DNV	FEA	DNV	FEA	DNV	FEA	DNV	FEA	DNV	FEA	DNV	FEA
C1	6.33	7.44	4.41	5.02			6.82	4.74	4.41	4.10		
C2	6.33	6.90	4.41	6.31			6.82	5.55	4.41	5.89		
C3	6.33	7.22			15.94	13.27	19.43	16.83			11.75	12.67
C4	6.33	7.20			15.94	13.27	19.43	16.81			11.75	12.68
B1	4.01	4.17	3.30	2.30			2.31	3.27	3.30	2.50		
B2	4.01	1.41	3.30	1.18			2.31	1.76	3.30	1.42		
B3	4.01	6.11			11.12	11.53	9.80	11.52			11.31	9.66
B4	4.01	6.13			11.12	11.62	9.80	11.62			11.31	9.72

By taking aforementioned considerations into account it can be concluded that the approach for acquiring values of hot-spot stress using stress extrapolation technique is a viable option, as overall it shows good agreement between stress concentration factors calculated using equations provided in DNVGL-RP-C203 [20] and stress values directly extracted from finite element analysis simulations. Since the same simulation setup procedure is performed for the analysed problematic crane upper arm joint - chosen method for hot-spot stress acquisition with FEA simulations is feasible and expected to provide representative stress results which can be used for fatigue assessment purposes.

4.4.4. S-N curve

According to DNVGL-RP-C203 [20], when defining a representative S-N curve for hot-spot fatigue assessment - all tubular joints are assumed to be class T, illustrated in figure 4.28. This is the defined S-N curve used for chord-brace connection welds in the analysed tubular joint.

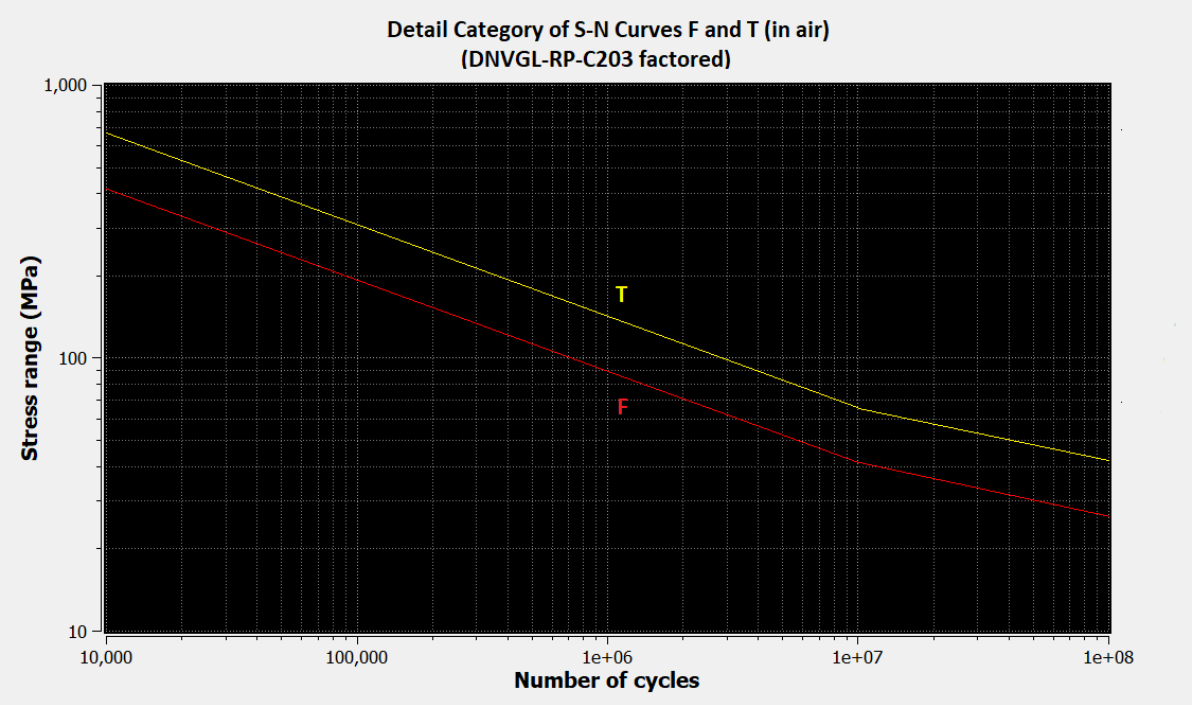

Figure 4.28: S-N curves used for evaluation of hot-spot stress fatigue damage in crane upper arm joint

However, although forestay and backstay beams are considered as a joint chord - it contains a weld, with an intermediate stiffener plate attached in the middle between both beams. For this purpose it requires a

separate weld definition which is not representative by class-T S-N curve. For this purpose, based on the weld specifics and according to recommendations of Lotsberg [57] - weld containing points F1-F8 and B1-B8 is treated as a circular hollow section of thickness above 8mm, welded end-to-end with an intermediate plate. This definition defines S-N curve of class-F (refer to figure 4.28). Additionally this description of weld type is comparable to S-N curve definition for specified points in nominal stress analysis - this should provide results which are corresponding well between fatigue damage results acquired using nominal and hot-spot stress methods.

4.4.5. Fatigue damage estimation

Using established hot-spot stress values for each measurement point at all time steps - Rainflow cycle counting is performed to acquire number and range of stress cycles. From here fatigue damage is assessed in relation to representative S-N curve and crane lifetime duration of 23 years (1.31 million work cycles). Fatigue damage calculations are performed based on fatigue damage formulation of DNVGL-RP-C203 [20] standard, with the using hot-spot fatigue damage calculation algorithm of SFAT software package. Damage accumulation factor D_i for 1 cycle is calculated using the principle formula 4.3 defined in section 4.3.7. Each contributing damage factor to the same measurement point is then summed up to acquire total hot-spot fatigue damage at specific location.

4.4.6. Results

Fatigue damage factor value calculations was performed for all measurement points defined in figure 4.17. These results for hot-spot fatigue damage factor at 1.31 million loading cycles are summarized in table 4.7, with colours highlighting point damage factor values based on their magnitude.

Table 4.7: Accumulated fatigue damage factor $D_{i_{HS}}$ of welded joint measurement points, acquired using conventional hot-spot fatigue assessment method (for 23 years of operation).

Brace	**Point**	**P1**	**P2**	**P3**	**P4**	**P5**	**P6**	**P7**	**P8**
	$D_{i_{HS}}$	3.139	0.078	0.233	0.066	0.299	0.081	4.548	0.314
	Point	**P9**	**P10**	**P11**	**P12**	**P13**	**P14**	**P15**	
	$D_{i_{HS}}$	0.169	0.009	0.094	0.263	0.184	0.000	0.140	
Chord	**Point**	**C1**	**C2**	**C3**	**C4**	**C5**	**C6**	**C7**	**C8**
	$D_{i_{HS}}$	3.235	0.321	0.191	0.209	0.220	0.408	4.449	0.896
	Point	**C9**	**C10**	**C11**	**C12**				
	$D_{i_{HS}}$	0.194	0.268	0.168	0.617				
Forestay	**Point**	**F1**	**F2**	**F3**	**F4**	**F5**	**F6**	**F7**	**F8**
	$D_{i_{HS}}$	0.011	2.946	0.081	0.095	0.013	0.020	2.023	1.414
Backstay	**Point**	**B1**	**B2**	**B3**	**B4**	**B5**	**B6**	**B7**	**B8**
	$D_{i_{HS}}$	0.012	2.563	0.124	0.143	0.013	0.020	4.420	3.067

Results show that for defined lifetime, joint structure is incapable of surviving experienced stress cycles. In total 10 points (out of 43) indicate fatigue failure with their values exceeding fatigue damage limit of $D_{i_{HS}} < 1$ (with points P7, C7 and B7 exceeding the limit 4-fold). This is an indication that the structure is not safe for operation under defined loading conditions as it accumulates a large amount of fatigue damage along its welds. Figure 4.29 illustrates positions of critical failure points and their distributions.

In terms of critical failure point positions - they are concentrated at the brace saddle locations on both sides of the joint, as well and along the bottom weld between forestay and backstay beams. This is an interesting observation which correlates well with positions of crack propagation which has been observed in the crane joint of Cornelis Tromp 25T as well as other cranes of the same model. As it has been detected in real crane joint structures - fatigue cracks are present both at the saddle position as well as along the length of the lower part of forestay-backstay weld, however it is not fully clear where these cracks initiated or whether it happened in one or multiple positions. Nevertheless this indication shows that performed hot-spot fatigue assessment is capable of distinguishing points of crack initiation in the analysed geometry. The only question concerning this approach lies in the magnitude of fatigue damage and whether performed hot-spot fatigue assessment which uses Von Mises stress is too conservative and overestimates the magnitude of experienced fatigue damage.

Finally, based on the positions of failure in the assessed upper arm joint - it appears that most points

experiencing highest fatigue damage are in inaccessible locations both for inspection and repair (hidden by structure of pylon legs). Accessibility of critical potential failure points is a crucial aspect of well-established and safe structural design which in the analysed joint structure has not been properly taken into account.

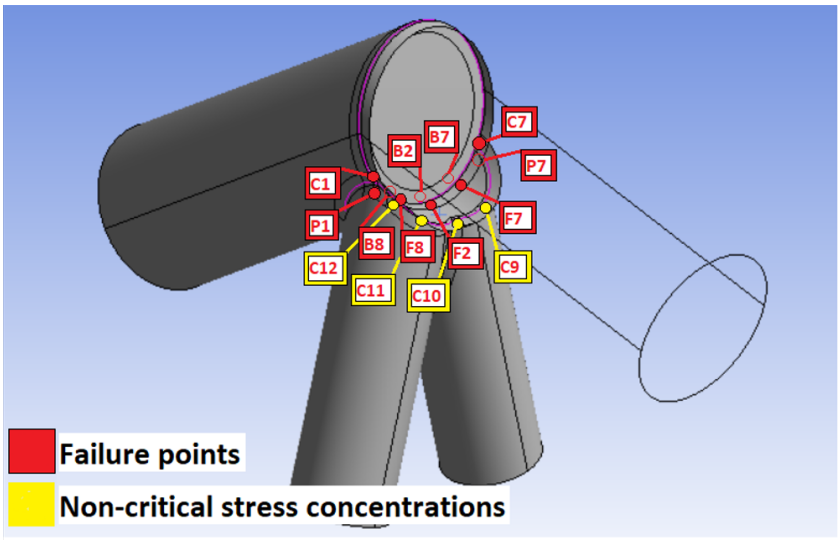

Figure 4.29: Locations of failure points (D > 1) and non-critical stress concentrations (0.5 > D > 1) as measured using hot-spot stress fatigue assessment approach (marked in red and yellow respectively)

4.5. Result comparison

This section provides a comparison of fatigue assessment results between nominal stress and hot-spot stress approaches. It also provides main observations acquired from result comparison to potentially find the reason of crane failure.

Having concluded fatigue analysis with both nominal and hot-spot stress approaches, it is now possible to compare acquired results and assess how incorporation of stress concentration effects into fatigue assessment affects fatigue damage estimation results.

Table 4.8 presents a comparison of fatigue damage factor magnitude results acquired using nominal stress approach D_{i_N} and hot-spot stress approach $D_{i_{HS}}$. Here negative values (highlighted in blue) indicate where nominal stress fatigue approach acquired higher damage factor D_i value, while positive values (highlighted in red) show the opposite conclusion. Value comparison is established for identical point distribution setup in both analyses allowing for observing direct fatigue damage factor value contrast at all measurement points. For measurement point location setup and naming convention - refer to figure 4.17 of section 4.3.2.

Table 4.8: Comparison of accumulated fatigue damage factor $D_{i_{HS}} - D_{i_N}$ values around the welds of analysed lemniscate crane upper arm structure, acquired using nominal stress against acquired hot-spot stress fatigue assessment method (for 23 years of operation).

Brace	**Point**	**P1**	**P2**	**P3**	**P4**	**P5**	**P6**	**P7**	**P8**
	$D_{i_{HS}} - D_{i_N}$	2.763	-0.224	0.196	-0.033	0.253	-0.293	3.887	-0.067
	Point	**P9**	**P10.2**	**P11**	**P12**	**P13**	**P14**	**P15**	
	$D_{i_{HS}} - D_{i_N}$	0.087	-0.017	0.024	0.259	0.175	-0.232	0.135	
Chord	**Point**	**C1**	**C2**	**C3**	**C4**	**C5**	**C6**	**C7**	**C8**
	$D_{i_{HS}} - D_{i_N}$	3.217	0.266	0.121	0.137	0.141	0.340	4.425	0.816
	Point	**C9**	**C10**	**C11**	**C12**				
	$D_{i_{HS}} - D_{i_N}$	0.094	0.164	0.057	0.522				
Forestay	**Point**	**F1**	**F2**	**F3**	**F4**	**F5**	**F6**	**F7**	**F8**
	$D_{i_{HS}} - D_{i_N}$	-0.025	2.882	0.022	0.025	-0.027	-0.034	1.948	1.356
Backstay	**Point**	**B1**	**B2**	**B3**	**B4**	**B5**	**B6**	**B7**	**B8**
	$D_{i_{HS}} - D_{i_N}$	-0.030	2.502	0.052	0.083	-0.046	-0.023	4.363	2.993

Results show a very significant difference in accumulated fatigue damage between nominal and hot-spot

stress approaches. In total, 31 out of 43 measurement points show larger fatigue damage accumulation factor when it is calculated using a hot-spot stress approach - with 10 of these points showing a factor value difference above $|D_{i_{HS}} - D_{i_N}| = 1$ (specifically for points P1, P7, C1, C7, F2, F7, F8, B2, B7, B8). These are points located at the brace saddle connection with the chord (where a significant stress concentration has been observed in section 4.2.7), as well as at the bottom part of forestay-backstay beam weld. The difference in magnitude at these points (which also correlate well with the locations where the crane has experienced stress concentrations in FEA model and crack propagation in real crane) shows that a nominal stress fatigue assessment appears to severely underestimate fatigue damage appearing in the real structure. Additionally, when it comes to damage comparison between methods - points P2, P6 and P14 show larger damage accumulation using a nominal stress approach by a fairly reasonable margin (i.e. $|D_{i_{HS}} - D_{i_N} -| > 0.2$). However in the FEA model of the crane structure these specific locations do not appear to show a presence of stress concentrations.

There are two key reasons why results between both fatigue assessments are different.

1. Nominal stress approach cannot distinguish the area over which stress is distributed in the cross-section - this method averages force and moment reactions over the entire cross section, leading to less accuracy in results at specific measurement points. This is very likely the main reason why points P2, P6 and P14 show larger damage accumulation factor values for nominal stress results, as their measurements were taken at the end points of an elliptical cross-section, which based on linear beam theory tend to increase stress result due to larger distance from the center point of a specific cross-section.

2. Hot-spot stress fatigue assessment measures stress directly from an FEA simulation nodes meaning its stress values are localised and are able to assess presence and effects of stress concentrations, with S-N curves accounting specifically for presence of this factor in its stress results.

In a fatigue analysis, choice of S-N curve has a large effect on resultant values of fatigue damage factor. However, for both nominal and hot-spot stress approaches S-N curves were chosen on identical weld definitions. This means that both nominal and hot-spot S-N curves can be directly compared as they represent same points and weld types in uniform fashion, which indicates that choice of S-N curve is not the reason for difference in fatigue damage factor results. This means that the main reasons for result difference is mainly linked to how nominal stress approach is not able to account for and distinguish locations of stress concentrations. This already indicates that hot-spot stress approach is likely should be preferred if a structure is prone to forming stress concentrations. However there is an additional important reason - when performing finite element (FE) analysis for design of plated structures it is often found more convenient to extract hot-spot stress from the analysis than that of a nominal stress [**?**]. This is linked to stress acquisition principle of performing nominal stress fatigue assessment with a 2D or 3D mesh element FEA model, which:

1. Does not allow for nominal stress extraction directly from FEA simulation - stress acquisition has to be performed through manual calculations based on linear beam theory, with extracted force and moment reaction measurements.

2. Definition of cross section placement is not straightforward for more complex geometry as in the case of pylon leg setup of analysed tubular joint. Location and angle of a cross-section used for performing measurements is partially affected by subjective judgement of a person performing the measurements – meaning that the same result model might acquire partially different results depending on who is performing the setup. This is however only an issue for complex geometry setups and simple beam element models do not indicate pressence of this problem.

3. Stress calculation for complex geometry which contains continuously changing profile calculates less representative stress results. This is the case because definition of cross-sectional area moment of inertia for uncommon profiles or profiles that do not represent moment of inertia for the entire length of the geometry calculate stress results with an potential added error factor.

On the other hand, hot-spot stress approach, as mentioned previously, includes stress concentration effects which are localized to a specific measurement location, without increasing the complexity of performed calculations. This is an observation which shows that fatigue assessment results acquired using hot-spot stress method provides more significant level of accuracy than its nominal stress counterpart, without sacrificing computational efficiency. These factors indicate that not only the entire process of acquiring nominal

stress with a multi-dimensional FEA element model is prone additional presence of error for complex geometry, but also that the calculation process is not particularly easier than performing fatigue assessment using a hot-spot stress approach. Overall the entire process of nominal stress fatigue assessment is prone to providing less accurate results than hot-spot stress method which incorporates stress concentration effects into its formulation, while requiring amount of setup that is heavily comparable, leading to a conclusion that fatigue assessment of detailed geometry should be performed using a hot-spot fatigue assessment method, rather than nominal stress approach.

4.5.1. Reason for failure of crane tubular joint

After evaluating differences between two damage estimation methods it is now possible to get a better idea why the analysed crane upper arm joint is experiencing problems of crack propagation which (as observed in a crane of the same model) can even lead to fatal crane failure. Hot-spot stress fatigue results show presence of serious stress fluctuation range during crane operation, which accumulates a very large amount of fatigue damage. This is a result of stress accumulation during performance of hoisting operations, when stress values at critical points significantly increase. With the large fatigue damage factor values at multiple weld locations reaching magnitudes up to 4.5 - it is clear that the joint structure has been poorly assessed in terms of its fatigue resistance during its design phase. Additionally the locations of fatigue damage accumulation are in positioned in a way which does not allow for their inspection or repair without crane disassembly, making the entire joint design inherently flawed. A very likely reason for why this happened is based on most likely conclusion that during design phase - crane structure has not been very well evaluated in terms of its stress concentration magnitude and effects. This is likely a result of using simple nominal stress approach for fatigue assessment, which has been the general norm for fatigue assessment in the industry for the last several decades. Additionally - use of static load establishment (compared with time-dependent load setup applied in this research) and potential assessment of fatigue by employing a beam element model of the crane (as performed in Tawjoeram [86]) could have been additional reasons why fatigue damage has been underestimated. However these factors are more difficult to assess without access to initial load and stress data used during crane design phase.

Overall, the fatigue assessment approach which takes into account stress concentrations is highly preferred for evaluating damage within complex geometries, as it allows to indicate well locations where cracks appear to propagate in the real structure.

4.6. Conclusion

This section concludes results and observations made and provides answers to research questions indicated at the beginning of this chapter.

In this chapter, a finite element analysis has been established in detail which explains the main principles of its setup in terms of research scope, geometry, mesh setup and boundary conditions. FEA model setup is acquired in a way which allows extraction of accurate results of stress, force reaction and moment reaction responses relevant to the problematic upper arm tubular joint. During crane setup, presence and effects of stress concentrations have been evaluated to determine whether measured large magnitude of a stress response in the shell model of the joint structure is a result of stress singularity or a stress concentration. Methods on how to distinguish both variants is discussed. Using the established FEA model, gathered responses were used for performing fatigue assessment using nominal stress and hot spot stress approaches. This has been done to determine whether inclusion of stress concentration effects into fatigue assessment affect resulting fatigue damage factor response. (which is possible with hot-spot stress method, but is not accounted for using nominal stress approach)

Using result of performed fatigue analysis it is possible to answer following research questions:

How does incorporation of stress concentrations into fatigue assessment affect resultant fatigue life estimation in relation to nominal stress fatigue analysis?

Results of fatigue assessment has shown significantly different results between nominal and hot-spot stress fatigue analyses. Nominal stress approach indicated that the structure is safe for 23 years of operation (1.31 million loading cycles), while hot-spot stress approach showing critical failure at 25% of measured points, with fatigue damage factor reaching values up to 4.5. It is estimated that hot-spot stress approach provides more accurate results due to its ability to account for stress concentration effects. Additionally it has been observed that locations which were distinguished in fatigue analysis to experience critical failure also correlate well with locations where fatigue cracks appear to propagate in multiple cranes of the same model

as the analysed Cornelis Tromp 25T lemniscate crane.

What is the main reason of joint failure for the analyzed lemniscate crane?

Main reason why the crane failed is likely the result of large stress concentration, appearing at the brace saddle connection with the chord and at the lower part of forestay-backstay weld. This location also experiences large stress fluctuation range during hoisting operation, which is the reason for fatigue damage accumulation that eventually lead to crack initiation and propagation in the joint. It is likely that during design phase the crane structure has been not been properly evaluated for its potential to develop stress concentrations and any fatigue assessment using a nominal stress approach would not have been able to capture their effects towards fatigue damage accumulation.

5

Multi-axial fatigue

Tubular joints are known to have a relatively complex directional distribution of stresses around its welds, which tends to vary heavily depending on joint setup. Additionally because analysed crane upper arm joint is also exposed to multiple time-varying loads - there is a possibility that the joint might experience significant multi-axial stresses that are also potentially non-proportional and/or out-of-phase. In the case of potential presence of multi-axial stress - assessing fatigue using only one stress direction (i.e. assessing only maximum principal stress) could lead to underestimation of fatigue damage, while assessing contribution of all stress component accumulative effect towards stress response (i.e. assessing fatigue using Von Mises stress) might prove to be an overestimation of fatigue damage, as not all stress components might be contributing towards fatigue damage or contributing at uneven proportions. These observations indicate that there is a possibility that conventional fatigue assessment method of hot-spot stress which was discussed in chapter 4) might not be sufficiently representative of real fatigue damage accumulation in the analysed crane joint and accounting for stress direction in fatigue formulation can potentially provide results that better represent real damage accumulation in the structure.

This chapter is meant to assess fatigue of the crane upper arm tubular joint using multi-axial fatigue assessment method which considers stress direction in its formulation. Its goal is to provide an answer for the research question of:

Is incorporation of stress direction into fatigue assessment beneficial for evaluating fatigue damage at the welds of problematic joint? How its results compare to more conventional hot-spot fatigue assessment approach?

5.1. Indication of multi-axial stress response

This section investigates the whether decision of performing multi-axial fatigue assessment on the problematic crane upper arm joint structure has a theoretical basis. Determination of the most optimal variant of multi-axial fatigue analysis approach is investigated in relation specific qualities of experienced structural stress.

Under the principles of conventional fatigue assessment, damage is evaluated by assessing cyclic loading effects without considering how stress direction can influence its results. However, most commonly under real life conditions stress direction has an effect on damage accumulation, potentially in a manner where more than one stress component is large enough to have a significant effect on fatigue damage results. Additionally multiple stress components can act both in-phase and out of phase with each other and vary in their frequency and amplitude. This can change principal stress direction during loading. All of these effects can factor into rate of fatigue damage accumulation.

As lemniscate cranes are commonly operated in a manner where multiple operations occur at the same time (e.g. grab hoisting and crane slewing, crane luffing and slewing, etc.) this means that the problematic tubular joint can be simultaneously loaded in multiple directions at varying amplitudes, leading to potential of complex stress states occurring at the points which are prone to fatigue damage accumulation. Combining this fact with the quality of tubular beams to develop complex stress distributions, it is possible that accounting for stress direction with the help of multi-axial fatigue assessment approach can help to better understand the real magnitude of fatigue damage where the joint is most prone to begin crack initiation. Nevertheless -

it is not clear whether there is a presence of significant multi-axial stress response in the analysed structure. For this purpose assessment has to be performed in a manner which is backed by theoretical reasoning.

In order to understand whether a multi-axial fatigue assessment is needed, there has to be evidence of multi-axial stress present in the analysed structure. Figure 5.1 illustrates how stress distributes in the analysed crane upper arm joint. This illustration shows that principal stress directions do indeed vary around the welds in terms of their direction and magnitude - this could potentially cause fatigue damage to be more complex than in structures where stress is distributed in a uniform manner.

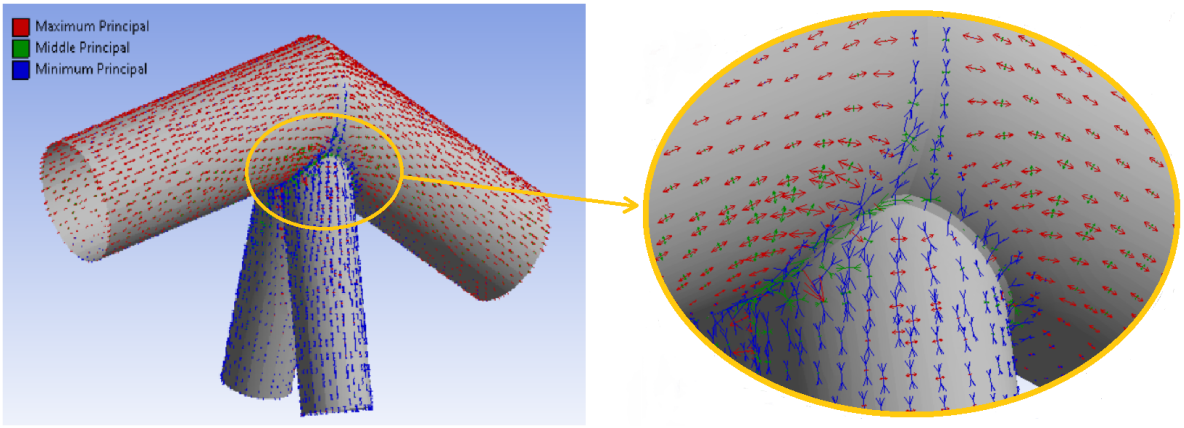

Figure 5.1: Principal stress vector distribution in the crane upper arm joint

General criteria is formulated, which indicate potential presence of significant multi-axial stress at an analysed location. In general - determination on whether application multi-axial fatigue approach might prove handy for increasing accuracy of fatigue assessment of a specific structure can be determined by three following indicators:

1. Exposure to multi-directional loads affecting analysed structure over its loading cycle.

2. Multiple (more than one) stress components of comparable magnitude affecting geometry locations sensitive to fatigue damage (e.g. stress concentrations, welds, etc.).

3. Presence of non-proportionality in the response of significant stress components, which in turn lead to significant change in principal stress direction during loading cycle of the structure.

It is important to note that in order to determine whether multi-axial fatigue analysis would be beneficial for result accuracy - all three indicators are not needed. However depending on which factors are present allows for determination of most optimal multi-axial fatigue assessment approach for the specific analysed case. In the upcoming sections each of the three indicators are evaluated one by one, in order to determine possible need for applying a multi-axial fatigue assessment approach.

5.1.1. Exposure to multi-directional loads

The first step in evaluating presence of multi-axial stress is to determine if joint geometry is exposed to multi-directional loading. It is already apparent from load establishment performed in chapter 3 that the upper arm structure is exposed to multiple body and acceleration loads. Nevertheless when assessment scope is localised to the geometry around only the problematic joint - load effects might not directly translate to presence of multiple load components simultaneously acting on specific joint beams. For this purpose tensile force and bending moment reactions were measured at each beam of the upper arm joint (forestay, backstay, right and left-right pylon legs), two meters away from the weld. Figure 5.2 illustrates these locations and orientation of taken force and moment reaction measurements.

From the assessment results indicated in figure 5.3, it has been observed that there is a significant presence of both axial force and bending moment affecting joint members - with forestay and backstay experiencing tensile force of up to $150kN$ and bending moment in Y direction of $150kNm$ (top graphs of figure 5.3). Additionally, some effect of non-proportionality has been observed when assessing magnitude of force and moment reactions over the time of crane operational cycle. This is more apparent in bending moment

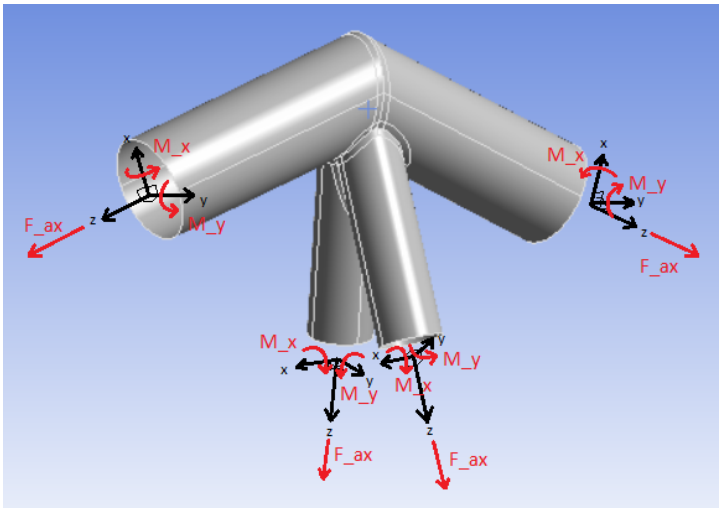

Figure 5.2: Directional load measurement setup for load reactions used to determine presence of multi-axial stress.

responses of pylon legs (bottom graphs of figure 5.3), where the magnitude and reaction direction does not fully conform between its axial force and bending moment responses (Example: around a 25 second mark, left pylon experiences a non-proportional 50% drop in its bending moment response in X direction, which is not seen at comparable proportion neither in axial force (which experiences a 19% drop) nor for bending moment in Y direction (7% drop in magnitude)). These observations are an indication that not only there is potential presence of multiple significant stress components affecting welds in the structure, but also that this phase shift might contribute to changing direction of principal stresses at critical locations over time. These factors can potentially affect fatigue damage accumulation rate and it might not be accurately captured with a conventional hot-spot fatigue assessment described in section 4.4. If that is the case - analysis of such structure would benefit from a multi-axial approach for fatigue assessment, which considers effects of stress direction and possibility of multiple stress components having considerable effect towards fatigue damage accumulation.

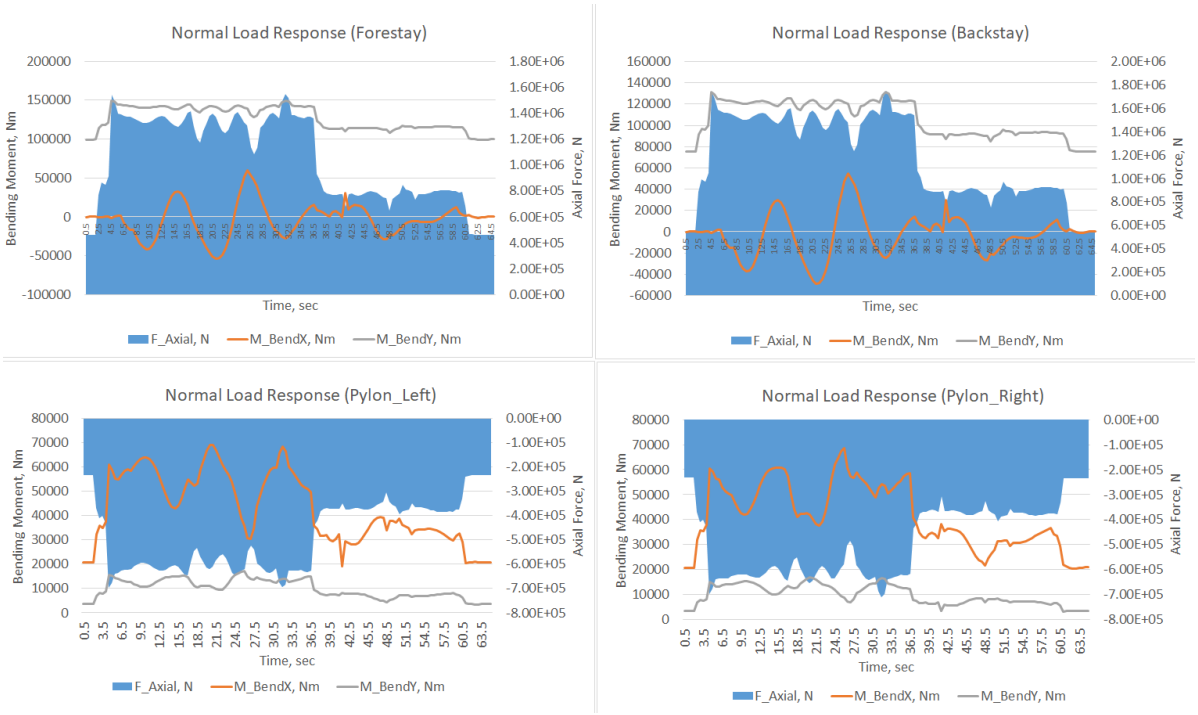

Figure 5.3: Overview of normal reaction load magnitudes.

5.1.2. Presence of multiple significant stress components

Since force and moment reaction response away from the welded joints alone is not enough to conclude significant presence of non-proportional stress - it does call for further investigation of whether multi-axial fatigue assessment might be needed for estimating fatigue damage in the critical upper arm joint.

The second step in the investigation is to determine if there is a presence of more than one stress components acting at the hot-spot locations around the length of tubular joint welds. For the purpose of this analysis - principal stresses are used as a assessment response.

Evaluation process is defined as follows:

1. Stress measurement locations are defined around welds of upper arm joint, based on the same distribution as it has been established for nominal and hot-spot fatigue assessment, presented in chapter 4. Please refer to figure 4.17 for point location setup and naming convention.

2. Stress extrapolation is performed by taking stress measurements $0.1\sqrt{rt}$ distance away from the weld at each hot-spot location at the closest mid-side mesh node. Here r and t are respectively radius and thickness of tubular beam, on which surface stress is being measured. This value is treated as extrapolated hot-spot stress result. Because for multi-axial stress assessment, direction of stress components is relevant - stress extrapolation technique used in chapter 4 is less reliable as here stress direction would have to be averaged for each of the measurement points to the extrapolation region and might not properly represent real stress direction close to the weld toe. Both approaches are considered as feasible for stress extrapolation in hot-spot fatigue assessment as per recommendations of DNVGL-RP-C203 [20].

3. Two largest principal stress components are evaluated at each location, in terms of their absolute magnitude. As it is apparent for thin tubular beam structures, these stress components are: one parallel and one perpendicular to the weld length. The third principal stress - parallel to the thickness of the beam - possess low values in comparison with two other components (<5% of the largest principal stress).

4. Magnitude of absolute values for parallel and perpendicular stress is used to determine which stress component is primary and secondary. Primary stress $\overline{\sigma_{1_i}}$ is the one with the larger absolute value of stress magnitude, with the lower value assigned as secondary stress $\overline{\sigma_{2_i}}$.

5. Primary and secondary stress components are compared with each other to assess whether both principal stress components are large enough to have a significant effect on the stress in the node. The threshold for secondary stress $\overline{\sigma_{2_i}}$ significance is assigned to being ≥ 30% to value of primary stress $\overline{\sigma_{1_i}}$. If stress at hot-spot points indicate that there is a presence of significant stress in both parallel and perpendicular direction it indicates presence of multi-axial stress response.

Table 5.1: Comparison of average absolute primary and secondary stress values. Percentage shows proportional value of secondary stress magnitude in comparison with the primary stress magnitude. Colors indicate significant values.

Brace	**Point**	**P1**	**P2**	**P3**	**P4**	**P5**	**P6**	**P7**	**P8**
	$\sigma_{1_i}/\sigma_{2_i}$	16.33%	55.74%	77.63%	25.56%	77.33%	56.80%	16.36%	34.41%
	Point	**P9**	**P10**	**P11**	**P12**	**P13**	**P14**	**P15**	
	$\sigma_{1_i}/\sigma_{2_i}$	87.83%	48.54%	87.61%	35.50%	32.90%	10.69%	0.30%	
Chord	**Point**	**C1**	**C2**	**C3**	**C4**	**C5**	**C6**	**C7**	**C8**
	$\sigma_{1_i}/\sigma_{2_i}$	18.86%	42.32%	95.61%	52.68%	96.03%	40.74%	12.58%	23.43%
	Point	**C9**	**C10**	**C11**	**C12**				
	$\sigma_{1_i}/\sigma_{2_i}$	67.18%	40.24%	69.98%	25.22%				
Forestay	**Point**	**F1**	**F2**	**F3**	**F4**	**F5**	**F6**	**F7**	**F8**
	$\sigma_{1_i}/\sigma_{2_i}$	11.04%	79.51%	59.33%	58.25%	82.35%	85.49%	42.16%	41.99%
Backstay	**Point**	**B1**	**B2**	**B3**	**B4**	**B5**	**B6**	**B7**	**B8**
	$\sigma_{1_i}/\sigma_{2_i}$	10.57%	80.84%	60.55%	59.54%	83.19%	86.32%	62.36%	98.54%

Which component of principal stress is considered as primary and secondary depends on the magnitude of the absolute stress value - larger component is always considered as primary stress σ_{1_i}, while the lower-valued component is defined as the secondary stress σ_{2_i}. Table 5.1 summarizes comparison of primary and

secondary stress absolute values for each measurement point. Highlighted percentage values indicate presence of significant secondary stress.

Extended result comparison which includes values for each evaluated principal stress component are summarised in table C.1 of Appendix C. According to acquired results presented in table 5.1 - 89% of the analysed hot spot points experience significant stress both along and perpendicular to the weld length direction (passing secondary stress percentage threshold of > 30%). This data concludes that there is a significant presence of multi-axial stress around the welds of problematic upper arm joint. Based on this observation it is safe to conclude that performing a multi-axial fatigue assessment is recommended for the crane upper arm joint.

5.1.3. Presence of non-proportionality in stress components

Tubular joints are specifically known to experience complex stress distribution. When stress is measured with an inclusion of time domain - under multi-directional loading it is possible to measure appearance of non-proportional stress and a possibility of phase shift between different stress responses (such as normal and shear stress). These factors (if present) result in a continuous variation of principal stress direction at critical locations that might be sensitive to fatigue damage. If that is the case and stress direction significantly changes - performance of multi-axial fatigue assessment with a method which accounts for stress non-proportionality is required to properly assess fatigue damage.

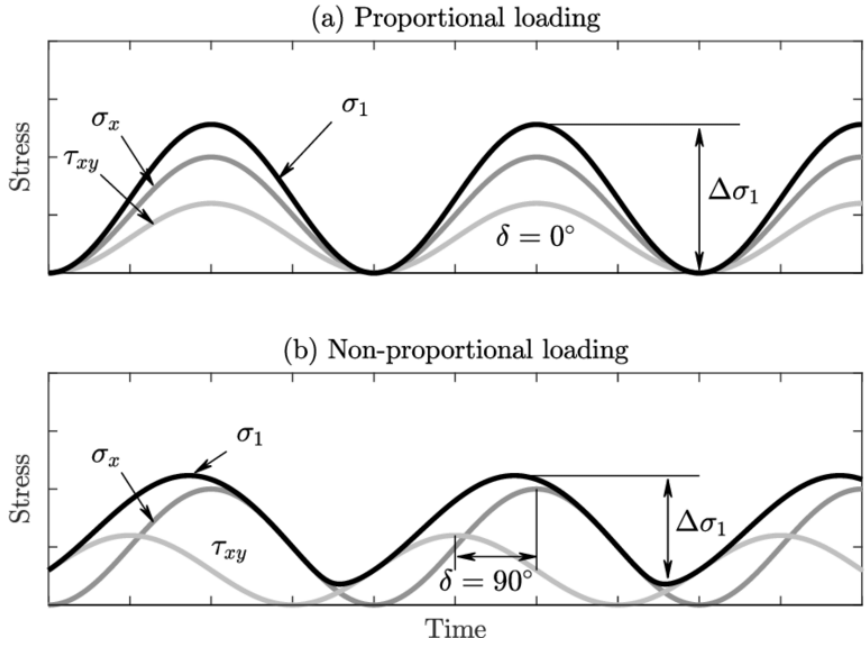

Figure 5.4: Illustration of proportional vs. non-proportional loading [72].

When it comes to the threshold of stress direction angle change that is large enough to lead towards imposing significant potential effect in fatigue damage accumulation rate - is still up for debate. Linden [53] indicates that accounting for stress direction in fatigue analysis is recommended when principal stress direction changes more than 20° over its loading cycle, while DNVGL-RP-C203 [20] recommends accounting for it if this value exceeds 10°. To ensure that the chosen evaluation approach does not underestimate effects of changing stress direction, the lower limit of 10° is chosen as the threshold for indicating whether there is presence of stress non-proportionality.

For evaluating change of stress direction of the lemniscate crane upper arm joint - measurements are taken at all nodal hot-spot locations, as defined in section 4.3.2. Maximum change in stress angle $\Delta\theta_i$ is measured for each measurement point i over the total crane operational cycle. Table 5.2 summarizes these results. Results show that maximum change of stress angles at hot-spot locations vary between 0° and 7° degrees, with measurement point at chord crown (i.e. chord points P4 and P10) and lower part of the weld between forestay and backstay (i.e. forestay points F7 and F8) experiencing the highest fluctuations of 7°. However since even the points with largest fluctuations in stress direction do not reach the threshold of $\Delta\theta_i >$

10°, this means that effects of stress non-proportionality do not have to be accounted for in fatigue analysis of lemniscate crane upper arm joint.

Table 5.2: Maximum angle change $\Delta\theta_i, deg$ of principal stress direction for critical nodes around the weld of crane upper arm joint

Brace	**Point**	**P1**	**P2**	**P3**	**P4**	**P5**	**P6**	**P7**	**P8**
	$\Delta\theta_i$, **deg**	3.0	3.0	2.0	8.5	1.5	2.5	2.5	4.0
	Point	**P9**	**P10**	**P11**	**P12**	**P13**	**P14**	**P15**	
	$\Delta\theta_i$, **deg**	3.0	8.5	3.0	2.5	5.0	3.0	4.5	
Chord	**Point**	**C1**	**C2**	**C3**	**C4**	**C5**	**C6**	**C7**	**C8**
	$\Delta\theta_i$, **deg**	3.0	3.0	1.5	7.0	1.5	2.5	3.0	4.0
	Point	**C9**	**C10**	**C11**	**C12**				
	$\Delta\theta_i$, **deg**	3.0	7.0	3.0	3.0				
Forestay	**Point**	**F1**	**F2**	**F3**	**F4**	**F5**	**F6**	**F7**	**F8**
	$\Delta\theta_i$, **deg**	0.0	5.0	5.0	5.0	0.5	1.0	7.0	7.0
Backstay	**Point**	**B1**	**B2**	**B3**	**B4**	**B5**	**B6**	**B7**	**B8**
	$\Delta\theta_i$, **deg**	0.0	5.5	5.0	5.0	1.0	1.0	2.5	3.0

5.1.4. Assessment overview

By concluding results of all three evaluated indicators, following conclusions have been made:

1. Axial force and bending moment assessment has shown that there is a presence of multiple different load reactions present in the joint, as well some non-proportionality in load responses, indicating possibility of multi-axial stress response acting in the structure.

2. Principal stress magnitude comparison around joint welds has confirmed that most points have two principal stress components per point which can be considered as significant (second largest stress component being more than 30% of largest principal stress component magnitude).

3. Measurements of principal stress angle change during crane loading cycle has shown that effects of stress non-proportionality do not have to be accounted for in fatigue analysis of lemniscate crane upper arm joint.

Presence of two principal stress components of considerable magnitude leads to a conclusion that *multi-axial fatigue assessment is recommended for evaluating fatigue of analysed crane upper arm joint.* However, since the critical measurement locations around the weld do not experience significant change in stress direction during its stress cycle, it means that applied multi-axial fatigue assessment method does not need to account for non-proportionality in its stress response.

5.2. Multi-axial fatigue analysis setup

This section describes main steps and procedure of performing multi-axial fatigue assessment on the problematic crane upper arm joint.

5.2.1. Approach of multi-axial fatigue assessment

As it has been assessed in the literature review provided in chapter 2, there is a large number of multi-axial fatigue assessment methods which could be potentially applied for evaluating fatigue damage accumulation in welded structural joints, both when stress response is proportional and non-proportional. Since the change of principal stress direction in the case of analysed crane upper arm joint measurement points, does not significant change (remains under the threshold limit of 0-10%) - this reduces the complexity of multi-axial fatigue setup and thus more conventional multi-axial fatigue assessment methods can be applied. Specifically, chosen approach uses a multi-axial fatigue assessment method described in the 2020 edition of DNVGL-RP-C203 [20]. This is a critical plane method which uses a stress-based approach that is designed for evaluation of fatigue damage accumulation of welded tubular joints. It uses hot-spot stress responses within a critical principal stress plane to evaluate fatigue damage accumulation. This method addresses the challenges of multi-directional fatigue by evaluating two damage components for each hot spot: one representing the

damage due to stresses perpendicular to the weld toe, $D_{\perp}$, and one due to the damage accumulation from stress ranges more parallel with the weld toe, $D_{\parallel}$. This method has several benefits which makes it suitable for specific case analysed in this paper:

1. It is meant for evaluating stress of welded tubular joints and welded plates.
2. It is best suited for fatigue assessment for locations where stress direction is relatively constant as in the case of analysed joint.
3. It is applicable with the same method for stress extrapolation as used in the conventional hot-spot stress approach, which has been described in chapter 4.
4. It uses general Rainflow counting algorithm for defining stress cycles, simplifying the assessment.
5. It uses same damage rule as hot-spot stress method to calculate cumulative fatigue damage.
6. Specific S-N curves and their recommendations are readily provided in DNVGL-RP-C203 [20].

Combining all these reasons it is apparent that measuring multi-axial fatigue assessment using this method is sufficient for estimating directional fatigue effects in the crane upper arm joint, while at the same time being significantly less complex than more advanced multi-axial fatigue assessment approaches introduced in chapter 2.

5.2.2. Fatigue assessment methodology

Multi-axial fatigue assessment methodology used for the purposes of this research is built on the principles of conventional hot-spot fatigue assessment methods and thus share some similarities in terms of measurement point definition for stress extrapolation and fatigue damage calculation. However it includes some additional steps in stress definition stage which separates both methods. Figure 5.5 presents a general step workflow for assessing fatigue using applied multi-axial fatigue assessment approach.

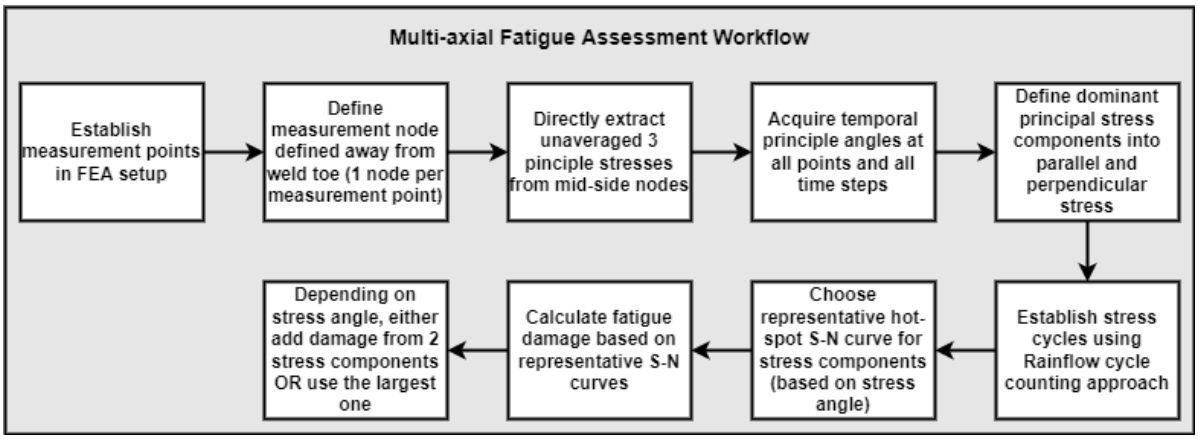

Figure 5.5: Workflow overview for multi-axial stress fatigue assessment procedure.

According to workflow graph presented in figure 5.5 approach of fatigue assessment methodology can be summarized as follows:

1. Stress measurement locations are defined around welds of upper arm joint, based on the same distribution as it has been established for nominal and hot-spot fatigue assessment methods presented in chapter 4. Please refer to figure 4.17 for point location setup and naming convention.
2. Stress extrapolation is performed by taking stress measurements $0.1\sqrt{rt}$ distance away from the weld at each hot-spot location at the closest mid-side mesh node. Here r and t are radius and thickness respectively of tubular beam on which surface stress is being measured. This value is treated as extrapolated hot-spot stress result.

3. Each principal stress component is assigned as parallel $\sigma_{\parallel}$ and perpendicular $\sigma_{\perp}$ based on its direction angle θ in relation to a coordinate system defined at each hot-spot location (as illustrated in figure 5.6). Which component has angle value of $< 45°$ in relation to perpendicular axis of its coordinate system axis (as presented in figure 5.6) is treated as perpendicular principal stress component $\sigma_{\perp}$ and vice versa.

4. Stress cycle for each measured stress component is established using conventional Rainflow cycle counting algorithm, which has been applied for both nominal and hot-spot stress fatigue assessment methods discussed in chapter 4.

5. Using defined principal stress values, fatigue damage is calculated separately for each stress component, meaning that two fatigue damage measurements are made per each point. S-N curve is chosen based on stress component angle as explained in section 5.2.3.

6. Depending on stress angle for parallel stress - fatigue damage factors for each stress component either sums up both component damage factor values (which happens when parallel stress angle is between $45° - 60°$). Otherwise the largest fatigue damage factor value is used.

Figure 5.6 illustrates how parallel and perpendicular principal stress components can be defined based on direction angle θ which coordinate system is located tangent to the weld at calculated measurement point position.

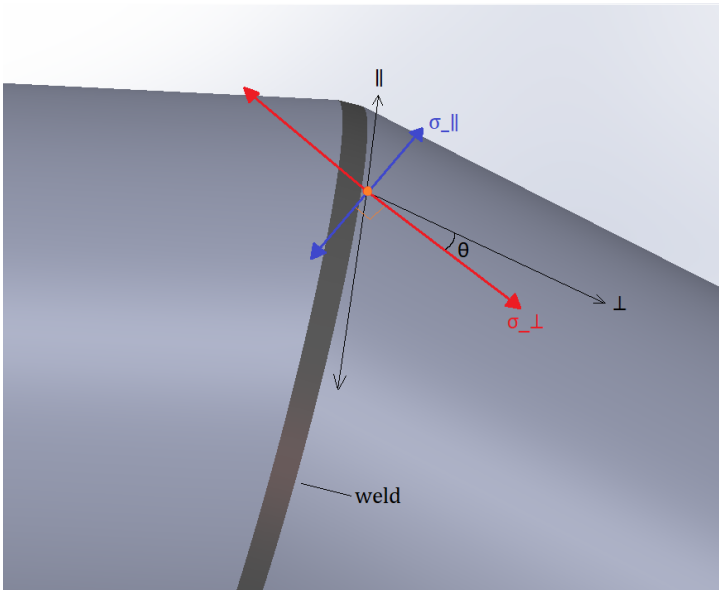

Figure 5.6: Directional principal stress measurements of stress angle θ used for determination of relevant S-N curve.

5.2.3. S-N curve

When it comes to used multi-axial fatigue assessment approach - two S-N curves used for calculating fatigue damage ratio at measurement points around the weld. Specifically hot-spot stress curves of class-T and class-C2 are applied. Because for multi-axial fatigue analysis each measurement point consists of two dominant stress components which are evaluated separately - two S-N curves are applied separately for each principal stress component of each measurement point. Figure 5.7 illustrates graphs of used hot-spot stress S-N curves.

The choice of which S-N curve is used for which stress component is dependent on the angle of stress component in relation to axis illustrated in figure 5.6. For each point 0 degree value is defined perpendicularly to the weld length with 90 degree value of stress angle θ appearing when stress component is parallel to the weld length. For principal stress components whose stress angle at measurement point location stays below $30°$ - class-T curve is applied. Otherwise class-C2 S-N curve is used. S-N curve choice for multi-axial fatigue assessment of original crane joint structure is summarized in appendix C.

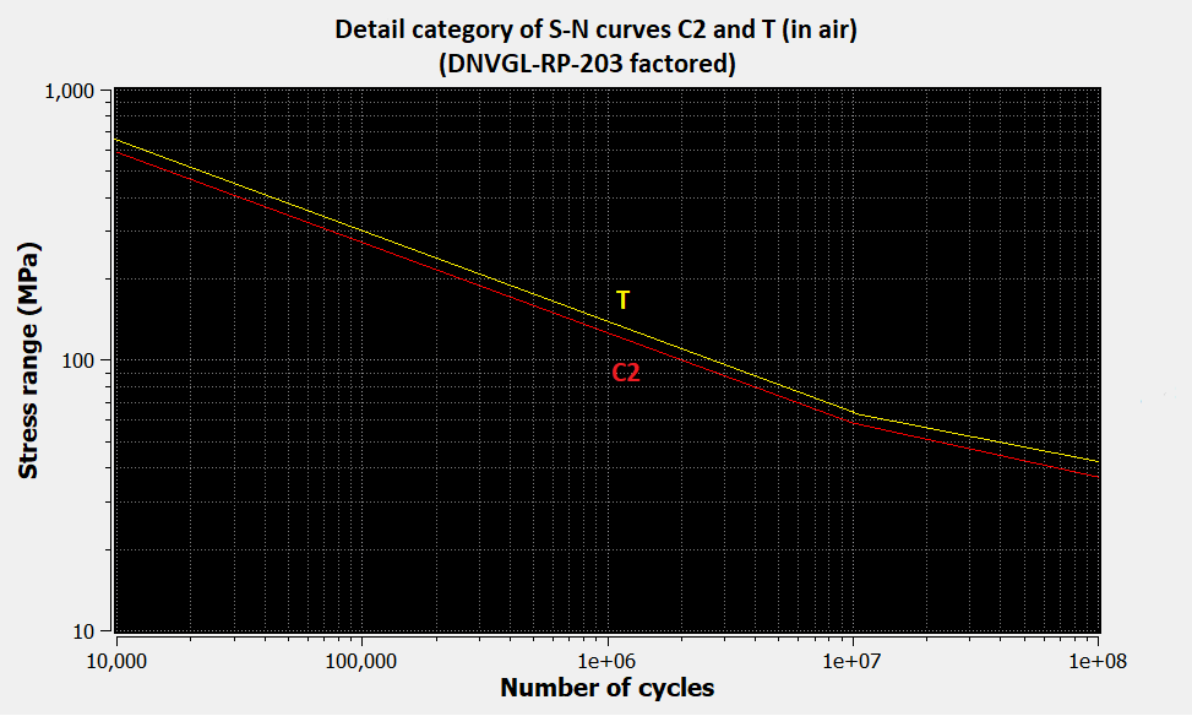

Figure 5.7: S-N curves used for evaluating fatigue damage accumulation using multi-axial fatigue assessment method.

5.3. Results

Table 5.3 presents fatigue damage factor result summary for measurement points defined for assessing hot-spot stress in problematic upper arm joint. All points are evaluated for fatigue life of 23 years - equalling to 1.31 million loading/unloading cycles.

Table 5.3: Accumulated fatigue damage factor of welded joint hot-spot nodes acquired using multi-axial fatigue assessment method (23 years of operation).

Brace	**Point**	**P1**	**P2**	**P3**	**P4**	**P5**	**P6**	**P7**	**P8**
	$D_{i_{HS}}$	2.944	0.056	0.172	0.000	0.193	0.053	4.236	0.236
	Point	**P9**	**P10.2**	**P11**	**P12**	**P13**	**P14**	**P15**	
	$D_{i_{HS}}$	0.157	0.001	0.139	0.162	0.121	0.003	0.061	
Chord	**Point**	**C1**	**C2**	**C3**	**C4**	**C5**	**C6**	**C7**	**C8**
	$D_{i_{HS}}$	3.371	0.958	0.397	0.564	0.487	1.236	2.916	0.241
	Point	**C9**	**C10**	**C11**	**C12**				
	$D_{i_{HS}}$	0.645	0.659	0.596	0.958				
Forestay	**Point**	**F1**	**F2**	**F3**	**F4**	**F5**	**F6**	**F7**	**F8**
	$D_{i_{HS}}$	0.001	0.990	0.054	0.066	0.000	0.000	1.898	1.402
Backstay	**Point**	**B1**	**B2**	**B3**	**B4**	**B5**	**B6**	**B7**	**B8**
	$D_{i_{HS}}$	0.001	0.866	0.083	0.102	0.000	0.000	1.601	0.368

Results indicate that when fatigue analysis takes into account stress direction - there is a large number of points which accumulate a critically high amount of fatigue damage. In particular pylon leg beam saddle positions from both chord and brace side (P1, P7, C1, C7) appear to accumulate the most damage with their fatigue damage factor values all exceeding $D_{i_{MA}} > 2.9$. Additionally there are 4 locations (C6, F7, F8 and B7) which accumulate fatigue damage above damage limit of 1, with additional four points (C2, C12, F2, B2) indicating fatigue damage above 0.8. All of these points should be considered as points for potential crack initiation. This distribution of critical point locations correlate well with crack propagation locations observed in real crane joint, which indicate that performance of fatigue assessment using multi-axial fatigue approach can distinguish potential locations for crack initiation with a good level of accuracy. Only magnitude of critical point stress is difficult to evaluate in terms of its accuracy due to lack of reliable data on

initial fatigue crack initiation timeline and position, as damage has been observed only after cracks have significantly propagated within the joint welds. However based on comparison between fatigue damage factor values presented in table 5.3 it can be assumed that most likely initial fatigue crack has initiated at the saddle location of the left pylon leg (point P7). This is a likely outcome as a large crack propagating from this position has been observed in the real crane structure as seen in figure 4.15 of chapter 4.

5.4. Result comparison

This section provides a comparison of fatigue assessment results between multi-axial and hot-spot stress approaches. It also provides main observations acquired from result comparison

Results of multi-axial fatigue assessment can be directly compared to a hot-spot stress approach to determine how acquired fatigue damage accumulation results differ when evaluated for identical operation lifetime of 23 years. Table 5.4 presents a comparison of fatigue damage factor magnitude results acquired using multi-axial fatigue approach $D_{i_{MA}}$ and hot-spot stress approach $D_{i_{HS}}$. Here negative values (highlighted in blue) indicate where hot-spot stress fatigue approach acquired higher damage factor D_i value, while positive values (highlighted in red) show the opposite result. Value comparison is established for identical point distribution setup in both analyses allowing to observe direct fatigue damage factor value contrast at all measurement points. For measurement point location setup and naming convention - refer to figure 4.17 of section 4.3.2.

Table 5.4: Difference in accumulated fatigue damage ratio $\Delta D_{i_{MA-HS}}$ between conventional Hot-spot fatigue and multi-axial fatigue assessment results. Colors indicate which method leads to higher damage factor value (red - multi-axial fatigue approach damage is higher, blue - hot spot stress approach damage is higher.)

Brace	**Point**	**P1**	**P2**	**P3**	**P4**	**P5**	**P6**	**P7**	**P8**
	$\Delta D_{i_{MA-HS}}$	-0.195	-0.023	-0.061	-0.066	-0.106	-0.028	-0.312	-0.079
	Point	**P9**	**P10**	**P11**	**P12**	**P13**	**P14**	**P15**	
	$\Delta D_{i_{MA-HS}}$	-0.012	-0.007	0.045	-0.101	-0.063	0.002	-0.079	
Chord	**Point**	**C1**	**C2**	**C3**	**C4**	**C5**	**C6**	**C7**	**C8**
	$\Delta D_{i_{MA-HS}}$	0.135	0.638	0.207	0.355	0.267	0.828	-1.533	-0.655
	Point	**C9**	**C10**	**C11**	**C12**				
	$\Delta D_{i_{MA-HS}}$	0.451	0.390	0.427	0.341				
Forestay	**Point**	**F1**	**F2**	**F3**	**F4**	**F5**	**F6**	**F7**	**F8**
	$\Delta D_{i_{MA-HS}}$	-0.010	-1.956	-0.026	-0.029	-0.013	-0.019	-0.126	-0.013
Backstay	**Point**	**B1**	**B2**	**B3**	**B4**	**B5**	**B6**	**B7**	**B8**
	$\Delta D_{i_{MA-HS}}$	-0.011	-1.698	-0.041	-0.040	-0.013	-0.019	-2.819	-2.699

The change in how each measurement point is loaded using multi-axial fatigue is especially significant in the case of points C7, F2, B2, B7 and B8, where hot-spot stress fatigue assessment approach shows significantly larger damage accumulation value than multi-axial fatigue assessment approach. This is likely linked to the fact that at these points for multi-axial fatigue assessment only a single principal stress component has been used (damage has not been summed up due to parallel stress angles not being between angle threshold of $45° < \theta < 60°$).

Another important observation is presented for fatigue damage accumulation factor values calculated for measurement points located on the chord. Here majority of damage results indicate that calculations measured using multi-axial fatigue assessment method acquire larger amount of fatigue damage. This is mainly linked to the application of S-N curve for dominant principal stress component that is based on the angle value for parallel and perpendicular stress. Most of these points indicate that parallel stress is the dominant and accumulate more fatigue damage than its perpendicular stress counterpart - this results in application of more dangerous S-N curve (C2 for multi-axial fatigue and T for hot-spot stress approach), leading to higher estimated fatigue damage when stress direction is taken into account.

Overall, when it comes to critical locations for fatigue damage accumulation - both methods appear to indicate critical fatigue damage at same locations. Figure 5.8 presents locations of critical damage points which were distinguished using both multi-axial and hot-spot stress fatigue approaches and how magnitude of damage factor compare at each stress position. As seen from the results, both methods appear to indicate presence of critical fatigue damage at majority of same points (excluding points B2 and B8 within multi-axial fatigue assessment). This means that for the purposes of indicating presence of fatigue damage accumula-

tion, both methods can be considered as feasible, with hot-spot stress approach which uses Von Mises stress as response, in general providing more conservative results.

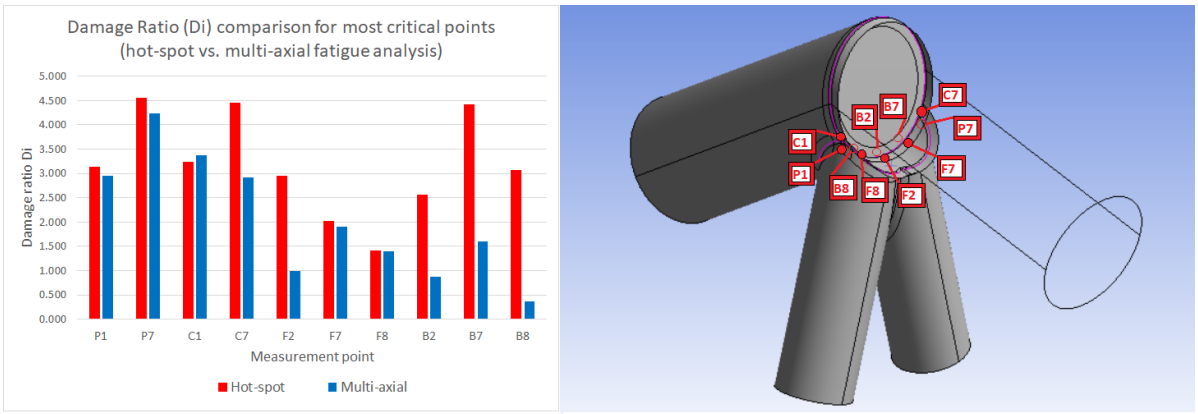

Figure 5.8: Resulting fatigue damage accumulation factor value comparison for conventional Hot-spot fatigue analysis (red) and performed Multi-axial fatigue analysis (blue) at points most critically affected by fatigue damage in both analyses (marked on illustrated joint).

Since there is not enough empirical data to assess which fatigue assessment approach is more accurate - it is worth considering the principle properties of analysed structure to make an assumption towards accuracy of both methods. As it has been assessed in section 5.1 - there is an indication that multi-axial fatigue assessment is beneficial for assessed joint structure due to presence of two significant principal stress components acting at most measurement point, which indicate effects of multi-axial stress. Additionally, when evaluating material properties of structural steel used for manufacturing upper arm structure for analysed crane - it is a ductile material, for which stress direction is an important factor. For these reasons it can be presumed that multi-axial fatigue assessment results are indeed beneficial for estimating fatigue life of problematic crane tubular joint. However the accuracy of multi-axial fatigue assessment results should have to be backed with data on crack initiation location and propagation rate, which are not present due to late observation of crack in the joint when it has already significantly propagated, both in the brace saddle and within forestay-backstay weld.

5.5. Conclusion

Based on the observed fatigue assessment results, the following research question can be answered:

Is incorporation of stress direction into fatigue assessment beneficial for evaluating fatigue damage at the welds of problematic joint? How its results compare to more conventional hot-spot fatigue assessment approach?

Benefits of fatigue assessment method which incorporates effects of stress direction into its formulation depend on material properties - for ductile materials stress is directional – thus additionally multi-axial fatigue approach is expected to provide benefit towards result accuracy of fatigue damage accumulation. Additionally it has been observed though principal stress magnitude assessment that most evaluated hot-spots in analysed joint experience significant stress in two principal directions - meaning there is a basis for assessing fatigue using multi-axial fatigue approach. For most locations – multi-axial fatigue approach shows a variation of fatigue damage (in comparison with hot-spot stress approach that is considerable for multiple critical locations), with majority of points showing lower damage when using multi-axial method. However both methods appear to be capable of establishing critical hot-spot locations as critical points based on simulation results in both cases match well with crack propagation locations observed in real crane structure. This means that both methods are feasible for assessing locations of potential crack initiation. Nevertheless to fully conclude which approach is more accurate, there is a lack of available data for measurement validation - thus it has been concluded that both methods are feasible in a general case, with indication that assessing fatigue damage using a conventional hot-spot stress approach which uses Von Mises stress is potentially more conservative than performing fatigue assessment using multi-axial fatigue assessment approach. Nevertheless both methods are likely applicable for estimating fatigue damage in crane upper arm joint.

6

Reducing fatigue damage accumulation

With fatigue assessment performed on the problematic joint structure - it is worth investigating ways on how to improve its fatigue life. Countering effects of stress concentrations or removing them altogether and understanding ways how to best reduce stress effects within the structure is beneficial for longevity of cyclically loaded constructions such as the crane upper arm, which makes it a worthy topic for investigation. This chapter is specifically focused on counteracting effects of the observed flaws within the original upper arm joint setup and evaluating ways on how to increase its operational lifetime.

Here the following research question will be answered along with its two main sub-questions:

- What is the best potential method to increase fatigue life of crane upper arm?
  - How can problematic joint structure be redesigned to reduce the rate of fatigue damage accumulation?
  - How can fatigue damage of the structure be reduced without changes to crane design? Can this be done without reducing efficiency of crane operation?

6.1. Increasing fatigue life of a structure

This section provides a general overview of potential methods for increasing fatigue life of welded joint structures and presents which approaches will be tested and compared in greater detail within this chapter.

In order to reduce fatigue damage accumulation in the crane - stress accumulation within the structure has to be reduced. This can be done either though increasing capability of the structure to handle stress or by reducing the external load sources which induce stress within the structure. Capability to handle stress generally requires a certain amount of design adjustments which change the composition of the construction, while reduction of load source magnitude is done on the original structure and does not include changes to structural design. Both methods however have to be investigated.

There are several ways to reduce stress accumulation and increase fatigue life of a structure from a standpoint of redesign. Some of the most common approaches include:

1. Increasing structural capacity of elements by adjusting thickness of construction components.
2. Redistributing stress through increase of loaded area.
3. Inclusion of stiffeners in the design setup.
4. Increase of weld quality through removal of impurities within weld surface.

All of these approaches can potentially prolong operational lifetime of the analysed construction. Improvement of weld quality in particular is a method which can be applied during assembly stage through weld grinding or hammer peening operations, regardless of any other design improvements. It is proven to have a strong benefit towards reducing fatigue damage accumulation, due to its quality of reducing potential flaws in the weld surface that can cause appearance of stress concentrations which are difficult to predict and model. According to fatigue damage formulation defined in standards of DNVGL-RP-C203 [20] - increase of

weld quality can reduce fatigue damage accumulation up to 2.5 times, significantly boosting fatigue life of the structure. To confirm this statement, fatigue assessment of original joint has been simulated with a by performing multi-axial fatigue damage calculations based on the damage formulation of DNVGL-RP-C203 [20], which includes factor for improved weld quality. Results have shown a reduction in fatigue damage equaling between 2.3 and 2.5 times over original analysis, which assumes the welds have not been additionally treated. Other aforementioned methods for increasing fatigue life of lemniscate crane are to be discussed in upcoming sections, specifically separated in two groups - those within the boundary of increasing structural capacity and redistribution of stress in the construction.

Along with redesign methods, there is also potential to increase fatigue life of a structure by adjusting external load effects acting on the structure. Most common methods can include:

1. Reduce loads exerted on the structure - in the case of the lemniscate crane boom this could be in the form of reducing hoisted mass of transported material, which in turn would reduce the load and stress accumulation.

2. Adjust potential motion of the construction - in the case of analysed crane it can be adjustment of motion operations such as hoisting, luffing and slewing. Adjustments could potentially reduce acceleration load effects on the hoisted load and entire structure.

As reducing the main load will likely negatively affect work efficiency of the crane - it is a questionable approach for increasing fatigue life and is left out of the scope of this report, however it might prove noteworthy if investigated further. On the other hand, adjustment of crane motion could potentially reduce stress and fatigue damage accumulation without negatively affecting crane cycle time, which makes it a potential method for damage reduction worthy of further investigation.

In summary, three main methods are to be evaluated in terms of their potential to reduce fatigue damage accumulation:

1. Increase of structural capacity of the original joint structure through adjustments to thickness values of upper arm joint elements.

2. Stress redistribution though crane refurbishment with inclusion of a different upper arm joint design.

3. Reduction of loads affecting the crane upper arm through introduction of adjustments to the crane motion cycle, in a way which does not increase the cycle time of crane loading/unloading operation.

Each method, its process, reasoning and results are described in more detail in sections 6.2, 6.3 and 6.4.

6.2. Adjustment of joint element thickness

This section describes the process of increasing crane upper arm structural capacity through adjusting joint element thickness. Screening of statistically significant values is performed and paired with sensitivity analysis which is used for acquiring optimal thickness values that allow joint to survive a predefined fatigue life.

For welded tubular structures, increasing thickness of its elements is linked with increased fatigue life [57]. Increasing structural capacity of the crane joint and reducing fatigue damage accumulation can be done by adjusting the thickness of current crane joint elements. This is an approach which in principle does not change structural design of the joint, but rather adjusts its load carrying capabilities through different beam thickness setup. It allows to determine whether the original crane joint design is flawed or rather its load carrying capacity has been underestimated and chosen beam thicknesses could have been adjusted without radical joint design changes. Figure 6.1 highlights (in blue) the scope of upper arm geometry which is to be varied in terms of its thickness, to reduce fatigue damage accumulation in the joint.

Since varying thickness simultaneously for multiple components based on a trial-and-error method is inefficient and does not ensure acquisition of optimal result for a specific fatigue lifetime - a methodical sensitivity analysis optimization approach is used. Sensitivity analysis - is a method for simultaneously acquiring optimal values of multiple analysed factors based on their relation with assessed experiment response/-s. This is an approach of establishing factor-response relations based on the principles of design of experiments (DoE) methodology. This is acquired with two main steps:

1. Parameter screening - which establishes which joint element thickness changes have an effect on evaluated fatigue damage accumulation.

2. Sensitivity analysis - where direct relations are established between statistically significant factors and defined response to acquire optimal factor values.

Both steps for acquiring optimal joint element thickness are described in this section.

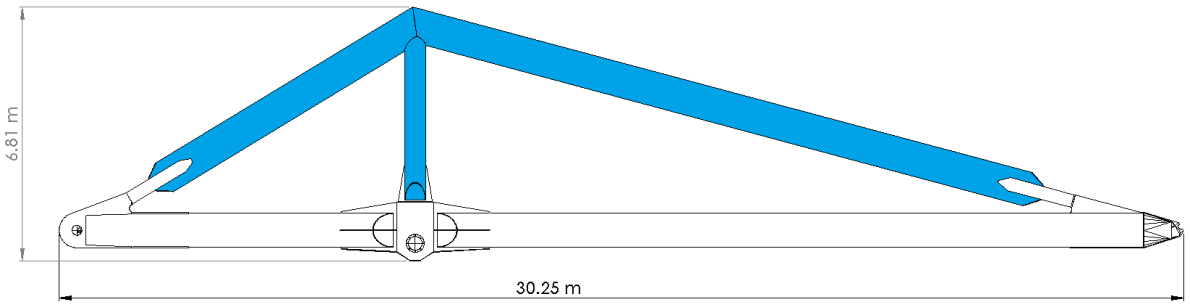

Figure 6.1: Scope of beam thickness adjustment in relation to the rest of upper arm structure (marked in blue).

6.2.1. Factor screening

First step in a sensitivity analysis is to assess whether change in magnitude of assumed relevant factors lead towards change in desired response/-s. This can be done through performing screening experiments and assessment of factor statistical significance, based on the principles as described in section 3.3.

This specific experiment evaluates whether independent and combined change in pylon, forestay/backstay and mid-plate thickness affect magnitude of stress accumulation in the joint. Stress range is chosen as screening experiment response because increase in stress magnitude and its fluctuation range correlate with increased accumulation of fatigue damage in the structure. Stress range is measured at 10 points within the joint, with points chosen that indicate presence of fatigue accumulation in original analyses of hot-spot and multi-axial fatigue assessment, described in chapters 4 and 5.

When it comes to choice of specific joint elements to be tested - all components which are a part of the joint element are evaluated. These factors and reasoning for their assessment can be summarized as follows:

1. Chord element thickness - Forestay and backstay beams contain the majority of hoisting load and serve the purpose of providing support for the upper arm structure in tension and bending directions. Thus in accordance to tubular joint classification, they are classified as a unitary chord beam setup. For this purpose their thickness is always assessed and varied uniformly. Due to chord beams supporting majority of the load in this lemniscate crane setup - it is expected to reduce stress accumulation in the joint with an increase of chord thickness.

2. Brace element thickness - brace beams (which in the case of analysed joint are right and left pylon legs) when under bending, they are assumed to provide stiffness to the structure during hoisting operation. Additionally, these beams support the forestay-backstay beam weight. It is expected that increase in thickness of pylon legs will provide reduction to stress magnitude especially for critical stress concentration points P1 and P7, located at the brace saddle locations.

3. Mid-plate thickness - this deals with the inner support plate that is welded between forestay and backstay beams. It is assumed that the inclusion of stiffener plate at the aforementioned beam connection is likely meant to reduce stress concentration at the saddle position. This has been evaluated when assessing presence of stress singularity effects described in section 4.2.7 and results have shown that removing stress plate does indeed increase stress magnitude in the main weld up to material yield limit. This concludes that its presence is important and increase in plate thickness can potentially reduce fatigue damage accumulation. However it is unclear whether further thickness increase indeed does significantly help with reduction of stress range at critical points, which is the reason it might be worthy of screening assessment.

Table 6.1 summarizes the setup of performed screening experiments, indicating low and high values of analysed factors (component thickness, [m]), and acquired responses (stress range at specific points, [Pa]). Low and high values have been chosen based on principles of the original joint setup (which consist of varied

thicknesses between 0.0095 m and 0.0127 m), with a slight limit increase to both low and high side. For this purpose low value is set at 0.008 m and high value at 0.02 m. All factor values are set to be uniform between different assessed joint elements to ensure consistency of evaluation to which factors are significant from statistical standpoint towards reducing stress range magnitude.

Table 6.1: Screening experiment setup for joint beam thickness evaluation.

Marking	**Factors**	**Tested values**	
		Low	**High**
A	Thickness of Chord elements, m	0.008	0.02
B	Thickness of Brace elements, m	0.008	0.02
C	Thickness of Mid-plate, m	0.008	0.02
Responses:	Nodal stress range [Pa] at points: P1, P7, C1, C7, F2, F7, F8, B2, B7, B8.		
Screening design type:		Factorial	
Resolution level:		Full	
Number of runs:		8	

Based on the defined factors and their value levels, screening experiment was formatted within Minitab software environment to acquire combinations of low and high values of each factor. This has concluded in a total number of eight experiments which had to be performed. Figure 6.2 provides a graphical setup overview of the analysed screening analysis experiments with definitions of factor value distribution for each of performed 8 experiments in table format.

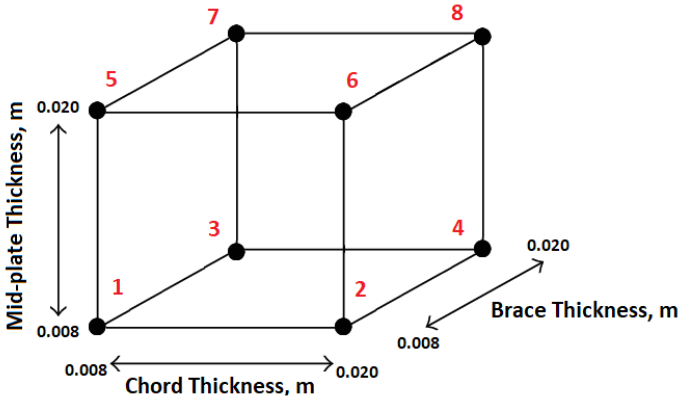

Run	Chord thickness, m	Brace thickness, m	Mid-plate thickness, m
1	0.008	0.008	0.008
2	0.02	0.008	0.008
3	0.008	0.02	0.008
4	0.02	0.02	0.008
5	0.008	0.008	0.02
6	0.02	0.008	0.02
7	0.008	0.02	0.02
8	0.02	0.02	0.02

Figure 6.2: Setup of full-factorial screening analysis for evaluating statistical significance of joint element thickness towards affecting experienced stress range.

Each experiment is performed within finite element analysis environment to acquire response data. All parameters in each experiment setup are kept identical, with only variation of specified upper arm structural element thickness. Maximum principal stress responses are then extracted using hot-spot extrapolation methodology described in section 4.4.2, at measurement points summarized in table 6.1. Results are evaluated based on their statistical significance using Minitab software, which acquires both independent factor effects (A, B, C) on responses as well as combined effects (AB, AC, BC).

Due to the amount of screening responses, factor significance is summarised in a compact format in table 6.2, with statistically significant values (P-value < α) highlighted in blue. All factor significance results in Pareto chart graphical format can be found in figure D.1 of appendix D.

Results show that all three factors are significant for most critical hot-spot locations. Chord thickness in particular has shown to have significant effect on stress response for all evaluated points - out of all responses chord thickness does have the most significant effect (lowest p-value) at all hot-spot locations. This means that change in chord thickness value will have the largest effect. Only combined effect of brace and mid-plate thickness (BC) does not show statistical significance at defined confidence interval of 95%.

Based on this observation a conclusion is made that all three independent joint elements are statistically significant and contribute towards structural capacity of the joint. This leads to a conclusion that to acquire

desired fatigue life through adjustment of component thickness - all three components should be varied. However it is still needed to determine optimal combined thickness setup of the joint, which requires a more detailed look into finding a direct relation between joint element thickness and resulting stress. This will be discussed in the section 6.2.2.

Table 6.2: Joint element thickness factor significance p-values for confidence level of 95%. Highlighted values considered statistically significant.

Point	P-values (significance limit: $\alpha = 0.05$)					
	A	B	C	AB	AC	BC
P1	0.004	0.006	0.085	0.007	0.164	0.643
P7	0.004	0.006	0.084	0.007	0.165	0.645
C1	0.034	0.420	0.270	0.603	0.236	0.386
C7	0.034	0.437	0.285	0.579	0.222	0.384
F2	0.006	0.013	0.069	0.050	0.093	0.309
F7	0.041	0.085	0.249	0.172	0.710	0.527
F8	0.041	0.086	0.249	0.173	0.715	0.526
B2	0.004	0.009	0.032	0.030	0.098	0.263
B7	0.013	0.017	0.041	0.029	0.047	0.179
B8	0.013	0.017	0.041	0.029	0.047	0.180

A - Chord thickness
B - Brace thickness
C - Mid-Plate thickness
AB - Chord thickness * Brace thickness
AC - Chord thickness * Mid-Plate thickness
BC - Brace thickness * Mid-Plate thickness

6.2.2. Sensitivity analysis

Next step of optimizing joint element thickness is linked to establishing direct relation between thickness of evaluated joint elements and desired response. This is done by applying sensitivity analysis algorithm that is based on Design of experiments methodology.

In principle, sensitivity analysis is a method which through a finite number of ran experiment allows to derive relation between more than one factor and evaluated response/-s. This approach is meant to limit the number of experimental runs while still finding desired solution to a specific problem. General principle of performing sensitivity analysis is based on comparable methodology as Screening analysis described in section 6.2.1. However, unlike factor screening - sensitivity analysis is capable of establishing relation between defined factors and analysed responses. Schepdael et al. [78] provides an in-depth introduction to sensitivity analysis, where additional information about the method and can be found. It explains the theory behind setting up the model as well as for analysing results of such design.

Figure 6.3 provides an overview of the main steps for acquiring optimal thickness of defined joint elements, which would allow upper arm structure to handle desired fatigue life.

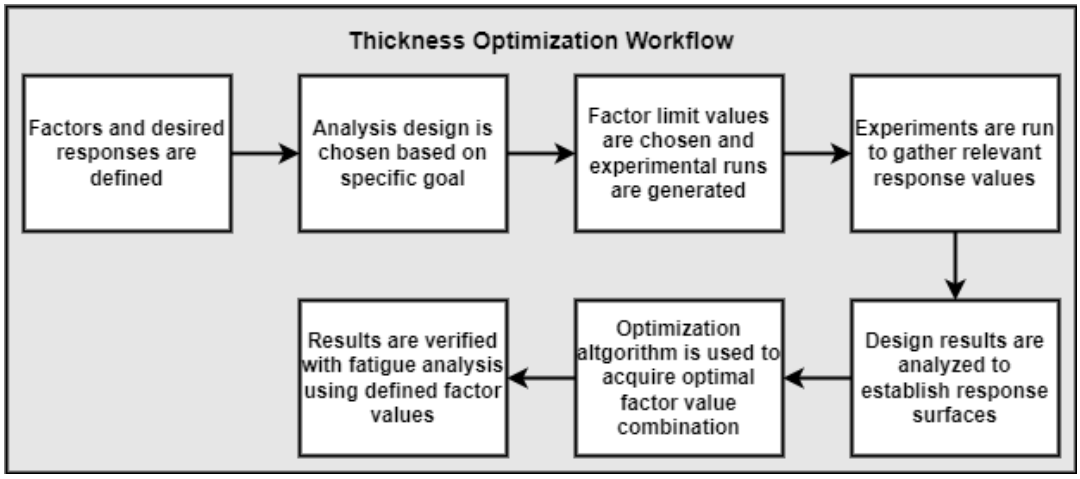

Figure 6.3: Workflow overview for establishment of joint element thickness using principles of sensitivity analysis.

The principle of assessing optimal joint element thickness based on steps defined in figure 6.3 can be summarised as follows:

1. Based on screening analysis results described in section 6.2.1, statistically significant factors are defined for evaluation using sensitivity analysis. Relevant responses are established in relation to optimization goal for surviving cyclic loads of 23 years.

2. Design type is chosen to accommodate optimization goal. This includes number of factors and the range of factor values that should be evaluated. This is done to reduce analysis complexity limiting number of experiments to a reasonable amount.

3. Maximum and minimum values used for testing factor sensitivity are established and experimental runs are generated. Assessed factor value limits are defined to evaluate mainly realistic values depending on factor type to maintain result accuracy within chosen value bounds. Experimental runs are generated on principles of design of experiments using statistical analysis software *Minitab*.

4. Based on defined experimental run setup - experiments are performed to acquire relevant responses. In the case of joint element thickness adjustment - maximum principal stress result data is collected at each critical hot-spot point to define stress range which accumulates fatigue damage.

5. Response results are evaluated to establish response surfaces of factor value combinations.

6. Optimization algorithm incorporated within Minitab software is applied to acquire optimal values from response surfaces, which should be capable of surviving desired fatigue life.

7. Results are then verified for accuracy with a detailed FEA analysis as applied in chapter 5. This approach uses multi-axial fatigue assessment method, a full stress cycle range and calculation of damage accumulation ratio for each hot-spot.

This method is used to acquire an optimal solution of upper arm joint structural capacity that is meant to handle 23 years of cyclic loading, through adjustment of joint element thickness (i.e. for chord, brace and mid-plate elements). Table 6.3 summarizes main parameters of performed sensitivity analysis. Key components, such as the type of analysis design is explained in more detail further in the section.

Table 6.3: Sensitivity analysis experiment setup for joint beam thickness calculation.

Marking	Factors	Tested values	
		Low	High
A	Thickness of Chord elements, m	0.008	0.03
B	Thickness of Brace elements, m	0.008	0.03
C	Thickness of Mid-plate, m	0.008	0.03
Responses	Nodal stress range at points: P1, P7, C1, C7, F2, F7, F8, B2, B7, B8.		
Screening design type		Box-Behnken	
Factor levels		3	
Resolution type		Unblocked	
Number of Runs		13	

Design type

For performing specific sensitivity analysis - Box-Behnken design is chosen. This is a response surface design approach which is capable of establishing relation between multiple assessed factors and needed responses in a format which can be represented in planar surfaces, showing response results of two or more factor combinations.

The Box-Behnken design is an independent quadratic design, as it does not contain an embedded factorial or fractional factorial design. In this design the treatment combinations are at the midpoints of edges of the process space and at the center. These designs can be rotated and require 3 levels of each factor [65]. It has the benefit over more conventional response surface designs (e.g. central composite) by reducing the needed number of experimental runs for establishing relations with the same number of analysed factors. This is due to the fact that Box-Behnken design does not evaluate corner points in the setup (illustrated in figure 6.4), which reduces the range of assessed values to a limited range within the middle of assessed value range, this way reducing computational complexity. This approach is best fitted when assessment range is

relatively well defined as it is in the case of performing joint element thickness adjustments, making it the perfect choice for sensitivity analysis in question.

Factor limit setup
Low and high values have been chosen based on observations of screening experiment described in section 6.2.1, which indicates following choices for limit points:

1. Lower limit of 0.008 m - based on measured stress range, choosing low value of any factor thickness below 0.008 m is not likely to provide results in a feasible region.

2. Higher limit of 0.03 m - measured stress range at 0.02 m provided reasonable stress for fatigue analysis that could potentially serve desired limit of 23 years, but to insure establishment of potential further increase of fatigue life and to allow more combination options - upper limit has been increased to 0.03 m.

Since Box-Behnken skips corner points of its setup, the analysis does not evaluate factor combinations where all factor values have defined either maximum or minimum values. Figure 6.4 graphically illustrates performed setup of Box-Behnken design with full experimental run setup.

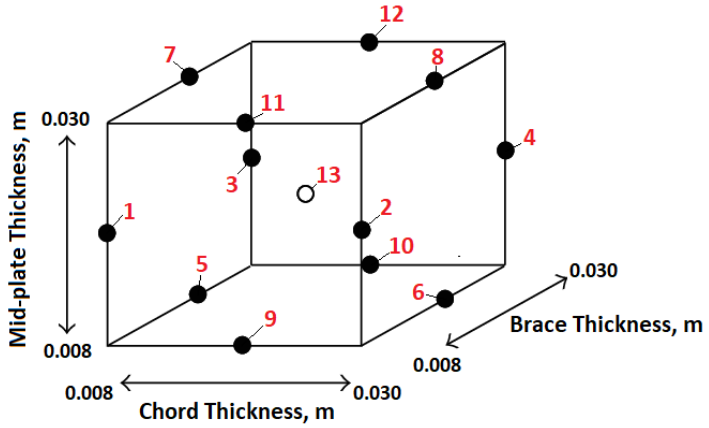

Run	Chord thickness, m	Brace thickness, m	Mid-plate thickness, m
1	0.008	0.008	0.019
2	0.030	0.008	0.019
3	0.008	0.030	0.019
4	0.030	0.030	0.019
5	0.008	0.019	0.008
6	0.030	0.019	0.008
7	0.008	0.019	0.030
8	0.030	0.019	0.030
9	0.019	0.008	0.008
10	0.019	0.030	0.008
11	0.019	0.008	0.030
12	0.019	0.030	0.030
13	0.019	0.019	0.019

Figure 6.4: Setup of Box-Behnken sensitivity analysis for evaluating relation between joint element thickness and stress range magnitude.

The geometry of this design suggests a sphere within the process space such that the surface of the sphere protrudes through each face with the surface positioned tangential to the midpoint of each edge [78].

Analysis response definition
The key purpose of increasing structural capacity through adjustment of structural element thickness is to reduce accumulation of fatigue damage to an optimal magnitude for defined fatigue life. However, performing fatigue analysis of each evaluated experiment is an inefficient process that requires a significant amount of manual data formatting. For the purpose of increasing efficiency of the sensitivity analysis - the testing process has been simplified to assess effects of the maximum stress cycle range that contributes most to fatigue damage ratio.

According to detailed fatigue damage ratio assessment of analysed loading cycle, in a general case the maximum stress cycle approximately contributes to 85% of the damage for the most critical point. This indicates that in order to efficiently assess optimal fatigue damage ratio with a large amount of tests, required fatigue life can be increased by a safety factor of 1.15 (to artificially counteract effects of smaller stress cycles). When estimating fatigue damage using S-N curves, this approach increases the optimal fatigue life from 1.31 million to 1.5 million cycles, thus reducing maximum allowable stress cycle range. This value is then used for estimating whether the stress range is safe when performing a sensitivity analysis. According to this procedure, allowable stress cycle range for the purposes of sensitivity analysis is set to 110 MPa for stress components which use T-curve and 125 MPa for components using C2-curve.

This approach allows to quantify fatigue damage with a response of reduced complexity in comparison with the case where fatigue damage accumulation ratio were to be used. It is worth noting that main stress

cycle not always contributes to 85% of total fatigue damage at each measurement point, but it serves as a good reference point to provide a cornerstone for reasonably accurate evaluation of each thickness combination.

Thickness optimization

With experimental run setup and desired responses defined - response surfaces can be established. In principle, response surfaces provide a relation between two or more factors to achieve a desired response. Figure 6.5 presents acquired response surface relation between analysed joint element thickness factors and resultant stress range response at point P1, which is located at the left brace saddle. Based on the same principle - response surfaces are establishes for responses at all measurement points defined in table 6.3.

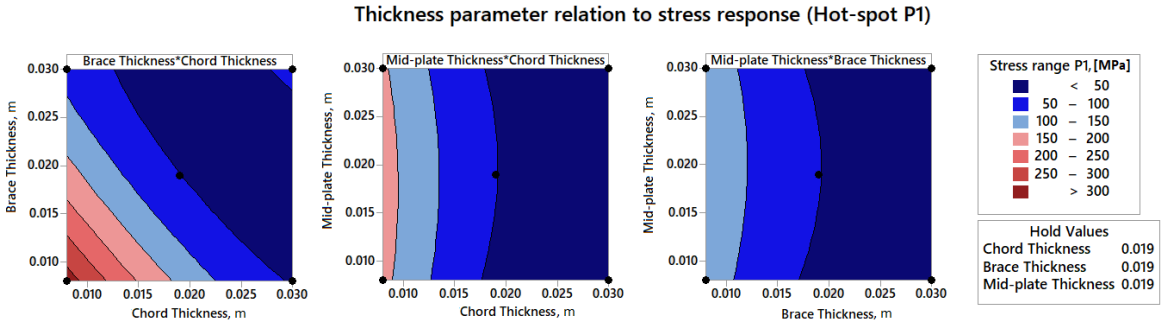

Figure 6.5: Combined joint element thickness relation to stress response at brace saddle measurement position P1. Acquired using DoE sensitivity analysis.

Using established response surfaces - *Response optimizer* algorithm embedded within Minitab software is applied to acquire optimal responses. Optimization target is established for all relevant responses to acquire stress range values below 110 MPa that is supposed to be enough to survive 23 years of cyclic loading. Since there are multiple possible joint element thickness combinations available which can acquire feasible values - 10 potential combinations are extracted and one variant is chosen. The variant is chosen with only one specific rule - that acquired brace and chord diameters should be different, because equal thickness setups have been observed to fail from the weld root at the saddle position even with relatively low stress concentrations [20]. The chosen setup of chord, brace and mid-plate thicknesses of the original joint and its optimization result are summarized in table 6.4. Along with thickness values table also presents change in total mass of the joint, as well as the entire crane upper arm structure.

Table 6.4: Comparison of joint element thickness and structure mass between original and optimised joint setups.

	Original	**Optimised**	**Change, %**
Chord thickness, mm	12.7	16.0	+26%
Brace thickness, mm	9.5	12.0	+26%
Mid-plate thickness, mm	12.0	14.0	+17%
Joint Mass. Kg	8248.3	10388.9	+26%
Upper arm Mass, kg	36770.0	38910.6	+6%

According to optimization setup both chord and brace element thicknesses had to be increased by 26% along the entire length of the beams, with mid-plate thickness increase of 17%. This leads to joint mass increase of approximately 26% with mass of the total upper arm structure increasing by 6%.

6.2.3. Results

To verify whether joint element thickness increase actually leads to sufficient fatigue life of the joint structure - a detailed fatigue analysis is performed. Finite element analysis is setup with original time-dependent loads and adjusted thickness setup. From here multi-axial fatigue damage is measured using the methodology presented in chapter 5. Table 6.5 summarises fatigue damage factor results for all measurement points of original joint structure. Results show that thickness optimization for 23 years has concluded to good results where all measurement points accumulate damage that is below critical failure limit of 1, with points B7 F7 and F8 accumulating most damage (above $D_{i_{AT}} > 0.8$). This observation indicates that optimization has been

performed successfully with all values staying below failure limit, with several points kept close to limit that is meant for 23 years of operation.

Table 6.5: Accumulated fatigue damage $D_{i_{AT}}$ results of crane upper arm with adjusted thickness of forestay, backstay, pylon leg beams and chord mid-plate. Calculated using multi-axial fatigue approach, (for 23 years of operation).

Brace	**Point**	**P1**	**P2**	**P3**	**P4**	**P5**	**P6**	**P7**	**P8**
	$D_{i_{AT}}$	0.175	0.002	0.014	0.000	0.015	0.002	0.225	0.007
	Point	**P9**	**P10.2**	**P11**	**P12**	**P13**	**P14**	**P15**	
	$D_{i_{AT}}$	0.010	0.000	0.009	0.005	0.024	0.001	0.011	
Chord	**Point**	**C1**	**C2**	**C3**	**C4**	**C5**	**C6**	**C7**	**C8**
	$D_{i_{AT}}$	0.525	0.273	0.081	0.115	0.090	0.302	0.474	0.007
	Point	**C9**	**C10**	**C11**	**C12**				
	$D_{i_{AT}}$	0.092	0.128	0.133	0.270				
Forestay	**Point**	**F1**	**F2**	**F3**	**F4**	**F5**	**F6**	**F7**	**F8**
	$D_{i_{AT}}$	0.001	0.337	0.000	0.000	0.000	0.000	0.939	0.683
Backstay	**Point**	**B1**	**B2**	**B3**	**B4**	**B5**	**B6**	**B7**	**B8**
	$D_{i_{AT}}$	0.001	0.282	0.000	0.000	0.000	0.000	0.730	0.526

Table 6.6 presents comparison of accumulated damage between adjusted thickness joint and original joint setups, with negative values indicating points where thickness adjustment led to reduction of fatigue damage accumulation when joint element thickness has been increased. As results show, there is also one point (i.e. B8) where damage has increased. This is mainly a result linked to the principles of multi-axial fatigue where due to specific principal stress angle fatigue damage components were summed up. This specific aspect presents the weakness of proposed approach as it is not always possible to accurately define damage accumulation as performed response surface optimization does not take into account stress angle effects into sensitivity analysis response formulation. However, for this particular case - optimization has not ran into this specific issue for any critical points where damage had the potential to exceed failure limit of 1, concluding optimization as verified and successful.

Table 6.6: Comparison of accumulated fatigue damage $D_{i_{AT-OG}}$ results for crane upper arm with adjusted thickness and the original upper arm setup. Calculated using multi-axial fatigue approach, (for 23 years of operation). Color represents which model accumulates more fatigue damage (blue (negative value) - if thickness adjustment reduces damage, red (positive) - if original model creates less damage).

Brace	**Point**	**P1**	**P2**	**P3**	**P4**	**P5**	**P6**	**P7**	**P8**
	$D_{i_{AT-OG}}$	-2.769	-0.054	-0.158	0.000	-0.178	-0.051	-4.011	-0.229
	Point	**P9**	**P10.2**	**P11**	**P12**	**P13**	**P14**	**P15**	
	$D_{i_{AT-OG}}$	-0.147	-0.001	-0.130	-0.157	-0.097	-0.002	-0.050	
Chord	**Point**	**C1**	**C2**	**C3**	**C4**	**C5**	**C6**	**C7**	**C8**
	$D_{i_{AT-OG}}$	-2.846	-0.686	-0.316	-0.450	-0.397	-0.934	-2.442	-0.234
	Point	**C9**	**C10**	**C11**	**C12**				
	$D_{i_{AT-OG}}$	-0.553	-0.531	-0.463	-0.689				
Forestay	**Point**	**F1**	**F2**	**F3**	**F4**	**F5**	**F6**	**F7**	**F8**
	$D_{i_{AT-OG}}$	0.000	-0.653	-0.054	-0.066	0.000	0.000	-0.959	-0.719
Backstay	**Point**	**B1**	**B2**	**B3**	**B4**	**B5**	**B6**	**B7**	**B8**
	$D_{i_{AT-OG}}$	0.000	-0.583	-0.083	-0.102	0.000	0.000	-0.870	0.158

Defined results exhibit that increasing fatigue life through adjustment of original joint element thickness is a feasible approach that could yield good fatigue life results. However it is worth noting that points which accumulate most damage (i.e, B7, F7 and F8) are located at the bottom of forestay-backstay weld and are hidden by pylon leg beams. This means that even with increase of structural capacity - critical failure points are in locations that do not allow inspection or repair without crane disassembly. For this purpose alternative approaches of increasing structural capacity should be investigated. This is done in the next section.

6.3. Redesign of problematic joint

This section investigates potential for adjusting structural design of the problematic upper arm joint with a goal to reduce accumulation of fatigue damage through stress redistribution.

As the observed weaknesses of original joint structure contain stress concentrations at locations which are not observable or repairable without crane disassembly - it is safe to determine that increasing structural capacity through increase of beam thickness still leaves this issue unresolved. Thus an alternative approach can be taken to increasing fatigue life of the crane - specifically through redesign of flawed joint structure.

Figure 6.6 present stress distribution during hoisting that is present in the joint. Figure highlights that majority of critical stress concentrations are located around the welds between forestay-backstay and chord-brace connections. There are two main ways how to reduce effects of illustrated stress concentrations:

1. By increasing structural capacity of the construction.
2. By redistributing stress within the construction.

The approach for increasing structural capacity has been introduced in section 6.2. Joint redesign goal however is meant to follow the principles of redistributing stress over larger areas, in a manner which increases fatigue life of crane upper arm.

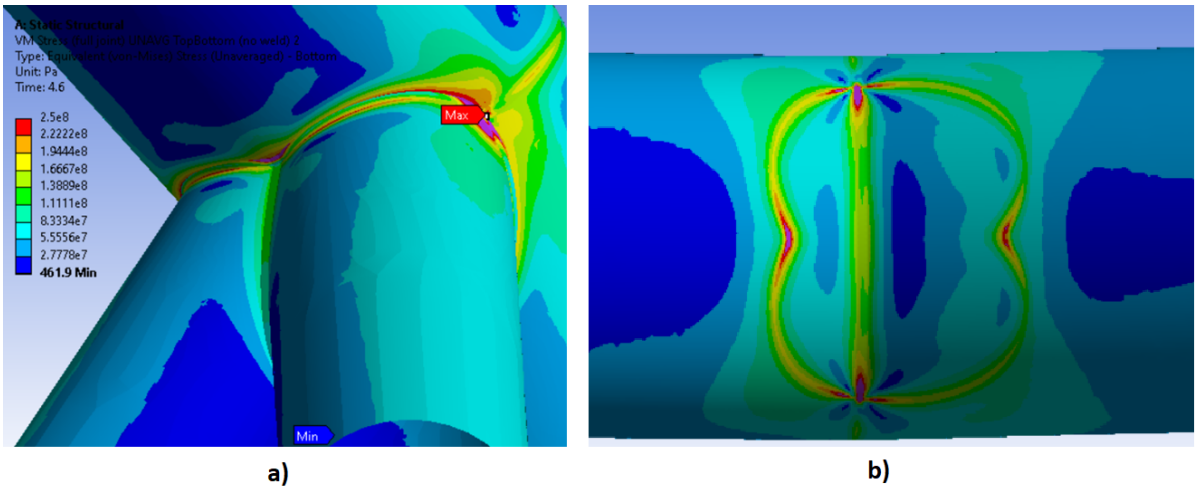

Figure 6.6: Problematic areas which accumulate stress in the problematic upper arm joint with a) outside view and b) pylon leg beams hidden.

Accomplishment of the main goal is performed from the perspective of crane refurbishment, where changes applied to the upper arm construction are kept localised to the main joint. For this purpose several constraints are set which are meant to realise design within reasonable bounds which would establish adjusted joint design as an improvement over the original. These limitations are expressed in the form of following aspects that are taken into consideration when implementing a new joint setup:

1. The scope of structural changes of the upper arm should be limited to the problematic joint, with only 2 meters of each joint beam allowed for removal (illustrated in figure 6.7).
2. Weight of the upper arm is not increased above 5% of the original weight.
3. Any potential stress concentrations should be in locations which allow easy access for inspection and repair, without requiring complex disassembly of the crane.

The approach for redesign (unlike that which have been applied in section 6.2 for increasing beam thickness) now adjusts only a very limited amount of the upper arm construction. This contains the majority of the length of forestay, backstay and pylon leg beams unchanged with only 2 meters of length being removed for each beam connection, as shown in figure 6.7. This not only makes potential crane refurbishment cheaper but also has more potential to limit weight increase of the upper arm, this way meeting its constraint goals.

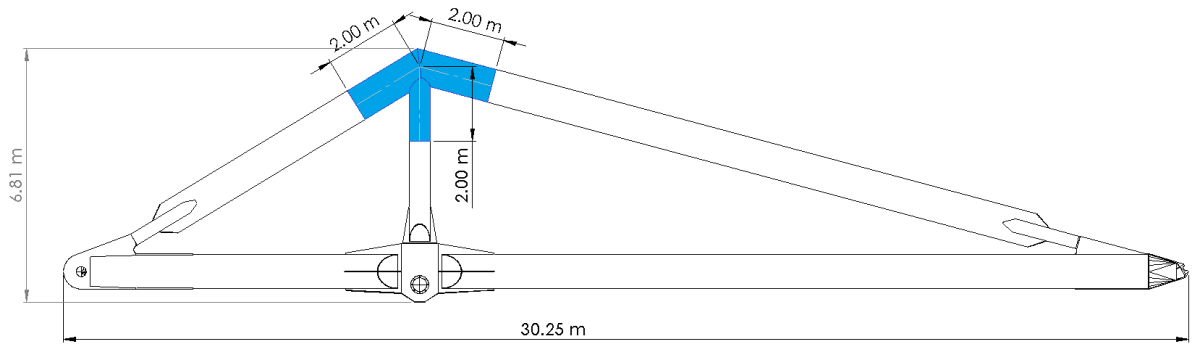

Figure 6.7: Scope of joint redesign in relation to the rest of upper arm structure (marked in blue).

Joint redesign process

Adjustment to the joint setup is performed and implemented in multiple iterations with each variant meant to redistribute stress, in a manner which reduces magnitude of stress concentrations observed in the original joint (illustrated in figure 6.6). Each variant is assessed in FEA environment by exchanging original joint in the main FEA analysis setup with the particular design iteration. In order to quantify improvement - upper arm structure is exposed to identical loads experienced by the crane (as used in previous fatigue assessments defined in chapters 4 and 5), from where locations and magnitude of stress response is measured in the joint at each step. Figure 6.8 illustrates main iterations which have lead to establishment of the final joint design that is used for assessing fatigue damage accumulation.

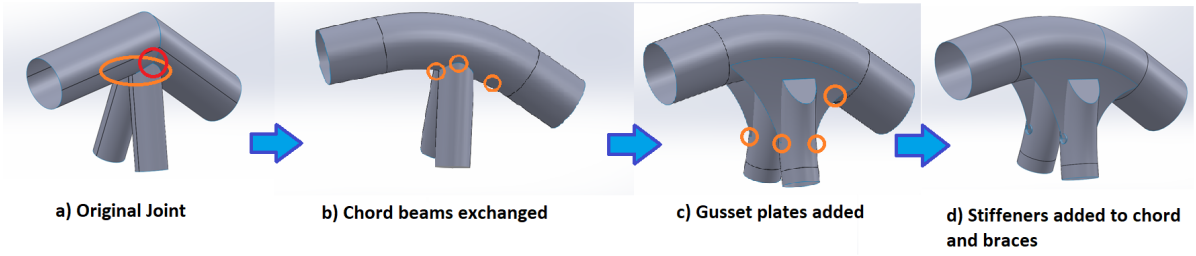

Figure 6.8: Step-by-step iterations of the chosen joint redesign and locations of noteworthy stress concentration for each setup (marked in orange or red it signals potential yielding of material).

Steps leading to final chosen design can be summarised as follows:

1. Welded forestay-backstay beam connection (picture A of figure 6.8) is exchanged by a uniform bent beam with a predefined bending radius of 3 m (picture B of figure 6.8) - this is done to move any potential stress concentration away from direct connection between chord and angle point and distribute it over a larger area that is not condensed to a sharp angled corner. This step does reduce the severity of aforementioned stress concentration, however it keeps critical stress concentration at the brace saddle.

2. Chord-brace tubular connection is remodelled to include gusset plates in between pylon leg tubes and forestay-backstay beam (picture C of figure 6.8). Included gusset plates are angled to connect to chord beam sides and avoid potential compression effects. Unlike the original setup, the adjusted connection is meant to mainly support forestay/backstay bending during hoisting operations rather than supporting compression loads. Most importantly - gusset plates connect to chord beam with a large edge, thus removing any serious potential to concentrate stress at a single connecting location. Critical stress concentration at the brace saddle in the original joint is eliminated.

3. As stress concentration described in step 1 is still left at a relatively significant magnitude - a stiffener ring is included within the angled chord beam (location illustrated in figure 6.11 with its location determined by analysing stress distribution in the chord). Only one stiffener has been added, because using too many stiffeners also might not be optimal for fatigue in some cases, as stiffeners tend to even out stress distribution which can potentially lead to fatigue cracks initiating at multiple positions [56], potentially leading to a long crack that could significantly reduce fatigue life of the structure. Inclusion

of stiffener ring reduced stress magnitude of specified stress concentration to manageable levels which avoids yielding or potential high stress fluctuations.

4. Finally, stiffeners are added at gusset plate endings where they intersect pylon leg beams. As direct connection creates a significant stress concentration - addition of stiffeners in this position distributes stress over a larger area, thus reducing maximum stress magnitude and solving final potential critical stress concentration.

Aforementioned steps provide a final design which is used as a solution for fixing main issues present in the original upper arm construction. The model of adjusted upper arm structure with changed joint setup is represented in figure 6.9.

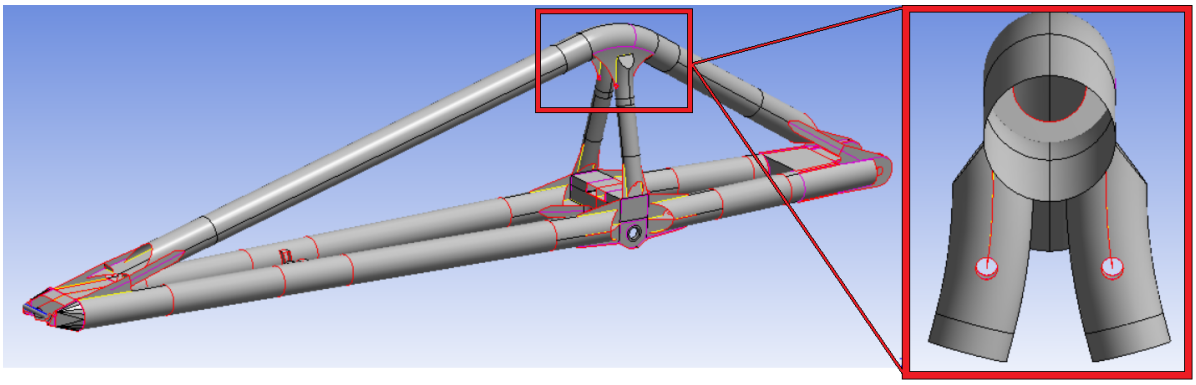

Figure 6.9: Crane upper arm structure with redesigned joint structure.

As it can be seen from definition of a final design setup - this joint incorporates longer welds in joint connections than the original design variant. It is important to note that as a rule - longer weld length is prone to lead towards higher chance of fatigue failure [57]. This is based on the principle that weld quality is a reason for failure in many cases and increasing the length of welded area leads to higher chance of failure, especially for welds along the length of beam elements. For the analysed tubular joint, increasing the length of the welded area through joint design changes can potentially reduce fatigue life, however the magnitude of the increase is highly dependant on weld quality and stress concentration distribution. Since it is apparent from observed stress distribution that stress concentration along the welds have been reduced - the increase of weld length is unlikely to pose an issue.

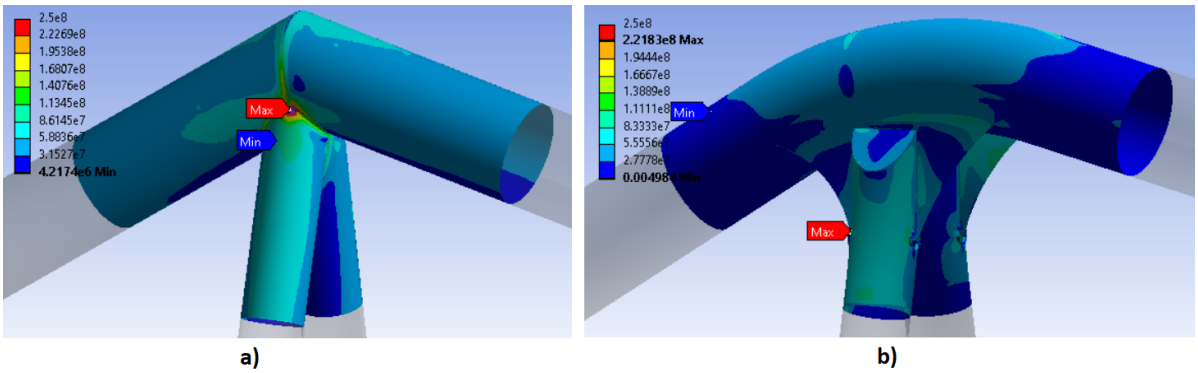

Figure 6.10: Stress distribution and magnitude comparison between a) original joint and b) redesigned joint structure.

On the other hand, figure 6.9 also presents the key drawback of redesigned joint structure - particularly that it is composed out of angled beams for brace and chord components. This setup is relatively difficult to manufacture using conventional manufacturing methods, without casting. Nevertheless, this design is meant to be a significant improvement from the standpoint of damage accumulation. This is exemplified in figure 6.10, which illustrates how stress distributes in the original and adjusted joint design at the moment when the load is being hoisted up. Here *Max* and *Min* shows locations of maximum and minimum stress

in the analysed geometry, with stress highlights capped at yield limit of structural steel, which is used for modelling the joint structure.

To ensure result consistency, finite element analysis for this geometry is defined based on the same principles described in chapter 4, with mesh set in a way to accommodate performance of hot-spot and multi-axial fatigue assessment around all relevant welds. With identically setup FEA models, it is still apparent in figure 6.10 that adjusted joint design does not have any significant stress concentrations between chord beam and pylon leg connections, with the maximum stress position located around the weld of left pylon leg beam stiffener ring. This also keeps any present stress concentrations at locations which are predictable and observable from the outside, with potential to repair occurring flaws without crane disassembly.

6.3.1. Fatigue assessment setup

To determine whether structure does not possess significant stress fluctuation around its weld connection - fatigue assessment is performed. Figure 6.11 illustrates measurement point locations and their naming definitions for evaluating fatigue damage. Picture A marks points for forestay-backstay chord, pylon legs and gusset plates weld connections on the right side, while picture B marks measurement points around stiffener ring and pylon leg stiffeners. An identical measurement point distribution of points illustrated in picture A are used for measuring fatigue on the left part of the joint, with a total of 80 measurement points defined.

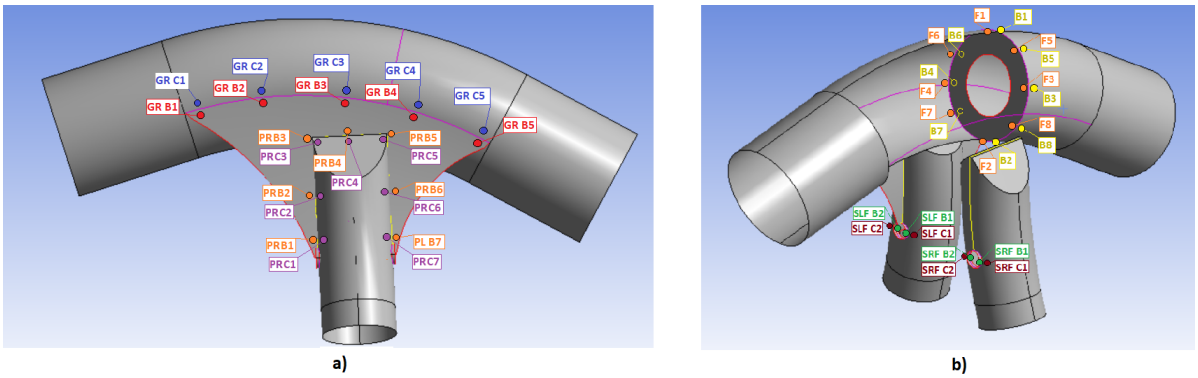

Figure 6.11: Measurement point distribution of hot spots for the redesigned joint multi-axial fatigue damage assessemnt

Fatigue assessment is performed using multi-axial fatigue method described in chapter 5, using same concept for defining stress angle, stress range and choosing appropriate S-N curves between T-curve and C2-curve.

6.3.2. Results

Table 6.7 summarizes fatigue damage factor results of redesigned joint for 23 years of operation (1.31 million cycles), when it is exposed to identical loading conditions as the original joint within original multi-axial fatigue analysis. Results show a good survival rate of the structure, with all measurement locations capable of surviving full assessed lifetime (keeping damage factor values <1).

In addition to that, according to performed fatigue assessment there is only a limited number of noteworthy stress concentrations with enough stress fluctuation during crane operation to accumulate fatigue damage above 0.5 over a 23 year operational period. Figure 6.12 highlights these points of interest - specifically points *F7, F8* located at the lower part of stiffener ring that is welded to the bent chord, and points *SLF C1* and *SLB C1* located around front and back stiffeners of the left pylon leg. Based on the damage ratio, these locations are safe as the rest of the structure, however these specific points should be observed during the lifetime of the crane for crack initiation. As all points of interest are in predictable locations which allow easy access for inspection and repair, joint can be conveniently serviced if needed.

Additionally, in terms of upper arm mass change - structure which incorporates adjusted joint design increases the mass of the total upper arm structure by just 2.6% - well outperforming its weight increase constraint limit of 5%. This means that redesigned joint is capable of increasing fatigue life of the upper arm structure without significantly increasing weight of the upper arm.

It is also worth noting that since the goal of joint redesign was not to provide the most optimal design possible, but rather to provide an alternative construction of original joint, which would be an improvement

Table 6.7: Fatigue damage factor results of measurement points of crane with redesigned joint structure, using multi-axial fatigue approach (23 years of operation).

Forestay-Backstay Chord	**Point**	**F1**	**F2**	**F3**	**F4**	**F5**	**F6**	**F7**	**F8**
	Damage	0.016	0.011	0.000	0.000	0.006	0.001	0.761	0.712
	Point	**B1**	**B2**	**B3**	**B4**	**B5**	**B6**	**B7**	**B8**
	Damage	0.048	0.008	0.000	0.000	0.016	0.004	0.037	0.161
Gusset-Chord Weld	**Point**	**GR B1**	**GR B2**	**GR B3**	**GR B4**	**GR B5**			
	Damage	0.001	0.011	0.026	0.013	0.000			
	Point	**GR C1**	**GR C2**	**GR C3**	**GR C4**	**GR C5**			
	Damage	0.001	0.001	0.003	0.002	0.000			
	Point	**GL B1**	**GL B2**	**GL B3**	**GL B4**	**GL B5**			
	Damage	0.000	0.001	0.001	0.001	0.000			
	Point	**GL C1**	**GL C2**	**GL C3**	**GL C4**	**GL C5**			
	Damage	0.001	0.001	0.003	0.001	0.000			
Pylon Stiffeners	**Point**	**SRF B1**	**SRF B2**	**SRB B1**	**SRB B2**	**SRF C1**	**SRF C2**	**SRB C1**	**SRB C2**
	Damage	0.006	0.001	0.001	0.001	0.121	0.015	0.476	0.020
	Point	**SLF B1**	**SLF B2**	**SLB B1**	**SLB B2**	**SLF C1**	**SLF C2**	**SLB C1**	**SLB C2**
	Damage	0.005	0.001	0.005	0.027	0.537	0.254	0.598	0.106
Gusset-Pylon Weld	**Point**	**PR B1**	**PR B2**	**PR B3**	**PR B4**	**PR B5**	**PR B6**	**PR B7**	
	Damage	0.000	0.050	0.117	0.000	0.006	0.007	0.001	
	Point	**PR C1**	**PR C2**	**PR C3**	**PR C4**	**PR C5**	**PR C6**	**PR C7**	
	Damage	0.013	0.010	0.061	0.080	0.010	0.003	0.055	
	Point	**PL B1**	**PL B2**	**PL B3**	**PL B4**	**PL B5**	**PL B6**	**PL B7**	
	Damage	0.001	0.152	0.004	0.000	0.034	0.074	0.009	
	Point	**PL C1**	**PL C2**	**PL C3**	**PL C4**	**PL C5**	**PL C6**	**PL C7**	
	Damage	0.000	0.028	0.010	0.013	0.016	0.020	0.002	

in terms of its ability to reduce accumulation of fatigue damage - there is a possibility to additionally improve the construction. However, since the proposed design is capable of handling desired operational fatigue life of 23 years, it can be judged that result of joint redesign is successful.

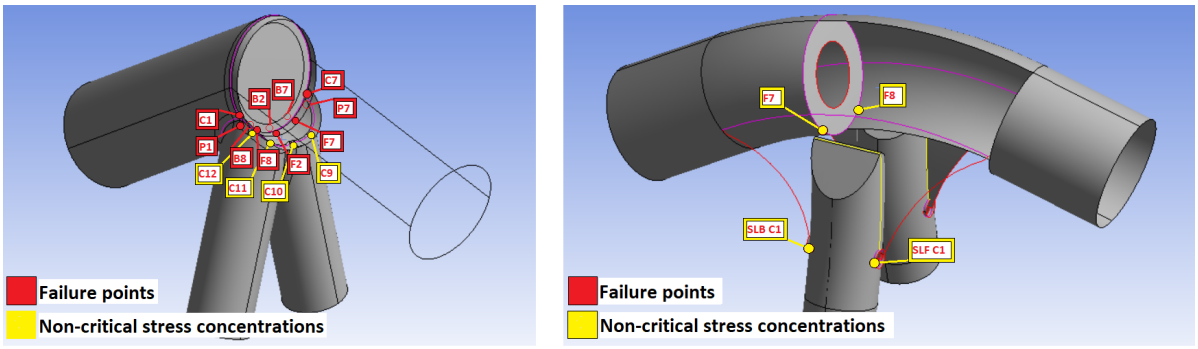

Figure 6.12: Comparison of failure points and non-critical stress concentrations between a) original joint and b) its redesigned variant.

All of the aforementioned factors conclude that because the adjusted variant is safe for operation of 23 years, is relatively light and provides good access to observe and address any potential crack initiation in the joint over routine checks of the structure - adjusted design of the crane fulfills all of its design criteria and is a significant improvement over the original joint.

6.4. Load reduction

This section investigates potential to increase fatigue life of the original crane upper arm without reduction in its work efficiency through adjustments of crane motion profile.

Damage accumulation is heavily dependent not only on structural capacity of analysed construction,

but also on exerted loads which affect the structure. As it has been deducted in load parameter screening presented in chapter 3 - weight of hoisting load is the most significant factor towards increasing average stress in the upper arm construction. This means that reducing lifted weight can potentially increase fatigue life of the structure, yet it also reduces crane work efficiency. On the other hand crane motion effects such as luffing, slewing and hoisting also have significance towards imposing stress in the analysed upper arm structure, however it might be possible to adjust their setup in such a manner where loading/unloading operation is completed with reduced load magnitude, but without increased overall cycle time of this operation. This forms the following supposition, which will be investigated for its accuracy:

- Hypothesis: *by adjusting crane motion profile it is possible to reduce fatigue damage accumulation in the critical upper arm joint without reducing operational efficiency of the crane.*

Finding an optimal motion profile which minimizes load impact is not the objective of this assessment - the scope of this analysis is meant to provide mainly an introductory assessment on whether aforementioned hypothesis is true and if it is possible to reduce loads acting the crane upper arm without increasing overall cycle time of crane operation and without reducing capacity of carried weight.

Approach

The principle of assessment is based of modelling an alternative motion setup within multi-body dynamic simulation environment, with the goal of reducing magnitude of load output that will be then used within FEA simulation to acquire stress response for fatigue analysis.

It has been observed during MBD model parameter screening in chapter 3 that crane movements can be modelled to complete a motion operation either by increasing overall magnitude of velocity or by increasing magnitude of acceleration. Increase of acceleration has been linked to higher resultant load when compared to increase of velocity magnitude, which means that in order to reduce loads it is more preferable to accelerate slower but to a higher overall velocity value rather than to take the opposite approach. Adjustment of crane motion cycle is based on the aforementioned principles - specifically on reduction of acceleration/deceleration magnitude as well as selective increase of motion velocity magnitude for hoisting, luffing and slewing motions.

To achieve the goal of reducing fatigue damage accumulation through motion adjustments, specific changes have been made:

1. Initial hoisting operation is done by lifting the grab from the ground at a reduced rate, instead of two quick pull steps which are present in original setup that is based on real crane operation.
2. Acceleration and braking time is increased throughout all motions of slewing, luffing and hoisting by 0.8-4.5 times.
3. Magnitude of velocity is selectively adjusted to account for potential time losses appearing from slower acceleration. Adjustment is varied by 0.8-1.85 times, changing velocity for specific motions.
4. Unnecessary intermediate speed changes have been removed to keep motion more stable and efficient.

Full list definition of both motion setups is summarized in table E.1 of appendix E. Aforementioned changes have led to acquisition of a new motion cycle within multi-body dynamic analysis that is of comparable length, with adjusted cycle being 5.3% shorter - saving approximately 3 seconds of cycle time. This fulfills the first requirement of analysis which states that adjusted motion cycle should not increase the cycle time of crane operation.

Figure 6.13 illustrates how hoisting load response differs between original crane motion setup and its adjusted counterpart. It is visible that the main difference between two variants is lower and less pronounced load peaks present within adjusted motion setup. The initial hoisting of the load happening between 5-10 second mark contains the largest reduction, which is expected to also reduce stress and in turn fatigue damage within analysed joint structure.

From acquired analysis results, load responses are extracted using the same principle as for original load assessment described in chapter 3. Hoisting load of front pulleys illustrated in figure 6.13 are then imported to finite element analysis environment of original upper arm setup (established and discussed in chapter 4) along with adjusted hoisting load on the back pulleys, cabin suspension load and all present inertia loads. FEA simulations are then run with adjusted loading setup to acquire adjusted stress response that is present within analysed geometry of original upper arm joint.

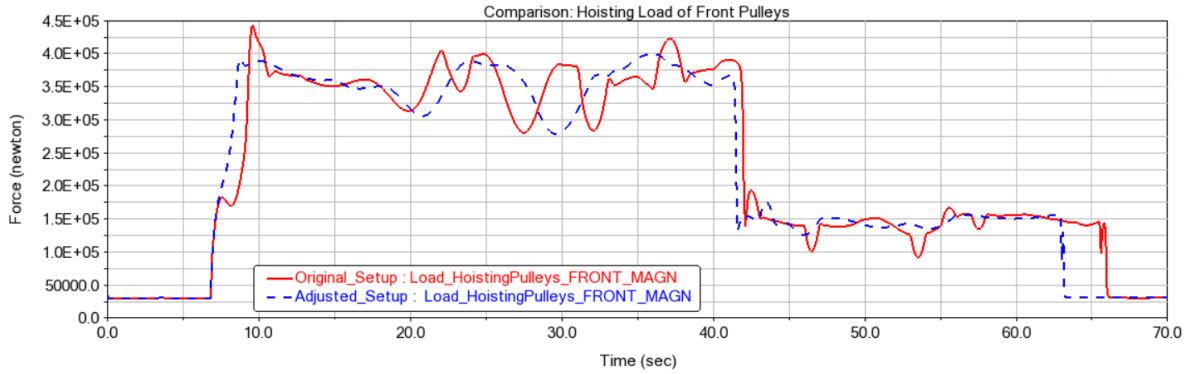

Figure 6.13: Comparison of hoisting load response affecting upper arm at the front pulley location between original (Red) and adjusted (Blue) motion setups.

Results

To assess how difference in crane motion affects damage accumulation in the joint, fatigue analysis is performed using multi-axial fatigue assessment method, with stress results acquired for adjusted motion profile. Measurement points are defined based on the distribution and naming convention presented in figure 4.17. Fatigue analysis results are summarised in table 6.8. Results show a directly comparable distribution of critical failure points (as it has been seen in table 5.3 in chapter 5 where original motion cycle fatigue results are presented). This strengthens the conclusion that distribution of failure points is not particularly linked to crane motion definition, but rather is a result of flawed design which is not fit for long-term use under cyclic loading.

Table 6.8: Accumulated fatigue damage factor $D_{i_{AA}}$ for original upper arm joint with adjusted acceleration profile setup. Measured at hot-spot nodes and acquired using multi-axial fatigue assessment method (23 years of operation)

Brace	**Point**	**P1**	**P2**	**P3**	**P4**	**P5**	**P6**	**P7**	**P8**
	$D_{i_{AA}}$	2.552	0.040	0.140	0.000	0.099	0.026	3.291	0.090
	Point	**P9**	**P10.2**	**P11**	**P12**	**P13**	**P14**	**P15**	
	$D_{i_{AA}}$	0.060	0.001	0.081	0.134	0.055	0.002	0.024	
Chord	**Point**	**C1**	**C2**	**C3**	**C4**	**C5**	**C6**	**C7**	**C8**
	$D_{i_{AA}}$	2.889	0.886	0.353	0.366	0.306	0.696	2.219	0.092
	Point	**C9**	**C10**	**C11**	**C12**				
	$D_{i_{AA}}$	0.301	0.380	0.420	0.924				
Forestay	**Point**	**F1**	**F2**	**F3**	**F4**	**F5**	**F6**	**F7**	**F8**
	$D_{i_{AA}}$	0.000	0.576	0.038	0.028	0.000	0.000	1.340	1.347
Backstay	**Point**	**B1**	**B2**	**B3**	**B4**	**B5**	**B6**	**B7**	**B8**
	$D_{i_{AA}}$	0.000	0.510	0.057	0.042	0.000	0.000	0.970	0.346

To better visualise changes within damage accumulation - table 6.9 provides a comparison of multi-axial fatigue damage factor results for original joint structure between adjusted and original crane motion setups. Here negative values (highlighted in blue) show where adjusted motion cycle leads to lower damage accumulation at the measurement point, while positive values (highlighted in red) present where original motion cycle leads to higher damage. As it is visible from the comparison - adjusted motion cycle reduces damage at all relevant measurement positions, with a maximum damage reduction of 0.945 at point P7.

Critical points which are prone to fatigue failure (i.e. P1, P7, C1, C2, C6, C7, C12, F2, F7, F8, B2, B8) as seen in original analysis have experienced reduced fatigue damage of approximately 24%. However the reduction is not significant enough to decrease damage to safe levels - a large amount of points accumulate enough damage to cause fatigue failure with both crane motion setups.

To reiterate the purpose of analysis - the current assessment has been established to test hypothesis of whether there is a potential to reduce fatigue damage through changes of crane movement and without reduction of operational efficiency. The presence of damage reduction presented in table 6.9 and comparable cycle time illustrated in figure 6.13 conclude that hypothesis is true. It is worth to additionally note that acquired adjusted motion cycle is not representative of most optimal crane motion setup, which maximizes

Table 6.9: Accumulated fatigue damage factor $D_{i_{AA}} - D_{i_{OA}}$ result comparison between crane using adjusted and original motion profile. Measured at hot-spot nodes and acquired using multi-axial fatigue assessment method (23 years of operation)

Brace	**Point**	**P1**	**P2**	**P3**	**P4**	**P5**	**P6**	**P7**	**P8**
	$D_{i_{AA}} - D_{i_{OA}}$	-0.391	-0.015	-0.032	0.000	-0.095	-0.027	-0.945	-0.145
	Point	**P9**	**P10.2**	**P11**	**P12**	**P13**	**P14**	**P15**	
	$D_{i_{AA}} - D_{i_{OA}}$	-0.097	-0.001	-0.059	-0.029	-0.066	-0.001	-0.038	
Chord	**Point**	**C1**	**C2**	**C3**	**C4**	**C5**	**C6**	**C7**	**C8**
	$D_{i_{AA}} - D_{i_{OA}}$	-0.482	-0.072	-0.044	-0.198	-0.182	-0.540	-0.697	-0.149
	Point	**C9**	**C10**	**C11**	**C12**				
	$D_{i_{AA}} - D_{i_{OA}}$	-0.345	-0.279	-0.176	-0.034				
Forestay	**Point**	**F1**	**F2**	**F3**	**F4**	**F5**	**F6**	**F7**	**F8**
	$D_{i_{AA}} - D_{i_{OA}}$	0.000	-0.415	-0.016	-0.039	0.000	0.000	-0.557	-0.055
Backstay	**Point**	**B1**	**B2**	**B3**	**B4**	**B5**	**B6**	**B7**	**B8**
	$D_{i_{AA}} - D_{i_{OA}}$	0.000	-0.356	-0.026	-0.060	0.000	0.000	-0.631	-0.022

reduction of fatigue damage - there is a definite potential to reduce fatigue damage further with a more in-depth methodical motion adjustment. This could be done by implementing an optimization algorithm to define a single cycle or by incorporating a dedicated controller for adaptive motion adjustments. Additionally, there might be a possibility to define a specific reduced hoisting weight magnitude which would be safe for operation of the original upper arm structure. Nevertheless, these two research extensions are left for future exploration.

6.5. Result comparison

This section evaluates damage reduction approaches to assess which method is best applied for increasing fatigue life of analysed crane upper arm structure. Structural capacity increase approach is compared with load response reduction method in terms of their potential to reduce fatigue damage. Additionally two structural capacity increase methods are compared with each other to assess their benefits and weaknesses.

6.5.1. Thickness adjustment vs. joint redesign

Two redesign methods have been tested in terms of their feasibility to increase fatigue life:

1. Thickness adjustment approach - which reduces accumulation of fatigue damage through increase of structural capacity of the structural elements of the upper arm, without changing the actual structural design setup of the joint.

2. Structural redesign of the problematic joint - which reduces accumulation of fatigue damage in the upper arm joint through stress redistribution within the structure.

Fatigue assessment of resulting designs have shown that both approaches provide good potential for improving fatigue life of the analysed upper arm joint. However even with their capabilities proven - they differ quite significantly and possess different strengths and weaknesses. For this purpose it is worth evaluating how these methods compare with each and which method should be favoured for refurbishment of the specific lemniscate crane.

The main benefits of performing thickness adjustment lie in:

1. This method does not require specific design changes to be made to the joint design beside the change of joint thickness. This simplifies the process of assessment for fatigue capacity as it allows to perform changes to an analysed finite element model structure quickly and efficiently.

2. Assessment method is based on a statistical optimization approach and is able of defining a direct relation between element thickness and imposed stress fluctuation range for the same loading conditions. This allows acquisition of thickness setup for multiple elements simultaneously in a manner that makes analysed construction capable of surviving desired fatigue life.

The main weakness of thickness optimization approach is rooted in the fact that location of the measurement points which accumulate most damage are always positioned in locations which are difficult to reach

for maintenance purposes, as they are situated behind pylon leg elements. This means that damage positions which might initiate fatigue cracking first are not possible to inspect and repair without crane disassembly, and this creates a large risk for longevity of the structure.

In a similar fashion, the main benefits of joint redesign can be summarised as follows:

1. Stress in the redesigned joint is distributed more evenly with significantly lower amount of stress concentrations present in the construction.
2. Joint redesign approach is more efficient in terms of weight increase when compared with thickness adjustment approach. Increasing the overall mass of the upper arm structure by 6% when thickness optimization method is used, and increasing mass by 2.6% when joint redesign method is applied.
3. Stress concentrations which could possess most danger towards potential crack initiation are in positions which are easily accessible for inspection and repair.
4. there is potential to further improve the design as joint redesign approach is not limited by the single variant which is used in this specific report - different design approaches can be taken if needed or the current setup further improved.

The main drawback of redesigned joint is linked to potential manufacturing issues. Because chosen design approach uses beams for pylon legs and the forestay-backstay chord that are manufactured out of large tubular cross-sections with preset radial bends. Producing bent structural steel beams with conventional manufacturing methods which do not rely on casting is difficult and at least more expensive than to rely on welded straight beams. This means that in terms of ability to manufacture - the original joint has a benefit over redesigned variant, however the benefits that adjusted joint design brings cannot be ignored.

In order to decide which design is better - it is worth summarising how each method deals with design requirements of handling cyclic loads for 23 years and predefined design constraints. These benefits and weaknesses of both methods can be summarised as follows:

1. Both approaches are capable of fulfilling their fatigue resistance requirements.
2. Joint redesign approach is capable of keeping upper arm structure lighter, but thickness adjustment approach uses design that is easier to manufacture.
3. Joint redesign approach keeps all points of interest for fatigue assessment in locations that are accessible for inspection and repair, while the thickness adjustment approach does not solve this issue.

Considering that the accessibility to locations where cracks are most prone to initiate is critical for maintenance purposes and overall safety of the crane structure - the joint redesign approach takes the lead. This concludes that most efficient method for extending fatigue life through design adjustments is to refurbish the crane upper arm by installing a new joint which is capable of solving the issues of original construction.

6.5.2. Load reduction vs. joint redesign

It has been shown that both load reduction approach and methods for increasing structural capacity can reduce accumulation of fatigue damage, this way potentially prolonging life of the analysed crane upper arm structure.

Comparing results of both approaches - the effective magnitude of what is possible to achieve is a lot more limited when it comes to load reduction approach. Assuming that the weight that is being hoisted cannot be reduced in magnitude - adjustments of motion effects can likely provide only a bounded benefit towards reducing fatigue damage accumulation per operational cycle. As it has been established in section 6.4 - reduction of loads through motion profile changes is not sufficient to fully counteract the damage accumulation effects which lead to crane failure. This means that it can act only as a supplementary method for increasing fatigue life of crane upper arm structure, rather than being a direct solution to the issue.

Design adjustments however have a lot more space for improvement as it is bounded only by available space and limited allowable increase of internal weight for the upper arm structure. They do however have a weakness of requiring significant downtime and increase in maintenance expenses to adjust design of the upper arm structure. Because original joint is flawed - redesign approach requires large-scale disassembly of the crane and refitting of original crane upper arm with a re-welded variant of a new joint model. This significantly impacts the effort and investment needed to prolong lifetime of the crane. Nevertheless this

is the best singular method to solve the apparent fatigue damage accumulation issues in the joint, due to methods versatility and observed good fatigue assessment results presented in section 6.3.

It is important to finally note that important aspect about two compared methods lie in the fact that - both fatigue life prolongation approaches are not mutually exclusive and it is possible to combine adjustment of crane design with a more efficient crane motion profile to potentially acquire best fatigue life results.

6.6. Conclusion

This section concludes results and observations made and provides answers to research question indicated at the beginning of this chapter.

In this chapter methods for increasing fatigue life of crane upper arm structure have been investigated. Overview of potentially beneficial approaches have been defined and three specific damage reduction methods have been implemented and evaluated. First potential for increasing structural capacity of original joint model has been assessed, following with an alternative joint design approach that attempts to redistribute stress without significantly increasing the weight of upper arm structure. Finally potential to reduce fatigue damage without changing design of the structure has been evaluated, which was focused on adjusting crane motion profile to reduce exerted loads on the joint construction. All methods were evaluated in terms of accumulated fatigue damage over 23 years of operation using multi-axial fatigue assessment approach for damage estimation.

Based on the observed fatigue assessment results, the following research questions can be answered:

How can problematic joint structure be redesigned to reduce the rate of fatigue damage accumulation?
Fatigue damage accumulation can be reduced with two main methods:

1. Through increase of structural capacity - which can be achieved by adjusting thickness of original upper arm joint elements.

2. Through redistribution of stress within problematic construction - which can be achieved through structural redesign of problematic joint.

Both methods have shown to be capable of achieving sufficient fatigue life for the structure (23 years of operation), however joint redesign is a more preferred method out of the two due to its savings in total mass that is added to the upper arm structure (6% vs. 2.6%) and because it provides access to points of interest for inspection and repair, which could be most prone to fatigue damage accumulation. Additionally, along with the aforementioned approach, improvement of weld quality when joint is being constructed is strongly recommended at locations which appear to be prone to experience stress concentrations. This is based on fatigue damage calculation principles of applied fatigue analysis method, which show that improvement of weld quality can potentially reduce fatigue damage in the structure up to 2.5 times.

How can fatigue damage of the structure be reduced without changes to crane design? Can this be done without reducing efficiency of crane operation?
Fatigue damage accumulation in the crane upper arm can be decreased with adjustments of the crane motion profile, that are based on reducing magnitude and fluctuation of loads exerted on the construction. It is possible to reduce load effects without reducing the hoisted mass of material or without increasing operational cycle time by:

1. limiting acceleration magnitude of luffing, slewing and hoisting motions; and

2. in exchange (if needed) increasing the maximum velocity magnitude of luffing, slewing and hoisting motions.

This allows to reduce fatigue damage by a relatively significant margin of 25% with potential additional increases if a more sophisticated motion control algorithm is implemented. However it has been shown that using only motion adjustments is not enough to maintain structure within safe level for 23 years of operation, thus this method can act only as a supplement to increasing structural fatigue life rather than being an independent solution.

What is the best potential method to increase fatigue life of crane upper arm?

Based on result comparison between two types of joint redesign and assessed approach for increasing fatigue life through adjustment of crane motion profile - it can be concluded that the best method for increasing fatigue life of the crane upper arm is by refurbishing the construction with a newly redesigned joint. Load adjustments have a limited potential to reduce the damage of the original upper arm setup and might not capable of being an independent solution to extending fatigue life to a safe level. On the other hand, joint redesign approach is capable of reducing fatigue damage accumulation within its welds to a safe level for 23 years of operation. This is achieved through stress redistribution principles, with only a limited increase of construction weight (<5% increase of the total weight for upper arm structure), while keeping all its potential failure points at locations which are accessible for inspection and repair. Thickness adjustment approach for the original joint structure, although providing good potential for increasing fatigue life - also possesses an inherent design flaw which keeps majority of critical points without clear access for inspection, leading to its main weakness in comparison with what complete joint redesign could provide. This concludes that joint redesign is the best approach for prolonging fatigue life of the analysed Cornelis Tromp 25T crane upper arm joint.

7

Conclusions and recommendations

This chapter summarises main observations made within the report and provides answers to its research questions. Additionally recommendations for future research are provided to conclude the thesis.

7.1. Research questions

Based on performed experiments and fatigue assessment results - all research questions can be summarized and answered in the following manner:

What is the current state of fatigue analysis methodology for structural joints?

Fatigue damage accumulation is heavily dependent on experimental data and on a large number of factors which are difficult to quantify. Because it is hard to account for all factors and situations based on performed fatigue experiments, the entire science of fatigue assessment relies on principle of estimation. Conventional methods, such as nominal, hot-spot and notch stress approaches are commonly applied in the literature and the industry to evaluate fatigue life of designed structures, however each method has its own benefits and weaknesses. Since stress direction can potentially play a significant role towards fatigue damage accumulation for different materials - a large amount of multi-axial fatigue assessment methods which could be applicable for fatigue damage estimation have been surveyed. Methods of multi-axial fatigue assessment are different both in terms of their application (whether they are capable of measuring proportional or non-proportional stress/strain response), as well as in terms of their proposed application. Although there are many approaches present in the literature, a large number of them still lack validation data to ensure their applicability towards estimating fatigue damage accumulation within welded structural joints. It is critical to choose a method which is applicable for specific analysis both in terms of stress response and evaluated geometry.

How can multi-body dynamic simulation approach help with establishing representative loading conditions of a crane work cycle within the time domain?

Multi-body dynamic (MBD) simulation of crane motion allows to establish load setups experienced by the crane within the time domain - meaning that loads acquired using this method include data of any potential load fluctuation and acceleration effects at multiple time steps, which are not present when establishing loads using static loading approach (which uses one time step for each load). MBD approach is less conservative when compared to static method as static approach uses safety factors to account for any potential dynamic load effects, while multi-body dynamic simulations capture all load responses in real time making it potentially more accurate. With enough data for model verification, MBD method for load acquisition is a very accurate approach that allows users to quickly compute large amount of load responses that are specific to needed motion profile of modelled mechanism. This however requires verification to be performed with enough reliable data available to conclude accuracy of the model. Finally this load acquisition method also allows to perform multi-axial fatigue analysis which generally require FEA stress responses that are evaluated within the time domain. Measuring how stress angle changes over time during crane operation can indicate whether there is a significant presence of non-proportionality within stress response. This factor influences both the choice of multi-axial fatigue assessment method as well as potentially having effect on the magnitude of fatigue damage accumulation. Static load approach does not enable this possibility of assessing fatigue damage using multi-axial methods.

How does incorporation of stress concentrations into fatigue assessment affect resultant fatigue life estimation in relation to nominal stress fatigue analysis?

Results of fatigue assessment has shown significantly different results between method which includes and doesn't include effects of stress concentration. Nominal stress approach shows that the structure is safe for 23 years of operation (1.31 million loading cycles). Hot-spot stress approach, on the other hand, shows critical failure at 25% of measured points, with fatigue damage factor reaching values up to 4.5. It is estimated that hot-spot stress approach provides more accurate results due to its ability to account for stress concentration effects and based on the fact that locations which were distinguished using this fatigue analysis to experience critical failure also correlate well with locations where fatigue cracks propagate in multiple cranes of the same model as the analysed Cornelis Tromp 25T lemniscate crane.

What is the main reason of joint failure for the analyzed lemniscate crane?

Main reason why the crane has failed is the large stress concentrations appearing at the brace saddle connection with the chord and at the lower part of forestay-backstay weld. These locations also experience a large stress fluctuation range during hoisting operation, which is the reason for fatigue damage accumulation that eventually lead to crack initiation and propagation in the joint. It is likely that during design phase crane structure has been not been properly evaluated for its potential to develop stress concentrations - any fatigue assessment which uses a nominal stress approach would not have been able to properly capture stress concentration effects towards fatigue damage accumulation in the crane upper arm structure.

Is incorporation of stress direction into fatigue assessment beneficial for evaluating fatigue damage at the welds of problematic joint? How its results compare to more conventional hot-spot fatigue assessment approach?

Benefits of fatigue assessment method which incorporates effects of stress direction into its formulation depend on material properties. For ductile materials stress is directional – thus multi-axial fatigue approach is expected to have some benefit towards potential increase of accuracy of fatigue damage accumulation results. Additionally it has been observed though assessment of principal stress magnitude, that most measurement points in analysed joint welds experience significant stress in two principal directions - meaning there is a basis for assessing fatigue life using multi-axial fatigue approach. For most locations – multi-axial fatigue approach shows some variation of fatigue damage in comparison with hot-spot stress approach, with majority of points showing lower damage when using multi-axial fatigue assessment method. Nevertheless both methods appear to be capable of establishing crack initiation locations, because based on simulation results - in both cases positions of points with critical damage accumulation values match well with crack propagation locations observed in real crane structure. Nevertheless to fully conclude which approach is more accurate, there is a lack of data available for measurement validation - thus it has been concluded that both methods are feasible in a general case, with indication that assessing fatigue damage using a conventional hot-spot stress approach that uses Von Mises stress is potentially slightly more conservative than performing fatigue assessment using a multi-axial fatigue assessment approach.

How can problematic joint structure be redesigned to reduce the rate of fatigue damage accumulation?

Fatigue damage accumulation can be reduced with two main methods:

1. Through increase of structural capacity - which can be achieved by adjusting thickness of original upper arm joint beams.

2. Through redistribution of stress within problematic construction - which can be achieved through structural redesign of problematic joint.

Both methods have shown to be capable of achieving sufficient fatigue life for the structure (23 years of operation), however joint redesign is a more preferred method out of the two, due to its savings in total mass that is added to the upper arm structure (6% vs. 2.6%) and provided access to points of interest for inspection and repair that are most prone to fatigue damage accumulation. Additionally, along with the aforementioned approach - improvement of weld quality when joint is being constructed is strongly recommended at locations which appear to be prone to experience stress concentrations. This statement is based on fatigue damage calculation principles of applied fatigue analysis method - removal of flaws within the weld can potentially reduce fatigue damage in the structure up to 2.5 times.

How can fatigue damage of the structure be reduced without changes to crane design? Can this be done without reducing efficiency of crane operation?

Fatigue damage accumulation in the crane upper arm can be decreased with adjustments of the crane motion profile that are based on reducing magnitude and fluctuation of loads exerted on the construction. It is possible to minimize load effects without reducing the hoisted mass of material or without increasing operational cycle time by:

1. limiting acceleration magnitude of luffing, slewing and hoisting motions; and
2. in exchange (if needed) increasing the maximum velocity magnitude of luffing, slewing and hoisting motions.

This allows to reduce fatigue damage by a relatively significant margin of 25% with potential additional increases if a more sophisticated motion optimization or control algorithm is implemented. However it has been shown that using only motion adjustments is not enough to maintain structure within safe damage limit for 23 years of operation. For this reason this method can likely act only as a supplement to increasing structural fatigue life rather than being an independent solution.

What is the best potential method to increase fatigue life of crane upper arm?

Based on result comparison between two joint redesign approaches and assessed method for increasing joint fatigue life through adjustment of crane motion profile - it can be concluded that the best method for increasing fatigue life is to refurbish the upper arm construction with a newly redesigned joint. Load adjustment has a limited potential to reduce the damage of the original upper arm setup and is not capable of being an independent solution to extending fatigue life to a safe level. Both joint redesign approaches however are capable of reducing fatigue damage accumulation within joint welds to a safe level, for 23 years of operation. This can be done both through principles of stress redistribution and increase of structural capacity. Stress redistribution approach however is most optimal because it achieves is fatigue life goals with only a limited increase of construction weight (<5% increase of the total weight for upper arm structure), while keeping all its potential failure points at locations which are accessible for inspection and repair. Thickness adjustment approach for the original joint structure, although providing good potential for increasing fatigue life - also possess an inherent design flaw which keeps majority of critical points without clear access for inspection, which leads to its main weakness in comparison with what complete joint redesign could provide. This concludes that joint redesign focused on stress redistribution is the best approach for prolonging fatigue life of the crane analysed Cornelis Tromp 25T crane upper arm.

7.2. Future research

1. Since there is not a clear agreement in the relevant literature on the optimal choice of stress type for hot-spot stress analysis - it is recommended to perform an in-depth evaluation on how choice of stress type influence hot-spot stress fatigue damage accumulation rate. Choice of stress type is expected to have significant consequences for hot-spot fatigue results. It has been observed that using Von Mises stress for hot-spot stress fatigue assessment leads to a conclusion that joint accumulates more damage at most critical locations when compared to calculation results acquired using multi-axial fatigue assessment approach. It is assumed that accounting for stress direction should increase damage rather than reduce it, but instead the opposite conclusion has been observed. Comparison of results between multi-axial fatigue with hot-spot stress approach which uses first principal stress results could potentially lead to a different conclusion.

2. There is still a very large gap present within validation of most multi-axial fatigue assessment methods. Lack of well documented experimental data limits potential application of many multi-axial fatigue approaches for evaluating fatigue damage within welds of steel joint structures. Additionally it maintains a factor of uncertainty within fatigue damage estimation presented in this report - on whether applied multi-axial fatigue assessment method is more accurate than conventional hot-spot stress approach.

3. An incorporation of controller within MBD setup environment could potentially allow modelling crane motion in a manner which effectively reduces magnitude of relevant loads, thus potentially reducing fatigue damage accumulation in the structure. The initial motion adjustment approach performed in this report has shown that there is a precedent to increase fatigue life of the crane, without increasing cycle time of loading/unloading, if crane motion is altered to accommodate movements which impose less stress within the structure. If a sophisticated optimization algorithm or a dedicated controller would be introduced for modelling crane motion within multi-body dynamic environment, this could

potentially allow to discover new movement approaches increasing fatigue life by a relatively significant margin.

4. It is worth investigating how reduction of hoisting load can affect fatigue life of the structure. In addition to that - an assessment could be made on whether it is possible to decrease fatigue damage accumulation in the crane upper arm structure without reducing of crane transshipment capacity. One way to perform this would be by reducing the hoisted load limit and compensating loss of efficiency with increased motion speed for luffing, slewing and hoisting operations.

Bibliography

[1] MSC ADAMS. *Mechanical System Simulation with Adams View*. 2012.

[2] Hobbacher A.F. *Recommendations for Fatigue Design of Welded Joints and Components*. Springer, Cham, Switzerland, 2nd edition, 2016. ISBN 978-3-319-23757-2. doi: 10.1007/978-3-319-23757-2.

[3] AISC. *ANSI/AISC 360-16*. Specification for Structural Steel Buildings. American Institute of Steel Constructio, 2019.

[4] Fisseha M. Alemayehu and Stephen Ekwaro-Osire. Uncertainty considerations in the dynamic loading and failure of spur gear pairs1. *Journal of Mechanical Design*, 135(8), 2013. ISSN 1050-0472 1528-9001. doi: 10.1115/1.4023870.

[5] C. Amzallag and J.P. Gerey. Standardization of the rainflow counting method for fatigue analysis. *Fatigue*, 16:7, 1994.

[6] T. Anderson. *Fracture Mechanics - Fundamentals and Applications*, volume 3. CRC Press, Boca Raton, USA, 2005.

[7] Vitor Anes, Luis Reis, Bin Li, and M. de Freitas. New cycle counting method for multiaxial fatigue. *International Journal of Fatigue*, 67:78–94, 2014. ISSN 01421123. doi: 10.1016/j.ijfatigue.2014.02.010.

[8] ANSYS. Fea best practices. *Academic training*, page 105, 2019.

[9] API. *2A-WSD*, volume 22 of *Planning, Designing, and Constructing Fixed Offshore Platforms—Working Stress Design*. Americal Petroleum Institute, Washington D.C., USA, 2014.

[10] J. Araujo, L. Susmel, D. Taylor, J. Ferro, and E. Mamiya. On the use of the theory of critical distances and the modified wöhler curve method to estimate fretting fatigue strength of cylindrical contacts. *International Journal of Fatigue*, 29(1):95–107, 2007. ISSN 01421123. doi: 10.1016/j.ijfatigue.2006.02.041.

[11] Z. Barsoum. *Guidlines for fatigue and static analysis of welded and un-welded steel structures*. KTH Royal Institute of Technology, Stockholm, Sweden, 2020.

[12] B. Beers. *P-value definition overview*, volume 2021. 2021. URL `https://www.investopedia.com/terms/p/p-value.asp`.

[13] Denis Benasciutti, Davide Zanellati, and Alessandro Cristofori. The "projection-by-projection" (pbp) criterion for multiaxial random fatigue loadings. *Frattura ed Integrità Strutturale*, 13(47):348–366, 2018. ISSN 19718993. doi: 10.3221/igf-esis.47.26.

[14] Jean-Pascal Bilodeau, Louis Gagnon, and Guy Doré. Assessment of the relationship between the international roughness index and dynamic loading of heavy vehicles. *International Journal of Pavement Engineering*, 18(8):693–701, 2015. ISSN 1029-8436 1477-268X. doi: 10.1080/10298436.2015.1121780.

[15] C. Braccesi, G. Morettini, F. Cianetti, and M. Palmieri. Development of a new simple energy method for life prediction in multiaxial fatigue. *International Journal of Fatigue*, 112:1–8, 2018. ISSN 01421123. doi: 10.1016/j.ijfatigue.2018.03.003.

[16] M.W. Brown and K.J. Miller. A theory for fatigue failure under multiaxial stress-strain conditions. *Applied Mechanics*, 187:27, 1973.

[17] Yuguang Cao, Zhanbin Meng, Shihua Zhang, and Haiqing Tian. Fem study on the stress concentration factors of k-joints with welding residual stress. *Applied Ocean Research*, 43:195–205, 2013. ISSN 01411187. doi: 10.1016/j.apor.2013.09.006.

[18] J.J Caoa, G.J. Yanga, J.A. Packer, and F.M. Burdekin. Crack modeling in fe analysis of circular tubular joints. *Engineering Fracture Mechanics*, 61:17, 1998.

[19] CEN. *EN 1993-1-9 Eurocode 3*. Design of Steel Structures. European Committee of Standardization, 2005.

[20] DNVGL-RP-C203. *Fatigue design of offshore steel structures*. DNVGL-RP-C203. 2020.

[21] Pingsha Dong, Zhigang Wei, and Jeong K. Hong. A path-dependent cycle counting method for variable-amplitude multi-axial loading. *International Journal of Fatigue*, 32(4):720–734, 2010. ISSN 01421123. doi: 10.1016/j.ijfatigue.2009.10.010.

[22] A. Ekberg, E. Kabo, and H. Anderson. An engineering model for prediction of rolling contact fatigue of railway wheels. *Fatigue Fracture Engineering Material Structures*, 25:12, 2002.

[23] Anders Ekberg, Bengt Åkesson, and Elena Kabo. Wheel/rail rolling contact fatigue – probe, predict, prevent. *Wear*, 314(1-2):2–12, 2014. ISSN 00431648. doi: 10.1016/j.wear.2013.12.004.

[24] A. S. Elliott and M. Hutchinson. Fully-coupled nonlinear 3-d time-domain simulation of drilling dysfunctions using a multi-body dynamics approach. *Drilling Conference and Exhibition*, 1:18, 2015.

[25] D. Exterkate, M. Saraber, Schreuder C., and R. Bohemen. Measurement acquisition procedure of a lemniscate crane. Report, Delft University of Technology, 2020.

[26] Ali Fatemi and Nima Shamsaei. Multiaxial fatigue: An overview and some approximation models for life estimation. *International Journal of Fatigue*, 33(8):948–958, 2011. ISSN 01421123. doi: 10.1016/j.ijfatigue.2011.01.003.

[27] Liuyang Feng and Xudong Qian. A hot-spot energy indicator for welded plate connections under cyclic axial loading and bending. *Engineering Structures*, 147:598–612, 2017. ISSN 01410296. doi: 10.1016/j.engstruct.2017.06.021.

[28] A.M. Freundenthal. Fatigue and fracture mechanics. *Engineering Fracture Mechanics*, 5:12, 1973.

[29] C. Gagg and Peter Lewis. In-service fatigue failure of engineered products and structures – case study review. *Engineering Failure Analysis*, 16:1775–1793, 09 2009. doi: 10.1016/j.engfailanal.2008.08.008.

[30] J. Giesbers. *Contact Mechanics in MSC ADAMS: A technical evaluation of the contact models in multibody dynamics software MSC Adams*. Ba, 2012.

[31] A. Harish. *Meaning of the Von Mises Stress and the Yield Criterion*, volume 2021. Simscale, 2021. URL `https://www.simscale.com/blog/2017/04/von-mises-stress/`.

[32] J. Homan. *Principal Stresses vs. Equivalent Stresses in Fatigue*, volume 2021. Fatec Engineering, 2018. URL `https://www.fatec-engineering.com/2018/10/19/principal-stresses-vs-equivalent-stresses-in-fatigue/`.

[33] ISixSigma. *Design of experiments screening approach overview*. 2020. URL `https://www.isixsigma.com/dictionary/screening-doe/`.

[34] ISO. *ISO 19902:2020*. Petroleum and natural gas industries — Fixed steel offshore structures. International Organization for Standardization, London, U.K., 2020.

[35] Anderson M. J.; and S. L.; Kraber. Principle of application for design of experiments tools. *Quality Digest*, 1999. URL `https://www.qualitydigest.com/july99/html/body_doe.html`.

[36] Marzbanrad J. and Hoseinpour A. Structural optimization of macpherson control arm under fatigue loading. *Tehnicki vjesnik - Technical Gazette*, 24(3), 2017. ISSN 13303651 18486339. doi: 10.17559/tv-20150225090554.

[37] C. Jiang, Z. C. Liu, X. G. Wang, Z. Zhang, and X. Y. Long. A structural stress-based critical plane method for multiaxial fatigue life estimation in welded joints. *Fatigue and Fracture of Engineering Materials and Structures*, 39(3):372–383, 2016. ISSN 8756758X. doi: 10.1111/ffe.12369.

[38] Y. Jiang, O. Hertel, and M. Vormwald. An experimental evaluation of three critical plane multiaxial fatigue criteria. *International Journal of Fatigue*, 29(8):1490–1502, 2007. ISSN 01421123. doi: 10.1016/j.ijfatigue.2006.10.028.

[39] JMP. *Types of design of experiments*. 2018. URL `https://www.jmp.com/en_ph/statistics-knowledge-portal/what-is-design-of-experiments/types-of-design-of-experiments.html`.

[40] J.C.P. Kam and W.D. Dover. Mathematical background for applying multiple axes random stress histories in the fatigue testing of offshore tubular joints. *International Journal of Fatigue*, 5:8, 1989.

[41] Aleksander Karolczuk, Dariusz Skibicki, and Łukasz Pejkowski. Evaluation of the fatemi-socie damage parameter for the fatigue life calculation with application of the chaboche plasticity model. *Fatigue and Fracture of Engineering Materials and Structures*, 42(1):197–208, 2019. ISSN 8756758X. doi: 10.1111/ffe.12895.

[42] K. Karttunen, E. Kabo, and A. Ekberg. Estimation of gauge corner and flange root degradation from rail, wheel and track geometries. *Wear*, 366-367:294–302, 2016. ISSN 00431648. doi: 10.1016/j.wear.2016.03.030.

[43] Masanori; Kawahara and Toshio; Iwasaki. Analysis of fatigue crack growth behavior in welded tubular t joints. *Offshore Technology Conference*, 10:10, 1978.

[44] M. Kertész and F. Palčak. The role of the stiffly stable integrators in nonlinear dynamic simulations. In *Conference of Applied Matematics*, volume 14, page 10.

[45] N. Kornev. *Ship dynamics in waves*, volume 1 of *Ship Theory II*. University of Rostock, Rostock, Germany, 2012.

[46] P. G. Kossakowski. Influence of initial porosity on strength properties of s235jr steel at low stress triaxiality. *Archives of Civil Engineering*, 58(3):293–308, 2012. ISSN 1230-2945. doi: 10.2478/v.10169-012-0017-9.

[47] Naim Kuka, Riccardo Verardi, Caterina Ariaudo, and João Pombo. Impact of maintenance conditions of vehicle components on the vehicle–track interaction loads. *Proceedings of the Institution of Mechanical Engineers, Part C: Journal of Mechanical Engineering Science*, 232(15):2626–2641, 2017. ISSN 0954-4062 2041-2983. doi: 10.1177/0954406217722803.

[48] T. Langlais. Multiaxial cycle counting for critical plane methods. *International Journal of Fatigue*, 25(7):641–647, 2003. ISSN 01421123. doi: 10.1016/s0142-1123(02)00148-2.

[49] L. Lee and C. Ball. Nominal stress calculation based on fea element nodal forces. *SAE International*, 5:13, 2018. doi: 10.4271/2018-01-1898.

[50] S. H. Lee, T. W. Park, J. K. Park, J. W. Yoon, K. J. Jun, and S. P. Jung. A fatigue life analysis of wheels on guideway vehicle using multibody dynamics. *International Journal of Precision Engineering and Manufacturing*, 10:6, 2009.

[51] M. C. Levesley, R. Ramli, N. Stembridge, and D. A. Crolla. Multi-body co-simulation of semi-active suspension systems. *Proceedings of the Institution of Mechanical Engineers, Part K: Journal of Multi-body Dynamics*, 221(1):99–115, 2007. ISSN 1464-4193 2041-3068. doi: 10.1243/1464419jmbd69.

[52] Kai Ling Li, Li Li Wang, Nan Shan, and Wei Xiao Tang. Fea analysis for the trunk beam of the portal crane. *Applied Mechanics and Materials*, 529:291–295, 2014. ISSN 1662-7482. doi: 10.4028/www.scientific.net/AMM.529.291.

[53] M. Linden. *Multiaxial fatigue: The influence of principal stress directions on the fatigue assessment of a stinger structure*. Msc, 2016.

[54] Rong Liu, Bohai Ji, Manman Wang, Ce Chen, and Hirofum Maeno. Numerical evaluation of toe-deck fatigue in orthotropic steel bridge deck. *Journal of Performance of Constructed Facilities*, 29(6), 2015. ISSN 0887-3828 1943-5509. doi: 10.1061/(asce)cf.1943-5509.0000677.

[55] P. Lopez-Crespo, B. Moreno, A. Lopez-Moreno, and J. Zapatero. Study of crack orientation and fatigue life prediction in biaxial fatigue with critical plane models. *Engineering Fracture Mechanics*, 136:115–130, 2015. ISSN 00137944. doi: 10.1016/j.engfracmech.2015.01.020.

[56] I. Lotsberg. *Fatigue Design of Marine Structures*. Cambridge University Press, New York, USA, 2016.

[57] I. Lotsberg. *Fatigue Design of Marine Structures*. Cambridge University Press, New York, USA, 2016. ISBN ISBN 978-1-107-12133-1.

[58] Y. Lu. *Survey of multi-body dynamic software packages*, volume 2021. New York, USA, 2012. URL `http://www.cs.rpi.edu/~trink/sim_packages.html`.

[59] L. Ma and G. Sines. Fatigue behavior of a pyrolytic carbon. *Journal of Biomedical Materials Research*, page 8, 2000.

[60] M.A. Meggiolaro and J.T. Castro. A modified wang-brown method for multiaxial rainflow counting of non-proportional stress or strain histories. *Brazilian Congress of Mechanical Engineering*, 21:8, 2011.

[61] Minitab. *Minitab statistical software guidlines*, volume 2021. 2021. URL `https://support.minitab.com/en-us/minitab/21/`.

[62] R v Mises. On saint venant's principle. *Bulletin of the American Mathematical Society*, 51(8):555–562, 1945.

[63] S. Modaresahmadi, A. Hosseinpour, and Williams W. B. Fatigue life prediction of a coaxial multi-stage magnetic gear. *IEEE 2019*, page 6, 2019. ISSN 978-1-5386-9284-4.

[64] Cory Natoli. Classical designs: Full factorial designs. Report, STAT Center of Excellence, 2019.

[65] M. Natrella. *Handbook of Statistical Methods*. Sematech, 2012. doi: DOI:10.18434.M32189.

[66] NEN. *NEN2018: Cranes*. Loads and combinations of loads. Nederlands Normalisatie-instituut, Delft, Netherlands, 1983.

[67] NEN. *Crane safety - General design*. Part 2: Load actions. Nederlands Normalisatie-instituut, Delft, Netherlands, 2014.

[68] NEN. *en13001-3-1*. Limit States and proof competence of steel structure. Nederlands Normalisatie Instituut, Delft, Netherlands, 2018.

[69] N. Nist. *Engineering Statistics: Handbook of Statistical Methods*. US. Department of commerce, 2003. doi: https://doi.org/10.18434/M32189.

[70] T. Palin-Luc and S. Lasserre. An energy based criterion for high cycle multiaxial fatigue. *European Journal of Mechanics*, 17:15, 1998.

[71] S. Pargalgauskas. Time-critical coordination of transport systems. Literature survey, Delft University of Technology, 2020.

[72] Mikkel Pedersen. Introduction to metal fatigue - concepts and engineering approaches. 12 2018. doi: 10.13140/RG.2.2.25216.28163.

[73] L. Reis, B. Li, and M. De Freitas. Analytical and experimental studies on fatigue crack path under complex multi-axial loading. *Fracture of Engineering Materials and Structures*, 29(4):281–289, 2006. ISSN 8756-758X 1460-2695. doi: 10.1111/j.1460-2695.2006.01001.x.

[74] Camilla Ronchei, Andrea Carpinteri, Giovanni Fortese, Andrea Spagnoli, Sabrina Vantadori, Marta Kurek, and Tadeusz agoda. Life estimation by varying the critical plane orientation in the modified carpinteri-spagnoli criterion. *Frattura ed Integrità Strutturale*, 9(34), 2015. ISSN 19718993. doi: 10.3221/igf-esis.34.07.

[75] Murat Saatcioglu. *Design of Slender Columns*, book section 4, page 26. 1997.

[76] Dikshant Singh Saini, Debasis Karmakar, and Samit Ray-Chaudhuri. A review of stress concentration factors in tubular and non-tubular joints for design of offshore installations. *Journal of Ocean Engineering and Science*, 1(3):186–202, 2016. ISSN 24680133. doi: 10.1016/j.joes.2016.06.006.

[77] R.; Samchuk and W. Bos. Analysis of the ct crane at 32t of load capacity. Report, 2020.

[78] A. Schepdael, A. Carlier, and L. Geris. Sensitivity analysis by design of experiments. *Tissue Engineering and Biomaterials*, 17:40, 2016. doi: 10.1007/978-3-319-21296-8_13.

[79] Nima Shamsaei. *Multiaxial Fatigue and Deformation Including Non-proportional Hardening and Variable Amplitude Loading Effects*. Thesis, 2010.

[80] Hua Shen and Hong Wan. Controlled sequential factorial design for simulation factor screening. *European Journal of Operational Research*, 198(2):511–519, 2009. ISSN 03772217. doi: 10.1016/j.ejor.2008.09.005.

[81] Angelo Simone. *An Introduction to the Analysis of Slender Structures*. Delft University of Technology, Delft, Netherlands, 2011.

[82] B. Socie and J. Bannantine. Bulk deformation fatigue damage models. *Materials Science and Engineering*, 3:11, 1988.

[83] Seung-wan Son, Hyun-seung Jung, Tae-soo Kwon, and Jin-sung Kim. Fatigue life prediction of a railway hollow axle with a tapered bore surface. *Engineering Failure Analysis*, 58:44–55, 2015. ISSN 13506307. doi: 10.1016/j.engfailanal.2015.08.031.

[84] C.M. Sonsino. <multiaxial-fatigue-of-welded-joints-under-inphase-and-outofphase-local-strains-and-stressesinternational-journal-of-fatigue.pdf>multiaxial fatigue of welded joints under inphase and out-of-phase local strains and stresses. *International Journal of Fatigue*, 17:16, 1995.

[85] Luca Susmel. A simple and efficient numerical algorithm to determine the orientation of the critical plane in multiaxial fatigue problems. *International Journal of Fatigue*, 32(11):1875–1883, 2010. ISSN 01421123. doi: 10.1016/j.ijfatigue.2010.05.004.

[86] C.J. Tawjoeram. *Crane fatigue assessment using Multibody Dynamics and Finite Element Method*. Thesis, 2017.

[87] L. Trocine and L.C. Malone. An overview of newer, advanced screening methods for the initial phase in an experimental design. In *Proceeding of the 2001 Winter Simulation Conference (Cat. No.01CH37304)*, volume 1, pages 169–178 vol.1, 2001. doi: 10.1109/WSC.2001.977263.

[88] P.S. van Lieshout. *On the assessment of multiaxial fatigue resistance of welded steel joints in marine structures when exposed to non-proportional constant amplitude loading*. Phd, 2020. URL `https://doi.org/10.4233/uuid:afd39f40-7569-4cc6-ac1a-659342b45f9a`.

[89] C. H. Wang and M. W. Brown. Life Prediction Techniques for Variable Amplitude Multiaxial Fatigue—Part 1: Theories. *Journal of Engineering Materials and Technology*, 118(3):367–370, 07 1996. ISSN 0094-4289. doi: 10.1115/1.2806821. URL `https://doi.org/10.1115/1.2806821`.

[90] E. Wierenga. Development of a dynamic model of a lemniscate crane in msc adams. Report 2019.MME.8399, Delft University of Technology, 2020.

[91] Hao Wu, Pingbo Wu, Fansong Li, Huailong Shi, and Kai Xu. Fatigue analysis of the gearbox housing in high-speed trains under wheel polygonization using a multibody dynamics algorithm. *Engineering Failure Analysis*, 100:351–364, 2019. ISSN 13506307. doi: 10.1016/j.engfailanal.2019.02.058.

[92] Zhi-Rong Wu, Xu-Teng Hu, and Ying-Dong Song. Multiaxial fatigue life prediction for titanium alloy tc4 under proportional and nonproportional loading. *International Journal of Fatigue*, 59:170–175, 2014. ISSN 01421123. doi: 10.1016/j.ijfatigue.2013.08.028.

[93] Yangjian Xu and Huang Yuan. Computational modeling of mixed-mode fatigue crack growth using extended finite element methods. *International Journal of Fracture*, 159(2):151–165, 2009. ISSN 0376-9429 1573-2673. doi: 10.1007/s10704-009-9391-y.

[94] Jia Yao, Xiaoming Qiu, Zhenping Zhou, Yuqin Fu, Fei Xing, and Erfei Zhao. Buckling failure analysis of all-terrain crane telescopic boom section. *Engineering Failure Analysis*, 57:105–117, 2015. ISSN 13506307. doi: 10.1016/j.engfailanal.2015.07.038.

MULTI-AXIAL FATIGUE ASSESSMENT OF A LEMNISCATE CRANE

S. Pargalgauskas[1], X. Jiang[1], M. Edelkamp[2], D.L. Schott[1]
[1]Department of Maritime and Transport Technology, Delft University of Technology, Delft, Netherlands
[2] In Summa Innovation B.V., Raamsdonksveer, Netherlands

***Abstract* – The main purpose of this paper is to investigate the flaws within the joint of Cornelis Tromp 25T lemniscate crane upper arm joint. It is done to understand why the structure is experiencing significant crack propagation, which in the past have potentially led to a structural joint failure within a crane of the same model and killed its operator. Present work attempts to evaluate fatigue damage accumulation within toe of a problematic tubular joint structure welds using three fatigue assessment methods - nominal stress, hot-spot stress and a specific multi-axial fatigue assessment method. Load response for all experiments is acquired using a simulated multi-body dynamic model of the analysed crane, which has been verified using measurement data acquired from real operation of the crane. Finally joint redesign potential is investigated using two methods meant to reduce the magnitude of fatigue damage accumulation - through increase of structural capacity and through redistribution of stress.**

***Keywords* – Multi-axial fatigue; Multi-body dynamics; Structural joints; Stress concentration; Structural design;**

I. INTRODUCTION

According to [1], 60-90 % of the damage on mechanical parts belongs to fatigue damage, while fatigue failure accounts for the majority of mechanical failures worldwide (with the numbers ranging between 50% and 90% between different industry statistics). This is particularly important for load bearing welded joint structures which are cyclically loaded throughout their operational lifetime. When the structure and/or its loading conditions are complex in nature, it is difficult to determine in advance how much accuracy is needed to estimate fatigue life, in a manner which is representative of real damage accumulation.

In the literature there is a large number of approaches estanlished to evaluate fatigue damage of welded structural joints, based on desired accuracy and available data. Some of the most commonly used fatigue assessment approaches in the literature and industry are conventional nominal [2], hot-spot [3] and notch [4] stress methods, which all differ depending on the type of stress used in the fatigue assessment, as well as the amount of available data of joint element and weld geometry. However none of the aforementioned approaches account for stress direction, which is an important factor towards dictating the way cracks initiate and propagate. For this purpose, more detailed multi-axial fatigue assessment approaches have been in development. Each fatigue assessment approach does differ based on its damage model formulation, use of response component types, applicability towards different types of multi-axial stress, as well as general geometry that the method is designed for. Some fatigue assessment methods are best suited when structure does not experience non-proportional stress effects, which lead to direction change within the stress response (e.g. Liu Virtual strain [5], Modified Wöhler Curve [6]), while others are specifically used for evaluating non-proportional fatigue responses (e.g. Structural Stress Critical Plane [7],Modified Carpinteri-Spagnoli [8]) With aforementioned critical plane methods being among most popular, recently some additional integral [9], [10] and Invariant [11] methods have been gaining ground. Nevertheless, due to the lack of experimental data a lot of them lack information which could verify their applicability towards evaluating multi-axial stress effects towards fatigue damage accumulation in welded structural joints, thus accuracy of how particular method performs in relation to real life fatigue damage accumulation can be difficult to assess.

A. Problem definition

This paper attempts to evaluate fatigue damage accumulation within a particular floating lemniscate crane used for handling bulk material. In the past, flawed design of analyzed lemniscate crane variant has ended in structural failure of the boom and death of the operator. The main reason for crane failure is assumed to be the initiation of crack at the welded connection between forestay and backstay beams as shown in figure 1. An inspection of identical model variant crane - Cornellis Tromp 25T - revealed that it has experienced comparable damage accumulation at the same location, which could potentially lead to structural failure in near future if left unattended. This similarity shows that there is a pattern in the cranes of this design and since multiple cranes of this type are still in operation - it is worth investigating what is the main contributing factor towards this damage, and how different fatigue damage evaluation methods, which include stress concentration and stress direction effects, are able to evaluate damage accumulation within the problematic joint.

Additionally lemniscate cranes perform rotational motion operations (e.g. slewing motion in lemniscate cranes) are prone to continuously changing multi-directional loading. This means that slewing cranes maintain complex motion and loading profiles, thus potentially requiring a more intricate approach to assessing fatigue damage that is defined within a time domain.

Finally due to presence of the apparent flaws in the joint structure, methods have to be investigated on how to improve fatigue resistance in the upper arm through a specific redesign approach. All of the aforementioned aspects are discussed in this paper.

Fig. 1. Crack propagation within upper arm joint of Cornelis Tromp 25T lemniscate crane.

B. Contribution

The paper provides a comparison of three fatigue assessment methods to indicate how inclusion of stress concentrations and stress direction affects resultant damage accumulation in welded joint structure. Additionally it defines relevant loading conditions through the use of multi-body dynamic simulations. Finally it introduces two approaches to reduce damage accumulation through adjusting design of the joint structure.

C. Structure

This paper is organised as follows: *Load acquisition* presents the general overview of simulating crane work cycle with the help of multi-body dynamic simulations for the purpose of acquiring loads acting on crane upper arm structure; *Fatigue assessment* presents the process and results of fatigue analysis using three different approaches and determines reason why joint experiences crack propagation; *Joint redesign* proposes two approaches for reducing fatigue damage in the structure and compares them in terms of their strengths and weaknesses; *Conclusion* summarizes the paper contents and provide main findings.

II. LOAD ACQUISITION

A critical part of fatigue assessment is the establishment of a representative stress cycle. Stress in the analysed structure is dependant on loading conditions which affect its geometry - the accuracy of stress cycle is directly related to the accuracy of applied loads. As loads used in fatigue assessment are either static (i.e. having a single step of loading/unloading representing main loading increase/decrease) or temporal (i.e. including response acquired over a period of time with multiple time steps present per each loading cycle). For the purpose of establishing accurate loading conditions, temporal load setup can potentially increase the precision through inclusion of residual dynamic load effects, however these are difficult to define without relying on measurement data.

Multi-body dynamic (MBD) simulation is an approach that allows users to acquire loading profiles in the time domain for dynamically loaded structures, which in turn can provide more accuracy to the procedure of fatigue life assessment. However, in order for acquired loading results to be reliable, the specific MBD model has to be sufficiently accurate in representing real system. To establish load responses affecting analysed crane upper arm structure - a representative MBD model of Cornellis Tromp 25T lemniscate crane is used as initially developed by [12]. This setup allows performing simulations of crane loading/unloading operations in real time and enable extracting body and inertia loads affecting particular part of the model for use in stress acquisition. As Cornellis Tromp 25T is a floating crane, pontoon motion is modelled within the environment to represent its effects as well. Figure 2 presents crane model established within Adams View MBD software environment.

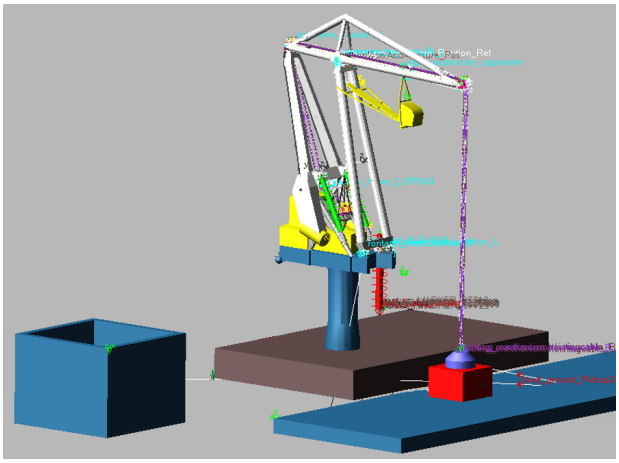

Fig. 2. Multi-body dynamic model of the crane used for load acquisition.

The original model has been assessed and additionally calibrated in terms of its component mass, inertia setup, as well as simulation setup parameters, such as use of particular dynamic integrator for modelling loads and accuracy of surface-to-surface contact model. Along with the aforementioned changes, a motion cycle setup has been introduced which has been modelled based on a representative work cycle of real crane operation. Motion setup in terms of time duration and displacement has been derived by analysing video footage of 57 consecutive work cycles of Cornellis Tromp 25T crane captured from the operators cabin. This resulted in modelling of a loading/unloading operation which lasts 66 seconds and completes a full work cycle.

Finally, to assess which loads have to be modelled with most accuracy to ensure precision of a stress response - statistical significance of several factors has been evaluated. A number of screening experiments based on Design of

Experiments [13] Screening analysis algorithms have been performed to find the answer. Following experiments were made:

1. Evaluation of body and inertia load effects towards imposing a stress response in the crane structure.
2. Evaluation of how inertia load effects affect dominant body loads.
3. Evaluation how pontoon motions affect dominant body load response.
4. Evaluation of how introduction of flexibility into slender crane components influences load response.

Slender part flexibility has been introduced to assess whether it affects loading response, however sensitivity analysis results have shown that it doesn't have a particular statistically significant effect.

Using the remaining three screening experiments, the effects of main load components affecting crane upper arm structure have been quantified based on their statistical significance. Six main loads have been determined: two body loads - hoisting load, cabin structure load; as well as 4 inertial accelerations appearing from crane slewing and luffing operations and from pitch and roll of crane pontoon rotation. As ensuring of accuracy for these loads is important to maintain accuracy of finite element analysis - they are verified using available data. Body loads have been established on the basis of crane rating and weight data published by crane owner, pontoon roll and pitch motions have been calibrated using sensor measurement data acquired during crane operation, while luffing and slewing acceleration values were defined based on extracted analog measurement data acquired from video footage for crane operation, which includes temporal displacement measurement information available to the crane operator. Figure 3 illustrates the resultant cartesian measurement of the hoisting load effects acting on the front pulleys of the crane upper arm throughout modelled crane operation cycle (in X Y and Z directions). This load has been determined to be most significant load towards imposing stress into the crane upper arm structure. It shows how much fluctuation is actually present in the load response which is not possible to accurately model using a static load approach. This and aforementioned body and inertia loads were then extracted and introduced into the finite element analysis for stress acquisition.

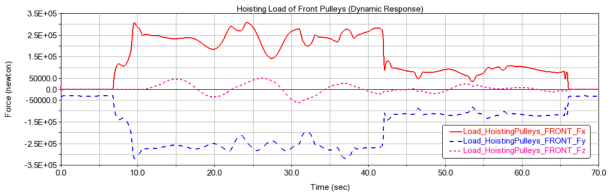

Fig. 3. Hoisting load response defined using MBD analysis.

III. FATIGUE ASSESSMENT

In order to choose an approach for fatigue assessment, it is important to investigate how inclusion of additional information into fatigue analysis (or its lack thereof) affects results of estimated fatigue damage and how weld it reflects crack propagation distribution based on what has been observed in the real structure.

A. Analysis Setup

Assessment is performed with the help of finite element analysis simulations using Ansys software, in which a detailed geometry variant of crane upper arm structure is defined for evaluation. For meshing of the geometry - using plane meshing approach presented in [14] and uniform quadratic Shell281 elements mesh has been established, with a significant mesh size refinement around evaluated joint. Mesh size and quality at measurement locations were defined in accordance to fatigue analysis requirements described in [15]. Loads were applied at identical locations as they have been extracted from MBD simulation results, with constraints defined at the locations where upper arm connects to front and rear arms of the crane, with allowed single rotational degree of freedom at both connection locations. Measurement points for evaluating fatigue damage were established at equal distances away around each weld line, with 8 points per each circular connection. Using the aforementioned finite element analysis setup, relevant stress responses were extracted to perform fatigue analysis with three specific methods which will described in this chapter.

B. Nominal stress fatigue

It is not always worth establishing a detailed fatigue assessment and commonly simplicity of fatigue analysis might be a preferred path. In such cases fatigue damage is evaluated using a Nominal stress approach which does not localize stress concentration effects to their specific location. Nominal stress, by definition, averages out stress response over entire beam element cross section using linear elastic beam theory, with stress values depending mainly on distance from cross-section center point.

Approach for evaluating nominal stress through finite element analysis that uses shell or solid elements is performed by extracting force and moment reactions at the cross section - small distance away from the actual weld position. As stress response cannot be directly obtained from the finite element analysis (FEA) response - it is then rather calculated using stress equations for linear beams, with appropriate surface area and area moment of inertia computed subsequently. As only normal stress components are used for nominal stress fatigue assessment - following equation is used to acquire relevant stress response σ_i [16].

$$\sigma_i = \frac{F_z}{A} - \frac{M_x y_i}{I_x} + \frac{M_y x_i}{I_y} \tag{1}$$

where F_z is force reaction in tension direction; A is cross-sectional area of measured cut; M_x and M_y is out-of-plane and in-plane bending moment reactions; y_i and x_i are planar distance values from center of cross-section to location of measurement point in X and Y directions; I_x and I_y being values of cross-sectional area moment of inertia in X and Y directions, established based on the shape of evaluated beam cross section.

As fatigue life for all methods described in this paper is evaluated with inclusion of time domain, cycle counting

was then performed using Rainflow cycle counting algorithm [17] to determine simplified stress cycles, which can then be evaluated in terms of fatigue damage accumulation using nominal stress-life (S-N) curves acquired from [2] and a damage rule derived from a combination of Haibach equation and Palmgren-Miner rule [12]. Fatigue damage accumulation is evaluated for 23 years, based on how long the crane has been operating before critical crack has been observed. Using crane transshipment data, this timeline has been determined to include a total number of approximately 1.31 million work cycles, which was the cycle number chosen for evaluation of fatigue damage. For comparative purposes the same number of fatigue cycles has been evaluated with nominal stress as well as all upcoming fatigue analyses described in this paper.

C. Hot-spot stress fatigue

One significant weakness of nominal stress approach is its inability to account for stress concentration effects within its stress formulation. Depending on geometry and loading conditions, stress concentrations commonly are a source and location of crack initiation which can potentially lead to accumulation of fatigue damage and eventual failure of the structure. By observing general stress response within FEA analysis, it has been observed that at the crack propagation position - there is at least one large stress concentration which is worthy of investigation. This is a serious point of interest for assessment of fatigue damage, thus including effects of stress concentrations into fatigue analysis is pivotal for understanding why this crane joint is prone to failure. This can be done using hot-spot fatigue assessment.

Hot-spot stress (also known as structural stress) method describes the stress raising effect caused by the global geometric discontinuity of the welded joints, without considering the local notch geometries of the welds [18]. Unlike nominal stress fatigue assessment - hot-spot stress approach uses stress values acquired from finite element analysis, however it is also not done directly at relevant measurement position. Instead - a linear stress extrapolation technique is used [3], which measures stress response at two points away from weld for each measurement position and then extrapolates stress value to the weld toe. These values are then used with Rainflow cycle counting algorithm and hot-spot S-N curves to calculate fatigue damage with the damage rule of [15]. Performed analysis uses Von Mises stress as a relevant response, in order to consider potential effects of all stress components acting at a measurement point location.

Method applicability has been verified by performing stress concentration factor calculations for a more conventional uniplanar K-joint, which were then compared with stress results acquired with FEA simulation.

D. Multi-axial fatigue

As stress distribution and failure for different materials is dependent on stress angle, it is worth evaluating how fatigue damage accumulation differs when stress direction is included within damage formulation. For this purpose multi-axial fatigue analysis can be performed. Is defined as assessment which takes into account effects of stress direction towards accumulation of fatigue damage. As the analysed joint is established out of four welded tubular joints - it is worth acknowledging that they have a tendency to experience complex stress distribution, generally along the surface of the tube [3]. This combined with the fact that the structure is loaded over a time with changing magnitude and direction of loads over operational cycle of the crane - there is potential for complex stress responses to develop around the welded connections, which would hint towards the need of multi-axial fatigue analysis.

It is important to note that there are different aspects of multi-axial fatigue which might be present in some stress/strain cases but missing in others. Generally the most critical ones include presence of multiple stress components acting on a single measurement point, as well as changing direction of stress components during its loading cycle, better known as stress non-proportionality. There is a large number of methods which could be used for assessing multi-axial fatigue [4], however some approaches are better suited for specific applications and types of multi-axial stress, which limits potential method choices. Stress response has been evaluated in the original structure to determine whether there are multiple significant stress components per each measurement point, as well as to observe whether principal stress direction changes over crane loading cycle - this could indicate stress non-proportionality. Inspection results have shown that indeed there is a presence of multi-directional stress of significant magnitude at majority of measurement points, however stress has been proportional (i.e. principal stress angle changes were limited at all positions - below threshold of 10 degrees). Combined with the fact that fatigue assessment has been performed using hot-spot stress on welded tubular joint structures - a hot-spot multi-axial fatigue method has been chosen, which is introduced in [15].

Applied multi-axial fatigue assessment method uses responses of two largest principal stress components within extrapolated hot-spot stress result to estimate fatigue damage. Aforementioned stress components are defined into parallel and perpendicular stress, based on value of principal angle θ illustrated in figure 4.

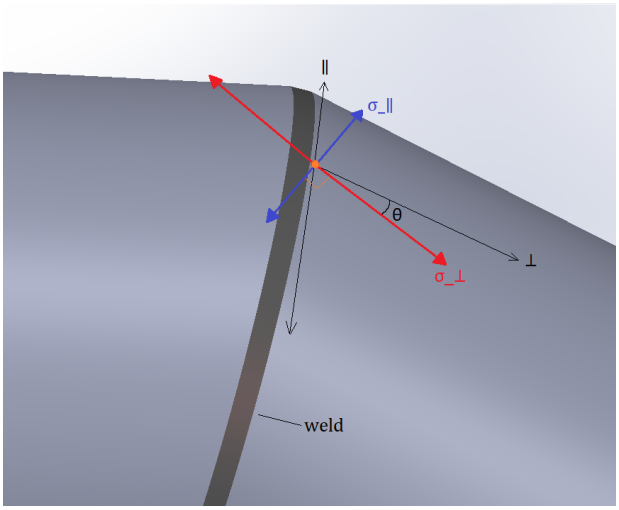

Fig. 4. Directional measurements of principal stress angle θ used for determination of relevant multi-axial fatigue S-N curve.

This approach uses a conventional Rainflow cycle counting algorithm to establish number of cycles and their magnitudes.

In order to evaluate fatigue damage - hot-spot stress S-N curves are used. Curve class is determined based on aforementioned stress measurement angle for each component, depending on whether $\theta \leq 30°$ or $\theta > 30°$, with an identical damage rule applied as it has been used for hot-spot stress approach. Calculated fatigue damage uses the following rule for choosing stress component inducing largest amount of damage D, based on principal angle θ value:

$$D = max \begin{cases} D_{\perp} = \sum_i D(\theta) \; for - 60° \leq \theta \leq 60° \\ D_{\perp} = \sum_i D(\theta) \; for - 45° \leq \theta \leq 45° \end{cases} \quad (2)$$

Since there is an angle overlap region between two rules - any measurement points with two stress components within overlap bounds are considered to experience combined effect, requiring summation of damage. This is evaluated for all measurement points to acquire final fatigue damage accumulation results. The aforementioned approach was applied to evaluate fatigue around all welds present in the joint at the same locations as for nominal and hot-spot stress fatigue approaches. Unlike most multi-axial fatigue assessment methods, the aforementioned approach is made specifically to assess fatigue damage within welded joints, which indicates that there is a basis to trust its results. An extended method overview can be found in [15].

E. Results

Main failure points are indicated with all fatigue assessment results in figure 5, with accumulated damage comparison of three fatigue assessment methods. As it can be seen from the graph, there is a significant distinction in magnitude of accumulated damage when stress concentration effects are included in the stress formulation, in comparison when they are missing. Results have shown significantly different results with nominal and hot-spot fatigue assessment. Nominal stress approach shows that the structure is safe for 23 years of operation (1.31 million loading cycles), while hot-spot stress approach showing critical failure at all 10 critical locations (which account for 25% of all measured points), with fatigue damage factor D_i reaching values up to 4.5. It is estimated that hot-spot stress approach provides more accurate results due to its ability to account for stress concentration effects and the fact that locations which were distinguished in fatigue analysis to experience critical failure also correlate well with locations where fatigue cracks appear to propagate in multiple cranes of the same model, as the analysed Cornelis Tromp 25T lemniscate crane.

A slightly different result can be seen when including stress direction effects into formulation. For most locations – multi-axial fatigue approach shows a variation of fatigue damage in comparison with hot-spot stress approach that is considerable for multiple critical locations, with majority of points showing lower damage when using multi-axial method. This is a presumed to be a result of using different S-N curves per each method requirements and due to the fact that Von Mises stress has been used for the hot-spot fatigue assessment approach, which has led to inclusion of stress component effects that might not properly account for increase in fatigue damage in

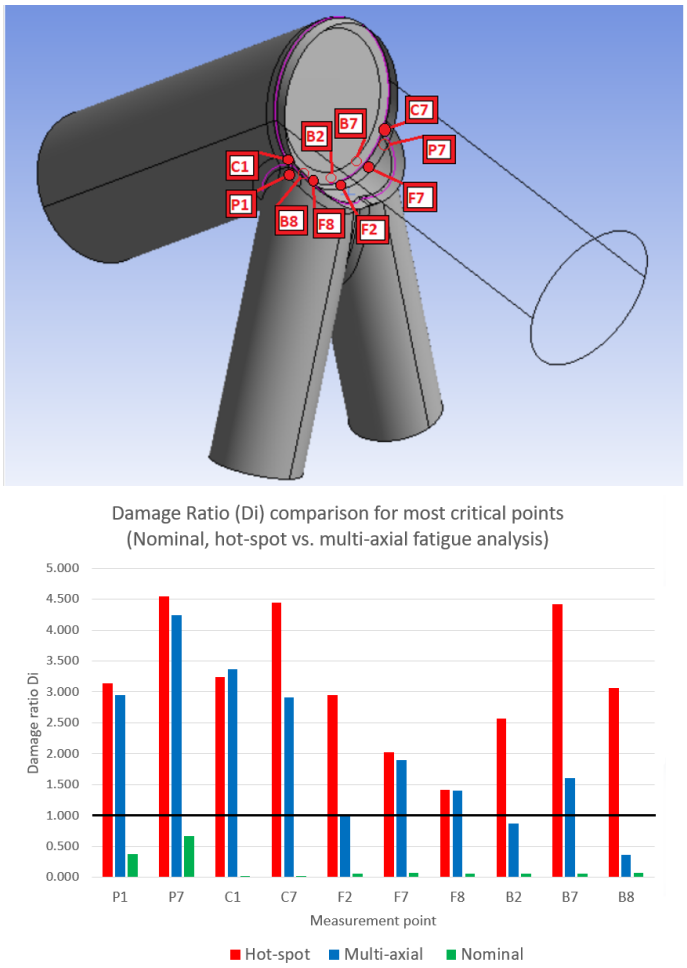

Fig. 5. Damage accumulation comparison between fatigue assessment approaches

real structures. However both methods appear to be capable of establishing noteworthy damage locations as critical points based on simulation results in both cases match well with crack propagation locations observed in real crane structure illustrated in figure 6 - meaning both methods are feasible for assessing locations of potential crack initiation, with some questions remaining towards magnitude of fatigue damage at each point. Nevertheless to fully conclude which approach is more accurate, there is a lack of data available - thus it has been concluded that both methods are feasible in a general case, with indication that assessing fatigue damage using a conventional hot-spot stress approach that uses Von Mises stress is potentially more conservative than performing fatigue assessment using multi-axial fatigue assessment approach. However both are likely applicable for estimating fatigue damage in the analysed structure.

IV. JOINT REDESIGN

As the original joint structure is incapable of surviving desired fatigue life - it is worth evaluating how the upper arm construction could be improved. The most common way is to approach the problem from the standpoint of refurbishment, where only a part of the structure is redesigned to provide better fatigue assessment results. Two design adjustments are performed - method for increasing structural capacity of

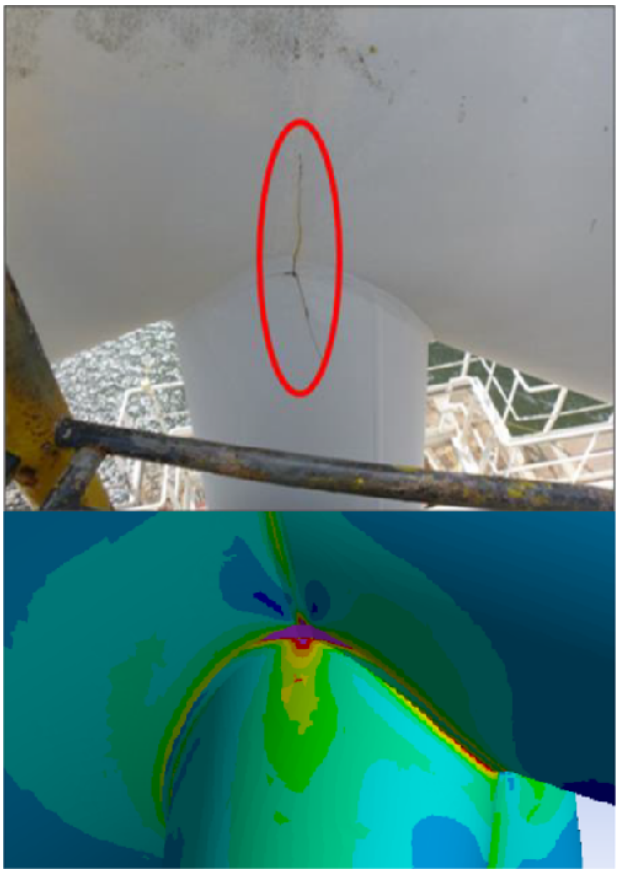

Fig. 6. Comparison of crack propagation location and FEA stress distribution.

the original construction and stress redistribution approach with introduction of a brand new joint design. Both variants are evaluated in terms of their stress response using an identical load and constraint setup, which are then assessed for fatigue damage accumulation at 23 years of operation, using previously introduced multi-axial fatigue assessment method.

A. Structural capacity increase

One of the most straightforward ways to reduce fatigue damage through the aspect of design change is to increase structural capacity of the construction. Better reinforced construction also induces lower stress response, thus potentially reducing range of stress fluctuation which is relevant for fatigue damage accumulation. For joint elements such as beams and plates this can be achieved by adjusting element thickness.

In order to approach the task effectively with decision basis covered by statistic evaluations - an optimization approach has been chosen to acquire optimal thickness setup capable of surviving desired fatigue life. This is performed in two main steps:

1. Factor screening - where each relevant joint component is evaluated in terms of whether there is statistical significance between component thickness and resultant stress response.
2. Factor sensitivity analysis - where a direct relation between statistically significant joint element thickness and imposed fatigue damage is established to find an optimal fatigue life.

Both approaches use algorithms based on Design of Experiments (DoE) methodology, performing multiple experimental runs with different factor value setups to extract and evaluate relevant response. For this redesign method beam thickness for forestay, backstay and pylon legs are adjusted throughout their entire length, meaning that increase of thickness tend to affect weight of the structure fairly significantly.

Screening analysis is performed using full factorial design [13] algorithm, which evaluates all possible factor combinations with two level values per factor (i.e. 8mm and 20mm of element thickness). This specific experiment evaluates whether change in pylon, forestay/backstay and mid-plate thickness separately affect magnitude of stress accumulation in the joint. Stress range was chosen as screening experiment response because increase in stress magnitude and its fluctuation range correlate with increased accumulation of fatigue damage in the structure. Screening response was used to evaluate statistical significance of thickness at all failure points from the original multi-axial fatigue analysis, illustrated in figure 5. Results have shown that change in thickness for all three evaluated elements are statistically significant at confidence interval of 95%. This concludes that thickness values had to be optimized for forestay/backstay, pylon leg beams, as well as for the chord mid-plate.

To acquire the optimized fatigue damage response relation between element thickness and fatigue damage accumulation - Sensitivity analysis algorithm is used. Chosen assessment employs DoE Box-Behnkhen [19] design which is a response surface design capable of establishing higher order relations between multiple factors and desired response/-s, while at the same time minimizing required number of experimental runs. Due to the fact that previous experiments have shown presence of statistical significance in all joint elements, this analysis uses identical factors (i.e. element thickness) for screening purposes, with adjusted low and high thickness value limits (8 mm and 30 mm respectively). Stress range is the chosen response, however it is established from the point of fatigue damage accumulation with a representative Stress-life curve indicating stress range limits for specific number of loading cycles.

Acquired factor-response relations allow to find an optimal thickness combination for desired fatigue life. Figure 7 illustrates a graphically established response surface relation between joint element thicknesses and imposed stress range at the critical failure point located within the brace saddle position shown in figure 6. Response surfaces show relations between two factors in a 2 dimensional surface format from where, depending on required fatigue life correlating to this stress range value, desired stress range can be chosen.

Using established response surfaces - *Response optimizer* algorithm embedded within Minitab software is applied to acquire optimal responses. Optimization target is established for all points of interest to acquire stress range values below 110 MPa that is supposed to be enough to survive 23 years of cyclic loading (1.31 million cycles). Since there are multiple

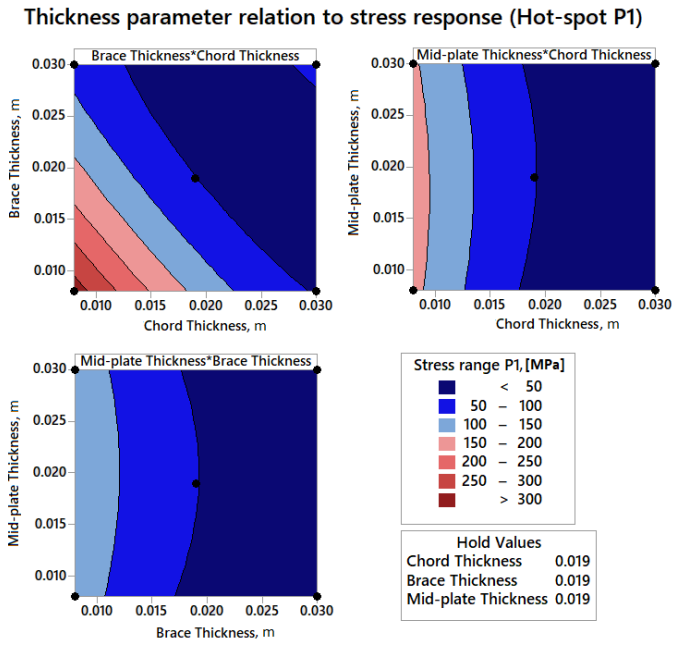

Fig. 7. Element thickness relation established using sensitivity analysis.

possible joint element thickness combinations available which can acquire feasible values - 10 potential combinations are extracted and one variant is chosen. The variant is chosen with only one specific rule - that acquired brace and chord diameters should be different, because equal thickness setups have been observed to fail from weld root at the saddle position even with relatively low stress concentrations [15]. The chosen setup of chord, brace and mid-plate thicknesses of the original joint and its optimization result are summarized in table I. Along with thickness values, the table also presents change in total mass for the joint and for the entire crane upper arm structure. These values are then verified using fatigue analysis to observe changes, summarized in *Results* subsection.

TABLE I

Comparison of joint element thickness T and structure mass between original and optimised joint setups, with change indicated in percentile values.

	Original	**Optimised**	**Change**
T Chord, mm:	12.7	16	26%
T Brace, mm:	9.5	12	26%
T Mid-plate, mm:	12	14	17%
Joint Mass. kg:	8248.3	10388.9	26%
Upper arm Mass, kg:	36770	38910.6	6%

B. Stress redistribution

It is not always possible to acquire desired damage distribution or fatigue life results simply by increasing structural capacity of the joint - this can be the case due to structural weight limitations or poor distribution of stress, which positions crack initiation points at inaccessible locations. This could require a change in the actual joint design, which goal is to redistribute stress in a manner where stress concentrations are released over a larger surface area and into locations which would be accessible for inspection and repair.

The main approach for redistributing stress is based on increasing surface area of the contact between structural elements in dominant loading direction/-s and removal of sharp re-entrant corners. Following changes have been made to provide a new joint design:

1. Original joint is removed from the entire structure, with only 2 meters of each beam element taken away (contrary to thickness adjustment approach which changes entire beam length). This is meant to limit the scope of changes and keep majority of upper arm intact.
2. Welded forestay-backstay beam connection is exchanged by a uniform bent beam with a predefined radius. This distributes stress concentration present at the original forestay-backstay beam weld. Stiffener ring is added to the chord at the location where majority of stress is present (shown in figure 9)
3. To even out stress distribution between chord and brace weld - the connection is remodelled to include gusset plates in-between pylon leg tubes and forestay-backstay beam.
4. Stiffeners are added at gusset plate endings where they intersect pylon leg beams. This distributes stress at plate-tube connection endings over a larger area.

Adjustment to the joint setup is performed and implemented in multiple iterations with each variant meant to redistribute stress in a manner which reduces magnitude of stress concentrations observed in the original joint. Each design is assessed in FEA environment by exchanging original joint in the main setup with the particular design iteration. Figure 8 illustrates how stress distributes within the original joint and its adjusted variant. It can be seen that there is a lack of strong stress concentration between chord and brace connections and any present stress concentration is located in positions which are easy to inspect for any potential crack propagation.

It is worth noting that the proposed design is relatively difficult to manufacture due to the use of bent tubular beams for both chord and brace elements. Nevertheless, the purpose of assessing alternative joint design is to estimate whether it is possible to reduce fatigue damage accumulation through a different distribution of stress under identical loading conditions, which would create lower stress concentrations. It is achieved using aforementioned design illustrated in figure 8. Detailed fatigue analysis is performed with the resultant stress responses measured at 80 points along joint welds.

C. Results

Table II summarizes damage accumulation results between original joint, thickness optimization and joint redesign approaches. Results show that compared to the original joint which indicates fatigue failure at 9 measurement locations - both redesign approaches no longer possess any failure points at tested fatigue life of 23 years. Maximum damage has been reduced more than 4 times for each design adjustment approach to safe levels. This shows that both increase of structural capacity and stress redistribution approaches

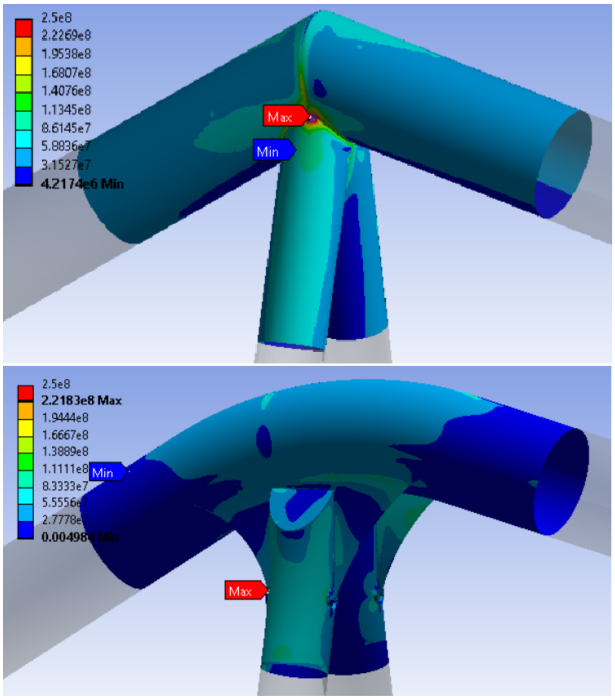

Fig. 8. Stress distribution and magnitude comparison between a) original joint and b) redesigned joint structure.

are capable of achieving desired fatigue life, with thickness optimization method increasing overall mass of the crane upper arm by 6.0% and stress redistribution method limiting mass increase to 2.6%.

TABLE II
Result comparison of joint redesign approaches

	Original Joint	Thickness adjustment	Joint redesign
Number of failure points:	9	0	0
Number of non-critical stress concentrations:	3	6	4
Maximum damage:	4.236	0.939	0.761
Tested life:		23 years	
Upper arm Mass Change:	-	+6.0%	+2.6%

However more difference between the two methods can be distinguished when assessing where stress concentrations accumulate in each structure. Figure 9 provides a visual definition of critical point locations prone to fatigue damage accumulation. Positions where damage accumulation is the highest remains inaccessible when lifetime is prolonged by increasing structural capacity of the joint. This is a critical issue, because a safe and well-designed construction that is prone to fatigue damage accumulation needs to have all of its points of interest (marked as non-critical stress concentrations) accessible for inspection and repair. Distribution of critical points does not change when structural capacity is increased for the same joint design, thus not fixing the main issue, which indicates that this joint setup is inherently flawed for loading conditions experienced by the crane upper arm. This issue is fixed by introducing a different joint design through stress redistribution approach - due to a different connection approach between joint elements - points which accumulate most damage are exposed and do not require crane disassembly to be inspected or for repairs to be performed. This indicates that in principle, when a structural joint is experiencing fatigue damage, it is important to assess whether damage is accumulating in accessible locations, because this determines whether it is even possible to efficiently apply thickness optimization approach which increases structural capacity. Otherwise redesigning the structure itself would be a preferable approach, as is the case for analysed upper arm joint of Cornellis Tromp 25T lemniscate crane.

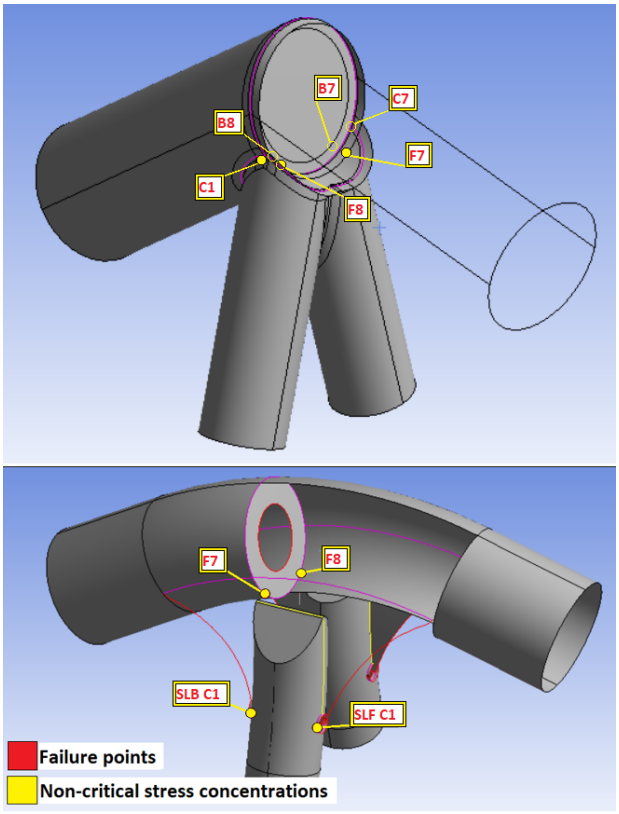

Fig. 9. Points of interest prone to fatigue damage accumulation in joint with adjusted thickness and redesigned joint model.

V. CONCLUSIONS

This paper has presented a structural evaluation of a problematic tubular joint of a lemniscate crane upper arm, in terms of its fatigue damage accumulation within the construction. A multi-body dynamic simulation approach allowed to model loads acting on the crane upper arm within a time domain, with the crane model verified based on measurements acquired from real crane operation. Fatigue analysis performed using nominal, hot-spot and multi-axial fatigue assessment approaches has shown that nominal stress fatigue analysis is not capable to predict fatigue damage based on how it has accumulated in the real structure. This is due to the fact that nominal stress does not contain enough information to distinguish stress concentration effects. On the other hand, both hot-spot and multi-axial fatigue assessment approaches are able to define most critical failure points,

although magnitude of accumulated damage does differ. It is expected that accounting for stress direction improves the accuracy of resultant damage accumulation, however more real-world data is needed to verify this statement.

Based on fatigue assessment results, it has been determined that joint structure experiences high stress concentrations which likely led to fatigue failure of this particular crane type, due to low structural capacity of the original joint. Two joint redesign methods have been introduced and compared - method to increase structural capacity using thickness optimization technique and stress redistribution method, implemented through full redesign of the joint. Both methods are capable of reducing fatigue damage to a desired level, however due to flawed design of original joint structure it has been shown that crack initiation points are located at non-accessible positions for inspection and repair, even when thickness is adjusted to safe levels. Proposed potential joint redesign model redistributes stress in a way which fixes this issue.

ACKNOWLEDGEMENTS

This paper is a documentation of the graduation project titled 'Multi-axial fatigue assessment of a lemniscate crane', which is one of the requirements to obtain the author's Masters of Science degree in Mechanical Engineering at Delft University of Technology, within the track of Multi-machine Engineering. Special appreciation goes to Dr. ir. X. Jiang for being a large part towards guidance and success within the project.

REFERENCES

[1] C. Gagg, P. Lewis, "In-service fatigue failure of engineered products and structures – Case study review", *Engineering Failure Analysis*, vol. 16, pp. 1775–1793, 09 2009, doi: 10.1016/j.engfailanal.2008.08.008.

[2] H. A.F., *Recommendations for Fatigue Design of Welded Joints and Components*, 2nd ed., Springer, Cham, Switzerland, 2016, doi:10.1007/978-3-319-23757-2.

[3] I. Lotsberg, *Fatigue Design of Marine Structures*, Cambridge University Press, New York, USA, 2016.

[4] P. van Lieshout, *On the assessment of multiaxial fatigue resistance of welded steel joints in marine structures when exposed to non-proportional constant amplitude loading*, Phd, 2020, doi:10.4233/uuid:afd39f40-7569-4cc6-ac1a-659342b45f9a.

[5] L. Reis, B. Li, M. De Freitas, "Analytical and experimental studies on fatigue crack path under complex multi-axial loading", *Fracture of Engineering Materials and Structures*, vol. 29, no. 4, pp. 281–289, 2006, doi:10.1111/j.1460-2695.2006.01001.x.

[6] J. Araujo, L. Susmel, D. Taylor, J. Ferro, E. Mamiya, "On the use of the Theory of Critical Distances and the Modified Wöhler Curve Method to estimate fretting fatigue strength of cylindrical contacts", *International Journal of Fatigue*, vol. 29, no. 1, pp. 95–107, 2007, doi:10.1016/j.ijfatigue.2006.02.041.

[7] C. Jiang, Z. C. Liu, X. G. Wang, Z. Zhang, X. Y. Long, "A structural stress-based critical plane method for multiaxial fatigue life estimation in welded joints", *Fatigue and Fracture of Engineering Materials and Structures*, vol. 39, no. 3, pp. 372–383, 2016, doi: 10.1111/ffe.12369.

[8] C. Ronchei, A. Carpinteri, G. Fortese, A. Spagnoli, S. Vantadori, M. Kurek, T. agoda, "Life estimation by varying the critical plane orientation in the modified Carpinteri-Spagnoli criterion", *Frattura ed Integrità Strutturale*, vol. 9, no. 34, 2015, doi:10.3221/igf-esis.34.07.

[9] C. Sonsino, "<Multiaxial-fatigue-of-welded-joints-under-inphase-and-outofphase-local-strains-and-stressesInternational-Journal-of-Fatigue.pdf>Multiaxial fatigue of welded joints under inphase and out-of-phase local strains and stresses", *International Journal of Fatigue*, vol. 17, p. 16, 1995.

[10] C. Braccesi, G. Morettini, F. Cianetti, M. Palmieri, "Development of a new simple energy method for life prediction in multiaxial fatigue", *International Journal of Fatigue*, vol. 112, pp. 1–8, 2018, doi: 10.1016/j.ijfatigue.2018.03.003.

[11] D. Benasciutti, D. Zanellati, A. Cristofori, "The "Projection-by-Projection" (PbP) criterion for multiaxial random fatigue loadings", *Frattura ed Integrità Strutturale*, vol. 13, no. 47, pp. 348–366, 2018, doi:10.3221/igf-esis.47.26.

[12] C. Tawjoeram, *Crane fatigue assessment using Multibody Dynamics and Finite Element Method*, Thesis, 2017.

[13] ISixSigma, *Design of experiments screening approach overview*, 2020, URL: `isixsigma.com/dictionary/screening-doe/`.

[14] J. Caoa, G. Yanga, J. Packer, F. Burdekin, "Crack modeling in FE analysis of circular tubular joints", *Engineering Fracture Mechanics*, vol. 61, p. 17, 1998.

[15] DNVGL-RP-C203, *Fatigue design of offshore steel structures*, 2020.

[16] L. Lee, C. Ball, "Nominal Stress Calculation Based on FEA Element nodal Forces", *SAE International*, vol. 5, p. 13, 2018, doi:10.4271/2018-01-1898.

[17] C. Amzallag, J. Gerey, "Standardization of the rainflow counting method for fatigue analysis", *Fatigue*, vol. 16, p. 7, 1994.

[18] L. Feng, X. Qian, "A hot-spot energy indicator for welded plate connections under cyclic axial loading and bending", *Engineering Structures*, vol. 147, pp. 598–612, 2017, doi:10.1016/j.engstruct.2017.06.021.

[19] A. Schepdael, A. Carlier, L. Geris, "Sensitivity analysis by design of experiments", *Tissue Engineering and Biomaterials*, vol. 17, p. 40, 2016, doi:10.1007/978-3-319-21296-$8_1$3.

A

Appendix: Load parameter screening procedure

A.0.1. Quantification methodology

In order to understand how changes in particular load magnitude affects the crane upper arm and which loads are particularly affect stress response (and in turn fatigue damage accumulation) - load effects should be quantified. This would allow to decide which specific loads should be accurately adjusted to realistically represent state of the upper arm during upcoming finite element analysis. There are a number of possible ways to statistically determine the significance of various model parameters. Karttunen et al. [42] uses a combination of latin hypercube sampling and regression analysis for determining combinations of parameters which create most critical loads in a multi-body dynamic simulation of a train wheel-rail contact. Some other approaches include trial and error approaches or implementation of modified genetic algorithms. However, one of the most common ways to determine whether a multiple independent variables have an effect on a specific response is the use of *Design of Experiments Screening* approach.

A Screening design, is one of the techniques based on design of experiments (DoE) technique. It is built on the principle of running a number of predefined experimental runs (which include combinations of specific changing screened factor values) and statistically interpreting their effects in term of their significance towards changing relevant response values. This technique is best used when a number of possible independent variables are present, which if used with a standard DoE design, would require running a large number of experiments [33]. With the help of DoE screening experiment setup, multiple factors can be screened at the same time and statistically significant factors can be derived while at the same time, minimizing number of experimental runs that have to be performed to find a reliable result.

Principle of screening design setup

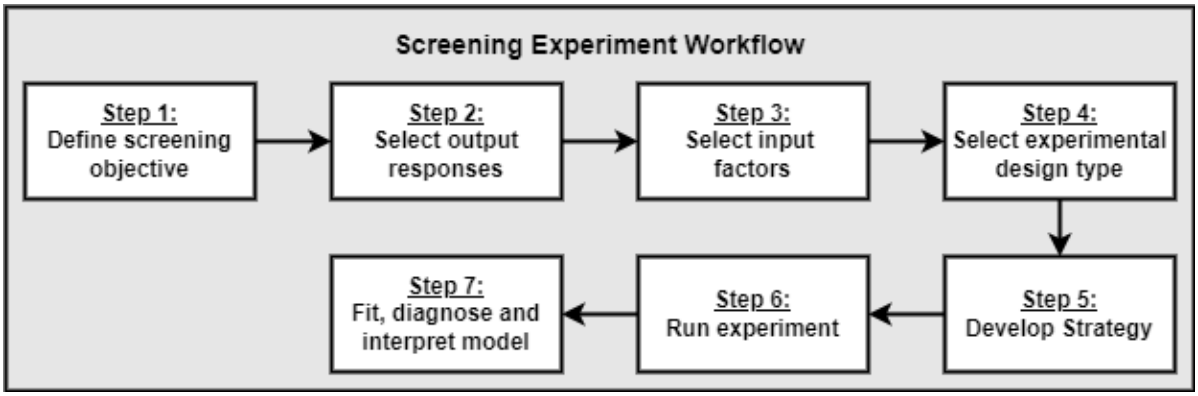

Figure A.1: Principle workflow steps of a design of experiments screening design

Figure A.1 illustrates a general steps of screening design experiment setup. It defines the process of performing screening in sequential manner. This principal idea of screening experiment execution can be defined with the following seven steps:

1. *Screening objective definition* - determination of analysis goal. It explains why this experiment takes place, its formulation is generally closely related to the relation between output response/-s and input factors.

2. *Output response selection* - it is a key performance indicator of a screening experiment. It defines what kind of model parameter/-s are used for evaluating changes when input factor value combinations with each experimental run. Depending on the observation goal and scope, there can be multiple responses used for each experiment.

3. *Input factor selection* - these are model parameters with adjustable values which are screened for their significance towards changing the output response values. A significant factor would have a direct impact towards increasing/reducing value of the response.

4. *Experimental design selection* - Choice of approach for running experiments, based on required level of interactions. Commonly used screening setups include Plackett-Burman, Mixed-level and various Factorial designs, which all evaluate a limited number of combinations to reduce the needed amount experimental runs, with mostly 2 level value setups for each input factor (high-low value approach). JMP [39] provides an overview of classical and modern screening designs and their use cases. The choice of a specific experiment heavily depends on the goal of experiment as well as on cost and resource constraints. Since screening of crane load effects is performed through simulations, the main limiting factors in terms of analysis choice is computation and data collection time limitations.

5. *Strategy development* - definition of how experiments will take place. This includes experimental run setups and approach for data collection.

6. *Experiment run* - performance of experimental runs and data acquisition. In the case of crane load analyses, this step concerns running of simulations and data extraction for further statistical analysis.

7. *Model fit, diagnosis and result evaluation* - statistical analysis of acquired response results in relation to experimental run setups. This step involves ensuring that collected data is reliable through evaluation of data fits using a specific R^2 value, removal of bias in the model and adjustments to experimental runs. This is where input factor significance is determined based on chosen significance level, which determines whether evaluated factors require additional attention to detail in terms of their accurate value definition.

It is important to note that screening design only establishes statistical significance of screened factors. Due to the low amount of screening points (2 per factor), it assumes only linear progression of factor values and in most cases does not have enough data to define direct relation between the factor and response that could be used for model parameter calibration.

Principle of strategy development

As previously mentioned, most common experiment types that are used for screening experiments include Full and Fractional factorial designs, Plackett-Burman, Cotter and Mixed-level designs, among others. Trocine and Malone [87] provides a detailed overview of conventional screening experiment types. More advanced screening experiment approaches are also available in the literature, especially for custom scenarios or when there is a large number of factors present which require screening. Shen and Wan [80] discusses applications of more unorthodox approaches for setting up a screening experiment and provides literature references towards detailed descriptions of such approaches. For the purpose of performing screening in this research, three approaches will be used, specifically:

1. *Full Factorial design* - designs where all possible factor combinations are run in order to acquire reliable data about all factors and all of their combined interactions. This approach provides most reliable data, but is often too expensive to run, especially if there is a large amount of factors which have to be screened for their significance.

2. *Fractional Factorial design* - an approach where a specific fraction of a full factorial design is run (commonly 1/2, 1/4, and 1/8 fractions are used). This approach reduces the number of experiments which have to be run, but in some cases might provide less reliable data than a full factorial experiment setup.

3. *Plackett-Burman design* - approach which uses a specific experiment setup algorithm meant to minimize the number of runs which have to be made in order to acquire enough data about factor significance. It is a very efficient approach, however it does not test any factor interactions besides their independent significance.

Each experiment type and setup is discussed in more detail in respective upcoming sections where they are specifically applied.

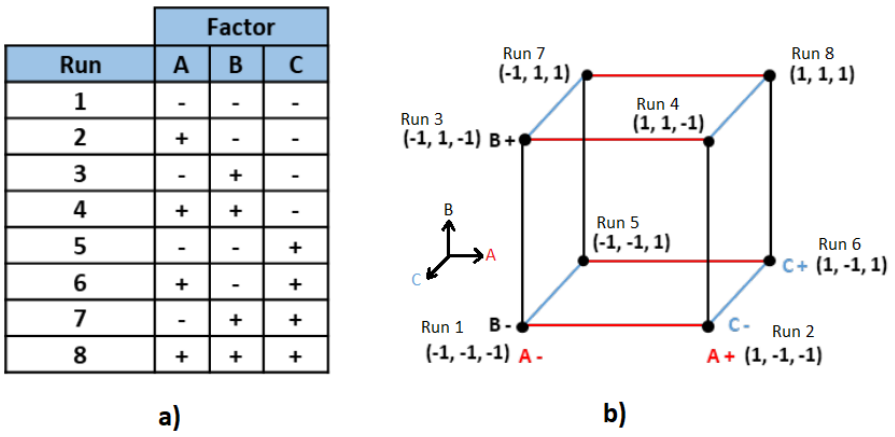

	Factor		
Run	A	B	C
1	-	-	-
2	+	-	-
3	-	+	-
4	+	+	-
5	-	-	+
6	+	-	+
7	-	+	+
8	+	+	+

Figure A.2: Example of experiment setup of a full factorial 2^3 screening design [64]

Figure A.2 presents a generic visual example for a three factor (2^3) full factorial design setup. In this example picture A shows a tabular representation how three unspecified factors (A, B and C) combine into eight experimental runs with varied factor level values (+ or - signs representing high and low level values of a 2 level factor design setup). Picture B illustrates same setup in a graphical coordinate format, where each factor is set on a separate axis and points are representing defined experimental runs. This explains the general principle of a how DoE approach establishes experimental runs. In the case of fractional factorial design or a Plackett-Burman design, only some of these points would be present in the analysis, present point assigned by a specific algorithm to provide enough information for establishing desired response statistical significance.

Principle of result evaluation

Evaluation of factors in a design of experiment screening design is based on evaluating whether each factor is statistically significant. This evaluation is based on determining whether the observed response result value exceeds the limit of value change that could possibly occur just by random chance [12]. A variable known as *p-value* is used to define the significance limit of screened factors. In order to measure whether the limit is exceeded, p-value for each factor is compared with chosen level of significance of specific experiment to assess the proposed null hypothesis. A basic null hypothesis for a screening design setup states that the evaluated response of experiment is equal to a hypothesized value [61]. P-value indicates that if there is a significant effect present from changing a value of a specific factor - determining whether the null hypothesis is true or false. If the observed difference in response value falls outside the limits of the chosen confidence interval - it is clear that the value change is not a result of random error (e.g. noise) and is in fact a result of change in factor value. As the distribution of performed test under null hypothesis H_0 is symmetric around zero, p-value p_{val} for a two-sided experimental significance of a screening test is calculated as follows [61].

$$p\text{-}value = 2P(T_s \geq |t_s| \quad | \quad H_0 \ is \ true) = 2(1 - f_{cd}(|t_s|)) \tag{A.1}$$

where P is the probability of the event; T_s is the test statistic, t_s is the observed value of the test statistic calculated from used experiment sample; and $f_{cd}()$ is the cumulative distribution function of the test statistic

T_s under the null hypothesis H_0. Each evaluated factor is assessed based on their acquired p-value in relation to the significance level α that is equal to 1 minus the chosen confidence interval I_c:

$$\alpha = 1 - I_c \tag{A.2}$$

Confidence level of all performed screening experiments in this report is set at 95%, which keeps value of significance level $\alpha = 0.05$ and compares p-value of each screened factor against significance threshold of $p\text{-}value = 0.05$. If $p\text{-}value \leq \alpha$ factor is statistically significant; if $p\text{-}value > \alpha$, then the screened factor is statistically insignificant and can be discarded.

Magnitude of significance level can be defined with the help of parameter called *t-value*. In general terms, this parameter is the calculated size difference relative to the variation of sample data [61]. It is represented in units of standard error. t-value value is calculated as follows:

$$t_{\hat{\beta}} = \frac{\hat{\beta} - \beta}{\frac{\sigma}{DoF}} \tag{A.3}$$

where $t_{\hat{\beta}}$ is the t-value, $\hat{\beta}$ is the mean of assessed factor response; β is the population mean; σ is the standard deviation of the error; and DoF is the degrees of freedom in the statistical model. Overall, larger t-value define higher significance of the factor it belongs to. The threshold of the t-value which has to be reached in order for the factor to be significant can be derived from significance level of the experiment. This value is generally used for graphical representations of factor significance as used in experiments, which are 1-4 described accordingly in sections A.0.2, A.0.3, A.0.4 and A.0.5.

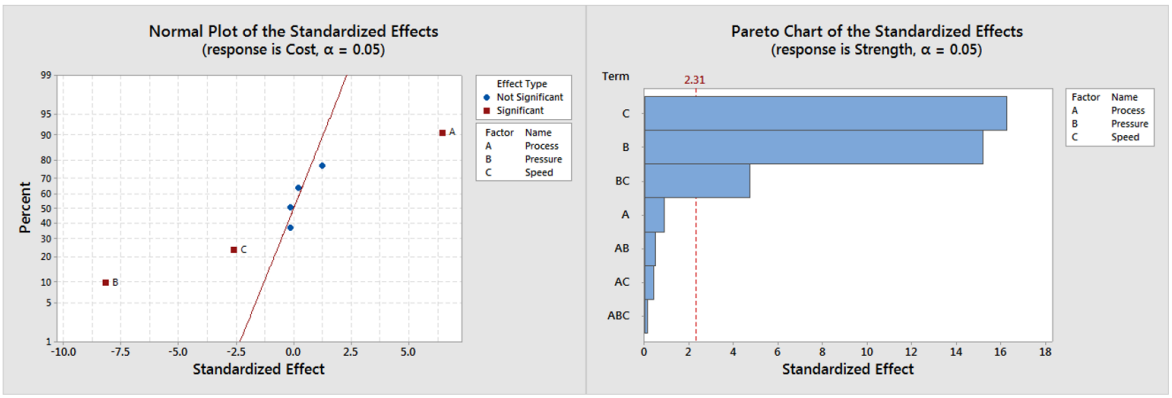

a) b)

Figure A.3: Generic example illustration of factor significance result evaluation formats: a) normal plot; and b) pareto chart [61].

Results of factor significance of each experiment are summarized with the help of two graph formats as presented with a generic example illustration in figure A.3 - a) normal plot or b) pareto chart. In order to understand the magnitude of significance, either graph can be used, however, each approach has its strengths and weaknesses and will be assigned to each experiment based on result type which has to be presented.

1. *Normal plots* can be used to determine the magnitude and direction of screened factor effects [61]. As shown in graph A of figure A.3, larger distance of a factor point (or factor combination) away from the red line expresses stronger factor significance, while the direction of each point shows whether positive change of assessed factor value (process, pressure, speed) increases or reduces response parameter value (cost). It is also best used when there is a large amount of screened factors and/or their combinations which all need visual reference for interpretation (as in the case of experiment 1).

2. *Pareto charts* (chart B of figure A.3) present only the absolute value of factor significance which contains data for significance magnitude but lack information on change of response direction. This format however expresses the threshold of significance with a reference line of t-value (dashed red line) that is the minimum amount of factor significance needed to make the result statistically significant. Any factor (or factor combination) bar above the red dashed vertical t-value threshold line is considered statistically significant.

Finally, as pareto chart does not contain information about response direction, factor effects graphs can compliment pareto charts well and provide information on how different factor values influence used response. Factor effect graphs are used to illustrate results for all experiments (1 to 4) and are shown along normal plots or pareto charts in figures A.6, A.5, A.8, A.10 and A.13. Detailed results of each assessed factor combination for all performed experiments can be found in tables A.8, A.9, A.10, A.11 of appendix A

A.0.2. Experiment 1: FE load effect on stress response

This experiment serves the purpose of evaluating each loading condition in terms of its effect on the stress response accumulated in the crane upper arm Finite element model. Additionally, by determining the dominant load in terms of its significance level - results of Experiment 1 provide a basis for the upcoming 3 experiments that are performed to establish which factors influence the response of the dominant load.

Motivation

Establishing a level of accuracy in a fatigue analysis that is performed with the help of Finite Element simulations requires accurate representation of stress response in the analysed structure. As the magnitude of stress/strain in any structural model is directly linked to the magnitude and direction of imposed external loads. For this reason effect and significance of loads acting on the crane upper arm should be investigated to understand which load/-s have largest effect on changing stress magnitude within the structure. Under this principle, statistically significant loads have to be correctly accounted for to acquire accurate stress and fatigue analysis results. In this screening setup all loads which realistically act on a generalized FEA model of the crane upper arm are evaluated in terms of their imposed stress response.

It is important to note that this screening analysis uses FEA model used for imposing flexibility in the MBD model described in section 3.2.6, rather than the detailed FEA upper arm setup for fatigue assessment which will be introduced in chapter 4. This means that in this screening experiment stress response acquired is not fully representative of stress acting in a real structure, but rather stress is used as a response for quantifying magnitude of change when load values are being changed. This means that a detailed stress response is not present in this experiment, however it provides enough data to determine load significance.

Screening setup

Table A.1 presents an overview of screening setup of discussed experiment. Here *Factors* column present the type of parameter used which is screened for its significance as well as (if applicable) its units ; *Marking* defines the letter used for illustrating each factor in result plots; *Tested Values* present high and low value setup of each screened factor; *Responses* indicate parameters used for evaluating factor significance, along with their units; *Screening Design Type* defines what kind of screening setup type is used for this experiment; *Fraction* indicates the fragment of full-factorial design that is accounted in the specific fractional factorial design setup (only applicable if a fractional factorial experiment design is used); *Resolution level* - describes the degree to which estimated main effects are aliased (or confounded) with estimated 2-level interactions [69]. ; and *Number of runs* show how many experimental runs had to be performed to acquire data for the aforementioned experiment to determine factor significance.

Setup of finite element (FE) stress evaluation screening experiment considers all major loads that will be applied during fatigue analysis - this allows for estimation of every possible source of stress present in upper arm structure during operation, leading to objectively reliable data of factor significance. These loads are defined as screened factors and can be summarized for the purposes of this experiment to:

1. *Hoisting load* - weight load present at the front and back locations of the upper arm, where cable pulleys are located.

2. *Operator cabin structure mass load* - mass due to presence of operator bridge, cabin and its suspension system, located at the connection point in the front part of the upper arm structure.

3. *Luffing acceleration* - translational acceleration along the length of the upper arm, which simulates crane forward/backward extension motion.

4. *Slewing acceleration* - radial acceleration around the upwards axis of the upper arm which simulates crane rotation.

5. *Roll acceleration* - radial acceleration of the upper arm around its width axis. It simulates pontoon roll motion.

Table A.1: Setup overview of screening experiment 1 (load effect on stress response)

Marking	Factors	Tested Values	
		Low	**High**
A	Hoisting load, N	25000	250000
B	Operator cabin structure load, N	9800	98000
C	Luffing acceleration, m/sec^2	0.14	1.40
D	Slewing acceleration, m/sec^2	-0.436	-0.044
E	Roll acceleration, m/sec^2	-0.03491	-0.00349
F	Pitch acceleration, m/sec^2	-0.03491	-0.00349
G	Heave acceleration, m/sec^2	0.012	0.120
H	Upper arm extension position	Retracted	Extended
Responses:	Maximum nodal stress, Pa Average nodal stress, Pa		
Screening design type:		Fractional factorial	
Fraction:		0.5	
Resolution level:		VIII	
Number of runs:		128	

6. *Pitch acceleration* - radial acceleration of the upper arm around its length axis. It simulates pontoon pitch motion.

7. *Heave acceleration* - translation acceleration of the upper arm along the upwards/downwards direction (height) of the upper arm structure of the crane. It simulates pontoon heave motion.

8. *Upper arm extension position* - determines whether crane upper arm is extended or retracted when a specific load is applied. It is a critical factor specifically for radial motion as depending on the center of rotation, the amount of angular momentum experienced by the structure changes. This is implemented in the FEA model by adjusting the location of coordinate system that is used for applying rotation position.

As it is customary for screening experiments - a two level analysis approach is used, where each screened factor set contains two different values - low level value and high level value. Such setup establishes only a linear relation between screened factors and used responses, but this is generally a sufficient amount of data for establishing factor statistical significance. Values chosen for each of the two factor levels are chosen in the following manner:

1. *High level* of the factor is based on the maximum value that is possible to acquire using normal crane operation. Limits for these values are based on measurements gathered from available data (example: pitch, roll, heave accelerations, crane extension length, operator cabin structure mass), as well as the crane rating data (example: maximum hoisted load, slewing and luffing acceleration).

2. *Low level* is based on the 10% value of the high level chosen for analysis. Zero values for the low level is also an option, however that makes all factors into conditional factors which are based on the ON/OFF principle, that provides a subjectively less reliable response between the combined effect of screened values. Chosen approach with low factor level kept at 10% always keeps a certain presence of each non-conditional load factor in the model. This way it ensures consistency in the definition of chosen values and that is important for estimating factor significance.

When it comes to responses according to which each factor is evaluated - a relevant quantifiable parameter should be used [35]. For the purpose of this experiment either stress or strain could be used. However, as this research deals with mainly elastic deformation of crane upper arm structure which is constructed using ductile structural steel S235 - only one of these parameters is sufficient. This is due to the fact that stress-strain relationship of S235 structural steel is constant in the region of elastic deformation [46]. Thus only stress is used for analysis - specifically two quantifiable aspects of stress response have been chosen to evaluate the effects of loads imposed on the crane structure:

1. *Maximum nodal stress* - defines critical value of stress in the model, indicating maximum averaged single node stress present in the detail crane upper arm structure without specifying its location.

2. *Average nodal stress* - defines nodal stress in the crane upper arm structure averaged over the entirety of nodes present in the model. It is worth noting that the average stress value depends on the size and the amount of nodes that are acquired through model meshing, so the response value is relevant only for the specific mesh and cannot be used for direct comparisons of different models. However, for the purposes of screening response of a constant mesh model, it is presumed to provide an accurate relation to stress change.

For evaluating the aforementioned stress responses, Von Misses Stress is used. Although it does not capture stress direction or sign, it has the benefit of acquiring 3-dimensional nodal stress in the form of its overall magnitude. This gives a good general overview on the significance of load factors towards imposing stress accumulation in the structure. This is a sufficient amount of data for this specific type of screening analysis.

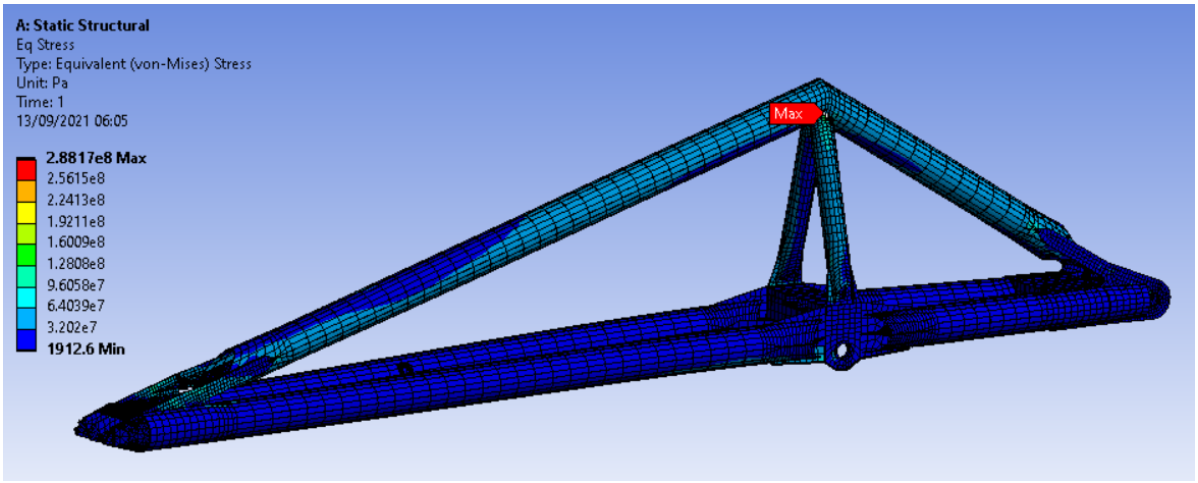

Figure A.4: Graphical illustration of Von Misses Stress distribution over the detailed upper arm structure when it is under maximum hoisting load. Red marker indicates location of maximum nodal stress in the model

Figure A.4 illustrates an example Von Misses Stress response result on the crane upper arm that is under a maximum screened hoisting load applied to the model. The red marker indicates location of the node that is under maximum stress imposed in the model, which is used for acquiring maximum nodal stress response. Average nodal stress is derived from the average stress value over the sum of all nodes present in the illustrated structure.

For the purpose of establishing significance of relevant factors, a 2^k fractional factorial design setup is used. This is a variant of a full factorial design, which follows a pattern that captures every possible combination of factor and level in the design matrix [64]. Here k defines the number of factors that are being screened, while the base number *2* establishes the number of value levels for each factor that is screened. This combination establishes the amount of runs which have to be made to acquire a full factorial design setup for an experiment. Fractional factorial design uses a specific fraction of runs from a full factorial design depending on the required screening resolution - general rule suggests that a higher resolution of performed experiment (the closer to a full factorial design setup) equals a higher reliability of results, especially for factor interaction screening. As the term *interaction screening* suggests, fractional factorial design estimates not only first order factor effects (how each factor separately influences its responses), but also the significance of possible factor combinations (how factor combined effect might influence responses in a way that is not predictable by first order estimations of separate responses), which can provide additional insight into load factor relations towards assessed stress responses. The number of possible interactions with a 2^k factorial design can be derived through the following relation:

$$\begin{bmatrix} k \\ n \end{bmatrix} = \frac{k!}{n!(k-n)!}, n \leq k \tag{A.4}$$

where k is the number of factors and n is the number of interactions to be found. Due to the ability of running simulations in batch mode, a large amount of simulation variants can be assessed in a computationally efficient manner. For this purpose a 2^8 fractional factorial screening design approach has been performed, which includes 128 simulation runs (full factorial design would include 256 runs for this experiment). Generally in DoE screening analysis experiments which are performed in real life also contain replicates to ensure

consistency of acquired data. However, since all experimental runs for screening analyses performed for this research concerns simulation screening - no experiment replicates are used, as additional replicates would not have any effect on acquired results. This maintains the total number of experimental runs for this experiment at 128.

Screening results

Screening results of this experiment is summarized with the help of normal plots, showing factor significance and direction of response change (whether increase of factor level increase or decrease response value). This plot is additionally supplemented with a factor effect plot which present how change of independent factor level affects specific response value. The format with a normal plot is used (instead of a pareto chart) due to a large number of factors and their interactions which were tested, that would not be clearly represented with a pareto chart. These results of load effect on stress response in the FEA model are illustrated in figures A.6 and A.5 (for Maximum nodal stress and Average nodal stress responses respectively). Results in the normal plots which include a combination of two letters per point (e.g. AB or DF, etc.) shows that a combination of two factor interaction have significant effect on the response that is independent from the effect that these two factors impose when not combined. For additional reference on how to interpret normal plots, please refer to *Principle of result evaluation* subsection of section A.0.1.

Figure A.5 illustrates the statistical significance results of tested factors and their linear combinations in relation to imposed average nodal stress in the crane upper arm FE model (upper graph) as well as the mean effects of how each factor level value change affects response (lower graph, with 2 levels per factor). Normal plot in the figure A.5 indicates statistical significance of tested factors, marked accordingly with the following letters: A) Hoisting Load; B) Operator cabin structure weight load; C) Luffing acceleration; D) Slewing acceleration; E) Pontoon roll acceleration; F) Pontoon pitch acceleration; G) Pontoon heave acceleration; and H) Crane upper arm extension position. Results show that the presence of hoisting load has by far the most significance (T-value = 3224) towards imposing average nodal stress to FE model of the crane upper arm. It can be considered as a dominant factor along with operator cabin structure load coming in second (T-value = 748, with more than 4 times less significance than the dominant load). This is an interesting observation which shows that most stress comes not from actual motion of the crane but rather from the presence or lack thereof of hoisted material. It is also visible that most inertial loads also have a statistically significant influence the average stress response with varying levels and directions of magnitude, however they are notably smaller than effects of the hoisting load (with effect of heave acceleration being the smallest - at). This means that there is likely a presence of directional stress in the model which has to be accounted for accordingly. Additionally, as the full factorial screening design setup has been run for this analysis, higher order factor relations have been evaluated as well. The normal plot presents combinations of two factors which impose statistically significant average nodal stress in the model. Significant factors and their combinations are presented in table A.8 with a more detailed variant of result overview present in table A.8 located in appendix A. It shows that a combined effect of several factors can also additionally affect average stress response in a manner which is not directly linked solely to the presence of a single first order term of a specific factor - an additional relation is present.

The lower graph of figure A.5 shows how each analysed factor and their tested level value influences the change the mean value of average nodal stress in the model. It helps to better understand the magnitude of change as well as change of direction between each factor level. Since the screening design which has been run contains only two levels for each factor, response value is interpreted as a linear relation. This graph further indicates that hoisting and operator cabin structure weight loads are the most dominant towards change of average nodal stress in the crane model (increase in stress value of 1.5E+09 Pa and 5.0E+08 Pa accordingly). Other load factors, although significant as seen from the graph, impact the value change of average stress significantly lower.

In terms of the maximum nodal stress (presented in figure A.6), screening results are comparable - with hoisting load being the dominant load (t-value = 469), being 3 times larger than second largest load factor (cabin structure load with t-value = 147), and other independent load factors (inertial loads) although statistically significant, but of comparatively low effect towards final maximum stress result. Additionally, as previously mentioned - although the screening response does not indicate the location of the node with the maximum stress, it is worth noting that the observations have shown that maximum stress is generally experienced at the approximately same node location as shown in the figure A.4. This is the multi-joint connection location, at which fatigue cracks have initiated in the Cornelis Tromp 25T crane, as well as is the point of failure of the same type of crane in the past that was discussed in the introductory chapter of this thesis. Thus it

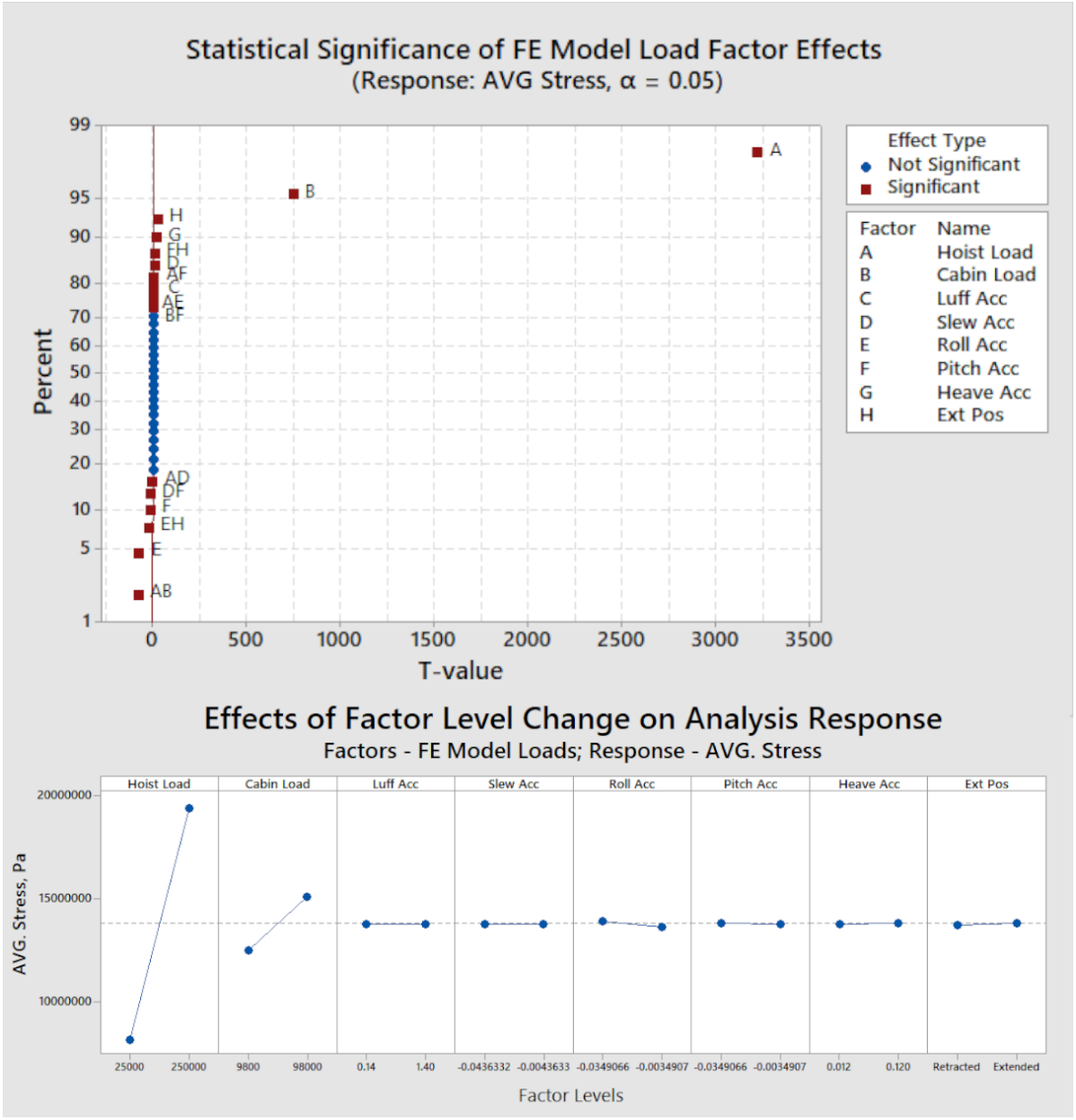

Figure A.5: Statistical significance of average nodal stress imposed on a detailed crane upper arm structure in relation to different load factor effects and their first order combinations. Analysed factors include: Hoisting Load, Cabin mass, Directional Accelerations due to crane luffing, slewing, roll, pitch and heave motions, as well as crane extension position

can already be observed that there is likely a direct correlation between the location of fatigue crack initiation and stress accumulation position in the crane upper arm structure.

Overview

Table A.2 lists factors as defined by this screening experiment based on their statistical significance. It marks most dominant loads on a green-white scale with green signifying large magnitude of significance. Based on the FE load screening analysis, it is clear that with both responses (average and maximum nodal stress), presence and effects of the hoisting load is most critical by a large margin over other loads (3-4 times larger than significance of cabin structure load and over 20-650 times larger than inertial load or extension position effects). This observation concludes that hoisting load is the dominant load towards imposing stress in the upper arm structure of the crane and thus has to be modelled with high level of accuracy. Additionally, extension position becomes relevant to both maximum and average stress when combined with roll and pitch accelerations due to increase of rotational distance travelled that appears as the motion radius increases with

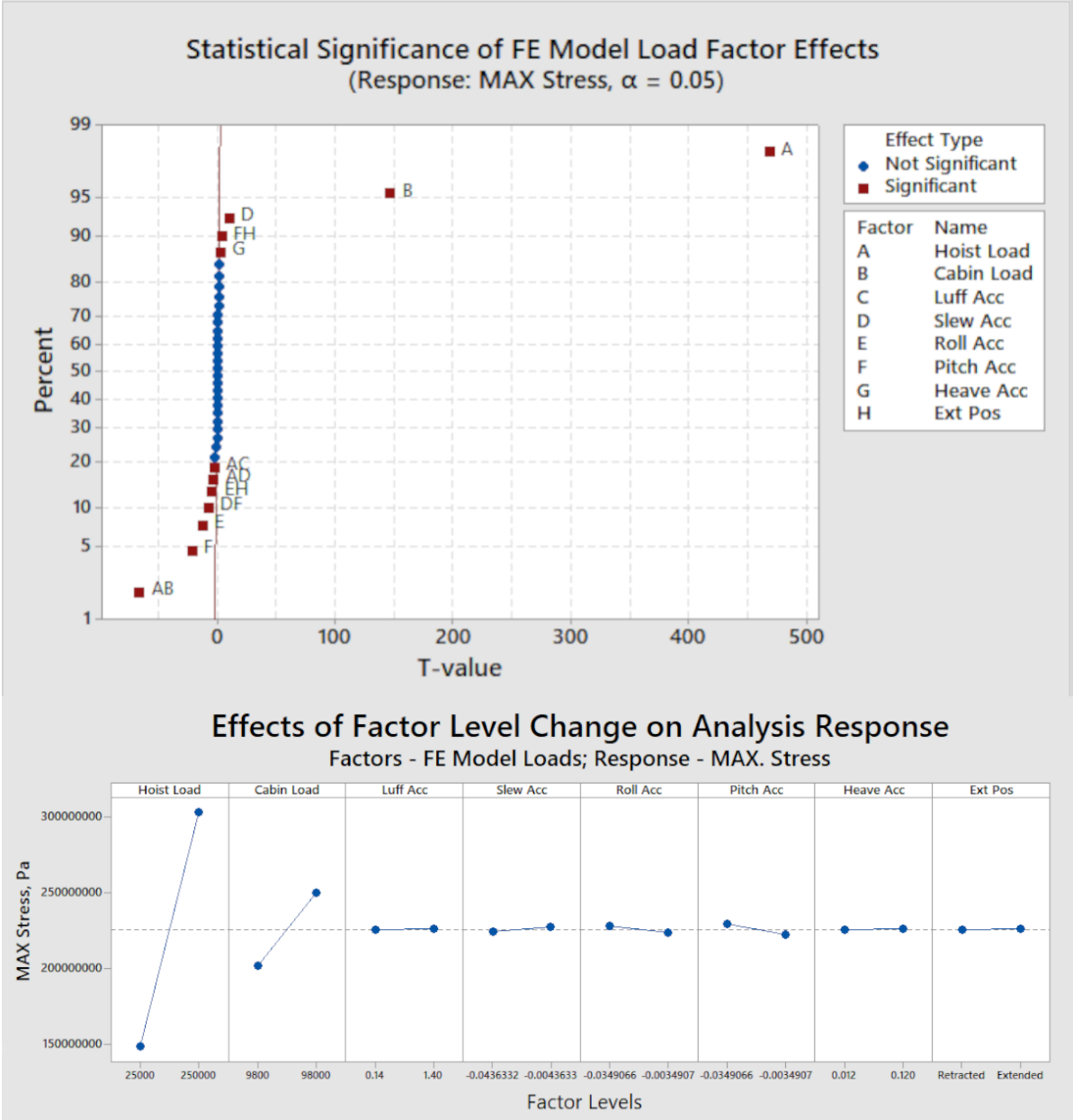

Figure A.6: Statistical significance of the maximum nodal stress imposed on a detailed crane upper arm structure in relation to different load factor effects and their first order combinations. Analysed factors include: Hoisting Load, operator cabin structure mass, Directional Accelerations due to crane luffing, slewing, roll, pitch and heave motions, as well as crane extension position

further crane extension. Overall, these results show that for result accuracy it is critical to accurately model hoisting and operator cabin structure loads as well as the radial accelerations in all three possible directions of motion.

Furthermore, hoisting load magnitude that is exerted onto the crane structure is assumed to be prone to fluctuation and change, which might be influenced by such aspects as the part deformation during inertial motion as well as the inertial load effects acting on the load during crane motion. These factors could impose cable swing and jerk-related effects which change load magnitude at specific moments in time. For this purpose additional screening experiments have to be performed which consider hoisting load as a response in order to determine which specific aspects have influence on its magnitude. These experiments will be discussed in the upcoming sections A.0.3, A.0.4 and A.0.5.

Table A.2: Overview of statistically significant factors for each response. Colour scale shows factors from most to least significance (most dominant factor coloured in green)

Magnitude of Significance							
Significance limit: P-value <0.05							
MAX Stress				AVG Stress			
Mark	**Factor**	**T-value**	**P-value**	**Mark**	**Factor**	**T-value**	**P-value**
A	Hoist Load	3224.34	0	A	Hoist Load	468.7	0
B	Cabin Load	747.9	0	B	Cabin Load	146.9	0
AB	Hoist L.*Cabin L.	77.69	0	AB	Hoist L.*Cabin L.	65.96	0
E	Roll Acc	73.68	0	F	Pitch Acc	21.36	0
H	Extension Pos	27.97	0	E	Roll Acc	12.9	0
F	Pitch Acc	15.57	0	D	Slew Acc	10.31	0
G	Heave Acc	15.06	0	AD	Hoist Load*Slew Acc	3.22	0.002
D	Slew Acc	6.62	0	AC	Hoist Load*Luff Acc	2.84	0.006
AF	Hoist Load*Pitch Acc	5.7	0	G	Heave Acc	2.6	0.011
C	Luff Acc	5.05	0				
AE	Hoist Load*Roll Acc	3.2	0.002				
AD	Hoist Load*Slew Acc	2.38	0.019				
BF	Cabin Load*Pitch Acc	2.22	0.029				

A.0.3. Experiment 2: Flexibility effect on hoisting load response

This part provides the description of screening experiment in which slender multi-body dynamic model components that incorporate flexibility in their inertia modelling setup are screened in terms of their significance towards changing the result of hoisting load (which is the dominant load for inducing stress response in the crane, as determined in experiment 1)

Motivation

This screening experiment deals with the effects of part flexibility on the hoisting load. Although the general approach of multi-body dynamic simulations deal with rigid component setups, this can potentially lead to results that do not provide a sufficient amount of accuracy. Tawjoeram [86] has suggested in the overview of the MBD setup of a lemniscate crane, that including flexible inertia modelling into part setup can potentially improve result accuracy. Additionally, visual observations of actual operation of the analysed Cornelis Tromp 25T crane has shown that during hoisting operation of the load lead to a visible elastic bending of the forestay and front jib beams of the upper arm. This presents an assumption that in order to acquire a realistic loading conditions of the upper arm through MBD analysis, flexibility should be incorporated into the crane structure for testing purposes. In some cases this can be done to yield more realistic loading results as it has been shown in [63] which used flexible parts in a magnetic gear systems to acquire loads for fatigue analysis. Similarly Wu et al. [91] uses flexible parts in a MBD simulation to acquire more precise loads for fatigue estimation of train gearbox housing and provides a comparison between rigid and flexible model results. The author concludes that flexibility in bodies experiencing high inertial loads is critical for result accuracy. Since addition of flexible components is yet to be tested in the analysed lemniscate crane structure, screening experiment in this section defines the process of flexibility implementation into the crane model.

Screening setup

As incorporation of complex flexible components into an MBD model is an effort-intensive task which additionally has an effect on computation time of the simulations - for efficient model establishment purposes it is preferable to limit the amount of flexible parts that are incorporated into the model to only those which require most serious attention. For the purpose of analysing crane structure, flexibility incurred elastic deformation is expected to have an effect on loading results. Thus, crane parts most prone to deformation are assessed in this screening setup with added flexibility. Generally the largest elastic deformation occurs in slender components due to apparent compression stress or exposition to other types of directional loading. Overall, slender columns resist lower axial loads than short columns having the same cross-section [75]. According to definition, slender components are defined as structures in which the cross-sectional dimensions are much smaller than their axial length [81]. As the analysed crane structure is predominantly made out of circular beam components, a level of slenderness λ for a circular component can determined through a ratio

relation between beam length L and outer beam thickness D:

$$\lambda = \frac{L}{D} \tag{A.5}$$

A component with $\lambda \geq 10$ can be considered as significantly slender and depending on its material properties, fixture setup, applied force magnitude and force direction it can potentially experience bending effects that could deform a structure in a way where load distribution and direction might differ from that of a perfectly rigid component.

Table A.3 presents an overview of a screening design setup of this experiment. For the explanation of presented data in the table, please refer to *Screening Setup* subsection of section A.0.2.

Table A.3: Setup overview of screening experiment 2 (Inertial loading effect on hoisting load response)

Marking	**Factors**	**Tested Values**	
		Low	**High**
A	Upper arm flexibility	Rigid	Flexible
B	Front arm flexibility	Rigid	Flexible
C	Rear arm flexibility	Rigid	Flexible
Responses:	Total Hoisting Force, N Maximum Hoisting Force, N Standard deviation of Hoisting Force, N		
Screening design type:		Full Factorial	
Number of runs:		8	

In accordance to the aforementioned description of slender components, - the following crane parts can be considered to be most susceptible to directional bending and thuse are considered as screening factors:

1. Upper arm (λ_{max} = 19.9) - This is a part that is analysed in terms of its fatigue damage resistance. It contains the point for analysis - the hoisting load at the front of the upper arm, where the cable connects load and the crane. It is predominantly made out of slender welded circular beams.

2. Front arm (λ_{max} = 18.8) - part connecting machine floor and the upper arm. It also supports one side of the operator cabin structure and significantly moves forward during luffing operation. It contains two slender circular beam members along its vertical length.

3. Rear arm (λ_{max} = 12.0) - part which connects the back of the upper arm with the tower and the hydraulic cylinders. It also contains counterweights on the other side of the structure, away from the upper arm. These counterweights reduce the fluctuation of center of mass when the crane extends forward or backwards. It is made out of slender H-beams along its vertical length.

Figure A.7 illustrates the outlines each of the aforementioned flexible parts. All three parts are made out of slender geometric components which also experience the largest motions. This is what makes upper arm, front arm and rear arm as viable candidates for affecting the loading response of dominant - hoisting load. Thus the flexibility of these three parts is the conditional factors used for experimental screening, which determine separated and combined significance of flexibility on the relevant response.

Since hoisting load has the most statistical significance towards stress accumulation in the upper arm structure as described in section A.0.2, it is important to determine how part flexibility affects this specific load response. For the purpose of fatigue analysis, the maximum load response is assumed to be the most critical as the magnitude of hoisting load generally translates to largest average and peak stress responses. To determine how hoisting load is affected by part flexibility when working in a time domain - a single response is not enough. It is important to capture force peaks, its average value, as well as the fluctuation of data that might not be visible only from the mean value. For this purpose three following responses linked to the hoisting load are evaluated:

1. *Total hoisting force* - this is the sum of hoisting force magnitude values at each time step (0.2 seconds). This provides a baseline for the overall force experienced by the body (in a comparative manner to average force).

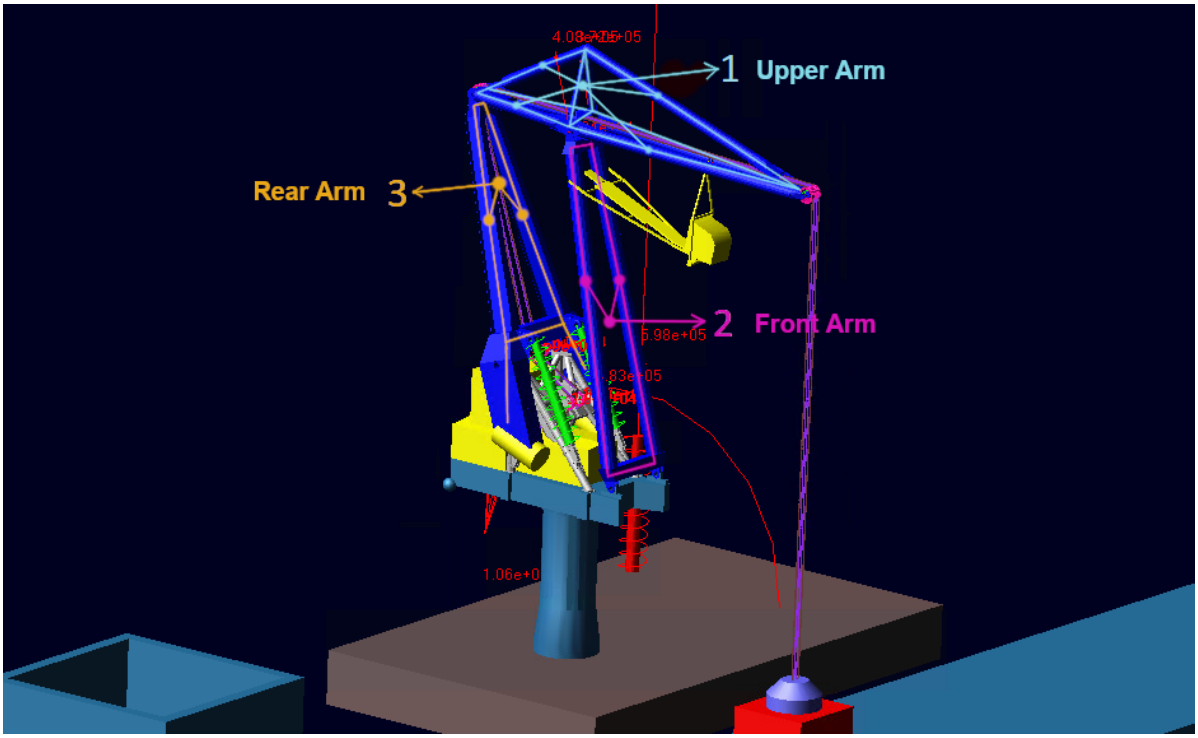

Figure A.7: Multi-body dynamic model of the crane with implemented flexibility into following components: 1. Upper arm (cyan outline); 2. Front Arm (purple outline) 3. Rear Arm (orange outline);

2. *Maximum hoisting force* - peak value of the force over the loading cycle, representing a specific time step when hoisting force has reached its maximum value.

3. *Standard deviation of force* - this the fluctuation of hoisting force meant to show whether there is a difference in how much hoisting force fluctuates over time compared to its mean value.

All responses are acquired by exporting time-dependent hoisting force information from MBD analysis and extracting relevant responses accordingly to determine changes in each experimental case.

Experimental setup for this analysis uses a 2^k full factorial design, with a total number of $2^3 = 8$ simulation runs needed to analyse aforementioned hoisting load responses. This is a full simulation setup which can be directly compared to the illustration of a 2^3 full factorial design presented in A.2, where each point of the setup is performed to gather the maximum amount of available data with a 2-level setup. A full factorial design is run due to the low amount of factors present in the experiment, which allows to acquire most reliable data with a relatively small amount of experimental runs.

Screening results

For the purpose of analysing the results of flexibility effects, a pareto chart is used (figure A.8, left side). Pareto chart shows the absolute T-value gain of screened factors from the largest effect to the smallest effect [61]. Each pareto chart presents analysed factors and factor combined responses in a horizontal bar graph format, where significance threshold is illustrated with a vertical red dotted line - any factor, which value exceeds the threshold can be considered as significant towards affecting a specific load response. Unlike normal plots used in section A.0.2, pareto charts do not provide information about the load direction as it shows only the absolute value of result significance. For this purpose, each response is accompained by the Factor effects plot as in result illustration (on the right) A.6 in section A.0.2 which presents the change in factor effects on gathered response. Same principle for result illustration is used in further screening experiments of sections A.0.4 and A.0.5. For a more detailed explanation on how to interpret pareto charts, please refer to *Principle of result evaluation* subsection in section A.0.1.

Figure A.8 illustrates the screening results of all three responses in a format which uses a combination of a pareto charts which show the magnitude of factor significance and factor effect plots that show how values of each independent factor change value of a specific response.

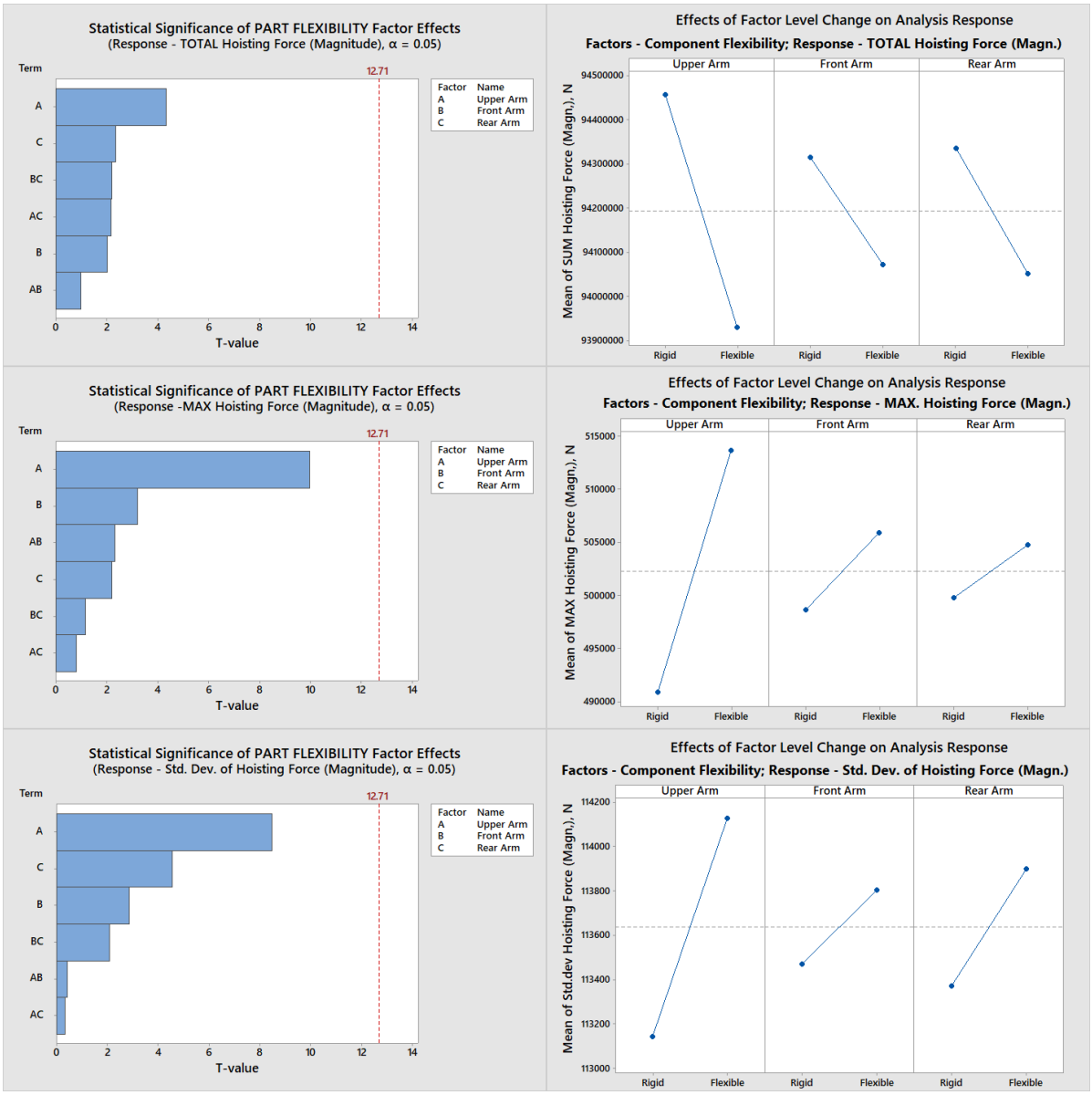

Figure A.8: Statistical significance of flexibility effects of front, rear and upper arm. A comparison between rigid and flexible part combinations in terms of total, maximum and standard deviation values of hoisting force magnitude

Based on the significance factor results at a 95% confidence level ($\alpha = 0.05$), part flexibility does not have any significant effect towards the total or maximum hoisting force, nor its relative variation level. This means that the flexibility of these specific parts do not create large enough change in load magnitude and load fluctuations to be worth of implementation. Additionally, higher level combined factor responses (AB, BC, AC) do not appear to have any effect on the changing response result. This is an interesting observation, which shows that the hypothesis made in Tawjoeram [86] - which speculated that inclusion of flexibility in crane components would increase the accuracy of results - is not true in the sense that increased accuracy does not provide a statistically significant change to argue inclusion of flexibility in MBD model for this analysis. However, for analysis of other parameters or components in the MBD model that fall outside of the scope for this research, the presence of flexibility might still me a valuable addition, but it falls outside of the research scope of this report.

Overview

Taking into account screening results along with the observations made about the significant increase of computation time with addition of extra flexible parts, further analysis and load acquisition steps will not

include added flexibility. This conclusion is based on the observation that presence of flexibility in the multi-body dynamic model setup of the lemniscate crane slender parts does not lead to significant change in any response of the dominant load (i.e. Hoisting load), at the confidence level of 95%. There are no significant factors present in this experiment - variations in maximum, total and standard deviation of the hoisting load are minimal or can be accrued to random error.

A.0.4. Experiment 3: Inertial loading effect on hoisting load response

This part provides description and results of a screening experiment in which the significance of inertial load effects on the hoisting load magnitude response are quantified. It allows to determine which specific inertial loads have to be accurately modelled in the MBD environment in order to acquire accurate hoisting load response.

Motivation

Establishing a realistic movement setup is an important step of load acquisition. As inertial loads are present in the load setup for upper arm structure of the crane, they have to be properly accounted for based on their significance towards affecting the relevant responses. Screening results of experiment 1 described in section A.0.2 has shown that, although hardly comparable to the effects of hoisting load, the inertial loads linked to crane and pontoon motion have effects on resulting stress response in the structure, which pass the threshold of statistical significance. Additionally, as hoisted mass of material is exposed to dynamic motion due to presence of inertial loads, an assumption appears which states that presence of inertial loads in the model might affect the magnitude and direction of hoisting load over its cycle of operation. This could change the loading profile, thus changing stress response experienced by the upper arm structure. This observation concludes that an accurate inertial load setup profile could potentially provide a more realistic loading setup and this effect of specific inertial loads has to be investigated.

The duration of crane each motion has been clarified - start and end times for each operation have been established in section 3.2.7, which defines a fixed time slot in which each operation has to be performed to reach the required displacement value from the initial position of the crane. It constrains possible acceleration values to a specific region that allows operation to fit inside the pre-established time window. However, this still leaves two possible ways to implement velocity into these constraints, based on:

1. *Increasing jerk magnitude (first order derivative of acceleration)*- this allows vehicles to reach desired acceleration and velocity faster and in turn requires lower maximum acceleration for equal amount of displacement. However this imposes sharper change in response values that could potentially create load spikes when the body is in acceleration/braking phase; or

2. *Increasing magnitude of maximum acceleration* - which tends to accelerate the body slower (reduces jerk), but requires higher overall acceleration value to reach the same amount of displacement during the pre-specified time window. This increase in acceleration magnitude is assumed to potentially reduce load spikes during acceleration/braking but at the same time should potentially increase velocity magnitude.

The two aforementioned approaches are illustrated in figure A.9, where luffing motion velocity measurements with two different acceleration setups are compared. Both result values are able to acquire equal displacement values in the same time window, which leaves the uncertainty open on how it is done in the actual operation and whether or not this difference in acceleration setup results in statistically significant change of dominant load (hoisting load). Thus acceleration effect screening has to be performed to determine if a more in-depth establishment of acceleration profiles has to be performed.

Screening setup

Screening setup is organized in a manner which attempts to reflect significance of crane motions and the presence of the uncontrolled pontoon motion. This is performed by using the established crane operation setup times from section 3.2.7, with changing magnitudes of main inertial accelerations, as well as pontoon motion - either by allowing pontoon motion or keeping the pontoon fixed in a static position. Data is collected throughout the total length of work cycle. Table A.4 presents an overview of a screening design setup of this experiment. For the explanation of presented data in the table, please refer to *Screening Setup* subsection of section A.0.2.

In accordance to the aforementioned setup, for the purpose of this acceleration effect screening - following screening factors are defined:

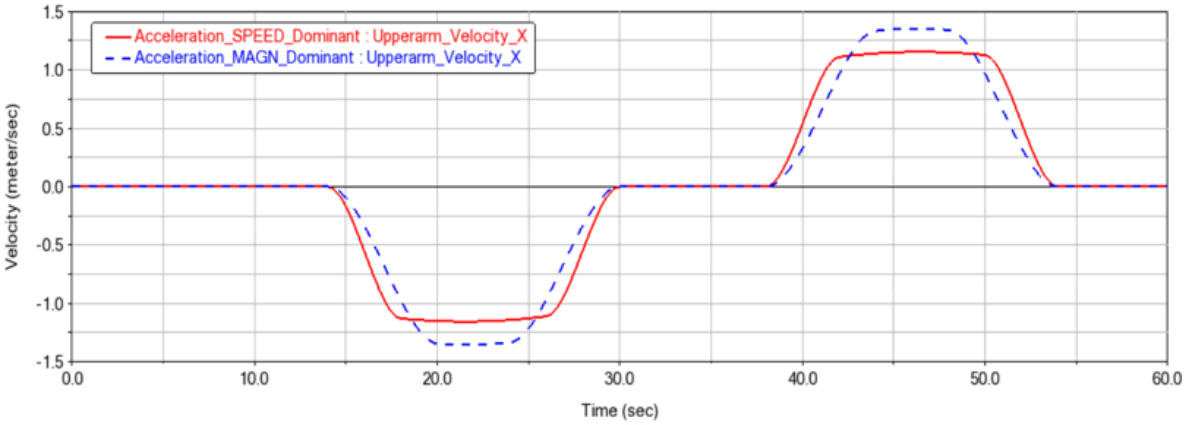

Figure A.9: Comparison of luffing velocity profiles over time between motion with dominant speed of acceleration (red) and dominant magnitude of acceleration (blue)

Table A.4: Setup overview of screening experiment 2 (Inertial loading effect on hoisting load response)

Marking	**Factors**	**Tested Values**	
		Low	**High**
A	Hoisting Acceleration, m/sec^2	1.12	1.40
B	Luffing Acceleration, m/sec^2	1.12	1.40
C	Slewing Acceleration, deg/sec^2	0.35	0.44
D	Pontoon Motion	OFF	ON
Responses:	Total Hoisting Force, N Maximum Hoisting Force, N Standard deviation of Hoisting Force, N		
Screening design type:		Full Factorial	
Number of runs:		16	

1. *Hoisting acceleration* - defines the pace at which load is lifted up/down by the cable system. It is assumed that the higher acceleration magnitude might have a significant effect towards reducing peak load imposed on the crane.

2. *Luffing acceleration* - dictates translation-based extension/retraction speed of the crane upper arm.

3. *Slewing acceleration* - determines how quickly crane accelerates in a radial direction around its center of rotation, which creates turning motion.

4. *Presence of pontoon motion* - this is a conditional factor which determines whether during motion the crane pontoon is in a fixed or active position. It allows to define whether pontoon motion has significant effect towards the change crane loading profile in relation to the aforementioned operational motion effects.

Each factor has its limited length of motion operation, which means that there is a possibility to acquire the same amount of motion by varying acceleration magnitude in these bounds as shown in figure A.9. Maximum and minimum values for each component are meant to achieve equal amount of displacement and fit into the available time bounds for each operation. These lower level values differ from high level values by 20%, making change magnitude comparable between all factors. This setup means - for a high level value magnitude of acceleration is increased, but magnitude of jerk (1st order derivative of acceleration) is decreased.

Responses for evaluating the effects of each inertial load is the chosen to be the magnitude of the hoisting load, as this is a factor which has most significance towards imposing stress in the analysed upper arm structure. This response is evaluated in the same manner as in section A.0.3, where it is separated into 3 related responses:

1. *Total hoisting force* - this is the sum of hoisting force magnitude values at each time step (0.2 seconds). This provides a baseline for the overall force experienced by the body (in a comparative manner to average force).

2. *Maximum force* - peak value of the force over the loading cycle, representing a specific time step when hoisting force has reached its maximum value.

3. *Variation of force* - this is the standard deviation (std. dev.) value of hoisting force sampled at each time step (0.2 seconds) over the duration of a single crane motion cycle. It is meant to capture a comparative level of how much the force value fluctuates from its mean.

Comparably to experiment 2, described in section A.0.3, experimental setup for this analysis of inertial acceleration effects uses a 2^k full factorial design, with a total number of $2^4 = 16$ simulation runs needed to analyse aforementioned hoisting load responses. This gathers significance of effects with all possible interactions up to the 3rd order (e.g. with three factors A,B,C - combined interactions considered would be A, B, C, AB, BC, AC and ABC).

Screening results

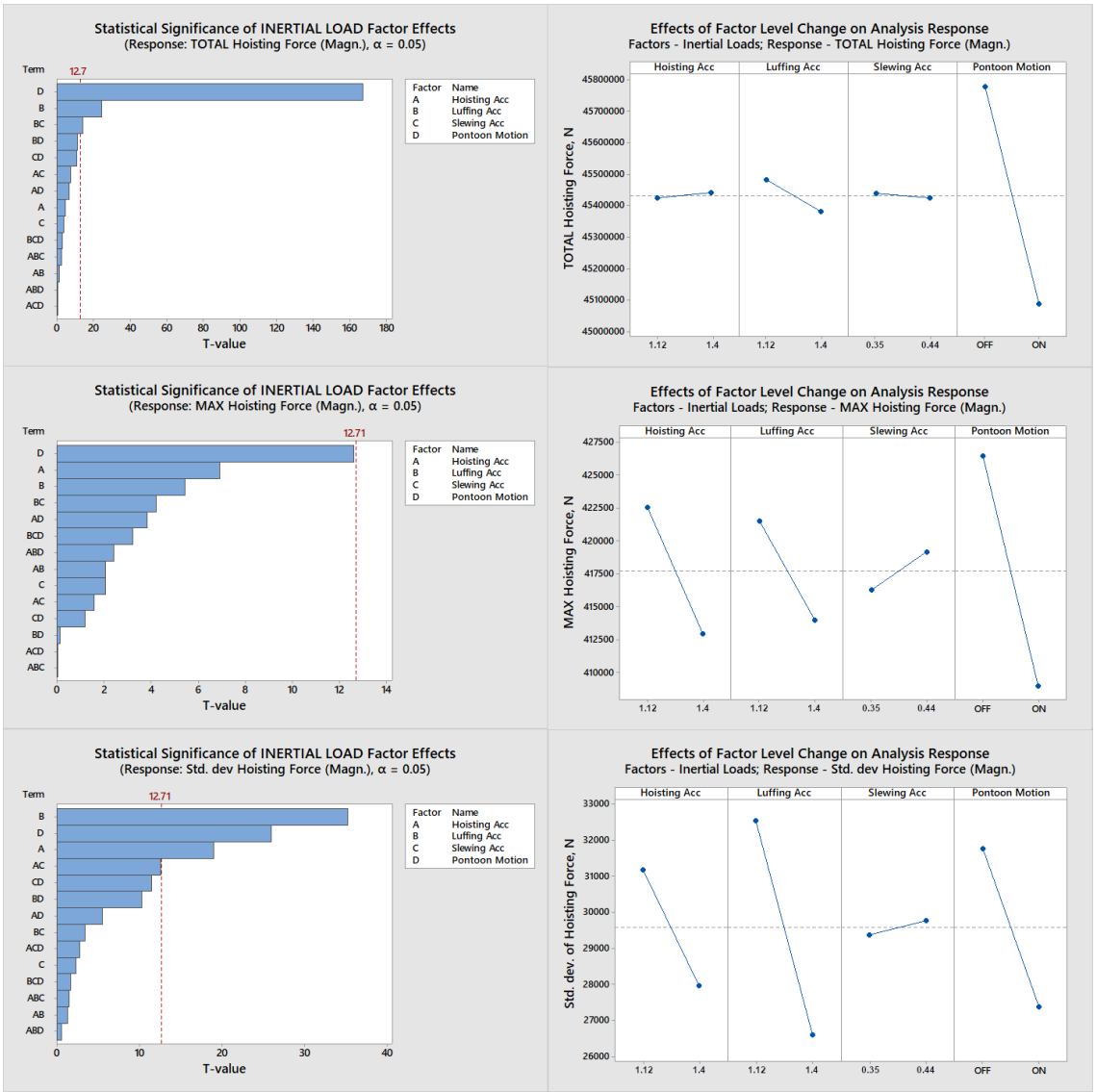

Figure A.10: Statistical significance of inertial loading imposed by different motions. A comparison between different inertial loading combinations in terms of total, maximum and standard deviation values of hoisting force magnitude

Figure A.10 illustrates screening experiment results for the inertial load effects in a pareto chart format (left side of figure A.10) complimented with factor effect plots (right side of figure A.10) of each analysed response. For the methodology on how to interpret the result chart, please refer to section A.0.1. Significant factor t-values and p-values are summarized in table A.5, with an in-depth overview of screening results summarized in appendix A.

Results show that pontoon motion effects significantly affect multiple hoisting force loading responses (Total hoisting force and standard deviation of hoisting force). It is the dominant factor for changing both response of total hoisting force (t-value = 167, threshold being equal to 12.71), reducing maximum hoisting force value by 3% (when pontoon motion is active) and also is an important factor for the standard deviation value of hoisting force (t-value = 26) reducing fluctuation of the response value throughout the cycle by 15% when compared with a rigid model. This effect is assumed to be a result of pontoon acting as a spring-damper system which dampens load spike effects during initiation phase of each acceleration induced motion thus leading to lower maximum, total and standard deviation of the load. However, since three separate degrees of freedom are active in the pontoon motion setup, it is worth to investigate which specific motions are affecting the hoisting load in a significant manner and determine which motions have to be calibrated to accurately mimic real motion of the crane. This will be performed in section A.0.5 and will be the final screening experiment discussed in this chapter.

Luffing acceleration is another factor which appears to provide a statistically significant change towards changing values of two relevant responses: total and standard deviation of hoisting force (t-values equal to 24 and 35 respectively). Increasing the magnitude of acceleration (reducing jerk) also leads to a reduction of total load by 0.5% and reduction of standard deviation of hoisting load by 19%. Luffing acceleration also has a significant higher order effect on total hoisting load response (t-value - 14), which indicates that when luffing acceleration is combined with slewing acceleration, there is additional load value change present which is not visible when these two factors act independently. This concludes that correctly establishing luffing motion profile and acceleration magnitude is an important task towards acquiring accurate hoisting load response.

In terms of motion significance, only slewing acceleration magnitude appears to be mostly irrelevant under allowed motion change threshold, meaning that in terms of calibrating hoisting load effects towards a realistic value, slewing acceleration magnitude setup is not particularly worthy investigation, with only some combined response with luffing acceleration showing significant change in result values. Other inertial load factors (especially pontoon motion and luffing acceleration) are more critical in terms of their independent effects. This leads to an assumption that for slewing acceleration setup, establishing displacement motion that can be completed within predefined temporal bounds is sufficient and further investigation into its accurate acceleration setup is not critical for result accuracy.

Standard deviation of hoisting force results show that hoisting acceleration setup is a factor that has significance towards affecting hoisting load value (t-value = 19), and its effect is comparable to pontoon motion and luffing acceleration effects (t-value equal to 26 and 35 respectively). This shows that establishment of hoisting acceleration setup is important for accurate result acquisition of hoisting force.

Results also show that no factor has enough statistical significance to change response value of maximum hoisting force at a confidence level of 95% ($\alpha = 0.05$), with pontoon motion effects being close to passing the t-value threshold of 12.71. Results of each p-value and t-value of this response is summarized in appendix A.

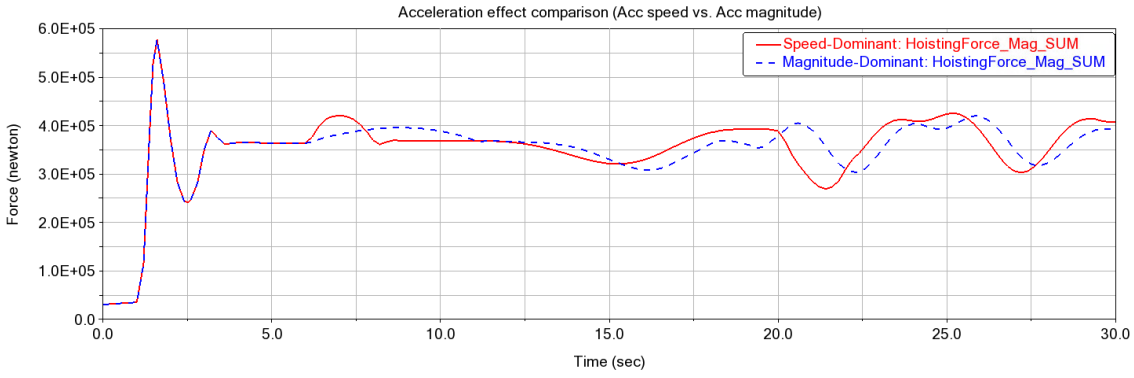

Figure A.11: Comparison of loading profiles of the hoisting force, between a setup which imposes motion through larger acceleration magnitude vs. larger jerk (speed of acceleration).

Based on the hoisting load magnitude response results illustrated in figure A.11, it appears that the change in two approaches (higher acceleration magnitude vs. higher jerk) lead to aforementioned expected effects on the body loads. Overall, the effects can be summarized as follows:

1. Increase of jerk does lead to higher load peaks, higher total load and more pronounced changes in load values seen on the profile; while

2. Increase in magnitude of acceleration change load value within a smoother profile (lower peaks and longer period), longer total value of hoisting force. Additionally it also creates a phase shift in load peak setup where peak values of hoisting force are reached at delayed moments in time compared to variant with jerk motion;

This quantification of motion profile and the pattern of observed results for the operator cabin structure load between these two implementation variants concern all three crane motions - luffing, slewing and hoisting, however as it has been discovered through screening experiments, this change is likely dominated by the effects of change in luffing acceleration magnitude. Concerning fatigue damage, and which setup is more desirable for optimal fatigue life - the variant with higher magnitude of acceleration is likely to provide better results. This is due to the fact that, as seen from results of screening experiment described in section A.0.2 - more drastic hoisting load magnitude changes translate to higher maximum and average nodal stress variations. Load peak magnitude and number of loading cycles increase chance of fatigue failure, and these two factors are more apparent in experiment setup where jerk magnitude is higher (when acceleration magnitude is reduced).

Overview
Table A.5 summarizes the list of statistically significant inertial load factors towards changing hoisting load response (with higher t-values signifying larger significance). Screening experiment of inertial loads has shown that all motion loads besides slewing acceleration have some significance toward at least one of the hoisting load responses: luffing acceleration being relevant for changing total hoisting force and std. dev. values; hoisting acceleration relevant for standard deviation value of hoisting force; slewing acceleration being significant only when combined with luffing acceleration effects; hoisting acceleration affecting mainly the load variation over time (standard deviation).

Table A.5: Overview of statistically significant inertia load factors and their magnitude of significance towards changing hoisting load responses

TOTAL Hoisting Load				**Std. Dev. of Hoisting Load**			
Significance limit: P-value <0.05							
Mark	**Factor**	**T-value**	**P-value**	**Mark**	**Factor**	**T-value**	**P-value**
D	Pontoon Motion	167.01	0.026	B	Luffing Acc	35.26	0.033
B	Luffing Acc	24.22	0.004	D	Pontoon Motion	26.05	0.018
BC	Luffing Acc*Slewing Acc	14.2	0.045	A	Hoisting Acc	19.05	0.024

An interesting observation has been made which shows that the presence of currently calibrated pontoon as it has been done in Wierenga [90] provides change to two responses in a very significant manner (especially for the value of total hoisting load where its statistical significance is higher by a very large margin against other relevant factors). This significant effect of pontoon motion towards changing results of a dominant load calls for a more detailed assessment of its possible motions to determine which factors of pontoon motion are worthy of adjustment. This will be performed in the upcoming section A.0.5.

A.0.5. Experiment 4: Pontoon motion effect on hoisting load response

This part describes the process of assessing the significance of pontoon motion effects on the resultant hoisting load response. It additionally checks whether crane extension and/or rotation angle position has any effect when pontoon motion is exerted on the crane.

Motivation
As inertial load screening analysis described in section A.0.4 has shown - presence of allowed pontoon motion have a significant effect on all relevant responses of the hoisting load (figure A.10). It is worth mentioning

that pontoon motion has been previously calibrated in Wierenga [90], however the significant MBD model accuracy adjustments towards part mass has led to possible discrepancies in the calibration result. Because current motion setup differs from default model and because this motion is affecting hoisting load response - it is worth estimating which specific pontoon motions have the strongest effect and might have to be adjusted.

Screening setup
This experiment tries to estimate what kind of effects how does a change of external motion imposed on the pontoon (when crane is in different boom extension positions and directions) affect response of hoisting load. Table A.6 presents an overview of a screening design setup of this experiment. For the explanation of presented data in the table, please refer to *Screening Setup* subsection of section A.0.2.

Table A.6: Setup overview of screening experiment 2 (pontoon motion effect on hoisting load response)

Marking	**Factors**	**Tested Values**	
		Low	**High**
A	Heave acceleration, deg/sec^2	0.012	0.120
B	Roll acceleration, deg/sec^2	0.0035	0.035
C	Pitch acceleration, deg/sec^2	0.0035	0.035
D	Crane slewing angle position	Pickup	Drop-off
E	Luffing extension position	Retracted	Extended
Responses:	Total Hoisting Force, N Maximum Hoisting Force, N Standard deviation of Hoisting Force, N		
Screening design type:		Plackett-Burman	
Number of runs:		12	

This analysis screens the effects of the following factors in accordance to possible pontoon motion directions and crane extension positions:

1. *Heave acceleration* - Motion imposed by upwards translational acceleration of the pontoon which is most commonly a product of load release.
2. *Roll acceleration* - radial acceleration of the pontoon around the axis of the pontoon length (see figure 3.2).
3. *Pitch acceleration* - radial acceleration of the pontoon around the axis of the pontoon width (see figure 3.2).
4. *Slewing position* - defines rotation position of the crane between its pickup (slewing angle = 0 deg) and drop-off rotation slewing angle = 115 deg) locations (pictures A and B of figure A.12). These specific angles are chosen as they are the points where hoisting load is picked up and released, leading to most significant natural pontoon motion. This factor is meant to determine whether rotation position of the crane has a significant effect on resultant value of the dominant load that imposes most stress to the upper arm structure (i.e. hoisting load).
5. *Luffing position* - defines the distance that the crane upper arm is extended forwards or kept in its natural position (pictures C and D of figure A.12). It includes two positions - when crane is in its general retracted point (extension length = 0 m) and general extended position (extension length = 20 m). It attempts to screen whether pontoon motions imposed when the crane is extended has an effect on resultant hoisting load.

Crane pontoon only has three active degrees of motion as it has been defined in Wierenga [90], thus only these three pontoon directional motion are screened in the form of imposed acceleration. Figure A.12 presents setup principle of conditional factors of slewing position and luffing position. Slewing position factor (figure A.12 picture A and B) defines most important angles of evaluation when largest displacements of pontoon are experienced - specifically when load is picked up (picture A) and dropped off (picture B). Luffing position factor (figure A.12 picture C and D) show two different setups of crane upper arm extension which is expected to have a significant effect on imposing hoisting load when accelerations of pontoon are initiated, due to increased distance of hoisting position away from the axis of rotation.

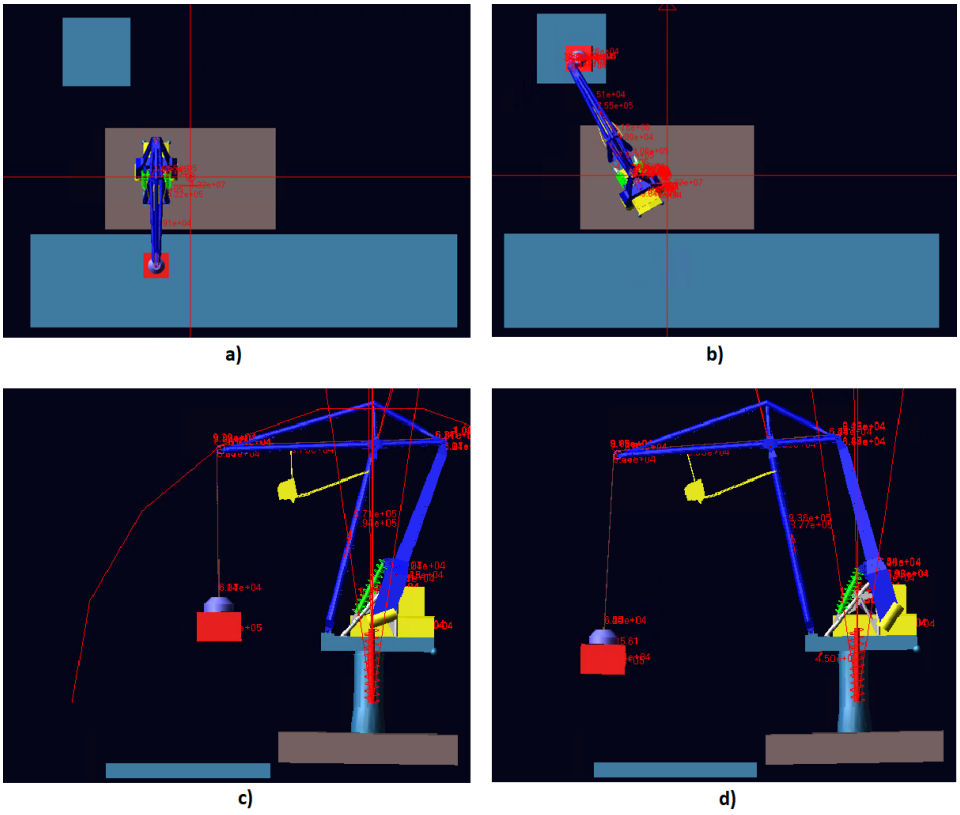

Figure A.12: Illustration of screened positional factors of experiment 4, when accelerations are initiated. Top pictures represent two slewing position factor values: a) pickup position and b) drop-off position. Bottom pictures illustrate Luffing position extension factor values: c) retracted crane and d) extended crane.

Maximum and minimum values of each motion were based on the measurement results made on the actual crane structure. This means that the maximum values of pitch, roll and heave were based on digital sensor measurements acquired for pontoon calibrations, while luffing and slewing positions were based on analog sensor measurements estimated through video footage of the crane operation taken inside the operator cabin. Low level values of acceleration factors are set to 10% of the maximum value, while luffing and slewing position factors do not have a real value, which makes them into conditional factors (ON/OFF principle).

Responses used for evaluating screening results are maximum, total and standard deviation of the hoisting load, just as defined in sections A.0.3 and A.0.4. This is due to the fact that hoisting load is the dominant load affecting the crane upper arm stress response and as it has been shown in A.0.4, it is as well significantly affected by presence of pontoon motion. Thus the relevant responses for this experiment can be summarized as:

1. *Total hoisting force* - this is the sum of hoisting force magnitude values at each time step (0.2 seconds). This provides a baseline for the overall force experienced by the body (in a comparative manner to average force).

2. *Maximum force* - peak value of the force over the loading cycle, representing a specific time step when hoisting force has reached its maximum value.

3. *Standard deviation of force* - this is value of hoisting force variation that is sampled at each time step (0.2 seconds) over the duration of a single crane motion cycle. It is meant to quantify how much the force value fluctuates from its mean.

The principle of how experiments are run for this screening setup is performed by moving the crane into required luffing and slewing positions, as it has defined by specific experimental run setup and then imposing accelerations in three directions at a predefined magnitude, then checking the results of gathered responses

at that moment in time. This provides a repeatable basis for experiment results as it removes external factors from evaluations that would not be possible to remove with an uncontrolled simulation setup.

For the purpose of running pontoon motion simulations, a different screening design has been used - specifically Plackett-Burman factorial design. This is a two level factorial design which is commonly used for parameter screening due to its ability to acquire results for factor significance with a relatively low amount of experimental runs needed. It is best used when there is a large amount of factors present (5 or more) as it requires less data collection to determine factor significance. The drawback of this approach lying in the fact that it assesses only independent relations of each factor without considering their combined effects. The main reason this specific approach is used was to minimize the amount of experimental runs that would be needed to complete the experiment - this is due to the fact that setting up each experimental run and gathering its data is significantly more complex than in experiments 1-3 discussed in previous sections of this chapter and acquisition of linear relations between factors and responses is sufficient for the purposes of this specific screening design of pontoon motions. In total, with a Plackett-Burman screening design setup and five factors in play, the amount of experimental runs needed to conclude this experiment is equal to 12.

Screening results

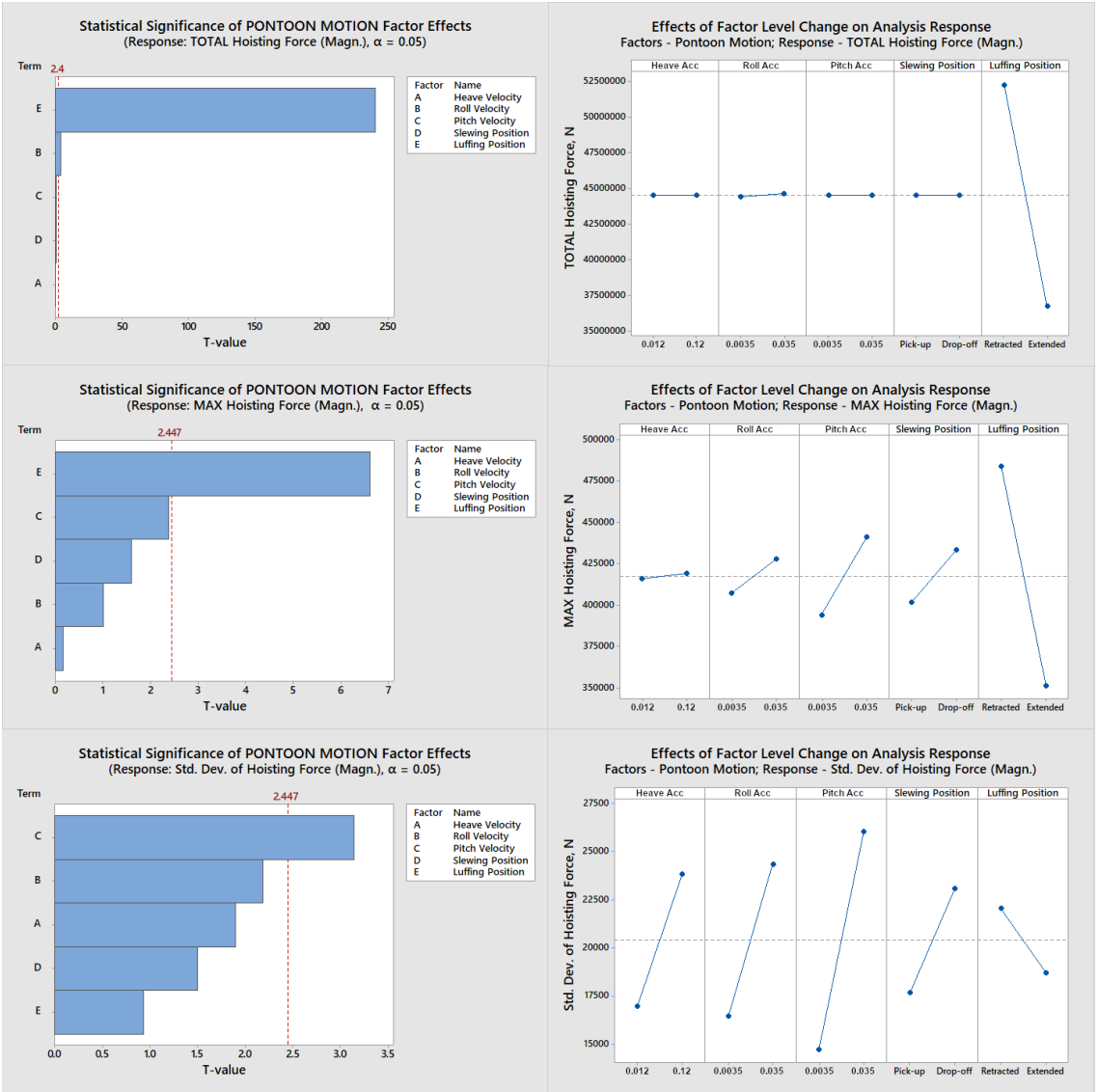

Figure A.13: Statistical significance of pontoon motion loads imposed on the upper arm at the front hoisting position of the crane. A comparison between different loading combinations at various rotation and extension positions are considered in terms of total, maximum and standard deviation values of hoisting force magnitude

Figure A.13 illustrates screening experiment results for the inertial load effects in a pareto chart format (left side of figure A.13) complimented with factor effect plots (right side of figure A.13) of each analysed response. For the methodology on how to interpret result chart, please refer to section A.0.1. Significant factor t-values are summarized in table A.7, with an in-depth overview of screening results summarized in appendix A.

Screening results show that in terms of maximum total hoisting force - the most significant factor is the luffing position. This means that hoisting load is significantly affected by whether crane upper arm is extended or retracted. In the case of maximum load, this is the only significant factor (t-value = 6.6 with threshold equal to 2.4), while for the hoisting load it is not the only relevant factor, but it is by far the most dominant (t-value = 240 with threshold equal to 2.5). This indicates that crane extension position is an important factor when determining how hoisting load is affected during pontoon displacement. An interesting observation here is that extension of crane pontoon leads to a reduction in maximum and total hoisting load.

Additionally, roll and pitch acceleration are relevant for the resultant hoisting load responses. Roll acceleration appears to affect the total hoisting load value (t-value = 3.7), leading to a 2% change in total hoisting load. Pitch acceleration on the other hand is relevant for response variation over time (t-value = 3.1), which results in a 42% increase of standard deviation value when magnitude of acceleration is increased.

Finally, this screening experiment has shown that heave motion effects are not significantly relevant for imposing loads onto the model of the crane. This means their accurate assessment is not required for establishing loading accuracy. Similarly, slewing position does not have a significant effect when motion is initiated to the model either, leaving it as a factor of small relevancy.

Overview

Table A.7: Overview of statistically significant pontoon motion setup factors and their magnitude of significance towards changing hoisting load responses

TOTAL Hoisting Load				**Std. Dev. of Hoisting Load**			
Significance limit: P-value <0.05							
Mark	**Factor**	**T-value**	**P-value**	**Mark**	**Factor**	**T-value**	**P-value**
E	Luffing Position	240.32	0	C	Pitch Velocity	3.14	0.02
B	Roll Velocity	3.74	0.01				

Table A.7 summarizes the list of statistically significant inertial load factors towards changing hoisting load response (with higher t-values signifying larger significance). Pontoon motion calibration has shown that it is most critical to establish correct values for crane luffing extension position in order to acquire accurate loading response. Additionally roll and pitch acceleration setup is important for acquiring an accurate hoisting load profile. For this purpose, hoisting loads will be calibrated in accordance to accurate pontoon motion setup which is dependent on accurate crane extension, pitch and roll motion effects. Heave effects and specific rotation angle of the crane (pickup and drop-off rotational angle setup) are factors which are not specifically relevant for accurate results. This experiment finalizes screening experiment process for finding which loads are most critical for imposing stress in the crane model and what factors are relevant towards establishing accurate response of the dominant load acting on the crane model.

A.0.6. Extended result overview

Table A.8: Factor significance result overview of Experiment 1: Load factor effects on FEA Von Misses stress responses (maximum and average stress). Significant factors and responses passing significance threshold are coloured in green.

No.	Factor	MAX Stress		AVG Stress	
		T-value	P-value	T-value	P-value
1	Hoist Load	3224.34	0	468.7	0
2	Cabin Load	747.9	0	146.92	0
3	Luff Acc	5.05	0	0.96	0.338
4	Slew Acc	6.62	0	10.31	0
5	Roll Acc	-73.68	0	-12.9	0
6	Pitch Acc	-15.57	0	-21.36	0
7	Heave Acc	15.06	0	2.6	0.011
8	Extension Pos	27.97	0	1.53	0.13
9	Hoist Load*Cabin Load	-77.69	0	-65.96	0
10	Hoist Load*Luff Acc	0.77	0.444	-2.84	0.006
11	Hoist Load*Slew Acc	-2.38	0.019	-3.22	0.002
12	Hoist Load*Roll Acc	3.2	0.002	-1.86	0.066
13	Hoist Load*Pitch Acc	5.7	0	1.55	0.126
14	Hoist Load*Heave Acc	-0.66	0.514	-0.4	0.69
15	Hoist Load*Extension Pos	-0.77	0.441	1.03	0.307
16	Cabin Load*Luff Acc	-0.52	0.603	0.01	0.992
17	Cabin Load*Slew Acc	-0.85	0.398	0.14	0.89
18	Cabin Load*Roll Acc	-1.14	0.258	0	0.998
19	Cabin Load*Pitch Acc	2.22	0.029	-0.14	0.888
20	Cabin Load*Heave Acc	0.06	0.956	0	0.999
21	Cabin Load*Extension Pos	0.27	0.786	-0.01	0.995
22	Luff Acc*Slew Acc	-0.03	0.974	0	1
23	Luff Acc*Roll Acc	0.2	0.842	0	1
24	Luff Acc*Pitch Acc	0.07	0.946	0	0.998
25	Luff Acc*Heave Acc	-0.03	0.978	0	1
26	Luff Acc*Extension Pos	0.01	0.991	0	1
27	Slew Acc*Roll Acc	0.03	0.975	-0.02	0.985
28	Slew Acc*Pitch Acc	-15.47	0	-7.19	0
29	Slew Acc*Heave Acc	-0.01	0.989	0	0.998
30	Slew Acc*Extension Pos	-1.07	0.287	1.61	0.112
31	Roll Acc*Pitch Acc	-0.09	0.931	0.02	0.987
32	Roll Acc*Heave Acc	0	0.998	0	1
33	Roll Acc*Extension Pos	-24.25	0	-4.18	0
34	Pitch Acc*Heave Acc	0.04	0.97	0	0.998
35	Pitch Acc*Extension Pos	7.19	0	4.05	0
36	Heave Acc*Extension Pos	0.01	0.991	0	1
Significance Limit		**2.00**	**0.05**	**2.00**	**0.05**
R^{2}		**100.00%**		**99.96%**	
Error Degrees of Freedom		**91**			
Total Degrees of Freedom		**127**			

Table A.9: Factor significance result overview of Experiment 2: Directional crane acceleration motion factor effects on hoisting load responses (maximum, total and standard deviation of hoisting load). Significant factors and responses passing significance threshold are coloured in green.

No.	Factor	MAX Hoist. Load		TOTAL Hoist. Load		Std. Dev. of Hoist. Load	
		T-value	P-value	T-value	P-value	T-value	P-value
1	Upper Arm	9.96	0.064	-4.34	0.144	8.49	0.075
2	Front Arm	3.2	0.193	-2.01	0.294	2.86	0.214
3	Rear Arm	2.21	0.271	-2.35	0.256	4.55	0.138
4	Upper Arm*Front Arm	2.31	0.261	0.98	0.506	-0.43	0.742
5	Upper Arm*Rear Arm	-0.82	0.564	2.16	0.276	0.33	0.797
6	Front Arm*Rear Arm	-1.15	0.455	2.2	0.271	2.07	0.287
Significance Limit		**12.71**	**0.05**	**12.71**	**0.05**	**12.71**	**0.05**
R^{2}		**99.19%**		**97.49%**		**99.06%**	
Error Degrees of Freedom		**1**					
Total Degrees of Freedom		**7**					

Table A.10: Factor significance result overview of Experiment 3: Directional pontoon motion factor effects on hoisting load responses (maximum, total and standard deviation of hoisting load). Significant factors and responses passing significance threshold are coloured in green.

No.	Factor	MAX Hoist. Load		TOTAL Hoist. Load		Std. Dev. of Hoist. Load	
		T-value	P-value	T-value	P-value	T-value	P-value
1	Hoisting Acc	-6.92	0.091	4.4	0.142	-19.05	0.033
2	Luffing Acc	-5.43	0.116	-24.22	0.026	-35.26	0.018
3	Slewing Acc	2.05	0.289	-3.54	0.175	2.31	0.26
4	Pontoon Motion	12.62	0.05	-167.01	0.004	-26.05	0.024
5	Hoisting Acc*Luffing Acc	-2.06	0.288	-1.15	0.455	1.33	0.41
6	Hoisting Acc*Slewing Acc	1.57	0.361	7.4	0.085	12.6	0.05
7	Hoisting Acc*Pontoon Motion	-3.84	0.162	-6.43	0.098	-5.49	0.115
8	Luffing Acc*Slewing Acc	-4.21	0.148	-14.2	0.045	-3.4	0.182
9	Luffing Acc*Pontoon Motion	0.13	0.917	11.27	0.056	10.33	0.061
10	Slewing Acc*Pontoon Motion	-1.18	0.448	-10.84	0.059	-11.44	0.055
11	Hoist Acc*Luff Acc*Slewing Acc	-0.02	0.989	-2.43	0.248	1.51	0.372
12	Hoist Acc*Luff Acc*Pontoon Motion	-2.41	0.25	-0.42	0.746	0.59	0.662
13	Hoist Acc*Slew Acc*Pont. Motion	-0.05	0.971	0.28	0.825	-2.78	0.22
14	Luff Acc*Slew Acc*Pont. Motion	3.2	0.193	2.91	0.211	1.69	0.34
Significance Limit		**12.70**	**0.05**	**12.71**	**0.05**	**12.71**	**0.05**
R^{2}		**99.67%**		**100.00%**		**99.96%**	
Error Degrees of Freedom		**1**					
Total Degrees of Freedom		**15**					

Table A.11: Factor significance result overview of Experiment 4:Crane part flexibility factor effects on hoisting load responses (maximum, total and standard deviation of hoisting load). Significant factors and responses passing significance threshold are coloured in green.

No.	Factor	MAX Hoist. Load		TOTAL Hoist. Load		Std. Dev. of Hoist. Load	
		T-value	P-value	T-value	P-value	T-value	P-value
1	Heave Velocity	0.15	0.883	-0.27	0.796	1.9	0.106
2	Roll Velocity	1.01	0.352	3.74	0.01	2.19	0.071
3	Pitch Velocity	2.38	0.055	0.6	0.573	3.14	0.02
4	Slewing Position	1.6	0.161	0.39	0.712	1.5	0.184
5	Luffing Position	-6.62	0.001	-240.32	0	-0.93	0.387
Significance Limit		**2.45**	**0.05**	**2.40**	**0.05**	**2.45**	**0.05**
R^{2}		**89.84%**		**99.99%**		**78.12%**	
Error Degrees of Freedom		**6**					
Total Degrees of Freedom		**11**					

B

Appendix: K-Joint stress concentration factor

This appendix includes information about the parameters and used formulas for calculating stress concentration factors of assessed load types and measurement positions for a K-Joint. This is a common joint variant which was used for verifying stress calculation principle used for Hot-spot finite element analysis.

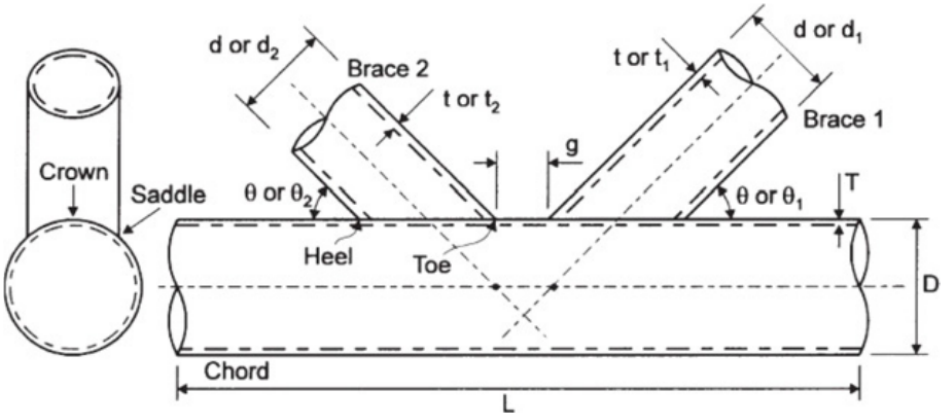

Figure B.1: Setup parameters of K-Joint used for FEA analysis method verification [17].

Table B.1: K-Joint parameter setup overview

Inputs										
$d =$	0.559	m	$t =$	0.0095	m	$C =$	0.70	$\alpha =$	32.8228	$\xi =$	0.1351
$D =$	0.914	m	$T =$	0.0127	m	$C_1 =$	0.40	$\beta =$	0.6116	$x =$	1.1562
$L =$	15.0	m	$g =$	0.1235	m	$C_2 =$	0.35	$\gamma =$	35.98425		
$\theta_1 =$	45.0	deg	$\theta_2 =$	45.0	deg	$C_3 =$	0.14	$\tau =$	0.748031		

Balanced axial load - Chord:

$$SCF_1 = \tau^{0.9}\gamma^{0.5}(0.67 - \beta^2 + 1.16\beta)sin(\theta)(\frac{sin(\theta_{max})}{sin(\theta_{min})})^{0.3} * (\frac{\beta_{max}}{\beta_{min}})^{0.3}(1.64 + 0.29\beta^{-0.38} * atan(8\xi)) \tag{B.1}$$

Balanced axial load - Saddle:

$$\begin{gathered} SCF_2 = 1 + (1.97 - 1.57\beta^2 + 1.16\beta)\tau^{-0.14}(sin(\theta))^{0.7} * (Eqn.(B.1)) + sin^{1.8}(\theta_{max} + \theta_{min}) \\ (0.131 - 0.084 * atan(14\xi + 4.2\beta)) * C\beta^{1.5}\gamma^{0.5}\tau^{-1.22} \end{gathered} \tag{B.2}$$

Unbalanced in-plane bending - Chord Crown:

$$SCF_3 = 1.45\beta\tau^{0.85}\gamma^{(1-0.68\beta)} * (sin(\theta))^{0.7} \tag{B.3}$$

Unbalanced in-plane bending - Brace Crown:

$$SCF_4 = 1 + 0.65\beta\tau^{0.4}\gamma^{(1.09-0.77\beta)} * (sin(\theta))^{0.06\gamma-1.16} \tag{B.4}$$

Unbalanced out-of-plane bending - Chord Saddle:

$$\begin{aligned} SCF_5 = \gamma\tau\beta(1.7 - 1.05(\beta^3)(sin(\theta))^{1.6})A * (1 - 0,08(\beta_B\gamma)^{0.5}e^{-0.8x}(\gamma\tau\beta(1.7 - 1.05 \\ (\beta^3)(sin(\theta))^{1.6}))B(1 - 0.08(\beta_A\gamma)^{0.5}e^{-0.8x})(2.05\beta_{max}^{0.5}e^{-1.3x}) \end{aligned} \tag{B.5}$$

Unbalanced out-of-plane bending - Brace Saddle:

$$SCF_6 = \tau^{-0.54}\gamma^{-0.05}(0.99 - 0.47 * \beta + 0.08\beta^4) * (Eqn.(B.5)) \tag{B.6}$$

Axial load on one brace only - Chord Saddle:

$$SCF_7 = (\gamma\tau^{1.1}(1.11 - 3(\beta - 0.52)^2)(sin(\theta))^{1.6}) + C_1(0.8\alpha - 6)\tau\beta^2(1 - \beta^2)^{0.5}(sin(2\theta))^2 \tag{B.7}$$

Axial load on one brace only - Chord Crown:

$$SCF_8 = \gamma^{0.2}\tau(2.65 + 5(\beta - 0.65)^2) + \tau\beta(C_2\alpha - 3)sin(\theta) \tag{B.8}$$

Axial load on one brace only - Brace Saddle:

$$SCF_9 = 1.3 + \gamma\tau^{0.52}\alpha^{0.1}(0.187 - 1.25\beta^{1.1}(\beta - 0.96))(sin(\theta))^{2.7-0.01\alpha} \tag{B.9}$$

Axial load on one brace only - Brace Crown:

$$SCF_{10} = 3 + \gamma^{1.2}(0.12e^{-4\beta} + 0.011\beta^2 - 0.045) + \beta\tau(C_3\alpha - 1.2) \tag{B.10}$$

In-plane bending on one brace only - Chord Crown:

$$SCF_{11} = 1.45\beta\tau^{0.85}\gamma^{(1-0.68\beta)} * (sin(\theta))^{0.7} \tag{B.11}$$

In-plane bending on one brace only - Brace Crown:

$$SCF_{12} = 1 + 0.65\beta\tau^{0.4}\gamma^{(1.09-0.77\beta)} * (sin(\theta))^{0.06\gamma-1.16} \tag{B.12}$$

Out-of-plane bending on one brace only - Chord Saddle:

$$SCF_{13} = \gamma\tau\beta(1.7 - 1.05(\beta^3)(sin(\theta))^{1.6})A * (1 - 0,08(\beta_B\gamma)^{0.5}e^{-0.8x} \tag{B.13}$$

Out-of-plane bending on one brace only - Brace Saddle:

$$SCF_{14} = \tau^{-0.54}\gamma^{-0.05}(0.99 - 0.47\beta + 0.08\beta^4) * (Eqn.(B.13)) \tag{B.14}$$

C

Appendix: Multi-axial fatigue

This appendix includes extended data on multi-axial fatigue analysis setup.

Table C.1 provides information on the magnitude difference between secondary and primary stress acting on each analysed hot-spot location. It is an extension of table 5.1 which includes only the percentage values without presenting stress magnitude results.

Table C.2 displays average angles of principal stress components for each point analysed in multi-axial fatigue assessment. These values are used for determining S-N curve used for each point as well as if fatigue damage both stress components had to be simultaneously used in fatigue assessment.

Table C.3 shows multi-axial fatigue assessment S-N curves for each of analysed hot-spot points used in the analysis of original crane joint.

Table C.1: Extended comparison of average absolute parallel $\sigma_{\parallel}$ and perpendicular $\sigma_{\perp}$ stress values. Percentage shows proportional value of secondary stress magnitude in comparison with the primary stress magnitude. Colors indicate significant values

Brace	**Point**	**P1**	**P2**	**P3**	**P4**	**P5**	**P6**	**P7**	**P8**
	$\overline{\sigma}_{\parallel}$	1.59E+08	4.55E+07	7.19E+07	7.76E+06	7.25E+07	4.51E+07	1.62E+08	1.91E+07
	$\overline{\sigma}_{\perp}$	2.59E+07	8.17E+07	9.27E+07	3.04E+07	9.37E+07	7.94E+07	2.65E+07	5.54E+07
	Point	**P9**	**P10**	**P11**	**P12**	**P13**	**P14**	**P15**	
	$\overline{\sigma}_{\parallel}$	5.15E+07	9.50E+06	5.11E+07	1.93E+07	2.33E+07	3.56E+06	1.43E+05	
	$\overline{\sigma}_{\perp}$	4.52E+07	1.96E+07	4.48E+07	5.43E+07	7.09E+07	3.33E+07	4.76E+07	
Chord	**Point**	**C1**	**C2**	**C3**	**C4**	**C5**	**C6**	**C7**	**C8**
	$\overline{\sigma}_{\parallel}$	1.64E+08	6.25E+07	1.14E+08	1.11E+08	1.15E+08	1.49E+08	1.43E+08	2.51E+07
	$\overline{\sigma}_{\perp}$	3.10E+07	1.48E+08	1.19E+08	5.84E+07	1.20E+08	6.07E+07	1.80E+07	1.07E+08
	Point	**C9**	**C10**	**C11**	**C12**				
	$\overline{\sigma}_{\parallel}$	7.15E+07	8.93E+07	7.19E+07	2.76E+07				
	$\overline{\sigma}_{\perp}$	4.80E+07	3.59E+07	5.03E+07	1.09E+08				
Forestay	**Point**	**F1**	**F2**	**F3**	**F4**	**F5**	**F6**	**F7**	**F8**
	$\overline{\sigma}_{\parallel}$	3.07E+07	9.00E+07	5.79E+07	5.82E+07	2.00E+07	1.99E+07	5.10E+07	5.00E+07
	$\overline{\sigma}_{\perp}$	3.39E+06	1.13E+08	3.43E+07	3.39E+07	1.65E+07	1.70E+07	1.21E+08	1.19E+08
Backstay	**Point**	**B1**	**B2**	**B3**	**B4**	**B5**	**B6**	**B7**	**B8**
	$\overline{\sigma}_{\parallel}$	3.09E+07	8.70E+07	6.04E+07	6.09E+07	1.99E+07	1.98E+07	8.15E+07	8.03E+07
	$\overline{\sigma}_{\perp}$	3.26E+06	1.08E+08	3.66E+07	3.62E+07	1.65E+07	1.71E+07	1.31E+08	8.15E+07

$SN\,\sigma_{\parallel}, deg$ $SN\,\sigma_{\perp}, deg$

Table C.2: Average angle values of parallel $\sigma_{\parallel}$ and perpendicular $\sigma_{\perp}$ principal stress components for each hot-spot point around joint welds. Colors (red, green, blue) indicate which principal stress component is represented by specific perpendicular or parallel stress angle (maximum, middle, minimum principal stress respectively)

Brace	**Point**	**P1**	**P2**	**P3**	**P4**	**P5**	**P6**	**P7**	**P8**
	$SN\,\sigma_{\parallel}, deg$	81.0	81.0	78.0	87.0	83.0	78.0	74.5	76.5
	$SN\,\sigma_{\perp}, deg$	9.0	9.0	12.0	3.0	7.0	12.0	15.5	13.5
	Point	**P9**	**P10**	**P11**	**P12**	**P13**	**P14**	**P15**	
	$SN\,\sigma_{\parallel}, deg$	77.5	63.0	76.0	67.0	83.0	84.0	87.5	
	$SN\,\sigma_{\perp}, deg$	12.5	27.0	14.0	23.0	7.0	6.0	2.5	
Chord	**Point**	**C1**	**C2**	**C3**	**C4**	**C5**	**C6**	**C7**	**C8**
	$SN\,\sigma_{\parallel}, deg$	67.5	57.5	70.0	87.0	66.5	49.5	86.0	49.5
	$SN\,\sigma_{\perp}, deg$	22.5	32.5	20.0	3.0	23.5	40.5	4.0	40.5
	Point	**C9**	**C10**	**C11**	**C12**				
	$SN\,\sigma_{\parallel}, deg$	51.0	87.0	51.5	68.0				
	$SN\,\sigma_{\perp}, deg$	39.0	3.0	38.5	22.0				
Forestay	**Point**	**F1**	**F2**	**F3**	**F4**	**F5**	**F6**	**F7**	**F8**
	$SN\,\sigma_{\parallel}, deg$	87.0	86.5	87.0	87.0	83.0	82.0	58.0	58.0
	$SN\,\sigma_{\perp}, deg$	3.0	3.5	3.0	3.0	7.0	8.0	32.0	32.0
Backstay	**Point**	**B1**	**B2**	**B3**	**B4**	**B5**	**B6**	**B7**	**B8**
	$SN\,\sigma_{\parallel}, deg$	87.0	87.5	86.5	86.0	81.0	81.0	84.5	84.0
	$SN\,\sigma_{\perp}, deg$	3.0	2.5	3.5	4.0	9.0	9.0	5.5	6.0

Table C.3: S-N curve classes of multi-axial fatigue damage calculations at specific hot-spot locations in relation to stress component direction ($\sigma_{\parallel}$ defining principal stress directed parallel to the weld; and $\sigma_{\perp}$ principal stress directed perpendicularly to the weld)

Brace	**Point**	**P1**	**P2**	**P3**	**P4**	**P5**	**P6**	**P7**	**P8**
	$SN\,\sigma_{\parallel}$	C2	C2	C2	C2	C2	C2	C2	C2
	$SN\,\sigma_{\perp}$	T	T	T	T	T	T	T	T
	Point	**P9**	**P10**	**P11**	**P12**	**P13**	**P14**	**P15**	
	$SN\,\sigma_{\parallel}$	C2	C2	C2	C2	C2	C2	C2	
	$SN\,\sigma_{\perp}$	T	T	T	T	T	T	T	
Chord	**Point**	**C1**	**C2**	**C3**	**C4**	**C5**	**C6**	**C7**	**C8**
	$SN\,\sigma_{\parallel}$	C2	C2	C2	C2	C2	C2	C2	C2
	$SN\,\sigma_{\perp}$	T	C2	T	T	T	C2	T	C2
	Point	**C9**	**C10**	**C11**	**C12**				
	$SN\,\sigma_{\parallel}$	C2	C2	C2	C2				
	$SN\,\sigma_{\perp}$	C2	T	C2	T				
Forestay	**Point**	**F1**	**F2**	**F3**	**F4**	**F5**	**F6**	**F7**	**F8**
	$SN\,\sigma_{\parallel}$	C2	C2	C2	C2	C2	C2	C2	C2
	$SN\,\sigma_{\perp}$	T	T	T	T	T	T	C2	C2
Backstay	**Point**	**B1**	**B2**	**B3**	**B4**	**B5**	**B6**	**B7**	**B8**
	$SN\,\sigma_{\parallel}$	C2	C2	C2	C2	C2	C2	C2	C2
	$SN\,\sigma_{\perp}$	T	T	T	T	T	T	C2	C2

D

Appendix: Joint design adjustment

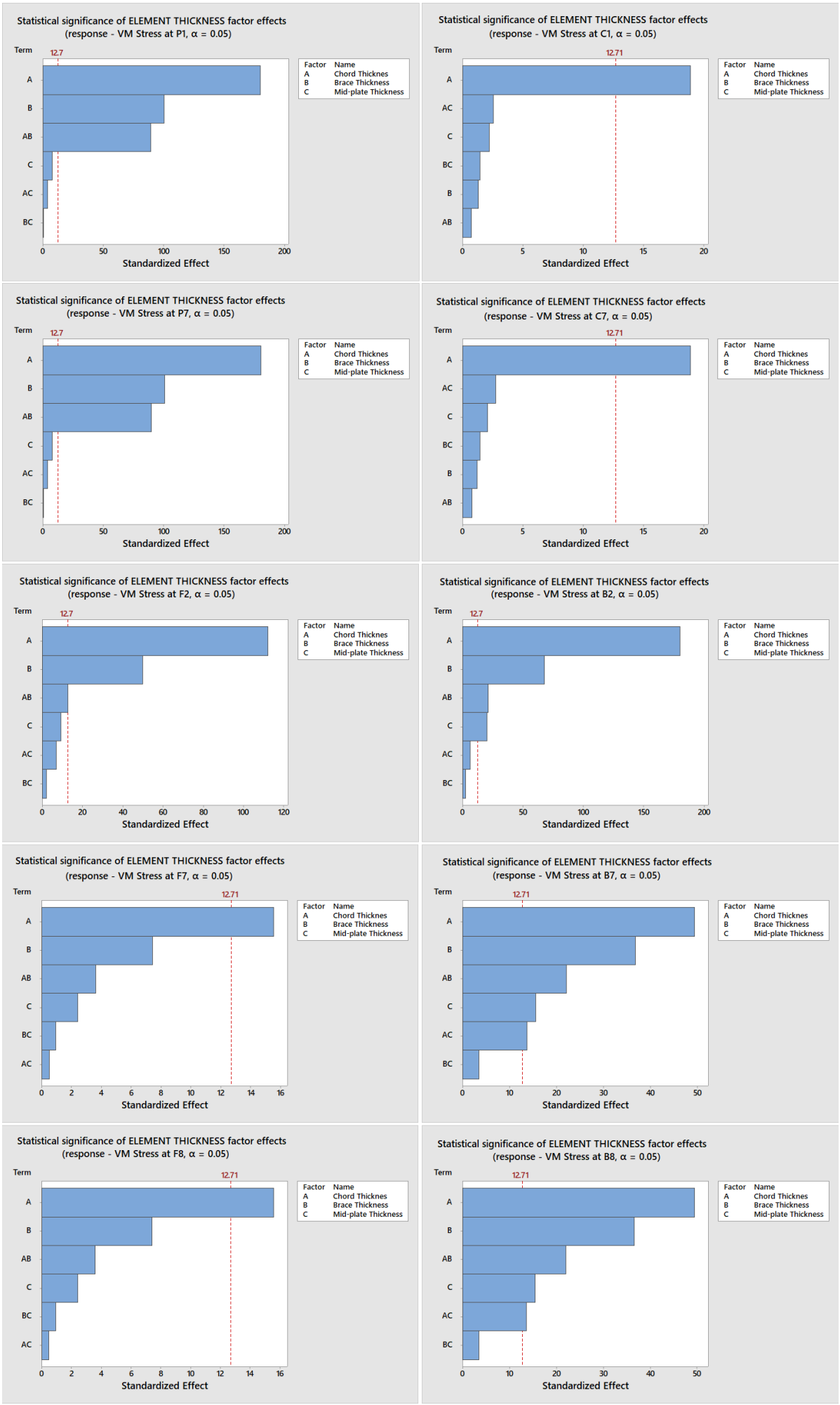

Figure D.1: Result overview - significance screening of joint beam thickness.

E

Appendix: MBD motion setups

Table E.1: Comparison of motion setup between original and adjusted motion profile.

Adjusted Velocity inputs			
Luffing Velocity, rot/min	**Hoisting Velocity, m/sec**	**Slewing Velocity, rot/min**	**Grab Load Switch**
step(time, 20, 0, 27, 3.0d) + step(time, 29, 0, 35, -3.0d)+ step(time, 43, 0, 52, -4.0d) + step(time, 53, 0, 61, 4.0d)	step(time, 6, 0, 7 , -0.2)+ step(time, 7, 0, 14 , - 2)+ step(time, 15, 0, 24 , 2.2)+ step(time, 28, 0, 32 , 2.8)+ step(time, 33, 0, 37 , -2.8)+ step(time, 40, 0, 42 , -0.5)+ step(time, 43, 0, 44 , -1.5)+ step(time, 45, 0, 47 , 2.0)+ step(time, 53, 0, 56 , 2.2)+ step(time, 58, 0, 68 , -2.2)	step(time, 11, 0, 16, -8.0d)+ step(time, 30, 0, 34, 6.0d)+ step(time, 34, 0, 38, 2.0d)+ step(time, 44, 0, 55, 9.2d)+ step(time, 60, 0, 66, -9.2d)	(step(time, 7, 0, 9, 1)+ step(time, 40, 0, 41.5, -1)
Original Velocity Inputs			
Luffing Velocity, rot/min	**Hoisting Velocity, m/sec**	**Slewing Velocity, rot/min**	**Grab Load Switch**
step(time, 20, 0, 22, 2.6d) + step(time, 33, 0, 35, -2.6d)+ step(time, 46, 0, 53, -4.2d) + step(time, 54, 0, 61, 4.2d)	step(time, 6, 0, 7 , -0.2)+ step(time, 9, 0, 10.5 , -1.6)+ step(time, 22, 0, 24 , 1.8)+ step(time, 31, 0, 33 , 3.5)+ step(time, 36, 0, 38 , -3.5)+ step(time, 40, 0, 42 , -0.5)+ step(time, 42, 0, 43 , -1.7)+ step(time, 46, 0, 47 , 2.2)+ step(time, 53, 0, 54 , 2)+ step(time, 55, 0, 56 , -1)+ step(time, 57, 0, 58 , 1)+ step(time, 62, 0, 68 , -2)	step(time, 11, 0, 13, -7.7d)+ step(time, 30, 0, 33, 7.0d)+ step(time, 33, 0, 38, 0.7d)+ step(time, 44, 0, 45.9, 3.0d)+ step(time, 46, 0, 47, 4.5d)+ step(time, 64, 0, 66, -7.5d)	step(time, 7, 0, 9, 1)+ step(time, 40, 0, 42, -1)